FAULTS AND FLUID FLOW: AN INVESTIGATION INTO THE PRODUCTION OF LOW PERMEABILITY FAULT ROCK IN WEAKLY LITHIFIED SILICICLASTIC SEQUENCES IN NEW ZEALAND

Gabrielle Watson

A dissertation submitted in partial fulfilment of the requirements for the Degree

of

DOCTOR OF PHILOSOPHY IN GEOLOGY

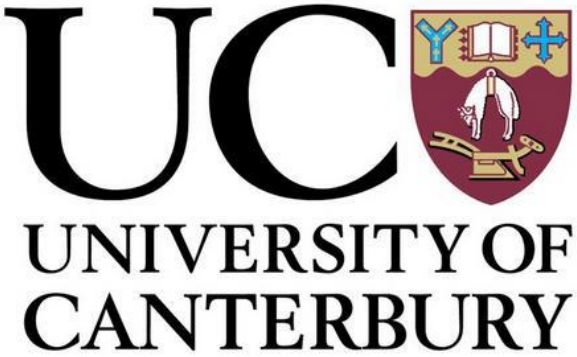

UNIVERSITY OF CANTERBURY 2020

Abstract

This PhD investigates the variability in fault rock generation, geometry and distribution for small normal faults with displacements of 2 cm to 1.1 m exposed along three coastal outcrops in New Zealand. The aim of the study is to quantify the geometries, frequency and fault seal properties of shale smears. The data and analysis contribute to improving predictions of the distributions, thickness and fault-seal properties of low-permeability fault-rock. We use measurements and analysis of 240 faults from the Mount Messenger Formation (MMF), Waitemata Group and Conway Formation, which were 100% exposed and displaced poorly lithified well bedded strata buried to maximum depths of 1.5 km. The majority of faults (N=184) were sampled from four beaches along a ~20 km exposure of the MMF deep-water turbidites. The data included a combination of displaced individual beds and six detailed down fault profiles. Shale-smear geometries are highly variable, ranging from continuous smears, to discontinuous smears with variable thickness, to faulted siltstone beds with no smear, to beds sliced by synthetic minor faults. Shale-smear geometries generally show few clear relationships with siltstone-bed thickness, proximity to siltstone bed or displacement. At outcrop scale smearing appears to be accommodated by both brittle and ductile processes with smeared siltstone beds being both dragged and faulted into fault zones. In thin sections shale smears that appeared ductile at outcrop comprised micro-scale synthetic faults that sliced the siltstone into the fault-zone. We suggest that all smears deform by brittle processes with the difference between ductile and brittle deformation being the scale of faulting. The incorporation of siltstone beds into fault-zones was less common than expected, with ~50% of beds showing more than 5% smear and only ~10% beds continuous smear. Formations with the highest phyllosilicate content siltstone beds display the greatest smearing, however, some beds exhibit both smear and no smear with these differences potentially related to fault-zone structure. As many of the siltstone beds are not incorporated into fault zones, siltstone wall rock may only comprise part of the low-permeability fault rock. The thickness of fault rock is heterogeneous varying by up to an order of magnitude over distances of 10s cm. These variations in fault-rock thickness do not reflect proximity to siltstone beds or the occurrence of shale smear, and at least partly reflect cataclastic processes. Using the available data and published shale-smear algorithms we calculate Shale Smear Factor (SSF), Clay Smear Potential (CSP) and Shale Gouge Ratio (SGR) for the faults studied. The algorithms generally do not replicate outcrop observations because they over simplify fault-zone structure and shale smear geometries, and do not explicitly account for processes other than shale smear that produce fault rock (e.g. cataclasis).

Acknowledgements

Submitting a PhD is no mean feat and it would have been near impossible for this to be completed if not for the following people:

Firstly, Sacha, Rob, Cathy, Sarah, Chris, John and Matt the geology techs for always being super helpful and kind when I asked for samples, equipment and training. Rob W for providing sample analysis, feedback and general support. My supervisor, Andy Nicol, for the guidance, support and opportunities to travel with fieldwork, conferences and internship.

Henry for all his help collecting and processing data, for doing most of the physical exertion on our last trip and for his ability to dive into the bush and return with cool NZ wildlife. Dale for help on fieldwork both collecting data and organising trips as well as his help in finalising this thesis.

Friends and family who fed me, kept me company and helped with anything/everything after my two surgeries.

Andrea for making sure I didn't just hide and become an office gremlin during my PhD. For showing me awesome places, fossil localities, keeping me company in hospital and encouraging me to explore more of the Port Hills! Ana for keeping me sane during my injuries and indulging my impulsive plans. Liz for the sarcasm, take downs and sound advice I didn't always want to hear but always kinda needed. Tabitha and Sam for listening to my office rants and helping out when I was incapacitated. My parents and brother for always thinking I could do this despite two major surgeries, strong medication and an apathy towards the finer details.

Last but not least: Astrid. Wouldn't have got this done if it wasn't for you being such an awesome human being.

Also Frostbite, Half-row and Ophelia. They know why.

Contents

Table of Tables

Table of Figures

1 Introduction

This thesis aims to quantify the geometry, frequency and continuity of shale smears using outcrops of small normal faults (<1.1 m displacement) in New Zealand. Shale smears are defined as 'Entrainment of clay or shale along the fault plane leading to an increase in capillary entry pressure' by Yielding et al. (1997) with variations of this definition having been proposed by various authors. The smearing of low permeability shales along a fault zone has been shown to create baffles or barriers to across fault fluid flow. To understand better the geometries of shale smears it is necessary to examine how they form and what factors influence their development. We propose to add to the current suite of shale smear outcrop studies which suggest a range of models for their geometries and formation mechanisms (Lehner and Pilaar 1997; Yielding et al. 1997; Van der Zee et al. 2003; Childs et al. 2009; M. B. Kristensen et al. 2013; Kettermann et al. 2016). Although these models are well established, many outcrop studies in siliciclastic sequences highlight the variability in the thickness and locations of shale smears relative to their source beds (Lindsay et al. 1993; Childs et al. 1997; Lehner and Pilaar 1997; Childs et al. 2009; Kettermann et al. 2016). By further constraining the range of shale smear behaviours it is hoped that the prediction of the distribution of low permeability fault rock along a fault trace will be improved. These improvements may help us understand how, where and when faults will impede the lateral flow of fluids including water, CO2, gas and oil (Fisher and Knipe 2001; Gartrell et al. 2004; Dockrill and Shipton 2010; Yielding 2012; Jenkins et al. 2015).

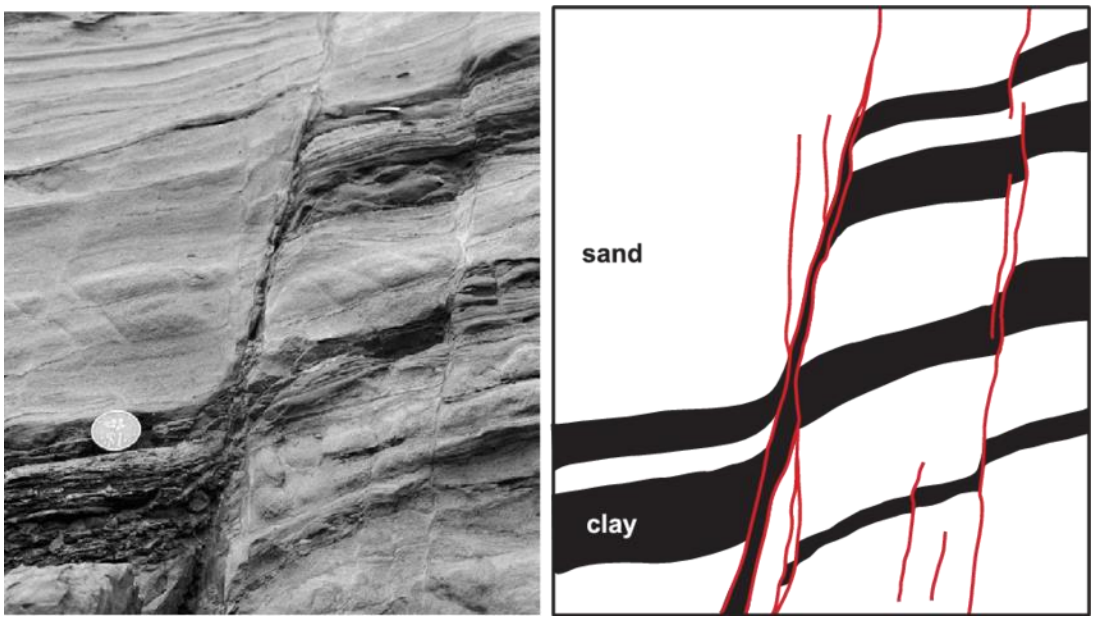

Figure 1.1 An example of a continuous shale smear taken in Miri, Malaysia by Van der Zee and Urai (2005). The schematic (right) is a sketch of the photograph and highlights the entrainment of clay along the small scale faults (red) clearly visible. The scales in both drawing and photograph are the same (see coin in photograph).

Many previous studies of shale smears have focused on faults characterised by smears that are well developed (Lindsay et al. 1993; Lehner and Pilaar 1997; Yielding et al. 1997; Van der Zee et al. 2003; M. B. Kristensen et al. 2013; Kettermann et al. 2016). Because these research projects have focused on studying shale smears they are unlikely to have sampled sequences where smear is infrequent or the smears are poorly developed. In this study, systematic sampling of faults was utilised to reduce the possibility of sampling bias and to constrain the natural variation in smearing of shale beds from no smear to complete smear between the source beds. We conduct this study using a number of different siliciclastic outcrops exposed in coastal cliffs along the North Canterbury, Taranaki and Auckland coastlines in New Zealand. At all study locations, normal faults displace poorly consolidated sequences of interbedded sandstones and siltstones. The bed thicknesses, siltstone compositions and water content of the faulted sequences are sufficiently different that we can examine the impact of sequence characteristics on the formation of shale smears. These stratigraphic differences and the number of faults studied (>250) may mean that the results of this thesis have application beyond the outcrops studied. Like many previous studies, our analysis has particular application to small normal faults and provides few insights into shale smears developed on strike slip or reverse faults. Despite the limited scale range of our data it remains possible that the conclusions of this thesis will have application for large faults observed in seismic reflection datasets.

1.1 Questions and aims

This PhD aims to further the current understanding of shale smear within fault zones by systematic sampling, testing the hypotheses and assumptions of previous authors. Our results and observations are used in conjunction with previous work to develop models of fault-zone structure. This thesis has been written as a collection of four stand-alone manuscripts, which may eventually be published, bookended by an introductory chapter and a conclusions (and further work) chapter. Each main science chapter (i.e. chapters 2-5) addresses a separate facet of shale-smear geometry and/or formation. The main questions addressed in each chapter are outlined below:

- **Chapter 2**: Most faults comprise an area of high strain, low permeability fault rock and lower shear strain fault-zone. Questions remain about how these high and lower shear strain fault-zone components relate to each other. For example, how is low permeability fault rock distributed within fault-zones, both in 2D and 3D? In addition, what relationships exist between displacement and fault architecture and what are the implications for predicting the impact of faulting on fluid flow?

- **Chapter 3**: Shale smears come in different shapes and sizes and questions remain about what are the range of geometries? Are different geometries representative of different processes (brittle or ductile), different shale-bed properties or a product of the scale of observation? Additional questions include, how do the geometries of shale smears vary between sequences? And what is the impact of shale smear and their varying geometries on fluid flow?

  Chapter 4: Implicit in many shale smear analyses is the assumption that all shale or siltstone beds smear, however, questions remain about the frequency of shale smears. For example, how common are shale smears and what percentage of smears are continuous between the host cut offs? What are the potential controls on smears on individual beds, for individual stratigraphic sequences and between different stratigraphic sequences? How do statistics on shale smear occurrence in this study relate to previous work?

- **Chapter 5**: Fault seal algorithms are widely used in industry to predict the influence of low permeability fault rock on across-fault flow. These algorithms primarily use parameters which assume that low permeability fault rock is primarily derived from shale and clay beds in the host sequence. The question is how accurate are the current shale-smear algorithms? Can they be used to predict the thickness of low permeability fault rock? What are the limitations of the current algorithms? What is the best way to use the algorithms going forward?

1.2 Previous work and thesis scientific contribution

Many studies have previously been conducted on shale smear and focus on specific questions regarding the formation, extent and predictability of smears (Lindsay et al. 1993; Lehner and Pilaar 1997; Yielding et al. 1997; Van der Zee and Urai 2005; Childs et al. 2007, 2009). This has led to a good understanding of the processes leading to the formation of shale smears and to the range of geometries of these smears. Previous authors have employed a range of methods to understand better the generation of low permeability fault rock. Previous work includes outcrop studies (Lehner and Pilaar 1997; Van der Zee and Urai 2005; Holland et al. 2006; M.B. Kristensen et al. 2013; Torabi 2014; Lommatzsch et al. 2015; Kettermann et al. 2016), grain scale investigations (Fisher et al. 2018), sand box modelling (Schmatz et al. 2010; Noorsalehi-Garakani et al. 2013), core studies (Revil and Cathles 1999; Fisher and Knipe 2001), analysis of seismic-reflection lines (Bouvier et al. 1989; Fristad

et al. 1997; Yielding et al. 1997), geomodelling (Childs et al. 2009; Manzocchi et al. 2010; Yielding 2012; Grant 2016) and combinations of the above. Rather than providing a detailed account of these studies we have summarised the salient points of each study in Table 1.1. The key conclusions from the table are that most previous studies of shale smear have been conducted on small normal faults (< 10 m displacement) formed in interbedded sandstones and shales buried to shallow depths (e.g., < 1.5 km). This study follows this previous work in that we focus on small normal faults that were not buried more than 2 km. As siliciclastic systems are mainly exploited by industry it makes sense that the vast majority of research is also focussed on siliciclastic reservoirs. This paper will concentrate not only on fault sealing behaviour in siliciclastic sequences but also entirely on across fault flow properties.

Table 1.1. Summation of previous studies that have aimed to quantify shale smearing through outcrop, lab or seismic studies. See Table 1.2 for acronym definitions.

AUTHOR	STUDY AREA	STRATIGRAPHIC UNIT(S)	AGE OF FORMATION	FAULT TYPE	THROW	NO. FAULTS	TIMING OF FAULTING	DEPTH OF FAULTING	OUTCOME
BOUVIER ET AL. (1989)	Nun River Field, Niger Delta	Shoreface sandstones separated by field-wide shales	Tertiary	Normal					Development of CSP, Seismic Study Seal not observed at an SSF >6
LINDSAY ET AL. (1993)	Round O Quarry, Lancashire	313ma – 304ma Westphalian A – Fluvio-deltaic sandstones and shale interbed	Pennsylvanian	Normal	Up to 15m, typically 1 m	80	Post-dating lithification	Maximum Burial Depth	Developed SSF, Outcrop study
GIBSON (1994)	Columbus Basin, Offshore Trinidad	Tertiary Sandstone and Shale Sequence	Tertiary	Normal			Late Pliocene and Pleistocene		Significant seals developed at SSF <4
FRISTAD ET AL. (1997)	Oseberg Syd, North Sea	Brent Group – Tarbert Fm and Ness Fm	Middle Jurassic	Normal		15-20	Mesozoic	<500 m	SGR Values <15% non sealing, 15%-18% <1-2bar pressure difference >18% significant seal, Seismic Study
YIELDING ET AL. (1997)	Fault K, Nun River Field, Niger Delta (Bouvier et al 1989) Oseberg Syd, Northern North Sea (Fristad et al 1996) Northern North Sea 2			Normal					Applied SGR to multiple locations using RFT data to calibrate Seismic Study SGR seal threshold at 10%-20% SGR

	Columbus Basin, Offshore Trinidad (Gibson 1994)								
LEHNER AND PILAAR (1997)	Frechen Lignite Mine	Deltaic Sediments, Moderately Cohesive		Synsedimentary Normal Faults	Up to 100 m		Upper Miocene and Lowermost Pliocene		Outcrop Study
VAN DER ZEE AND URAI (2005)	Miri, Sarawak	Deltaic Sediments	Miocene	Normal	Several cm to >25m	450		<1000 m	Outcrop Study
CHILDS ET AL. (2009)	Taranaki, New Zealand	Turbidite Sequence, Poorly lithified	Miocene	Normal, not synsedimentary	1 mm – 60 m		2 Ma – 6 Ma	~1-2 km	Outcrop Study
KRISTENSEN ET AL. (2013)	Nr. Lyngby Jensgaard Galgeløkke Denmark	Unlithified Shallow marine Unlithified Tidal flat Semi lithified Tidal Flat	Post Glacial Lower Miocene Jurassic	Normal	Up to 50 cm Up to 10 cm Up to 25 cm,		Synsedimentary	50m 300m – 500m 1400m	Outcrop Study
KETTERMAN ET AL. (2016)	Hambach Lignite Mine, Germany	Unlithified Deltaic sand clay sequence	Eocene to Pliocene	Normal, Synsedimentary	50-120cm		Late Oligocene to Pliocene	150m	Outcrop Study

1.2.1 Fault rock controls on permeability

Fault permeability is an important area of research for industries that require a detailed knowledge of fluid flow within the subsurface. Knowing the horizontal and vertical flow properties of faults allows the prediction of fluid pathways and storage in reservoirs (Childs et al. 1997; Cartwright et al. 2007; Dockrill and Shipton 2010; Manzocchi et al. 2010; Bense et al. 2013; Jenkins et al. 2015). Whether this is groundwater (cold water), geothermal systems (hot water), hydrocarbons or nuclear waste, knowing if faults will act as conduits, barriers or baffles to flow will be key to establishing efficient and safe operations. For petroleum systems this includes not only the current flow properties of faults, but also how their permeability may have changed through time as fluids migrated on geological timescales (Aydin 2000; Fisher and Knipe 2001; Cartwright et al. 2007; Collettini 2009; Faulkner et al. 2010; Manzocchi et al. 2010). The thickness of fault rock and the reduction in permeability required to retard fluid flow will vary depending on whether production or geological timescales are under consideration. For example, when producing from a field, a fault could present a barrier to flow, while the same fault on geological time scales may only provide a baffle to flow; in general increasing the timescale is likely to increase the probability that fluid will pass through (or around) the fault rock.

Within clastic reservoirs, there are two primary types of fault rock. These are; i) cataclastic fault rock produced by the breakdown of host sandstone grains and, ii) shale smear arising due to the incorporation of low permeability host beds into fault zones (Childs et al. 1997; Gartrell et al. 2004; M. B. Kristensen et al. 2013; Pei et al. 2015; Frischbutter et al. 2017). In addition to these two fault-rock generation processes, the development of phyllosilicate framework rocks, fault-zone mineralisation and post deformation diagenesis can influence the hydraulic properties of fault zones (Frischbutter et al. 2017). Childs et al. (2007) suggest that as the permeability difference between sandstone and shale host lithologies is greater than the difference between the host rock and resultant fault rock lithologies, the entrainment of low permeability shale into the fault zone (from the wall rock) has a bigger influence on fault permeability than production of fault rock via cataclasis. While this conclusion may be true in a sequence comprising clean sandstones, it may be less applicable in sequences where the sandstone units contain a significant amount of lithics or clay (i.e. dirty sands). As the incorporation of clay into a fault zone is considered to be a primary cause of permeability reduction within fault rock, it is often employed to calculate transmissibility multipliers for the purposes of modelling of fluid flow. Thus, cataclasis can often be overlooked and the contribution of cataclastic fault rock underestimated in studies of fault permeability (Nicol and Childs 2018).

The scale of observation and intended use of fault permeability data determines which characteristics are focussed on (Van der Zee and Urai 2005). For an exploration setting, the permeability of one fault may be of interest whereas on a production scale the combined permeability characteristic of all faults

across a field will be of more importance. The purpose of the study also discerns the timescale being investigated; exploration requires knowledge of how fault permeability has behaved through geological time whereas the focus shifts to the sealing behaviour of faults over several years to decades during production (Childs et al. 1997). Furthermore, the characterisation of a fault can vary according to the scale of observation. What at outcrop scale may appear as a series of individual faults may appear as one fault with multiple strands at seismic scale and vice versa. What appears as a fault within a thin section may only be a single slip surface taking up only part of the displacement at outcrop. This can be further complicated by variability in interpretations by different geologists depending on their focus and experience (Seebeck et al. 2014).

Despite cataclasis being thought to be a less viable barrier to fluid flow than shale smear there is evidence that this may not be the case. Grain reorganisation, cataclasis, pore collapse or preferred cementation can all lead to a loss of porosity and/or permeability (Lommatzsch et al. 2015). These reductions are not insignificant with cataclasis having been observed to reduce across fault permeability by up to four orders of magnitude across a single slip band with only a few centimetres displacement in high porosity sandstone (Yielding et al. 1997). Further studies have recorded permeability reductions across deformation bands of three to six orders of magnitude suggesting that they have the potential to prevent fluid flow (Awdal et al. 2014). This is most likely perpendicular to the deformation band as cataclastic bands tend to show permeability anisotropy (Bense et al. 2013). While low degrees of cataclasis may not produce a seal, it can produce a barrier or baffle to flow which can still impact fluid flow on production time scales (Ballas et al. 2014). It has been discussed whether the thickness and petrophysical properties of cataclastic bands is such that a single band would be unlikely to create a barrier or baffle to flow (Fossen et al. 2007; Torabi and Fossen 2009). Instead multiple bands would be required, with Ballas et al 2014 showing that multiple strands could lead to up to four orders of magnitude permeability reduction while cataclastic clusters could lead to reductions of over five orders of magnitude (Ballas et al. 2014).

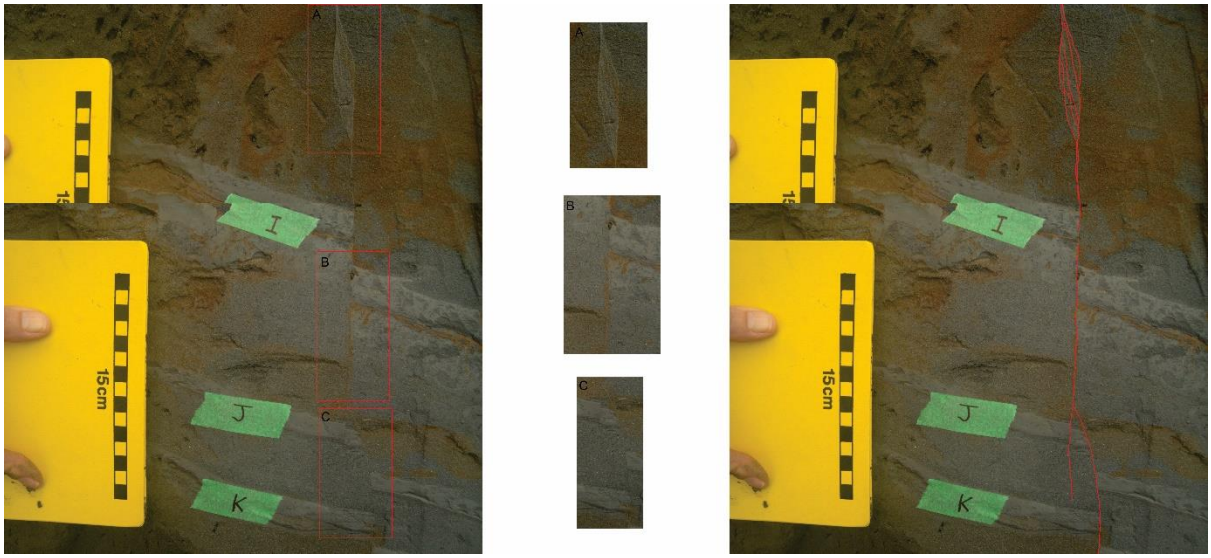

Figure 1.2. A photograph from fault RAP 95 showing the range in deformation band numbers with examples of a deformation band cluster (a), a single band (b) and a pair of deformation bands (c). It is thought a seal is much more likely when clusters are present rather than individual bands.

This study differs from those before as no specific attribute, parameter or relationship was explicitly investigated. Instead, data were collected systematically from outcrop. Every fault that was accessible and where the source bed cut offs could be located on both the hangingwall and footwall was studied while traversing each outcrop locality from one end to the other. The intention was that by taking measurements from every possible faulted bed any internal bias may be removed, or at least heavily reduced, and that a representative sample of the clay smears within the Mount Messenger Formation would be attained. Many measurements were taken so that the assumptions and questions raised through previous studies could be tested against the data from Taranaki.

1.3 Terminology

In the study of shale smears and fault-zones in general a wide range of terminology has been proposed and adopted both for the deformation structures and for the strata that they deform. These definitions can differ subtly, which can make comparison of results between different studies problematic. For example, measurement of fault thicknesses can vary depending on whether a damage zone or fault zone is being measured, and these differences may impact interpretation of how faults influence fluid flow or growth (for further discussion see Childs et al. 2009). To support interpretation of my results I provide a table below that summarises key terms used frequently throughout this thesis. These definitions are brief, and I encourage the reader to source the original reference if more detailed information is required.

Table 1.2 Summary of the terminology used throughout this thesis. Sources for the definitions can be found in the references on the right side of the table.

TERM:	DEFINITION:	REFERENCE:
FAULT ROCK	Deformed rock that has been entrained into the fault zone; includes fault gouge, breccia and cataclasite.	Childs et al. (2009)
FAULT ZONE	General definition: A fault or series of faults that influence or interact with each other within a relatively constrained zone. Outcrop definition: The distance between kinematically linked synthetic slip-surfaces that accommodate a portion of the overall offset.	General definition: Peacock et al. (2000) Outcrop definition: Childs et al. (2009)
DEFORMATION BAND	Thin areas of strain localisation resulting in grain deformation ranging from granular flow to intense cataclasis with mm to cm offset.	Nicchio et al. (2018)
FAULT SEAL	Reduction in fault permeability due to juxtaposition of low permeability host rock against reservoir or the production of a membrane seal by shale smear, cataclasis or cementation.	Foxford et al. (1998)
SHALE SMEAR FACTOR (SSF)	Equation aiming to quantify the likelihood of smear continuity between host cut offs based on the behaviour of abrasion style smears.	Yielding et al. (1997)
SHALE GOUGE RATIO (SGR)	Summation of the percentage of shale or clay that has passed a specific point on the fault plane.	Yielding et al. (1997)
CLAY SMEAR POTENTIAL (CSP)	Equation aiming to represent the proportion of clay that has been smeared from individual shale horizons for a given location on the fault plane.	Yielding et al. (1997)
CATACLASIS	Crushing of grains to form a finer grained fault rock leading to an increase in capillary entry pressure.	Yielding et al. (1997)
CLAY/SHALE SMEAR	Entrainment of clay or shale along the fault pane leading to an increase in capillary entry pressure.	Yielding et al. (1997)
SLIP SURFACE	Synthetic minor fault that accommodates a significant portion (>5%) of the slip of the overall fault zone.	Childs et al. (2009)
SLICE	Slicing is process of entraining segments of the host shale into the fault zone. Slices are commonly bound by slip surfaces with a distinct boundary between	Giger et al. (2013)

	the slice and juxtaposed units indicating a lack of mixing.	
CLAY*	Grains less than 3.8 µm in size.	Wentworth Grain Scale
DAMAGE ZONE	Zone outside of the fault core that is comprised of kinematically related fractures, minor faults and veins.	Caine et al. (1996)
FAULT CORE	Portion of the fault zone where the majority of displacement is accommodated, comprising anastomosing slip surfaces, shale smear, cataclasites and breccias.	Caine et al. (1996)
PHYLLOSILICATES	Layered silicates.	Brown and Nadeau (1984)

*Clay does not have a standard definition. There is discrepancy as to whether authors define clay by grain size or by composition. Several grain sizes are in use ranging from 1 µm to 4 µm depending on discipline (Velde and Meunier 2008). The Wentworth scale defines anything smaller than 3.8 µm to be a clay and that is the grain size used here. However, this can be problematic as kaolinite and illite can be found up to 50 µm and yet are regularly described as clay minerals (Velde and Meunier 2008). When defined by composition clays are often described as hydrated silicates with layered structures or as fine grained phyllosilicates (Brown and Nadeau 1984). Without a set definition is becomes difficult to identify what is and isn't clay and also to compare between studies that specify a clay percentage for host and/or fault rocks without defining would is being classed as clay.

Damage Zone/Fault Core are terms that are not used extensively in this thesis. Instead the terms fault-rock and fault-zone will be used to describe parts of a fault. Preference for the fault-rock and fault-zone terms is because they appear to be less subjective (than damage zone and core) and the definitions were easier to apply to the faults observed at outcrop (for further discussion see Childs et al., 2009).

Siltstone beds are here referred to as shales and the resulting fault rock derived from these units referred to as shale smear. The siltstones appear to meet the requirements of shale set by some authors, however there is a significant discrepancy in definitions and a lack of detail in the descriptions, with many simply describing it as a fine-grained rock comprising clay minerals and quartz. This is summed up by Grant (2016) who states 'the petrophysicial distinction between a shale and a silt is somewhat subjective, so what is called a silt may still have enough clay matrix to behave like a weak layer and generate a short smear during faulting'. Additionally, some definitions also require shale to split into layers rather than blocks when hit. While shales are often quoted to have a high percentage of clays it can be unclear as to whether this is clay sized grains or clay minerals regardless

of their size. While the units in Taranaki have a high proportion of silt-sized grains, as opposed to clay-sized grains, they do have an abundance of clay minerals and therefore due to the siltstone's fine-grained nature and high clay/phyllosilicate content I also refer to these beds as shales within this publication.

1.4 Data and methods

1.4.1 Outcrops studied

As part of this study I have searched New Zealand for interbedded sandstone and mudstone strata displaced by small normal faults. Of particular interest were localities where these faults exhibited displacements greater than the thickness of fine-grained beds (e.g., siltstone or claystone), individual beds could be traced across the fault zones and the fault zones were 100% exposed with resolution down to millimetre scales. The best locations that satisfied these requirements were coastal outcrops, which are continually 'cleaned' by wave action and generally only accessible approaching low tide. The three sample sites used in this study were outcrops of the Waitemata Sandstone at White Bluff, Auckland, the Mount Messenger Formation (MMF) exposed along the Taranaki coast and the Conway Formation in Gore Bay, North Canterbury (see Figure 1.3). At each of these outcrops the rocks were sufficiently soft to allow manual cleaning of the outcrop and the faults sufficiently numerous to permit sampling of≥15 faults. In total 214 faults were sampled across the three localities. The majority of samples (>80%) were taken from four key sites in the MMF distributed along a ~20 km section of the north Taranaki coast. Because the Taranaki faults provide our main dataset we briefly describe the stratigraphic and tectonic setting of the MMF in the next section.

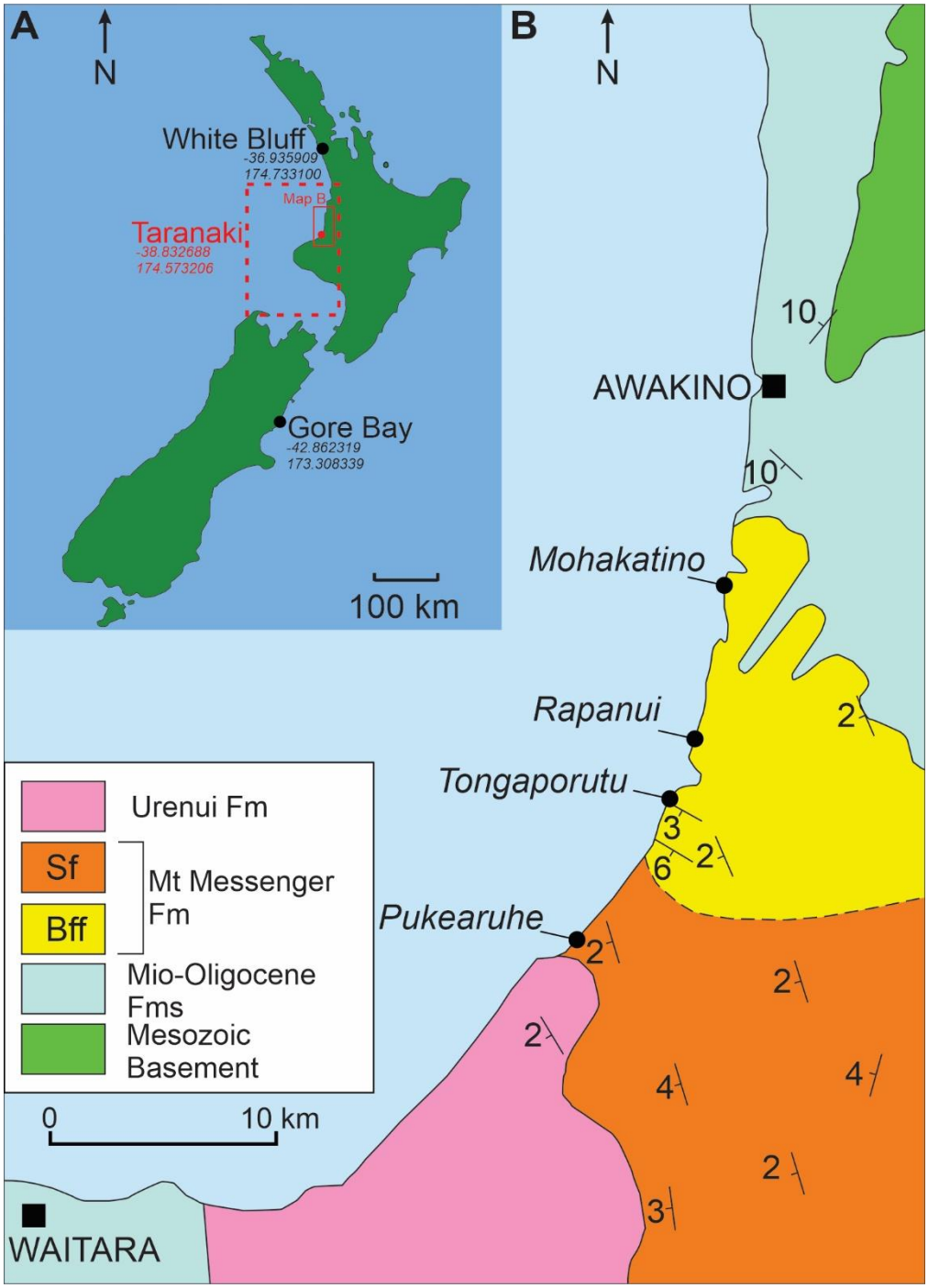

Figure 1.3 Map of New Zealand (A) and Northern Taranaki (B) showing the field sites used in this thesis. Sf=Shelf fans, Bff=Basin floor fans. Strikes and dips of bedding are shown.

The MMF in Taranaki was selected for this study for several reasons. Firstly, it is a well exposed turbidite sequence of sandstones, siltstones and clays that outcrops over a long (~20-30 km) section of coastline in large cliffs. The sequence is heavily faulted, predominantly by normal faults which allowed for a large amount of data to be collected from the same area. Secondly, the MMF is a targeted reservoir unit for some of the onshore Taranaki petroleum fields and therefore is a proven reservoir that both oil and gas, which is currently being produced from (See Figure 1.4). Some of these fields experience compartmentalisation due to faults within the area, which is attributed to internal

fault rock acting as a barrier to fluid flow. Finally, previous work has focussed on siliciclastic sequences predominantly with clean sands in deltaic environments, which have long been targets for oil exploration. As reservoirs become depleted, exploration is moving into deeper water sediments and silt-rich sands meaning that understanding the distribution of low permeability fault rock in turbidite sequences is becoming more pertinent.

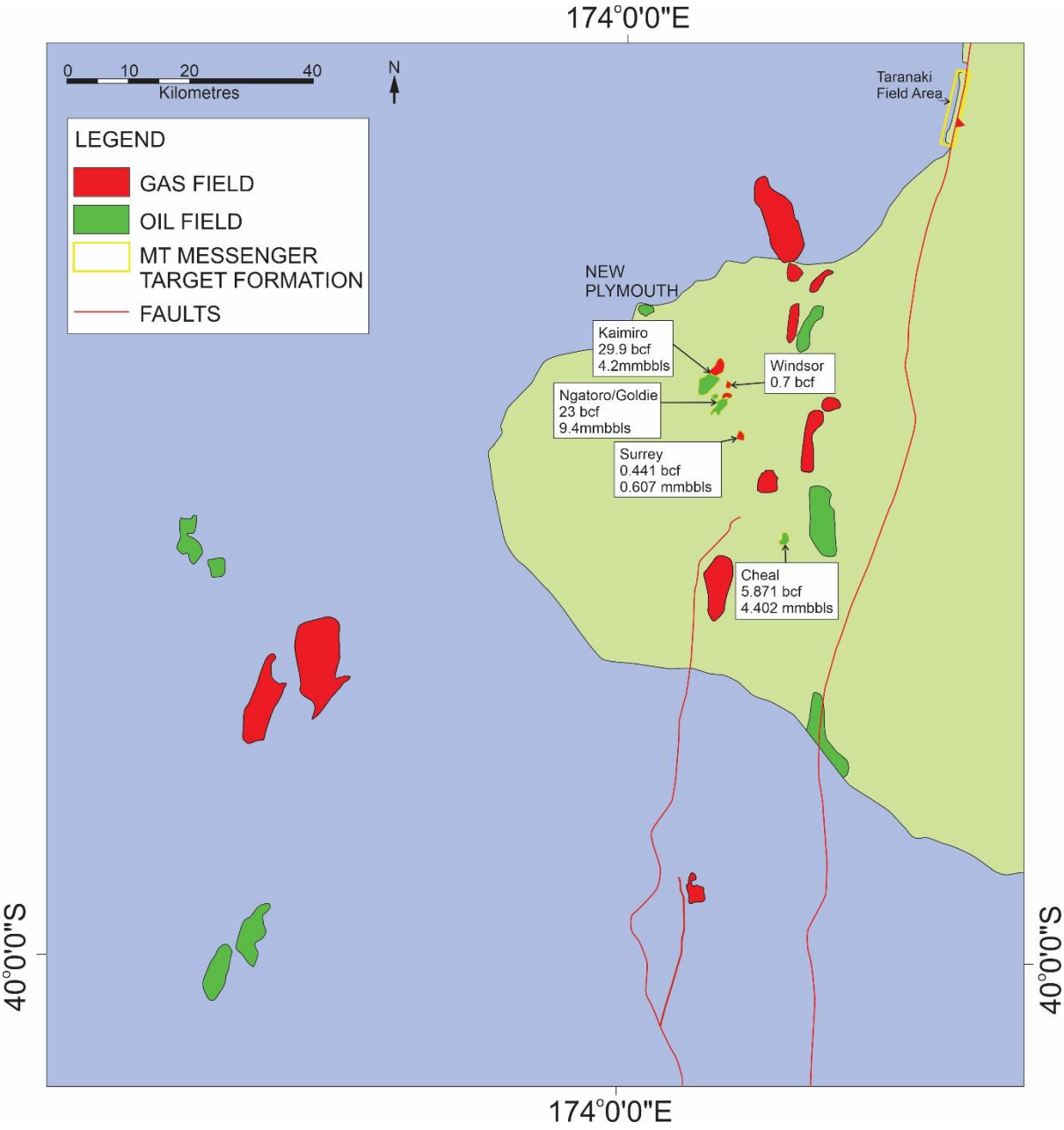

Figure 1.4 Map of the Northern Taranaki Basin showing producing oil and gas reservoirs,with fields that target MMF reservoirs highlighted annotated. Figure adapted from King et al. (2009).

Two additional stratigraphic units were investigated as part of this work, including an outcrop of the Conway Formation in Northern Canterbury and the Waitemata Sandstones in Auckland. The Conway Formation comprises Later Cretaceous age alternating sandstone, siltstone and mudstone beds, which

are exposed in coastal cliffs along the North Canterbury coast. The unit is poorly consolidated and has thin horizons of mudstone and organic rich layers displaced by small normal faults and slip surfaces (Rattenbury et al. 2006). The Waitemata Sandstone is an outcrop of Miocene turbidite deposits with interbedded sandstones, siltstone and claystones. The rocks are exposed in a small (<10 m high) coastal cliffs and show a high degree of smearing (Ballance 1964).

1.4.1.1 Geological setting of the Mount Messenger Formation (MMF)

The MMF outcrops along the eastern edge of the Taranaki Basin which extends from the north-western South Island to west of Auckland in the North Island. The basin covers ~100,000km^2 and is mainly situated offshore (King and Thrasher 1996; Strogen et al. 2017). The sediments infilling the basin range from Cretaceous to Quaternary in age - with a total thickness of up to 8 km (King and Thrasher 1996). The MMF is part of the upper basin fill and is a deep-water turbidite deposited during

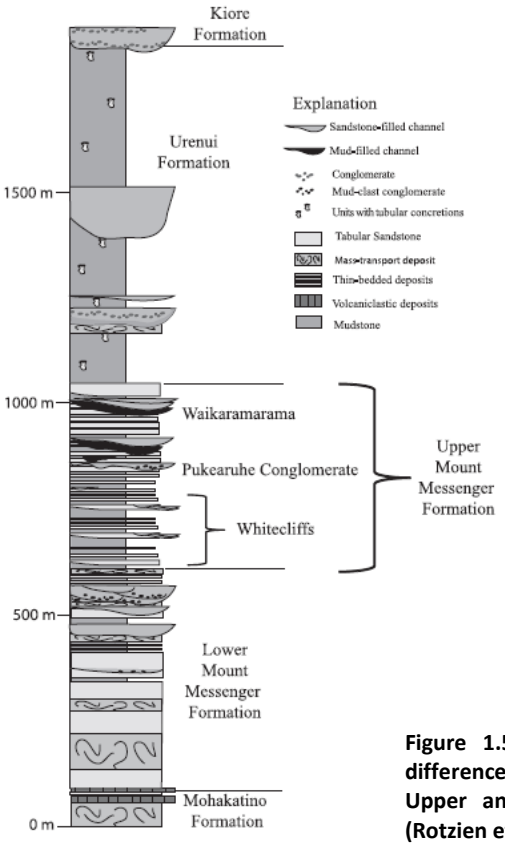

Figure 1.5 A stratigraphic column showing the difference in stratigraphic character between the Upper and Lower Mount Messenger Formation (Rotzien et al. 2014).

the Late Miocene (Figure 1.5). The MMF was deposited during extension (11 – 7 Ma) that is inferred to have formed in response to steepening of the subducting Pacific Plate slab (See Figure 1.6) (King and Thrasher 1996; Giba et al. 2010; Rotzien et al. 2014). Normal faulting contributed to basin deepening, with water depths at the time of MMF deposition reaching 1-1.5 km in the study area. Following MMF deposition, the western North Island was subjected to about 1-1.5 km of uplift which

raised the MMF to sea level and resulted in erosion of the overlying strata (King and Thrasher 1996; Pulford and Stern, 2004; Masalimova et al. 2016). The combination of subsidence followed by Plio-Pleistocene uplift is common along New Zealand's coastline and produces favourable conditions for exposure and preservation of faulted turbidites.

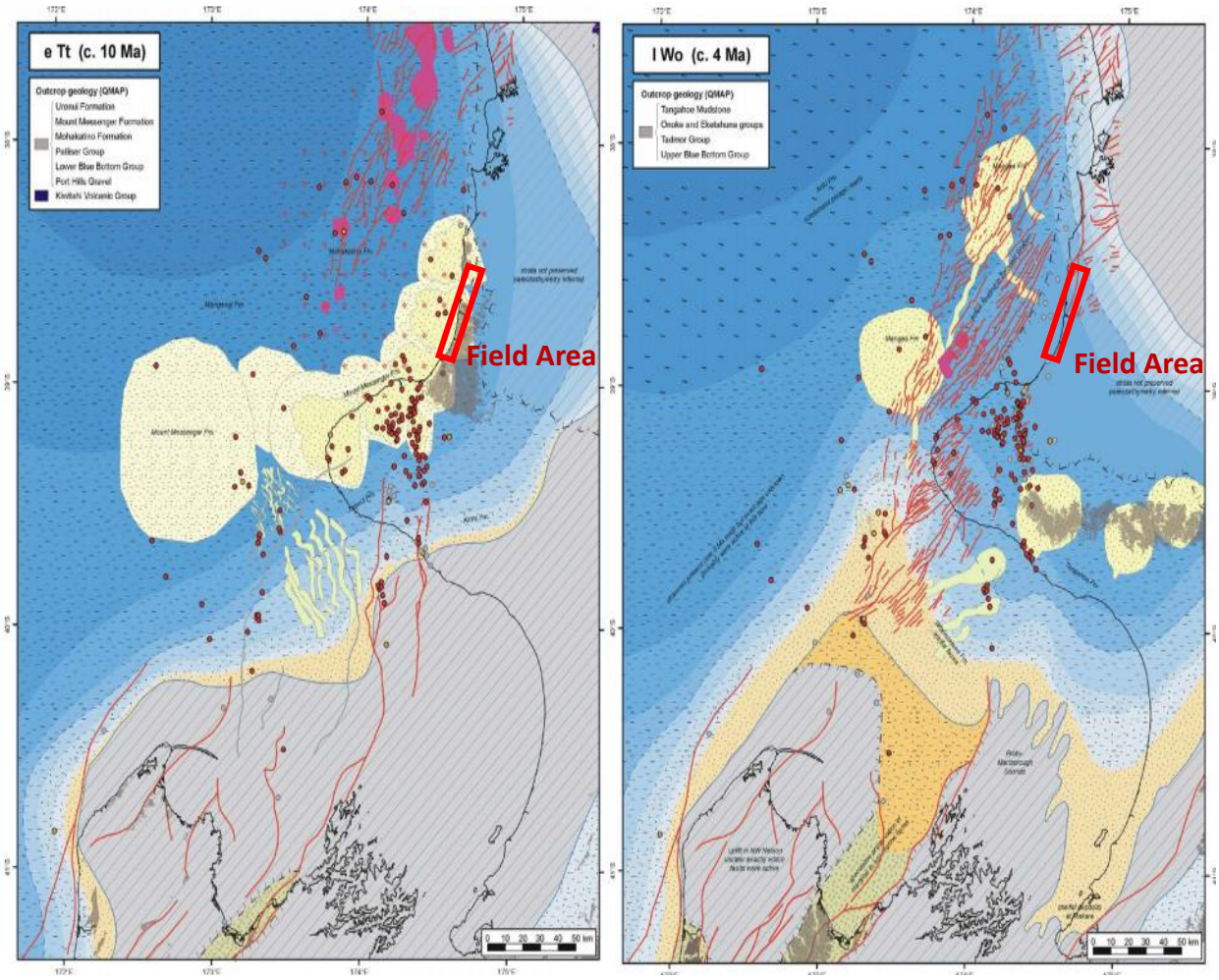

Figure 1.6 Palaeogeographic maps by Strogen et al. (2014) showing the Taranaki Basin during MMF depostion (A) at 10 Ma and during faulting (B) at 4 Ma. The area sampled during this study is highlighted by the red rectangle.

The MMF comprises between 700 m and 1200 m of sediment deposited along the eastern edge of the northern Taranaki Basin. It outcrops for ~25km in coastal cliffs up to ~200m high which stretch from Pukearuhe Beach in the south to north of Awakino (See Figure 1.3). The formation dips at ~2-6° to the southwest and youngs in the same direction along the coastal exposures (Browne et al. 1996; Masalimova et al. 2016). The formation encompasses a series of deep-water submarine fans that can be split into two sub groups: the Upper Mt Messenger and the Lower Mt Messenger. The Lower is characterised by a deep marine siliciclastic and volcaniclastic sequence of basin floor fans (Bff in Fig. 1.3) with thick (>30cm thick) to thin (<30cm thick) bedded sand rich turbidites, thick packages of very

thinly bedded muddy turbidites and occasional conglomerates (Browne et al. 2005). These were deposited as a slope fan system representing channel, levee, lobe and over bank deposits (Rotzien et al. 2014) (see Table 1.2 for further information). The Lower Mt Messenger comprises around 50% fine to very fine sandstones with lesser siltstone, mudstone and conglomerate deposits. The sands contain a high degree of lithic fragments (45-55%) and are generally described as being litharenites. Quantitative Evaluation of Materials by Scanning Electron Microscopy (QEMSCAN) data revealed MMF sandstones to have a high percentage of clays including kaolinite, smectite and illite (Higgs et al. 2015). The Upper Mt Messenger consists of thick bedded units of fine to very fine sandstone, medium to thin interbeds of sandstone and mudstone, volcaniclastic beds, and thick units of mudstone within a slope fan (see Sf in Fig. 1.3) system and mass transport deposits (Browne et al. 2005; Masalimova et al. 2016). In this study most of the sampling occurred in the Lower Mt Messenger, excluding the data from Pukearuhe Beach which samples the upper part of the sequence.

Table 1.2 Summary of the sedimentology of the MMF adapted from (Browne et al. 2005).

SEDIMENTARY FEATURE	BASIN FLOOR FAN: THICK-BEDDED FACIES	BASIN FLOOR FAN: THIN-BEDDED FACIES	SLOPE FAN
SANDSTONE BED THICKNESS	<2 m (typically <1.0 m). Often amalgamated	<0.6 m (typically <0.2 m)	<1.2 m (typically <0.3 m)
SILTSTONE BED THICKNESS	<0.15 m (typically <0.05 m)	<0.4 m (typically <0.1 m)	<1.5 m (typically <0.1 m)
SANDSTONE:SILTSTONE RATIO	9:1	7:3 to 6:4	Variable 2:8 to 8:28:2 to 2:8
SANDSTONE GRAIN SIZE	Fine to very fine	Fine to very fine	Fine to very fine
SANDSTONE SORTING	Moderately well sorted	Moderately well sorted	Moderately well sorted
SANDSTONE SEDIMENTARY STRUCTURES	Abundant massive sandstone (T_a). Tops of some beds rippled.	Abundant massive sandstone (T_a). Common parallel (T_b) and rippled (T_c) beds.	Abundant parallel (T_b), ripple and climbing ripple (T_c) beds with minor massive sandstone (T_a).
TRACE FOSSILS IN SANDSTONE*	Ophiomorpha, Chondrites, Thalassinoides, Diplocraterion, Zoophycos	Ophiomorpha, Chondrites	Scolicia

TRACE FOSSILS IN SILTSTONE*	Planolites, Anconichnus, Chondrites, Zoophycos, Thalassinoides, Spirophycus, Rorschacichnus, Cycloichnus, Paleophycus, Diplocraterion, Cardioichnus	Planolites, Anconichnus, Chondrites, Zoophycos, Thalassinoides, Spirophycus, Lophoctenium	Scolicia, Planolites, Anconichnus, Chondrites, Zoophycos, Rorschacichnus, Scalarituba, Subphyllochorda
PERMEABILITY RANGE	100-800 mD	20-150 mD	20-750 mD
POROSITY RANGE	30-35%	30-35%	30-35%
SANDSTONE CONTINUITY	Extensive in dip and strike orientation.	Extensive in dip orientation. In strike direction, controlled by depositional pinch-out of beds	Extensive—controlled by erosional cut-out of beds.

*Data from Manley & Lewis (1998).

1.4.2 Fault data

Fault data was collected during multiple field campaigns between January 2016 and December 2018. Due to the duration of field studies and the rates of coastal erosion some of the faults studied have now been partially or completely eroded (e.g. Rapanui 95, Chapter 2 Figure 2.6). Two main datasets were derived from the outcropping normal faults. These datasets are here referred to as 'individual faults' and 'fault profiles'. The individual fault dataset includes measurements from over 200 faults with the majority having been sampled from the MMF. The data was collected from individual siltstone/shale beds predominantly displaced by individual faults (>90% of the dataset). For each fault, the outcrop was cleaned using scrapers and water spray bottles and was photographed. Measurements taken in the field included bed thickness, fault vertical displacement, fault-rock thickness, fault-zone thickness, number of slip surfaces (See Figure 1.7). Further measurements of smear continuity and fault-bed apparent angle were derived from high resolution photographs. The fault profile dataset was collected from six sample lines approximately parallel to the dip of six normal faults. All the profiled faults displace sandstone and shale beds of the MMF. Measurements were taken at regularly spaced intervals (5 or 10 cm) along the profile sample lengths that spanned the accessible and exposed sections of the fault. Measurements of bed thickness, displacement, fault-rock thickness, fault-zone thickness, number of deformation bands were taken as well as Schmidt hammer readings.

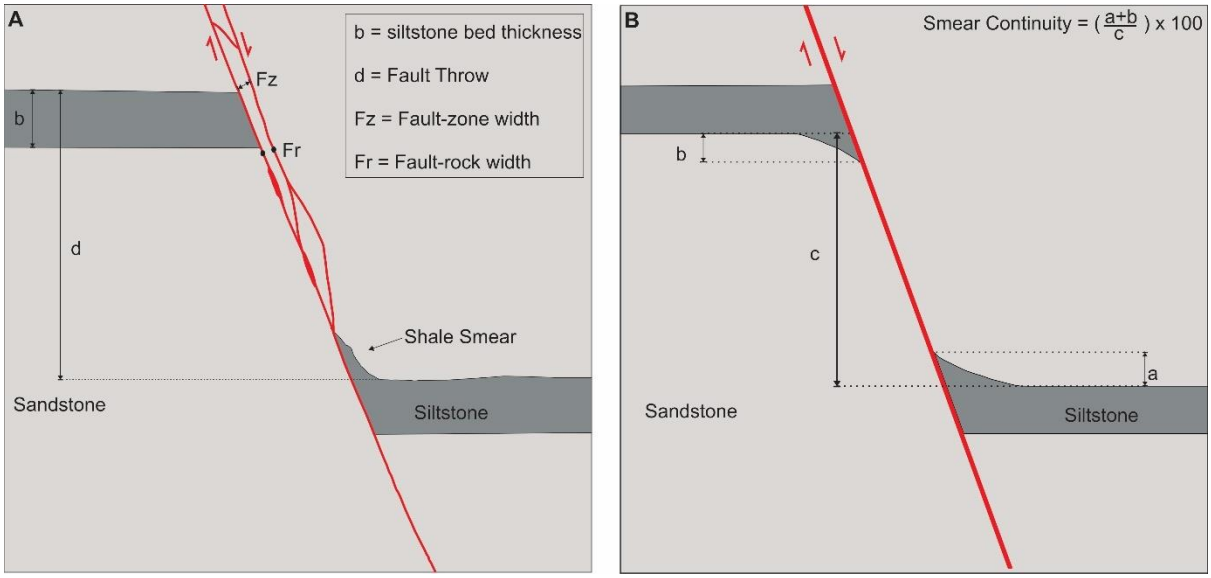

Figure 1.7 Schematic diagram showing fault measurements collected during outcrop sampling.

In addition to these fault measurements, thin-section analysis was conducted to determine the micro-structure of fault zones. Thin sections were viewed using a petrographic optical microscope and polarised light. Thin sections were difficult to produce due to the fragile nature of the rock and even when produced they often have rough surfaces with sections where resin is exposed. By taking pictures of the sample at 2µmx2µm scale across the entire area of each thin section a montage of the sample at 4x optical zoom was produced (the department did not have access to a thin section scanner). Once digitised, Coreldraw was used to highlight the key structural features within the specimens. Three thin sections of shales smears and fault rock were analysed in this way.

Scanning Electron Microscope (SEM) was also used to observe fault-zone micro-structure. For SEM analysis, samples were cut from larger rock and mounted onto plates before being coated in carbon. The top surface of a 1 cm^3 was flattened and mounted into the SEM to allow as much of the sample to be imaged as possible. Element mapping was used to analyse both the chemical composition of the sample itself and individual grains to highlight any patterns in composition with structures formed.

Grain-size analysis was conducted on more than 160 sandstone, shale, and shale smear and fault-rock samples to help constrain the grain-sizes of undeformed sedimentary beds and grain-size reduction associated with faulting. The utility of grain-size measurements for fault rock are dependent on being able to avoid contamination of the fault-rock sample with wall rock (this is particularly the case when fine-grained fault rock is juxtaposed against host sandstone). To limit the possibility of contamination fault-rock samples were carefully removed from the outcrop and scraped clean (see Figure 1.8). In cases where multiple samples were taken of the same fault rock the grain size distributions were comparable suggesting that random contamination is unlikely (for these samples), although

systematic contamination cannot be discounted.

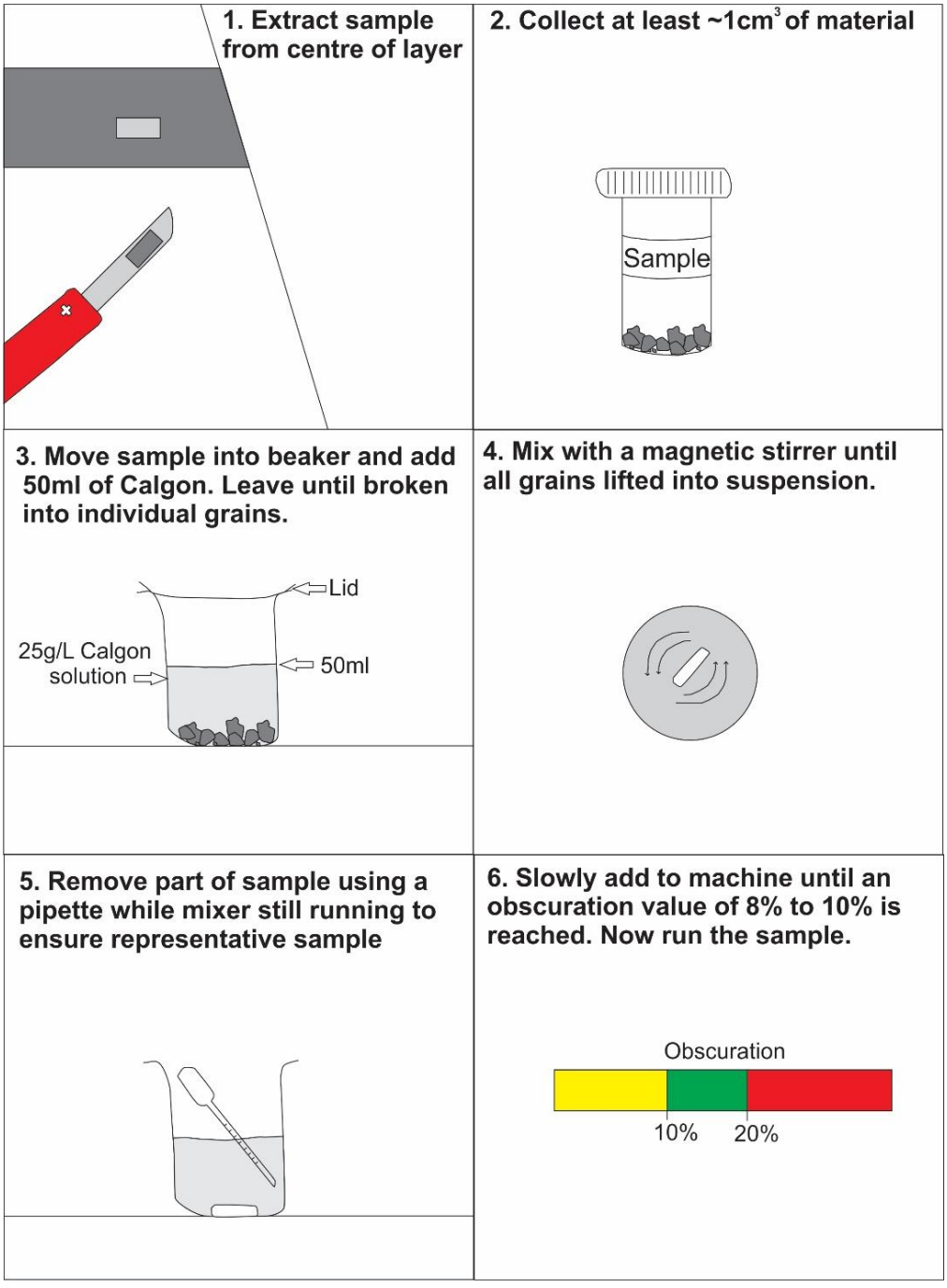

Figure 1.8 Schematic diagram showing the collection of grain-size samples and the process for analysing these samples using the Saturn Digitiser II Laser Diffraction Particle Size Analyser (LDPSA).

Grain sizes were analysed using a Saturn Digitiser II Laser Diffraction Particle Size Analyser (LDPSA). Samples of 1 cm^3 were prepared for analysis by disaggregating grains of 25mg sodium hexametaphosphate (Calgon) dissolved in 1L of water. This process could take a few days to several months depending on the clay content of the sample. In samples where breakdown was progressing slowly, the flasks were swilled to aid mixing between Calgon and the sample. While this process took

time, it was preferable to using physical force to break the samples as this could lead to human induced grain fracturing that was not present previously within the sample. Once the sample had broken down a magnetic stirrer was used to mix the grains into suspension. This allowed a representative sample to be taken by pipette as all grains would be in suspension. Samples were taken from the middle of the tube to try and increase the chance of capturing the entire grain size range. Material was consistently added to the laser sizer until an obscuration value of around 10-20% has been reached. Grain-size analysis was completed three times per sample at a flow velocity of 600 rpm. The LDPSA used has a minimum detection limit of <0.04μm, however, none of the samples tested were close to this lower limit. The resulting grain-size distributions were analysed to ensure that no erroneous responses were recorded. If unexpected grain sizes occurred, a test run of ash with a known particle distribution was used to determine if the measurements were the product of machine error or faithfully recorded the grain size population. In cases where the results were shown to be anomalous by measurement of a standard or by remeasurement of the origin sample they were discarded.

After grain-size samples are run, the data is converted from interval volume percent to cumulative volume with the values starting from the smallest particles to the largest. These are then binned into particle-size classes. This is done by using a SUMIFS formula in Excel to convert the laser sizer output into bins reflecting the Wentworth scale. This allows easy comparison of particle distribution peaks with grain sizes as well as comparison with other results from literature. Host rock and fault rock samples from the same fault can be plotted on the same graph to highlight the reductions in grain size and the changes in grain size distribution for those rock types over a certain displacement

Core samples were collected from 15 beds and fault zones for the purposes of measuring horizontal and vertical permeability. Drill cores 20 mm in diameter and at least 4 cm long were extracted from the outcrop. Unfortunately, we were unable to measure permeability for any of the samples collected because the rocks are poorly lithified and failed during the preparation and measurement process. In addition to permeability, three samples were collected and tested for unconfined compressive strength, however, due to the weak nature of the samples, all 3 failed before the minimum stress had been applied and readings could not be taken.

1.5 Thesis structure

This PhD research is presented in six chapters, four of which (chapters 2, 3, 4 & 5) are intended to be published as separate papers (Table 1.1). Preparing the chapters as first-drafts of these papers resulted in some duplication within the thesis, especially at the beginning of each chapter. Below we provide brief descriptions of the chapters (refer to Table 1.3 for summary information about the chapters).

Table 1.3. Summary of PhD thesis chapters.

CHAPTER	TITLE	COMMENTS
CHAPTER 1	Introduction	Thesis outline and contents
CHAPTER 2	Fault-zone Architecture and the Production of Low-Permeability Fault-rock	Quantifying the variability along down fault profiles and the effect this has on the distribution of low permeability fault rock.
CHAPTER 3	Shale Smear Geometries in a thinly bedded Turbidite Sequence	Investigating the variation in Shale Smear Geometries and the implications for fluid flow.
CHAPTER 4	Frequency of Shale Smear and Factors that Influence their Formation	Assessing whether all shale beds contribute to the fault rock and determining what may be controlling smearing
CHAPTER 5	Algorithms	Testing the current algorithms against the datasets gathered. Suggestions for why Taranaki does not conform and how algorithms may be improved
CHAPTER 6	Conclusion	Conclusions and future work

Chapter 1: Introduction

This chapter sets up the thesis and provides the technical background necessary to analyse and interpret the main body of the research presented in chapters 2-5. The chapter includes brief

descriptions of the faulted stratigraphic units and reader is referred to the cited publications for further information.

Chapter 2: Fault zone architecture and its impact on the production of low permeability fault rock

This chapter investigates the spatial distribution of structures within fault zones and the associated geometries of low permeability fault rock. This study focusses on normal faults from the MMF. Fault architecture was found to be highly variable with fault rock and fault zone thickness showing 1-2 orders of magnitude variation over short distances and at low displacements. While an increase in displacement showed an increase in fault-rock and fault-zone thickness, as well as in the number of slip surfaces and deformation bands, this relationship often showed a wide range over several orders of magnitude. The high degree of variability observed is likely due to fault propagation and linkage processes resulting in areas of higher complexity that produce increases in fault thickness and strain rate.

Chapter 3: Quantification of Shale Smear Geometries from a thinly bedded Turbidite Sequence

This chapter describes the geometries of shale smears from the MMF, a weakly lithified, thinly bedded turbidite sequence from the Taranaki Basin. We summarise information from the international literature (Lindsay et al. 1993; Lehner and Pilaar 1997; Yielding et al. 1997; Giger et al. 2013; Vrolijk et al. 2016; Kettermann et al. 2016) and compare these results to our observations. We explore the lengths and thicknesses of smears for a random sample of more than 180 small (< 1.1 m displacement) normal faults and for six along-fault profiles. The majority of smears had variable thicknesses which were often unrelated to source-bed thickness or distance from the source bed. These thickness variations can result from secondary faults within the fault zone, which locally thicken or thin the smear depending on the geometries and displacements of the secondary faults. The importance of ductile smear and smear associated with slicing of shale beds are considered. The scale dependence of brittle vs ductile deformation of shale smears is considered and used to develop a brittle faulting model for the formation of shale smears in the MMF. The impact of smearing on fluid flow is considered.

Chapter 4: Frequency of Shale Smear and Implications for Fault Seal

Here we test the assumption that all shale beds smear by quantifying the proportion of beds that smear for a turbidite sequence that comprises interbedded mudstone (~1-45 cm thick) and sandstone (~1-150 cm thick), from Gore Bay (North Canterbury), Pukearuhe to Mohakatino (northern Taranaki) and White Bluff (Auckland). The data suggest that many faults produce little to no smear of siltstone beds. Individual shale beds displaced by adjacent faults, with comparable orientations, kinematics and

timing of formation, can show smear and no smear, suggesting that in these cases bed composition (e.g. clay type), grain-size distribution, moisture content or lithification cannot account for the observed variations in smear occurrence. Instead, smearing appears to be common where fault deformation is most distributed and fault-zone thicknesses are greatest. We examine the implications that the results might have for the use of shale-smear algorithms.

Chapter 5: Shale Smear Algorithms

Using the available data and published shale-smear algorithms we calculate Shale Smear Factor (SSF), Clay Smear Potential (CSP) and Shale Gouge Ratio (SGR) for over 180 siltstone beds displaced on normal faults in a thinly bedded turbidite sequence. The algorithms were applied both to a series of detailed down fault profiles and to a larger dataset on individual faulted beds. As with previous studies, continuous smear (i.e. fault seal) is most likely for lower SSF and higher CSP or SGR values, although discontinuous and no smear cannot be discriminated by these methods (see Figure 5.2). The available data support the use of a probabilistic approach for estimating the location of smears between horizon cutoffs (e.g., Childs et al. 2007), an approach that could also be extended to the occurrence and length of the smears. Independent of which algorithm is used shale-smear calculations could over-estimate the seal potential because not all beds smear and many of the smears are short in length.

Chapter 6: Conclusions

A summary of the results and contributions to the field presented by this thesis. The primary questions from Chapter 1 are discussed and, in some cases, answers proffered. Ideas and questions that could not be addressed in this study, primarily due to time restraints, will be briefly expanded upon and recommended for further work.

The research described in this thesis was undertaken by me (Gabrielle Watson), however, others contributed to refining the ideas and their presentation. The chapters are all written in the first person plural ("we"), as is common practice for multi-authored publications. In particular, Andy Nicol (University of Canterbury), Henry Winter (University of Canterbury – Masters student), Dale Cusack (University of Canterbury, research assistant) and Robert Worthington (Equinor, Bergen, Norway) contributed guidance to design of the thesis, and to interpretations of the data. All of the fieldwork, analysis and preparation of field drafts of the chapters was conducted by me (Gabrielle Watson). Chapter 3 is in an advanced stage of preparation as a manuscript that will be submitted for publication following thesis submission with me as first author. Work on the remaining chapters will continue through 2020.

1.6 References

Awdal A, Healy D, Alsop GI. 2014. Geometrical analysis of deformation band lozenges and their scaling relationships to fault lenses. J Struct Geol. 66:11–23. doi:10.1016/j.jsg.2014.05.006.

Aydin A. 2000. Fractures, faults, and hydrocarbon entrapment, migration and flow. Mar Pet Geol. 17(7):797–814. doi:10.1016/S0264-8172(00)00020-9.

Ballance PF. 1964. The Sedimentology Of The Waitemata Group In The Takapuna Section,Auckland. New Zeal J Geol Geophys. 7(3):466–499. doi:10.1080/00288306.1964.10422096.

Ballas G, Fossen H, Soliva R. 2015. Factors controlling permeability of cataclastic deformation bands and faults in porous sandstone reservoirs. 76:1–21.

Ballas G, Soliva R, Benedicto A, Sizun JP. 2014. Control of tectonic setting and large-scale faults on the basin-scale distribution of deformation bands in porous sandstone (Provence, France). Mar Pet Geol. 55:142–159. doi:10.1016/j.marpetgeo.2013.12.020.

Bense VF, Gleeson T, Loveless SE, Bour O, Scibek J. 2013. Fault zone hydrogeology. Earth-Science Rev. 127:171–192. doi:10.1016/j.earscirev.2013.09.008.

Bouvier JD, Sijpesteijn K, Kleusner DF, Onyejekwe CC, Van Der Pal RC. 1989. Three-dimensional seismic interpretation and fault sealing investigations, Nun River field, Nigeria. Am Assoc Pet Geol Bull. 73:1397–1414.

Brown G, Nadeau P. 1984. rystal Structures of Clay Minerals and Related Phyllosilicates [and Discussion]. Philos Trans R Soc London Ser A, Math Phys Sci. 311(1517):221–240.

Browne G, King PR, Higgs KE, Slatt RM. 2005. Grain-size characteristics for distinguishing basin floor fan and slope fan depositional settings: Outcrop and subsurface examples from the late miocene mount messenger formation, New Zealand. New Zeal J Geol Geophys. 48(2):213–227. doi:10.1080/00288306.2005.9515111.

Browne GH, McAlpine A, King PR. 1996. An outcrop study of bed thickness, continuity and permeability in reservoir facies of the Mt. Messenger Formation, North Taranaki. In: New Zealand Petroleum Conference Preceedings. p. 154–163.

Caine JS, Evans JP, Forster CB. 1996. Fault zone architechture and permeability structure. Geology. 24(11):1025–1028. doi:10.1130/0091-7613(1996)024<1025.

Cartwright J, Huuse M, Aplin A. 2007. Seal bypass systems. Am Assoc Pet Geol Bull. 91(8):1141–1166. doi:10.1306/04090705181.

Childs C, Manzocchi T, Walsh JJ, Bonson CG, Nicol A, Schöpfer MPJ. 2009. A geometric model of fault zone and fault rock thickness variations. J Struct Geol. 31(2):117–127. doi:10.1016/j.jsg.2008.08.009.

Childs C, Walsh JJ, Manzocchi T, Strand J, Nicol A, Tomasso M, Schopfer MPJ, Aplin AC. 2007. Definition of a fault permeability predictor from outcrop studies of a faulted turbidite sequence, Taranaki, New Zealand. Geol Soc London, Spec Publ. 292:235–258. doi:10.1144/SP292.14.

Childs C, Walsh JJ, Watterson J. 1997. Complexity in fault zone structure and implications for fault seal prediction. Nor Pet Soc Spec Publ. 7:61–72. doi:10.1016/S0928-8937(97)80007-0.

Collettini C. 2009. Comment on “Structural controls on a carbon dioxide-driven mud volcano field in the Northern Apennines (Pieve Santo Stefano, Italy): Relations with pre-existing steep discontinuities and seismicity.” J Struct Geol. 31(8):853–856. doi:10.1016/j.jsg.2009.02.002.

Dockrill B, Shipton ZK. 2010. Structural controls on leakage from a natural CO2 geologic storage site: Central Utah, U.S.A. J Struct Geol. 32(11):1768–1782. doi:10.1016/j.jsg.2010.01.007.

Faulkner DR, Jackson CAL, Lunn RJ, Schlische RW, Shipton ZK, Wibberley CAJ, Withjack MO. 2010. A review of recent developments concerning the structure, mechanics and fluid flow properties of fault zones. J Struct Geol. 32(11):1557–1575. doi:10.1016/j.jsg.2010.06.009.

Fisher QJ, Haneef J, Grattoni CA, Allshorn S, Lorinczi P. 2018. Permeability of fault rocks in siliciclastic reservoirs: Recent advances. Mar Pet Geol. 91(July 2017):29–42. doi:10.1016/j.marpetgeo.2017.12.019.

Fisher QJ, Knipe RJ. 2001. The permeability of faults within siliciclastic petroleum reservoirs of the North Sea and Norwegian Continental Shelf. Mar Pet Geol. 18(10):1063–1081. doi:10.1016/S0264-8172(01)00042-3.

Fossen H, Schultz RA, Shipton ZK, Mair K. 2007. Deformation bands in sandstone: a review. J Geol Soc London. 164:755–769.

Foxford KA, Walsh JJ, Watterson J, Garden IR, Guscott SC, Burley SD. 1998. Structure and content of the Moab fault zone, Utah, USA, and its implications for fault seal prediction. Geol Soc London, Spec Publ.(147):87–103.

Frischbutter AA, Fisher QJ, Namazova G, Dufour S. 2017. The value of fault analysis for field development planning. Pet Geosci. 23(1):120–133.

Fristad T, Groth A, Yielding G, Freeman B. 1997. Quantitative fault seal prediction: a case study from Oseberg Syd. Nor Pet Soc Spec Publ. 7(C):107–124. doi:10.1016/S0928-8937(97)80010-0.

Gartrell A, Zhang Y, Lisk M, Dewhurst D. 2004. Fault intersections as critical hydrocarbon leakage zones: Integrated field study and numerical modelling of an example from the Timor Sea, Australia. Mar Pet Geol. 21(9):1165–1179. doi:10.1016/j.marpetgeo.2004.08.001.

Giba M, Nicol A, Walsh JJ. 2010. Evolution of faulting and volcanism in a back - arc basin and its implications for subduction processes. 29(November 2009):1–18. doi:10.1029/2009TC002634.

Gibson RG. 1994. Fault zones seals in siliciclastic strata of the Columbus Basin, offshore Trinidad. Am Assoc Pet Geol Bull. 78:1372–1385.

Giger SB, Clennell MB, Çiftçi NB, Harbers C, Clark P, Ricchetti M. 2013. Fault transmissibility in clastic-argillaceous sequences controlled by clay smear evolution. Am Assoc Pet Geol Bull. 97(5):705–731. doi:10.1306/10161211190.

Grant NT. 2016. A geometrical model for shale smear: implications for upscaling in faulted geomodels. Pet Geosci. 23(1):39–55. doi:10.1144/petgeo2016-021.

Higgs KE, Arnot MJ, Brindle S. 2015. Advances in grain-size, mineral and pore-scale characterization of lithic and clay-rich reservoirs. Am Assoc Pet Geol Bull. 7(7):1315–1348. doi:10.1306/01271513101.

Holland M, Urai JL, Zee W Van Der, Stanjek H, Konstanty J. 2006. Fault gouge evolution in highly overconsolidated claystones. J Struct Geol. 28:323–332. doi:10.1016/j.jsg.2005.10.005.

Jenkins C, Chadwick A, Hovorka SD. 2015. The state of the art in monitoring and verification—Ten years on. Int J Greenh Gas Control. 40:312–349. doi:10.1016/j.ijggc.2015.05.009.

Kettermann M, Thronberens S, Juarez O, Urai JL, Ziegler M, Asmus S, Krüger U. 2016. Mechanisms of clay smear formation in unconsolidated sediments-insights from 3-D observations of excavated normal faults. Solid Earth. 7(3):789–815. doi:10.5194/se-7-789-2016.

King P., Bland K.J., Funnell R., Archer R., Lever L. (2009). Opportunities for underground geological storage of CO2 in New Zealand -Report CCS -08/5 -Onshore Taranaki Basin overview. GNS Science Report. 58.

King P, Thrasher GP. 1996. Cretaceous-Cenozoic geology and petroleum systems of the Taranaki Basin, New Zealand. Institute of Geological & Nuclear Sciences.

Kristensen M. B., Childs C, Olesen N, Korstgård JA. 2013. The microstructure and internal architecture of shear bands in sand-clay sequences. J Struct Geol. 46:129–141. doi:10.1016/j.jsg.2012.09.015.

Lehner FK, Pilaar WF. 1997. The emplacement of clay smears in synsedimentary normal faults-inferences from field observations near Frechen , Germany. NPF Spec Publ. 7:39–50.

Lindsay NG, Murphy FC, Walsh JJ, Watterson J. 1993. Outcrop Studies of Shale Smears on Fault Surface. Int Assoc Sedimentol Spec Publ.(15):113–123.

Lommatzsch M, Exner U, Gier S, Grasemann B. 2015. Dilatant shear band formation and diagenesis in calcareous , arkosic sandstones , Vienna Basin (Austria). Marine and Petroleum Geology. 62:144–160. doi: 10.1016/j.marpetgeo.2015.02.002.

Manzocchi T, Childs C, Walsh JJ. 2010. Faults and Fault Properties in Hydrocarbon Flow Models. Geofluids:94–113. doi:10.1111/j.1468-8123.2010.00283.x.

Masalimova LU, Lowe DR, Sharman GR, King PR, Arnot MJ. 2016. Outcrop characterization of a submarine channel-lobe complex: The Lower Mount Messenger Formation, Taranaki Basin, New Zealand. Mar Pet Geol. 71:360–390. doi:10.1016/j.marpetgeo.2016.01.004.

Nicchio MA, Nogueira FCC, Balsamo F, Souza JAB, Carvalho BRBM, Bezerra FHR. 2018. Development of cataclastic foliation in deformation bands in feldspar-rich conglomerates of the Rio do Peixe Basin, NE Brazil. J Struct Geol. 107(July 2017):132–141. doi:10.1016/j.jsg.2017.12.013.

Nicol A, Childs C. 2018. Cataclasis and silt smear on normal faults in weakly lithified turbidites. J Struct Geol. 117(June):44–57. doi:10.1016/j.jsg.2018.06.017.

Noorsalehi-Garakani S, Kleine Vennekate GJ, Vrolijk P, Urai JL. 2013. Clay-smear continuity and normal fault zone geometry - First results from excavated sandbox models. J Struct Geol. 57:58–80. doi:10.1016/j.jsg.2013.09.008.

Peacock DCP, Knipe RJ, Sanderson DJ. 2000. Glossary of normal faults. J Struct Geol. 22(3):291–305. doi:10.1016/S0191-8141(00)80102-9.

Pei Y, Paton DA, Knipe RJ, Wu K. 2015. A review of fault sealing behaviour and its evaluation in siliciclastic rocks. Earth-Science Rev. 150(October):121–138. doi:10.1016/j.earscirev.2015.07.011.

Rattenbury M., & Townsend D., Johnston M. (2000). Geology of the Kaikoura Area. Tech. rep.. 13.

Revil A, Cathles LM. 1999. Permeability of shaly sands. Water Resour Res. 35:651–662.

Rotzien JR, Lowe DR, King PR, Browne GH. 2014. Stratigraphic architecture and evolution of a deep-water slope channel-levee and overbank apron: The upper miocene upper mount messenger formation, Taranaki Basin. Mar Pet Geol. 52:22–41. doi:10.1016/j.marpetgeo.2014.01.006.

Schmatz J, Vrolijk PJ, Urai JL. 2010. Clay smear in normal fault zones - The effect of multilayers and clay cementation in water-saturated model experiments. J Struct Geol. 32(11):1834–1849. doi:10.1016/j.jsg.2009.12.006.

Seebeck H, Nicol A, Walsh JJ, Childs C, Beetham RD, Pettinga J. 2014. Fluid flow in fault zones from an active rift. J Struct Geol. 62:52–64. doi:10.1016/j.jsg.2014.01.008.

Strogen DP, Seebeck H, Nicol A, King PR. 2017. Two-phase Cretaceous–Paleocene rifting in the Taranaki Basin region, New Zealand; implications for Gondwana break-up. J Geol Soc London. 174(5):929–946. doi:https://doi.org/10.1144/jgs2016-160.

Strogen P., Bland K., Nicol A., King P. (2014) Paleogeography of the Taranaki Basin region during the latest Eocene–Early Miocene and implications for the 'total drowning' of Zealandia, New Zealand Journal of Geology and Geophysics, 57:2, 110-127, DOI: 10.1080/00288306.2014.901231

Torabi A. 2014. Tectonophysics Cataclastic bands in immature and poorly lithi fi ed sandstone , examples from Corsica , France. 630:91–102.

Torabi A, Fossen H. 2009. Spatial variation of microstructure and petrophysical properties along deformation bands in reservoir sandstones. Am Assoc Pet Geol Bull. 93(7):919–938. doi:10.1306/03270908161.

Velde BB, Meunier A. 2008. Fundamentals of Clay Mineral Crystal Structure and Physicochemical Properties. In: The Origin of Clay Minerals in Soils and Weathered Rocks. p. 1–15.

Vrolijk PJ, Urai JL, Kettermann M. 2016. Clay Smear: Review of Mechanisms and Applications. J Struct Geol. doi:10.1016/j.jsg.2015.09.006.

Yielding G. 2012. Using Probabilistic Shale Smear Factor to Relate SGR Predictions of Column Height to Fault-zone Heterogeneity. Pet Geosci. 18:33–42. doi:10.3997/2214-4609.20147179.

Yielding G, Freeman B, Needham DT. 1997. Quantitative fault seal prediction. Am Assoc Pet Geol Bull. 81(6):897–917. doi:10.1306/522B498D-1727-11D7-8645000102C1865D.

Van der Zee W, Urai JL. 2005. Processes of normal fault evolution in a siliciclastic sequence: a case study from Miri, Sarawak, Malaysia. J Struct Geol. 27(12):2281–2300. doi:10.1016/j.jsg.2005.07.006.

Van der Zee W, Urai JL, Richard PD. 2003. Lateral clay injection into normal faults. GeoArabia. 8(3):501–522.

2 Fault-zone architecture and the production of low-permeability fault-rock

2.1 Abstract

We investigate fault-zone architecture using outcropping normal faults from the Miocene (7-11 Ma) Mount Messenger Formation (MMF), which are exposed in coastal cliffs in Taranaki, New Zealand. Fault data include measurements of fault dimensions and displacements from many individual faults (N=184) and from six down-fault profiles showing detailed variations in fault zone architecture. Outcrop data for the MMF place constraints on fault-zone thicknesses, fault evolution, fault-zone scaling properties and the impact of faults on fluid flow. Analysis of the available data confirms that fault-zone geometries are heterogeneous on length-scales of centimetres with fault-rock and fault-zone thicknesses ranging by 2-3 orders of magnitude for faults of uniform displacement. These variations are typically associated with slip surfaces and fault-rock defined by lens shapes. The frequency and size of these lenses are greatest at irregularities or asperities in the fault surface, where the number of slip surfaces and deformation bands increase in number with rising displacement. These lens geometries are observed on length scales of millimetres to metres and are accompanied by patches of low permeability fault rock, which occur frequently. Stochastic placement of thin patches of low permeability fault rock on fault surfaces (using the data from outcrop) may provide a basis to improved understanding of where and how frequently fault seals are likely to be leaking.

2.2 Introduction

Displacements and shear strains for faults are typically accommodated within volumes of rock which are here referred to as fault-zones (Childs et al. 1997; Walsh et al. 2002; Childs et al. 2009; Faulkner et al. 2010; Manzocchi et al. 2010) (Figure 2.1). The geometries and number of slip surfaces together with the distribution of shear strains and types of fault-rock generated can vary along the same fault and between faults. The resulting fault-zone architecture can be influenced by a range of factors including: the properties of the host rock, the stress conditions during faulting, finite displacement, and initial fault-surface geometries (Fisher and Knipe 1998; Ferrill and Morris 2002; Van der Zee and Urai 2005; Childs et al. 2009; Seebeck, et al. 2014; Pei et al. 2015; Yielding et al. 2016; Childs et al. 2017). Fault-zones are generally considered to comprise two main elements which include a high shear-strain component, often referred to as fault core or fault-rock, and a lower strain zone which

can be referred to as the damage zone (Chester and Logan 1986; Caine et al. 1996; Fisher and Knipe 1998; Peacock et al. 2000; Childs et al. 2009; Faulkner et al. 2010; Bense et al. 2013) (Figure 2.1). Fault-rock can comprise fault gouge, cataclasites, breccias and slip surfaces and the damage zone includes smaller faults and fractures associated with faulting (Caine et al. 1996). In many cases faults are highly heterogeneous with high and low shear strain components that form a continuum of deformation styles which is rarely quantified (Childs et al. 2009).

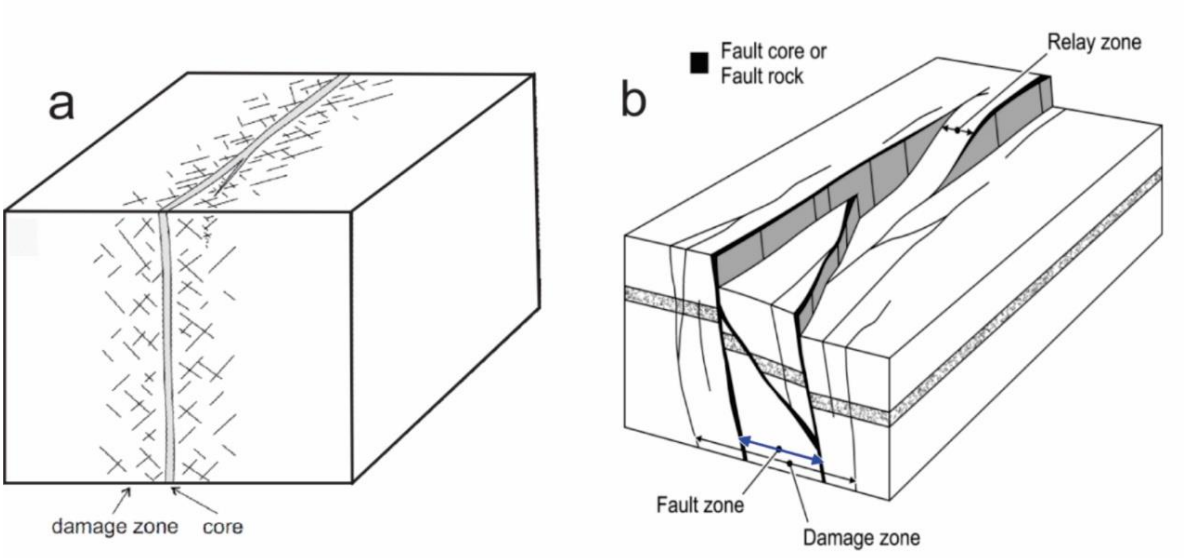

Figure 2.1 A) Proposed fault-zone model from Chester and Logan (1986) showing a simple single fault trace with fault core and surrounding damage zone and, B) schematic block diagram from Childs et al. (2009) of a fault with the fault-rock/core, fault-zone and damage zone highlighted. The diagram in B) also emphasises the 3D heterogeneity of fault zones.

The study of fault-zones can improve understanding of how faults evolve and have practical applications for predicting the flow of fluids (e.g. water, petroleum and CO_2 in the sub-surface). In this chapter we primarily consider the geometry of fault-zones in the context of how they might impact fluid flow. Fault-zones have the potential to both impede and enhance the flow of fluids in the sub-surface (Caine et al. 1996; Aydin 2000; Cartwright et al. 2007; Faulkner et al. 2010; Manzocchi et al. 2010; Bense et al. 2013; Seebeck et al. 2014; Vrolijk et al. 2016). Fault-rock accommodates the majority of displacement and is typically fine grained, of low permeability and has the potential to impede across-fault fluid flow. The fault-zone, which usually partially or entirely encloses the fault-rock, can comprise numerous synthetic and antithetic faults and joints that provide conduits for along-fault fluid flow.

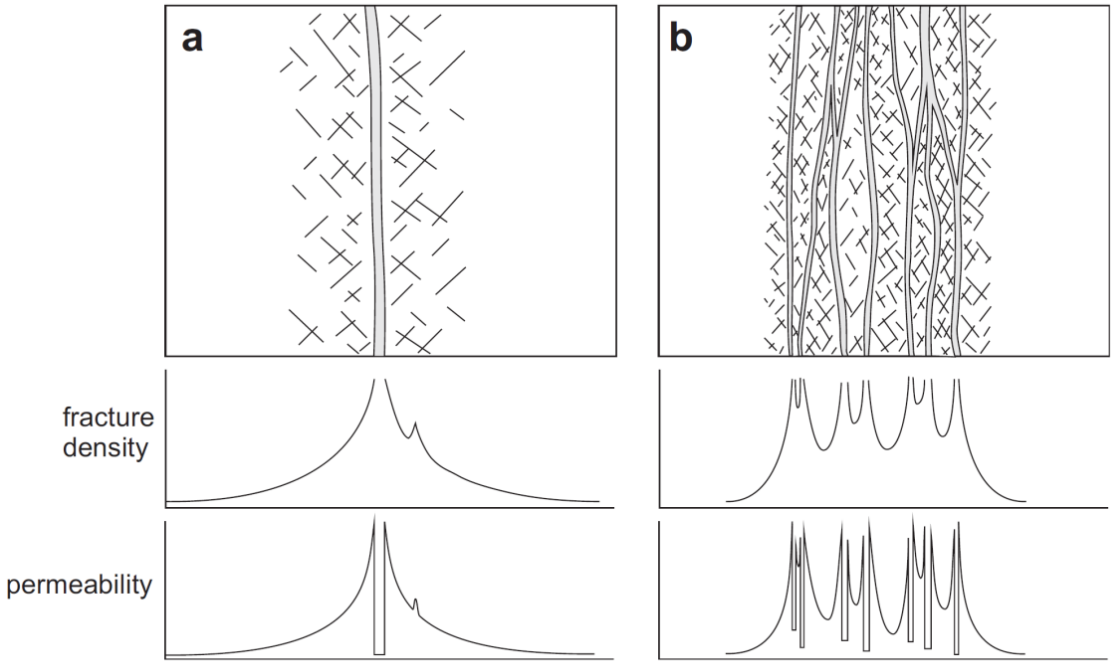

Figure 2.2 Schematic diagram showing the fault-zone architecture, fracture density and permeability across A) a simple fault structure contain one high strain zone and B) a complex fault zone comprising multiple anastomosing high a strain zones (Faulkner et al. 2010).

The geometries, evolution and fluid-flow properties of fault-zones are widely discussed and debated in the literature (Lindsay et al. 1993; Caine et al. 1996; Fristad et al. 1997; Yielding et al. 1997; Fisher and Knipe 1998; Foxford et al. 1998; Aydin 2000; Cartwright et al. 2007; Faulkner et al. 2010; Bense et al. 2013; Giger et al. 2013; Seebeck et al. 2014; Grant 2017). For example, there has been debate about whether or not the positive relationship between displacement and fault-zone thickness is a growth trend with thickness increasing as displacement accrues. Childs et al. (2009) have argued against such a widening model for fault zones and instead suggest that fault-zone widths are established early in the faulting process as part of propagation and controlled by the locations of irregularities (e.g. segment boundaries and bends) on the fault. The locations of these irregularities may also impact the length scales over which fault-zone architecture changes. However, few studies have been conducted to quantify these changes in three-dimensions (3D) over a fault surface. In this study we will measure and quantify changes in fault-zone geometry using a combination of along-fault profiles for individual faults and micro-structural analysis from the Mount Messenger Formation (MMF) in New Zealand (Figure 2.3). These data place constraints on fault-zone thicknesses, fault evolution, fault-zone scaling properties and the impact of faults on fluid flow. The results have implications for the distribution of

low permeability fault-rock over fault surfaces, fault-geometry upscaling and prediction of fault properties in reservoir models. An aim of this study is to provide information that can be used to assess fluid flow in the subsurface, both for Taranaki and elsewhere. By measuring fault-zone and rock variability along sample lines and across a large dataset of faults we hope to constrain better the relationship between fault architecture and permeability. Analysis of the available data confirms that fault-zone geometries are highly variable on length-scales of metres for fault displacements of 10s of centimetres. These variations are typically associated with slip surfaces and fault-rock defined by lens shapes. These geometries are observed from millimetre to metre length scales, appear to apply at the scale of seismic reflection lines (>10 m throw) and may be scale independent. Our analysis suggests that for the parts of the MMF studied here, 'holes' in the low permeability fault rock may occur frequently, meaning that fault seal is unlikely. This study may have application to faults elsewhere in New Zealand and globally.

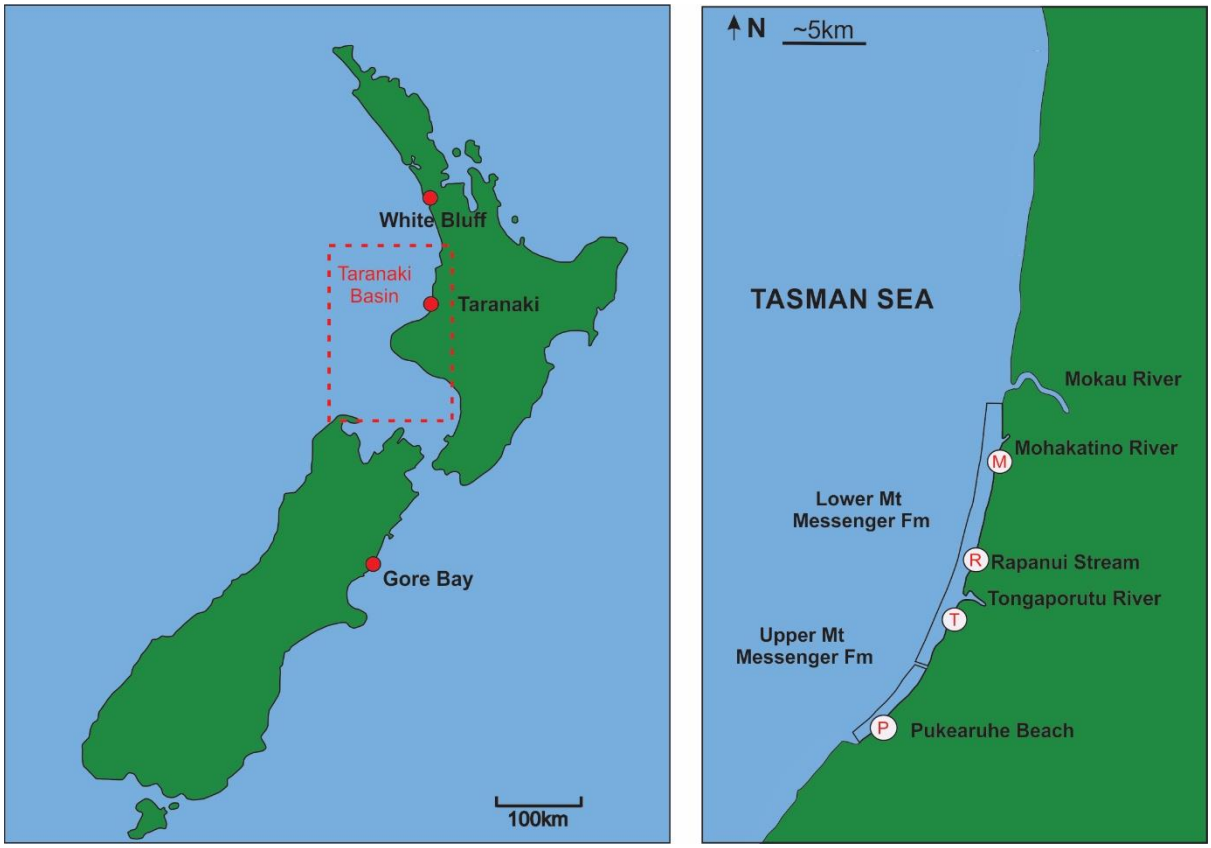

Figure 2.3 A) Map of New Zealand showing the location of the Taranaki Basin and field sites discussed in this thesis. B) Detailed map showing the outcrop field sites (P, T, R & M) for the MMF along the Taranaki Coast. At each MMF field site data are collected along coastal sections >100 m long.

2.3 Literature review

2.3.1 Fault-zone geometries

Fault-zones comprise anastomosing systems of interacting slip surfaces and fault-rock which vary in thickness from millimetres to kilometres (Caine et al. 1996; Childs et al. 1997; Evans et al. 1997; D.R. Faulkner et al. 2010) (Figure 2.2). Faults display a positive relationship between displacement and fault-zone/fault-rock thickness (Walsh and Watterson 1988; Blenkinsop 1989; Scholz et al. 1993; Childs et al. 2009) (Figure 2.4). However, this relationship can span up to four orders of magnitude for a given displacement and therefore thickness cannot be applied to precisely predict the thickness of fault-rocks or how these zones evolve through time (Foxford et al. 1998, Childs et al. 2009; Nicol et al. 2013, Seebeck et al. 2014). For example, along a 12 m sample length of a strike-slip fault with 23 m of displacement there was over an order of magnitude range in fault-rock thickness (0.07-0.9 m) (Blenkinsop 1989). These variations in thickness can be observed on individual faults and have been attributed to many processes including fault segmentation, bifurcation and intersection during fault propagation. Faults may comprise one primary slip surface or multiple fault surfaces, with the number of slip surfaces weakly related to the fault displacement (Seebeck et al. 2014). In their study of fault-zones Childs et al. (1997) describe structures with "two discrete bounding slip surfaces, enclosing fault-rock which may vary from intensely deformed to virtually undeformed".

Given the complexity of fault-zones and a paucity of detailed quantitative analysis, definitions of their geometries and component parts can vary, with authors having different opinions on the extent and structures that comprise a fault-zone. These variations may become problematic when comparing studies as measurements could vary by up to a factor of two for different definitions. For example, Peacock et al. (2000) suggested that fault-zones comprise related fault segments that span a narrow volume, while Childs et al. (2009) define the term fault-zone as "the distance between kinematicaly related synthetic slip surfaces (measured perpendicular to the strike), which accommodate at least 4% of the overall displacement". Childs et al. (2009) define fault rock as comprising deformed material within the fault including fault gouge, breccia and cataclasite. This is similar to the definition by Knott et al. (1996) who class fault-rock as the part of the fault zone that has accrued the majority of the displacement and usually comprises slip surfaces, gouge and cataclasites. Fault-rock is equivalent to the fault core described by Caine et al. (1996) and, in some instances, the terms can be used interchangeably. Both Knott et al. (1996) and Childs et al. (2009) do not consider underformed host rock that has been incorporated into a fault as fault-rock but rather as a part of the wider fault-zone. While this definition clearly emphasises the origin of fault-rock it doesn't cover all material within a fault-zone that may contribute to permeability reductions. For the purposes of this chapter we use the terms fault-zone as defined by Childs et al. (2009) (Figure 2.1B) and fault-rock comprises any

material entrained along and/or between the major slip surface(s). While of value, these terms typically do not capture the hetereogeneity of fault-zones (Figure 2.2). However, it has so far been difficult to accurately convey the variability that can occur over fault surfaces. Along-fault profiles, such as those presented in this chapter, offer an opportunity to better define this variability.

This thesis focusses on faults observed at outcrop scale with a limited number of thin sections and Scanning Electron Microscope (SEM) images. Upscaling these observations to larger faults is rarely tested and of critical importance for comparing the results of outcrop studies to the scale of faults likely to be important for reservoir compartmentalisation. The measurement of fault-rock and zone thicknesses can be subjective depending on the observer and the scale at which they normally work. What may appear to a seismic interpreter as a single fault-zone with multiple slip surfaces may, at outcrop scale, be assessed to be several individual fault-zones by someone else. This can mean the delineation between where one fault ends, and another begins can be highly dependent on the observer and the observation technique. Therefore, we have attempted to adhere to the definitions stated in the literature to ensure our results can be compared to other studies.

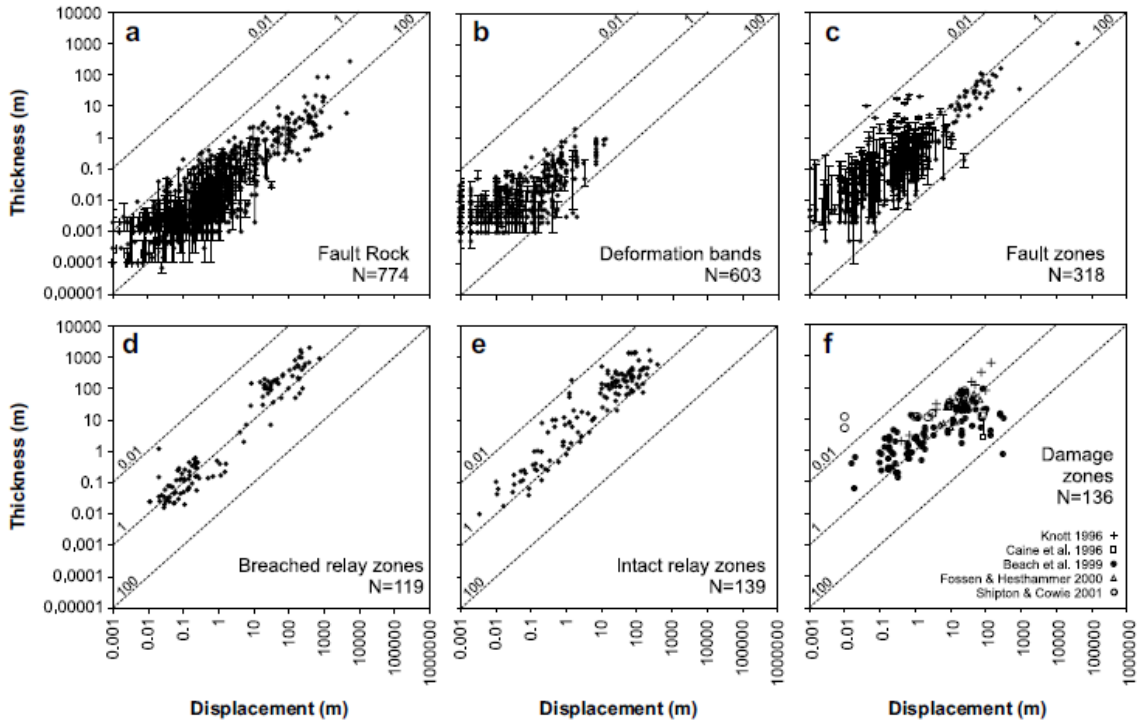

Figure 2.4 Summary of previously published data showing the positive relationship between the thickness of: A) fault rock, B) deformation bands, C) fault zones, D) breached relay zones, E) intact relay zones and F) damage zones versus displacement (Childs et al. 2009).Vertical bars show thickness variations on faults of decametre scales. Faults from the MMF are included in plots a-c.

2.3.2 Fault-zone permeability

Fault-zones can act as barriers, conduits or dual conduit/barrier systems for fluid flow on production and geological timescales (Cartwright et al. 2007; Faulkner et al. 2010; Manzocchi et al. 2010). The flow properties of faults can vary over the fault surface and with time, due to rupture events (e.g., earthquakes) and/or changes in stress conditions. The majority of studies have so far focussed primarily on normal faults in siliciclastic sequences and therefore the mechanisms and processes of fault seal discussed below are only applicable to these types of faults. As fault-zones increase in displacement, the dimensions of irregularities and heterogeneities attributed to the fault also increase. Therefore, it has been suggested that larger faults generally have wider maximum fault-zone thicknesses and both higher and lower permeabilities (compared to smaller faults), increasing their potential impact on fluid flow (Hermanrud et al. 2014). Local increases and decreases in fault permeability with fault size can lead to channelized flow (Caine et al. 1996; Wibberley and Shimamoto 2002; Childs et al. 2009; Faulkner et al. 2010; Seebeck et al. 2014).

Fault-related fluid flow has several controls, including: fault-zone architecture and structural permeability, pressure gradients, host rock anisotropy (including secondary mineralisation and alteration), and fluid viscosity (Seebeck et al. 2014). Evidence for fault seals/barriers to flow has been gathered from reservoir compartmentalisation, different pressure regimes in juxtaposing blocks, and accumulation of oil and gas against faults (Hooper 1991; Van Hulten 2010). Large-scale faults are often the boundaries to oil fields while smaller faults also have the potential to seal, leading to the compartmentalisation of reservoirs and reduction in the ultimate recovery volumes than was previously predicted from drilling data. An example of such an overestimation in connectivity was observed in the North Seas' Brent Field where fault seal led to a lower ultimate recovery than initially predicted (Fisher and Knipe 2001). However, it has been suggested that faults can also boost productivity, the Clair field (also in the North Sea) having shown evidence of this (Fisher and Knipe 2001).

Manzocchi et al. (2010) suggest that faults can affect sub-horizontal fluid flow in three ways: by juxtaposing permeable and impermeable beds against each other, the production of low permeability fault-rock between two permeable horizons, and the connection of two vertically separated permeable beds. Caine et al. (1996) indicate that fault-core permeability is defined by many different factors that vary according to fault size, fault type, geological history, and type and variability of the lithologies displaced. This chapter will focus on the effect of fault-rock on across fault fluid flow. Some mechanisms have been proposed for fault-rock production, including: shale smear, cataclasis, cementation, disaggregation/mixing and diffuse mass transfer (Hooper 1991; Annunziatellis et al. 2008; Faulkner et al. 2010; Seebeck et al. 2014, Pei et al. 2015). Although there are five of these

mechanisms, we are predominantly concerned with the first two (shale smear and cataclasis). Both Fisher and Knipe (1998) and Pei et al. (2015) highlight that these processes do not work in isolation and that fault sealing could be due to more than one of these processes working concurrently along a fault's length.

A tendency towards only modelling the larger structures has meant that smaller faults are often neglected during the modelling process (Manzocchi et al. 2010). However, these smaller faults can have a significant impact on fluid flow especially in thinly bedded units such as the MMF. In such finely bedded sequences small-scale faults can be very important for connecting thin permeable sandstone horizons across larger fault systems, potentially allowing conduits for flow that have not been modelled. By only modelling the larger structures, areas of increased complexity along fault-zone, such as in relay zones or at fault splays, may be simplified or unrepresented. This could affect fluid flow predictions, as segment boundaries and fault branch points are thought to be sites with increased chances of fault leakage (Childs et al. 1996; Dockrill and Shipton 2010).

Smaller-scale structures such as deformation bands are too small to model, but have been observed to reduce permeability by up to six orders of magnitude allowing them to affect the permeability of fault-zones (Fossen et al. 2007) and compartmentalise hydrocarbon reservoirs (Fossen et al. 2011). Cataclastic deformation bands within clean lithified sandstones have shown permeability reductions of up to four to five orders of magnitude with the largest permeability reductions observed perpendicular to the strike of the band (Bense et al. 2013). Within poorly consolidated arkosic or lithic-rich sands, feldspars and lithic grains preferentially break down first leading to the cataclasite becoming enriched with phyllosilicates. The production of catclastic rock can lead to both reductions in permeability (> 1 order of magnitude) and porosity (<20%) (Exner and Tschegg 2012; Nicol and Childs 2018).

2.4 Data and methods

Fault-zone data were collected from the Late Miocene MMF, which outcrops in coastal cliffs along the Northern Taranaki Coast in New Zealand (Figure 2.3). The formation consists of a series of deep water turbidites and submarine fans comprising interbeds of lithic-rich sands, silts and occasional volcaniclastics (King and Thrasher 1996; Browne et al. 2005; Rotzien et al. 2014; Masalimova et al. 2016). The MMF is one of the target reservoirs for the Ngatoro, Kaimiro and Windsor fields which are part of the onshore petroleum exploration area in Taranaki (see Figure 2.5). Therefore, faults in this formation may have direct application for fault seal in the Taranaki Basin. Normal faulting is estimated to have developed between 2 and 6 Ma at maximum burial depths of 1-1.5 km (Childs et al. 2007, Giba

et al. 2010). Due to the shallow burial depths, the absence of diagenesis, and only rare cementation the strata are poorly lithified, which aided cleaning and examination of the faults.

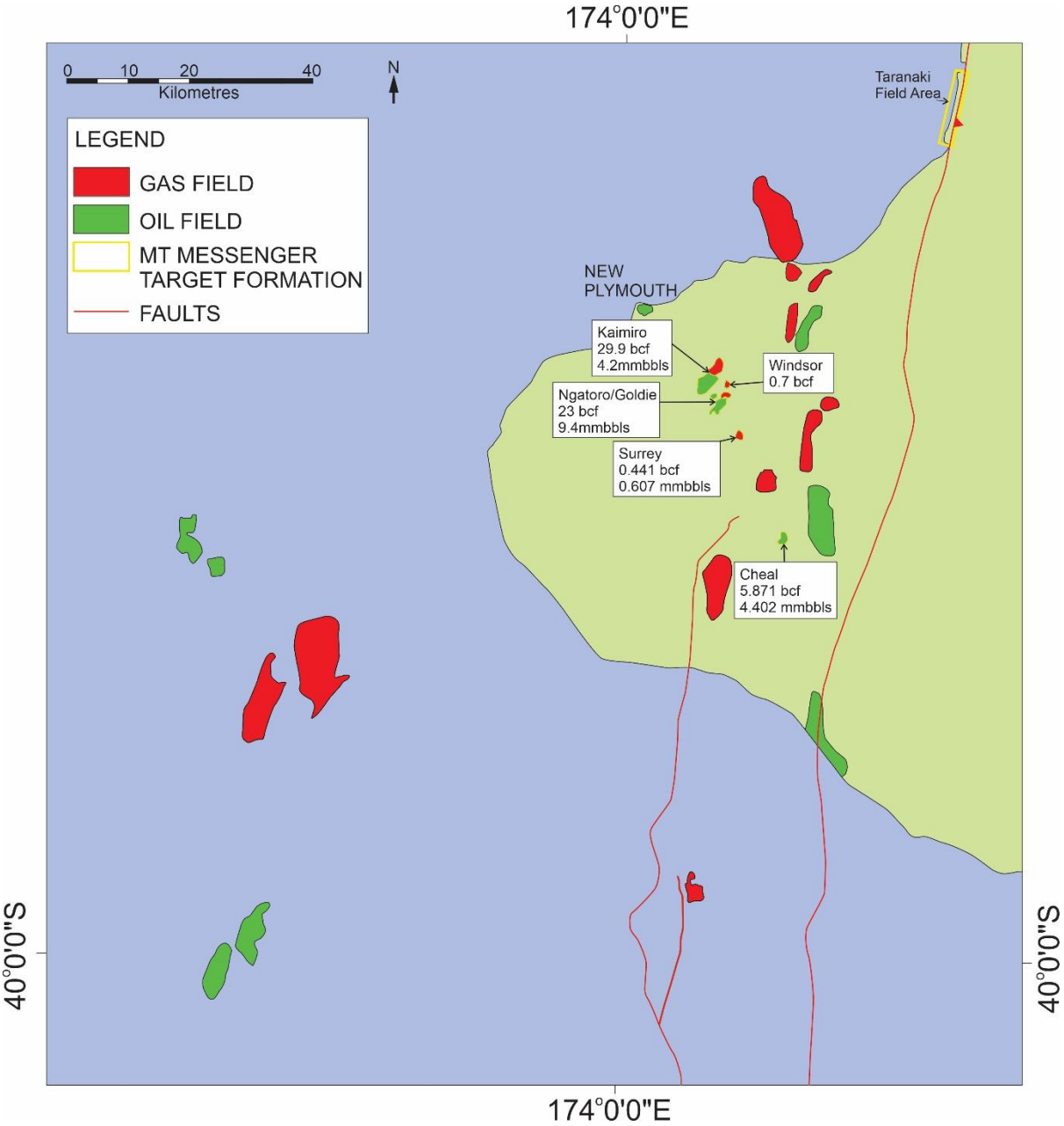

Figure 2.5 A map of the Taranaki region showing existing oil and gas fields with those targeting the Mount Messenger annotated. The location of sample collection is shown on the map by the yellow rectangle. Figure modified from King et al. (2009).

Fault-zone geometry data analysed in this chapter were derived from three primary sources. These are: i) compilation of previously published data on fault-zone and fault-rock thicknesses, ii) measurement of fault-zone geometries for ~180 faults (this study, see Chapter 3) and, iii) detailed fault-zone geometries observed from six along-fault profiles. Fault-zone and fault-rock thicknesses have been presented in previous studies of faults with displacement ranging up to ~35 m and exposed

along ~25 km of coastal Mount Messenger Formation outcrop from Pukearuhe to Mokau (Childs et al. 2007; Childs et al. 2009; Giba et al. 2010; Nicol et al. 2013; Nicol and Childs 2018) (e.g. Figure 2.3). As with the present study, these publications utilised data from faults with 100% exposure and included measurements of fault-zone and fault-rock thicknesses and fault displacements together with descriptions of fault-zone geometries (e.g. number, spacings and thicknesses of deformation bands). In many cases ranges of fault-zone and fault-rock thicknesses were measured along individual fault traces over dip lengths of up to 5 m in order to access the variability of fault-zone structure. These fault-trace measurements were distilled down to estimates of min, max and average fault-zone/fault-rock thicknesses (e.g. Childs et al. 2007; Childs et al. 2009).

In addition to the compilation of previous data we have acquired new information as part of this thesis. Information on the geometry of fault-zones has been collected for ~180 individual faults. These normal faults have been described in Chapter 3 (section 3.2) and range in displacement from 9 mm to 5.1 m (average 192 mm) and displace beds of 1.5 mm to 450 mm thickness. Lastly, data were collected from six along-fault (approximately parallel to fault dip) profiles. The characteristics of the faults and strata in each profile are summarised in Table 2.1 below.

These faults outcropped at Pukearuhe Beach (N=3), Tongaporutu Beach (N=2), and Rapanui Beach (N=1) (for locations see Figure 2.6), with displacements of 17-290 mm. For each profile the fault outcrop was cleaned and scraped approximately flat (to aid measurement and analysis), photographed and logged along lengths of 2.65-6.83 m. The resulting profiles represent 2D strip samples approximately 20-60 cm wide along which the fault-zones were 100% exposed at resolutions down to 1 mm. The strips enabled the full fault-zone width to be sampled. To simplify data acquisition, fault attributes were measured at 5 cm intervals along a section of the fault-trace length for five profiles, and at 10 cm sample intervals for the Rapanui 95 fault profile. Fault-rock and fault-zone thicknesses, and the number of deformation bands were recorded at each sample location (for definitions of fault-rock and fault-zone see Chapter 1). Fault-rock and fault-zone thicknesses ranged from 0.5 mm to 115 mm and 0.5 mm to 825 mm, respectively. The lower bounds of these ranges (i.e. 0.5 mm) is the lower resolution limit of the data and smaller thicknesses are possible but can only be reliably measured from thin section or SEM images.

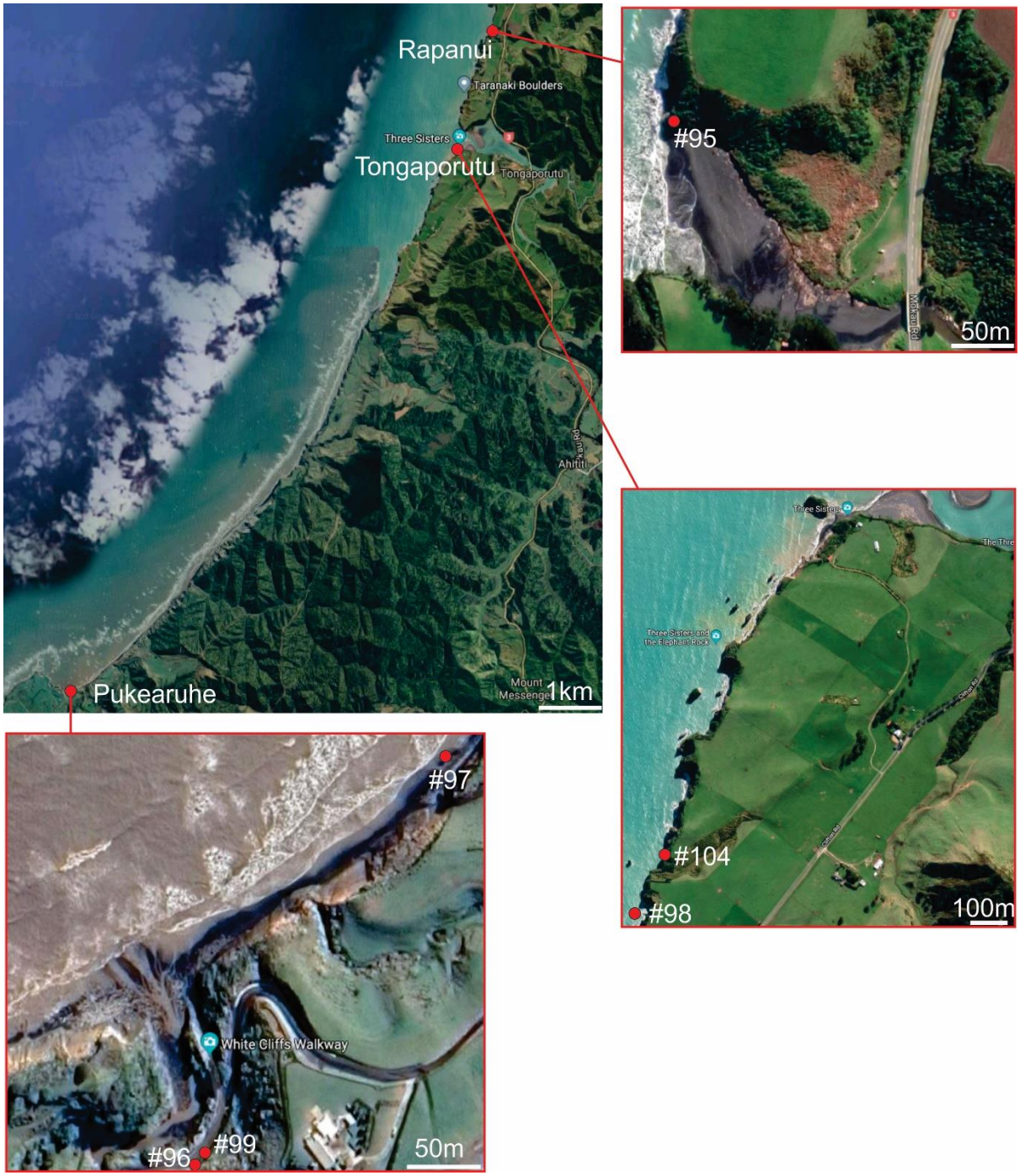

Figure 2.6 Locations of the six down fault profiles. The image in the top left shows the profile localities on a regional scale, while the more detailed photos show the precise location of each fault. All orthophotographs are from Google Earth (November 14 2019).

Table 2.1 Descriptions of faults studied in six along-fault profiles from the MMF, Taranaki. See Figure 1.3 for locations.

FAULT NAME	LAT./LONG.	DISPLACEMENT (MM)	SILTST BEDS	SST BEDS	SAMPLING	COMMENTS
RAPANUI 93/95	-38.799 174.591	Average: 23 Range: 17 - 26	12 beds, Average thickness 15 mm	13 beds Average thickness: 606 mm	6.8 m sampled at 10 cm intervals	- Displacement mainly on single band - Band number increases in sandstone often forming clusters - Very little shale smear, some shale slicing - Vertical segmentation at siltstone beds
TONGAPORUTU 98	-38.826 174.578	Average: 129 Range: 100 - 160	11 beds, Average thickness: 27 mm	13 beds Average thickness: 260 mm	3.4 m sampled at 5 cm intervals	- Displacement accommodated on 2 to 3 deformation bands - Some shale smearing and complicated slicing of siltstone beds - Segmentation common mainly in proximity to siltstone beds
TONGAPORUTU 104	-38.824 174.579	Average: 4 Range: 0 - 5	7 beds, Average thickness: 78 mm	9 beds Average thickness: 406 mm	2.7 m sampled at 5 cm intervals	- Most displacement on single deformation band except for splay at top of section. - Fault has few bends or segmentation and no evidence of shale smearing. - Siltstone beds barely displaced so little analyses of fault-rock
PUKEARUHE 96	-38.898 174.516	Average: 118 Range: 100 - 130	8 beds, Average thickness: 91 mm	10 beds Average thickness: 404 mm	3.6 m sampled at 5 cm intervals	- Displacement mainly accommodated along one deformation band. - Some deformation band clusters observed in sandstone, usually close to siltstone beds. - Fault predominantly planar with very little segmentation or bends. - Shale smear uncommon and shale slicing relatively common.
PUKEARUHE 97	-38.891 174.519	Average: 270 Range: 255 - 290	8 beds, Average thickness: 50 mm	10 beds Average thickness: 295 mm	3.05 m sampled at 5 cm intervals	- Majority of displacement and fault-rock accommodated by two deformation bands. - Shale mearing and shale slicing common.
PUKEARUHE 99	-38.893 174.516	Average: 154 Range: 130 - 165	20 beds, Average thickness: 59 mm	22 beds, Average thickness: 164 mm	4.5 m sampled at 5 cm intervals	- Displacement primarily accommodated by two to four anastomosing deformation bands which accounted for the majority of fault-rock. - Shale smearing and small-scale shale slicing of siltstone beds is common.

Samples of deformation bands, shale smear siltstone, and sandstone beds displaced by the faults along the profiles were collected for analysis of grain-size distributions. Small blocks (4x5x8 cm) of the fault-zones were also excavated from the outcrop for thin sections and SEM analyses at the University of Canterbury. Grain particle-size analysis was conducted on 143 >1 cm^3 samples from the profiles. In the laboratory the samples were placed in beakers with the decoagulant sodium hexametaphosphate (Calgon) and left to disintegrate into separate grains. The disaggregated samples were stirred with a magnetic flea so that a representative sample could be taken and run through the Laser Sizer. Measurements were taken using a Saturn DigiSizer II Laser Diffraction Particle Size Analyser (LDPSA) with a detection range of 0.04-2500 µm. All samples run in this study were well within this range and the results were not impacted by the detection limits of the equipment. Each sample was measured three times to ensure that the results were reproducible. In rare cases where anomalous results were produced, additional measurements were taken to check the reproducibility of the results. Grain sizes were binned according to the Wentworth Grain Scale and the three runs averaged to produce a single distribution per sample.

Thin sections were collected from seven samples along the profiles. Due to the poorly induration of the rocks, all samples were collected using small (5 cm x 10 cm x 5 cm) plastic boxes to keep the samples intact during transportation. Once back in the laboratory, the samples were dried, impregnated with resin and thin sectioned. Thin sections were photographed by taking a series of overlapping images from a microscope and then stitched together to form a composite image of the entire thin section. Detailed photographs of thin sections were taken at points of specific interest and used to analyse the grain-scale micro structures and deformation processes, including grain crushing and mixing. Samples collected to constrain cataclastic processes were taken from locations where no siltstone beds had passed the sample point on the fault. In addition to thin sections, locations of particular interest were sampled for SEM analysis. SEM samples were used for chemical mapping and panoramas through deformation bands, host rock or shale smear at scales of 200 µm.

Bed strength is a possible factor that may impact fault-zone architecture. Siltstone beds typically protrude out of the cliffs more than sandstone beds suggesting that they are mechanically stronger than the sandstone interbeds (or at least more resistant to erosion). The MMF is typically weak with Unconfined Compressive Strength (UCS) values of <12MPa (Nick Perrin pers comm. 2012). To determine UCS values for sandstone and siltstone beds 20 cores were taken, however, none of these cores remained intact for long enough for these tests to be completed and reliable UCS values recorded. Instead we have used Schmidt Hammer rebound measurements to provide a proxy for rock strength. These measurements were taken on all of the sandstone and siltstone beds displaced by the faults in the six profiles to estimate the relative strengths of these units. For each bed at least five

measurements were taken and the results averaged. All Schmidt Hammer measurements were conducted on the scraped outcrop to reduce the potential impact of weathering on the results.

2.5 Results

2.5.1 Fault-zone geometries

Fault-zone geometries have been analysed in this thesis using plots of distance vs fault parameter derived for individual faults (Figure 2.7) as well as from the six profiles sampled in detail (Figure 2.8). These graphs enable relationships between fault parameters (fault-rock and fault-zone thickness, displacement and deformation band count), stratigraphy (siltstone and sandstone beds) and shale smear predictions (SSF, SGR and CSP) to be assessed at points on individual faults. Results show a high degree of variability and hetereogenity both between faults and between different points on the same fault.

Despite differences in the displacements and stratigraphy of the profiled faults, the fault zones display some similar geometric elements (see Figure 2.8). Each of the fault-zones comprise anastomosing slip surfaces and deformation bands, with the latter being mainly present in the sandstone beds. Displacements are predominantly accommodated within the deformation bands and by slip surfaces that primarily bound the siltstone beds (Table 2.1). The siltstone beds may be smeared or faulted (at the scale of the outcrop) to produce slices of siltstone beds (see Chapter 2 for further discussion). These slices are generally bounded by a lens of slip-surfaces and deformation bands which are often at a maximum width in the sandstone beds and locally may bifurcate from a single band. This bifurcation is most often (but not exclusively) close to the tops and bottoms of siltstone beds, with faults in these finer beds often having a slightly steeper dip than in adjacent sandstone beds (difference <20°).

With increasing displacement there is increasing fault-zone complexity and an increase in the maximum number of deformation bands in sandstone beds and slip surfaces in siltstone beds. For both slip surfaces and deformation bands the right and lower bound of the data define a positive slope. This positive slope is consistent with a positive relationship between displacement and the maximum number of bands, and with data presented by Nicol et al. (2013). The range in the number of bands for each fault arises because deformation bands and slip surfaces both define anastomosing lens-shapes where, for a given displacement, the fault-zones may comprise a range of geometries from a single slip surface to fault-bound lenses comprising many slip-surfaces or deformation bands (Figure 2.8). Given the geometric similarities of the slip surfaces and the deformation bands, we argue that they are both high shear-strain manifestations of faulting, with the primary difference being that

slip surfaces are thinner and mainly associated with siltstone beds, while deformation bands are thicker and primarily confined to sandstone beds.

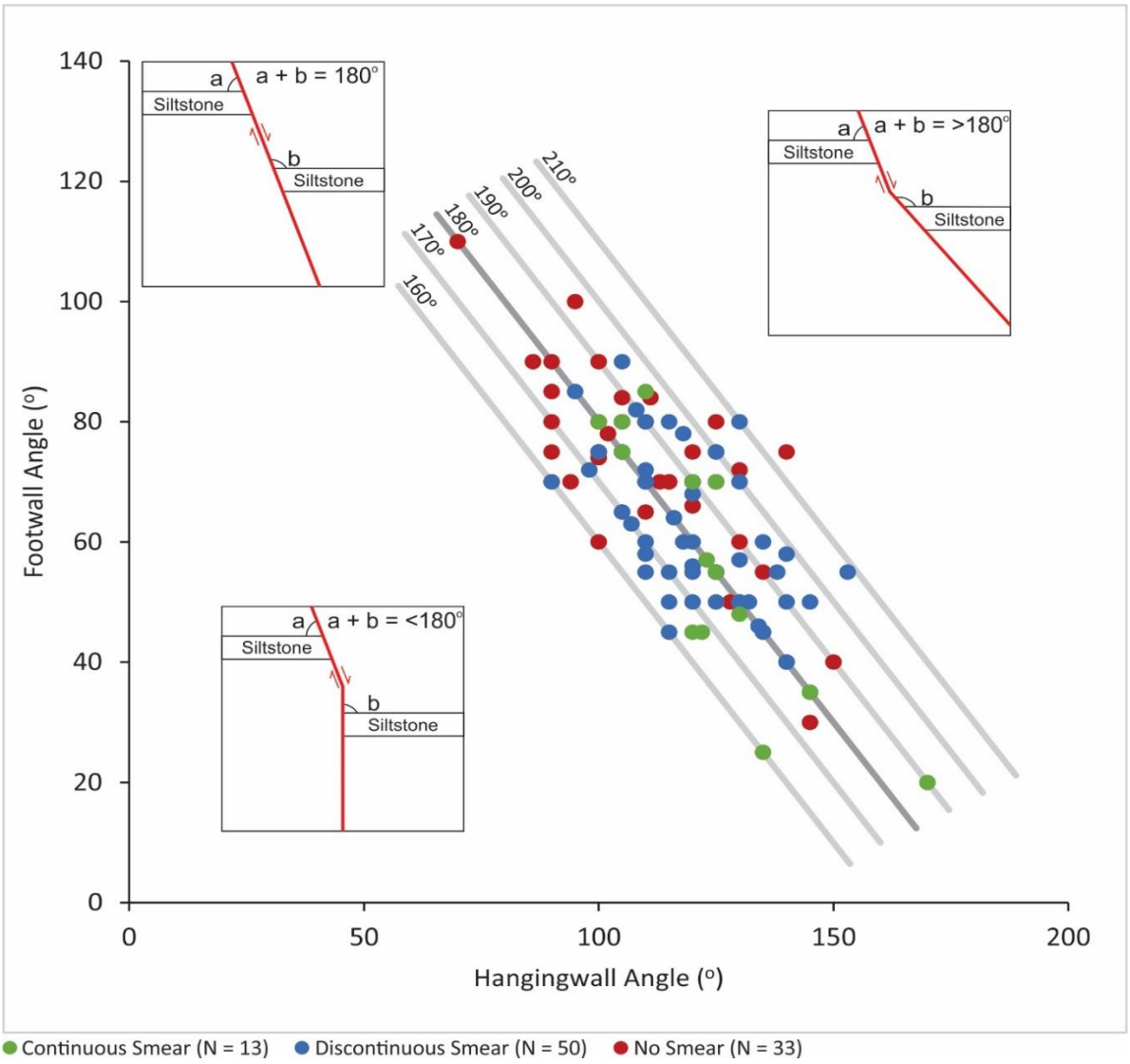

Figure 2.7 Graph depicting the angle between the footwall and hangingwall siltstone cut offs and fault trace for siltstone beds with no smear, discontinuous smear and continuous smear. Departure from angles of 180° indicates that the fault trace changes orientation between the siltstone bed cut offs.

Figure 2.7 shows the hangingwall and footwall angles between the host siltstone bed and the fault trace. If the fault maintained a constant orientation then the hangingwall and footwall angles would add up to 180°. However, there is variation around the 180° line suggesting that it is common for the fault orientation to change between the host cut offs despite most displacements only being of the order of 10s of centimetres. If the angle between the host bed and fault trace is found to correlate with the degree of smearing this could be an explanation of why beds may smear on one side of the fault and not another and how sub seismic resolution features could be influencing fault permeability.

Table 2.2 Summary of displacement, thickness and deformation-band numbers for the six fault profiles studied in detail.

FAULT	DISPLACEMENT (MM)	FAULT-ZONE THICKNES (MM)	FAULT-ROCK THICKNESS (MM)	NUMBER DEFORMATION BANDS
RAPANUI 93/95	Min: 17	Min: 0.5	Min: 0.5	Min: 1
	Max: 26	Max: 15	Max: 6	Max: 8
	Mean: 23	Mean: 4.6	Mean: 2.4	Mean: 3
TONGAPORUTU 98	Min: 100	Min: 1	Min: 1	Min: 1
	Max: 160	Max: 48	Max: 6	Max: 5
	Mean: 129	Mean: 12.5	Mean: 3.4	Mean: 2.5
TONGAPORUTU 104	Min: 0	Min: 0.5	Min: 0.5	Min: 1
	Max: 5	Max: 12	Max: 2	Max: 2
	Mean: 5	Mean: 1.1	Mean: 0.88	Mean: 1.2
PUKEARUHE 96	Min: 100	Min: 0.5	Min: 0.5	Min: 1
	Max: 130	Max: 55	Max: 12	Max: 10
	Mean: 118	Mean: 8.2	Mean: 3	Mean: 2.8
PUKEARUHE 97	Min: 255	Min: 1.5	Min: 1.5	Min: 1
	Max: 290	Max: 60	Max: 13	Max: 12
	Mean: 270	Mean: 19.7	Mean: 4.7	Mean: 3.8
PUKEARUHE 99	Min: 130	Min: 1	Min: 1	Min: 1
	Max: 165	Max: 40	Max: 8	Max: 15
	Mean: 154	Mean: 9.6	Mean: 2.4	Mean: 3.4

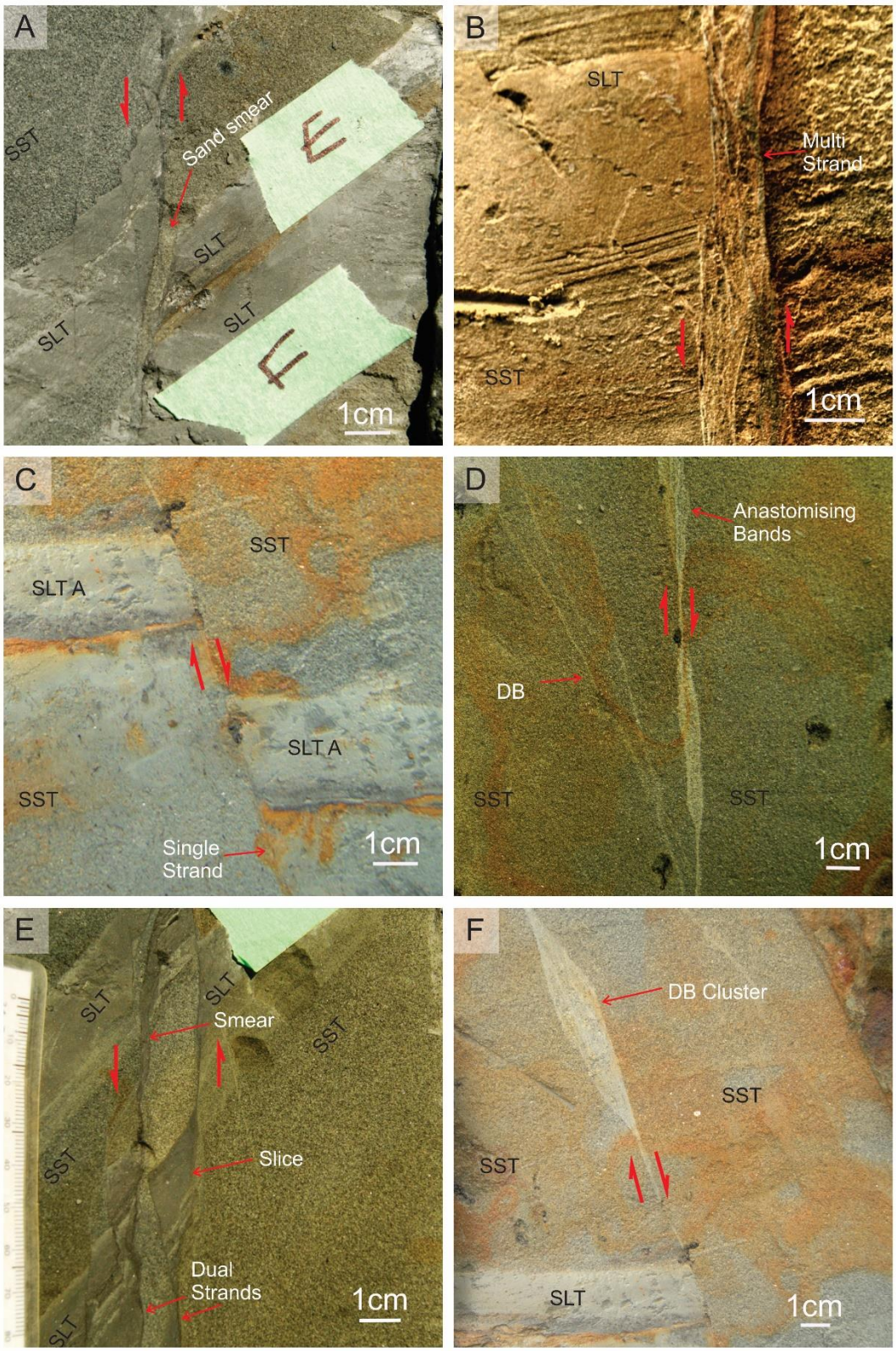

Figure 2.8 Collation of fault geometries from the six down fault profiles in Taranaki. A) Sand smear from Tongaporutu 98. B) Displacement is accommodated on multiple strands on Pukearuhe 99. C) Single strand controlling displacement between non-smeared beds from Rapanui 95. D) Anastomosing deformation-band clusters from Rapanui 95. E) Dual slip surfaces controlling displacement on Tongaporutu 98. F) Single deformation band cluster in close proximity to a siltstone bed on Rapanui 95. SST = Sandstone, SLT = Siltstone, DB = Deformation Band.

2.5.2 Micro-scale fault-zone structure

Thin sections were studied for each of the fault profiles. These thin sections provided information about the geometries, displacements and locations of micro-scale faults and cataclastic deformation processes (See Figure 2.9 for schematic). When analysed in thin section, siltstone smears, which appear to be deformed in a continuous ductile fashion, are typically deformed by complex arrays of micro-faults that bound sliced sections of siltstone (Figure 2.10). These micro-faults are primarily synthetic to the fault-zone dip and displace the siltstone beds down the fault in a series of steps where the risers on the steps are typically 1mm or less. Although the siltstone beds within the siltstone smears are heavily faulted, they retain some primary sedimentary structures and there is generally no evidence of mixing of siltstone beds or injection of silt into the fault-zone. At the edges of the slip surfaces some sandstone grains can be entrained into the smear, suggesting minor mixing at siltstone-sandstone boundaries. Collectively, these observations suggest that siltstone smear in the MMF is primarily a brittle process (see Chapter 3 for more detail). Therefore, we infer that both the siltstone slicing at outcrop scale and siltstone smear at a micro-scale are both brittle deformation processes and that the distinction between slicing and smearing is primarily due to the scale of observation (rather than reflecting a fundamental difference in the deformation processes). The distinction between ductile (i.e. brittle micro-faulting) and brittle faulting at outcrop scale is illustrated in Figure 2.9.

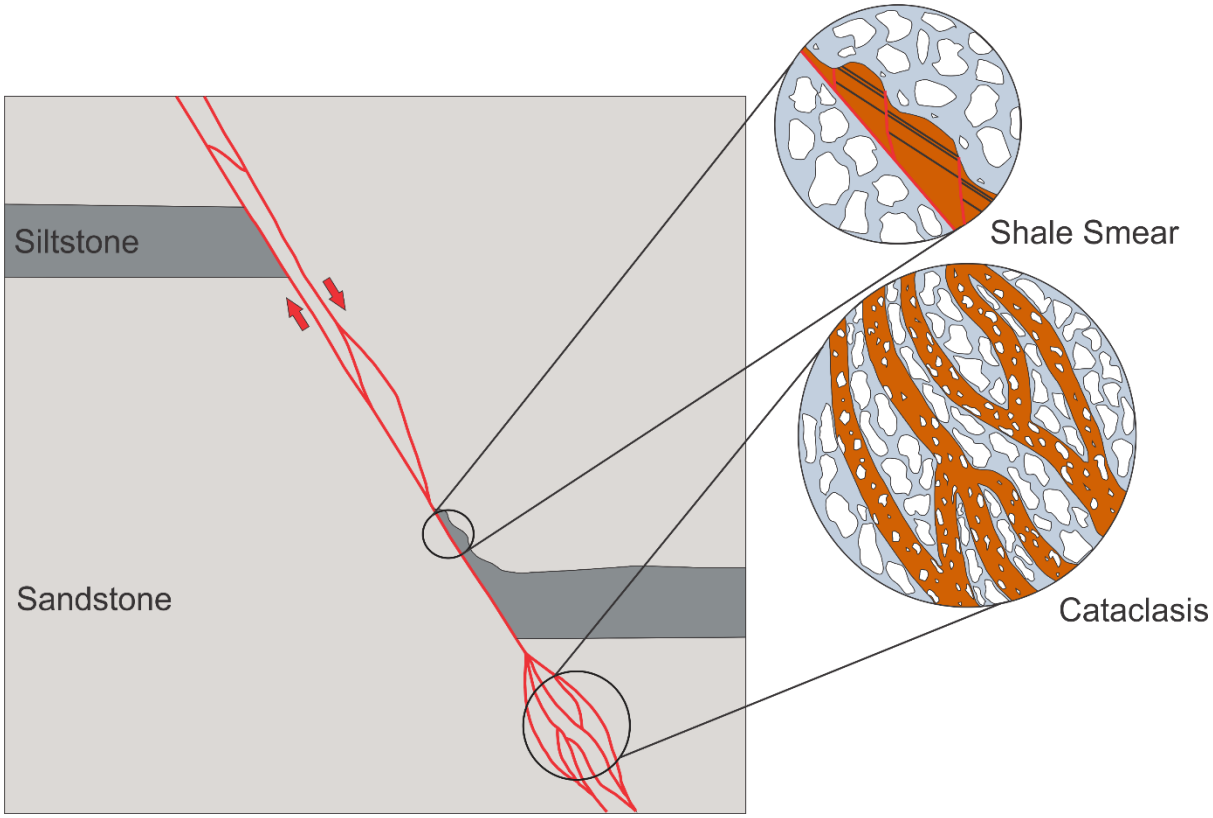

Figure 2.9 Schematic diagram showing examples of fault rock at outcrop scale (left) and at micro scale (right).

Thin sections and SEM images also provide information on the deformation processes that produce deformation bands in sandstones. These data clearly show that deformation bands are primarily produced by destruction of sand-size particles. Grain-size reduction is primarily achieved by break-down of lithic and altered feldspar sand-sized grains (this study, Nicol and Childs 2018). Cataclasis appears to be formed in association with reduction in the size and numbers of pores. In thin sections from this study we did not see any evidence for secondary mineralisation or dilation of the rock fabric associated with increased separation of grains. Despite the absence of mineralisation, deformation bands often stand proud in outcrops, suggesting that they are slightly harder and more resistant to erosion than the adjacent sandstone beds. The apparent relative hardness of deformation bands may lead to the conclusion that the clusters of bands observed in some outcrops form due to strain hardening (Aydin 1978, Mair et al. 2000, Fossen et al. 2007). However, Nicol et al. (2013) argue that strain hardening is unlikely to explain the formation of deformation-band clusters because these clusters frequently collect into a single band. The localisation of shear strain into a single band is consistent with strain softening and is difficult to rationalise with strain hardening of the same band mm to cm along the fault trace. Certainly, there are no data from outcrop to suggest that individual bands vary in hardness over short distances (e.g. < 10 cm).

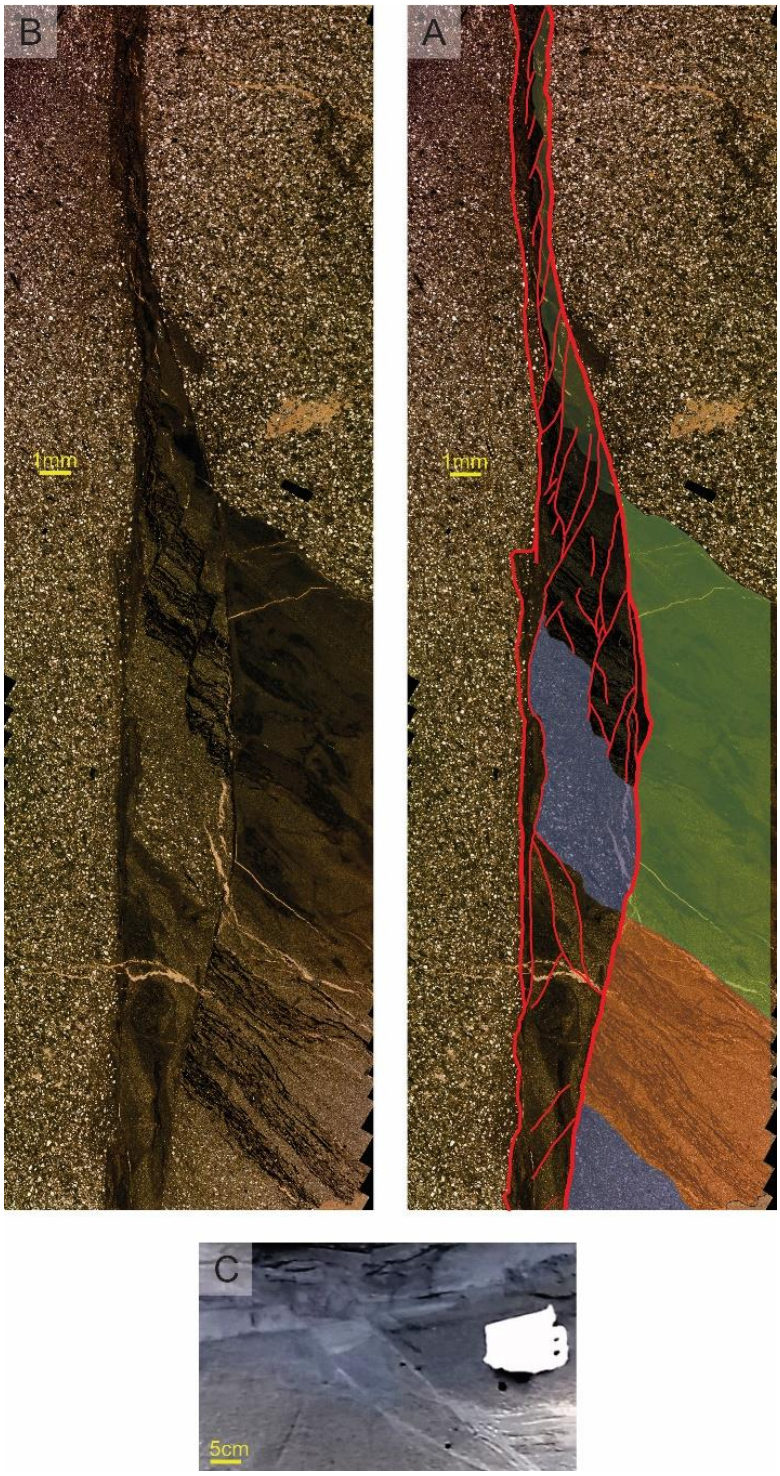

Figure 2.10 Interpreted (A) and uninterpreted (B) thin section from small-scale fault at Rapanui Beach (location: Lat. -38.796, Long. 174.591). Green, brown and grey are siltstone beds that are interpreted to have been incorporated into the fault-zone, which varies in thickness from 0.5-4.5 mm in the thin section. At outcrop scale (C) the siltstone beds appear to have been smeared into the fault-zone. At the micro-scale (B) the siltstone beds have been displaced by many small-scale slip surfaces (displacements generally < 1.8 mm). The host-bed origin was not clear for the lower ~15 mm of the thin section and was described as fault-rock. In thin section the original bedding stratigraphy can be observed and the silt would be interpreted as a fault-bound bed. The thin section illustrates the importance of the scale of observation for interpreting fault-rock.

2.5.3 Fault-rock and fault-zone thicknesses

Fault-rock and fault-zone thicknesses for each of the faulted beds in the individual fault dataset (N=184) were measured at the host siltstone cut offs, whereas for the fault profile dataset measurements were taken at regular intervals of 5 cm or 10 cm. The individual fault dataset allowed the comparison of fault-rock and fault-zone thickness measurements between faults to assess the variability in thicknesses for a range of displacements, slip surfaces and bed thicknesses. The fault profile dataset was used to quantify the variability (and the length-scales over which it occurs) for the two thickness measurements.

Fault-zone and fault-rock thicknesses for all fault profiles vary by up to two orders of magnitude, ranging from 0.5-55 mm and 0.5-13 mm, respectively (see Table 2.2). The lower bounds of these thicknesses are the resolution limit of the data and are mainly observed where single-slip-surfaces or deformation bands are present (individual bands range in thickness from 0.5 to 2 mm, mean 0.7 mm); single-slip-surface sites are the most likely sites of holes in the low permeability fault-rock (Figure 2.11 red polygons) (see section 2.6 for further discussion). Fault zones and fault rock thicknesses are positively related to each other, in part because wider fault-zones comprise more deformation bands and, in many cases, deformation bands and associated cataclasis of sandstone beds are the primary source of fault-rock (see section 2.5.4). Despite the relationships between fault-rock and fault-zone thicknesses, there is no clear relationship between displacement and these thicknesses along individual faults and only a weak relationship comparing data between faults (Figure 2.11).

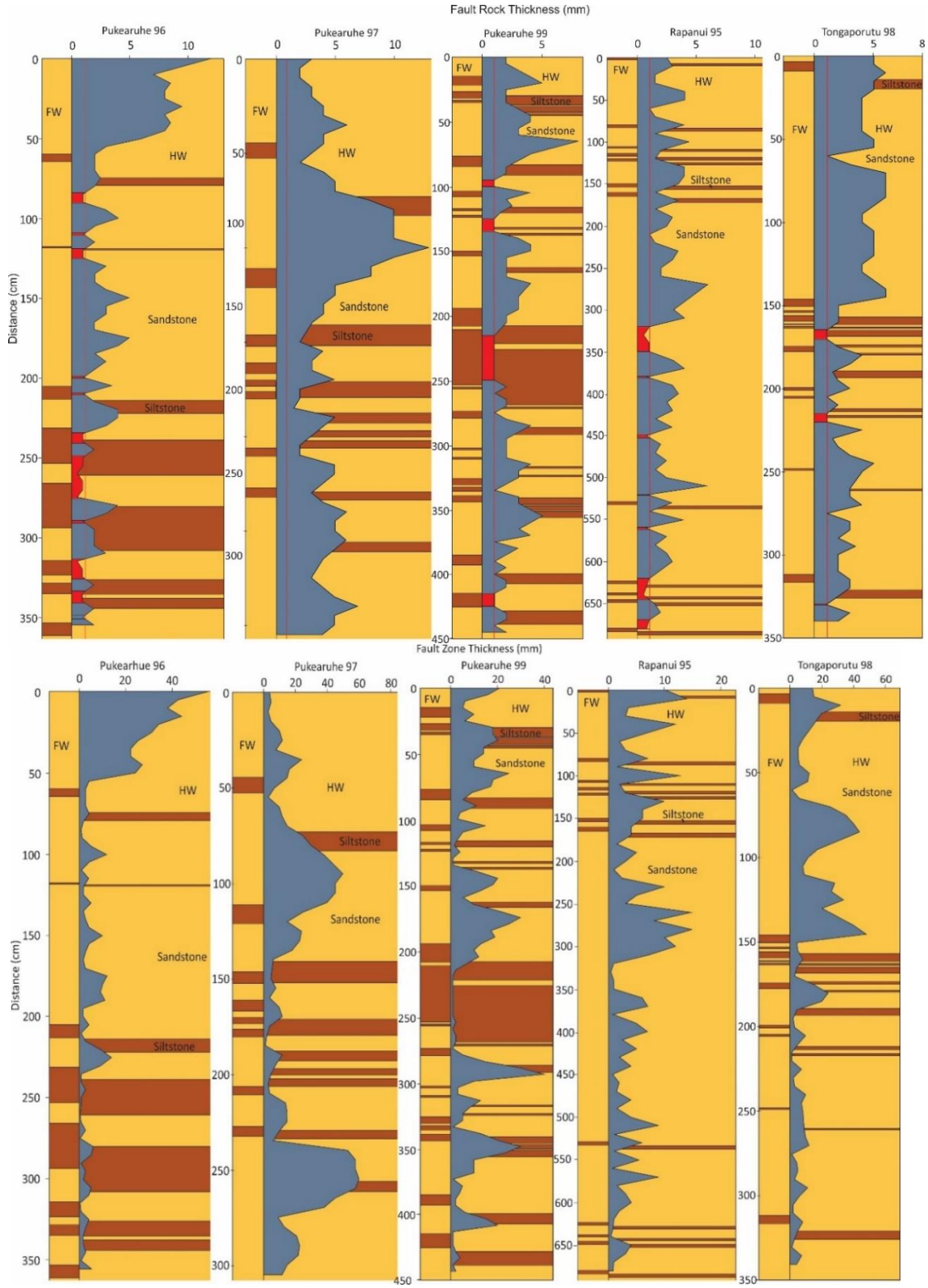

Figure 2.11 Diagram showing thickness variations of fault-rock (top panel) and fault-zone (bottom panel) for five down-fault profiles. For each profile grey polygons show thicknesses relative to the locations of siltstone (dark brown) and sandstone (yellow) beds. Red polygons show locations of potential 'holes' in fault-rock. Distances along each profile are in cm and thicknesses in mm. The average displacement for each profile is also given in mm. N.B. the Tonagporutu 104 fault was not included as the siltstone beds were not fully offset and the fault-rock and fault-zone thicknesses did not vary due to the low displacements.

The relationship between fault-zone thickness and distance from the nearest siltstone bed is examined in Figure 2.12. Taken collectively, the data suggest that the thinnest fault-zones can occur anywhere relative to siltstone beds, while the upper bound of the data has a negative slope suggesting that the thickest fault-zones most often occur within 70 mm of siltstone beds. However, for individual faults there is often no clear relationship between stratigraphy and fault-zone thickness (see Figure 2.11 and Figure 2.12). In fact, along-fault variations in thickness do not seem to correlate with any of the measured parameters and it is uncertain what is leading to the fault-rock and fault-zone thickness lows (see Figure 2.12).

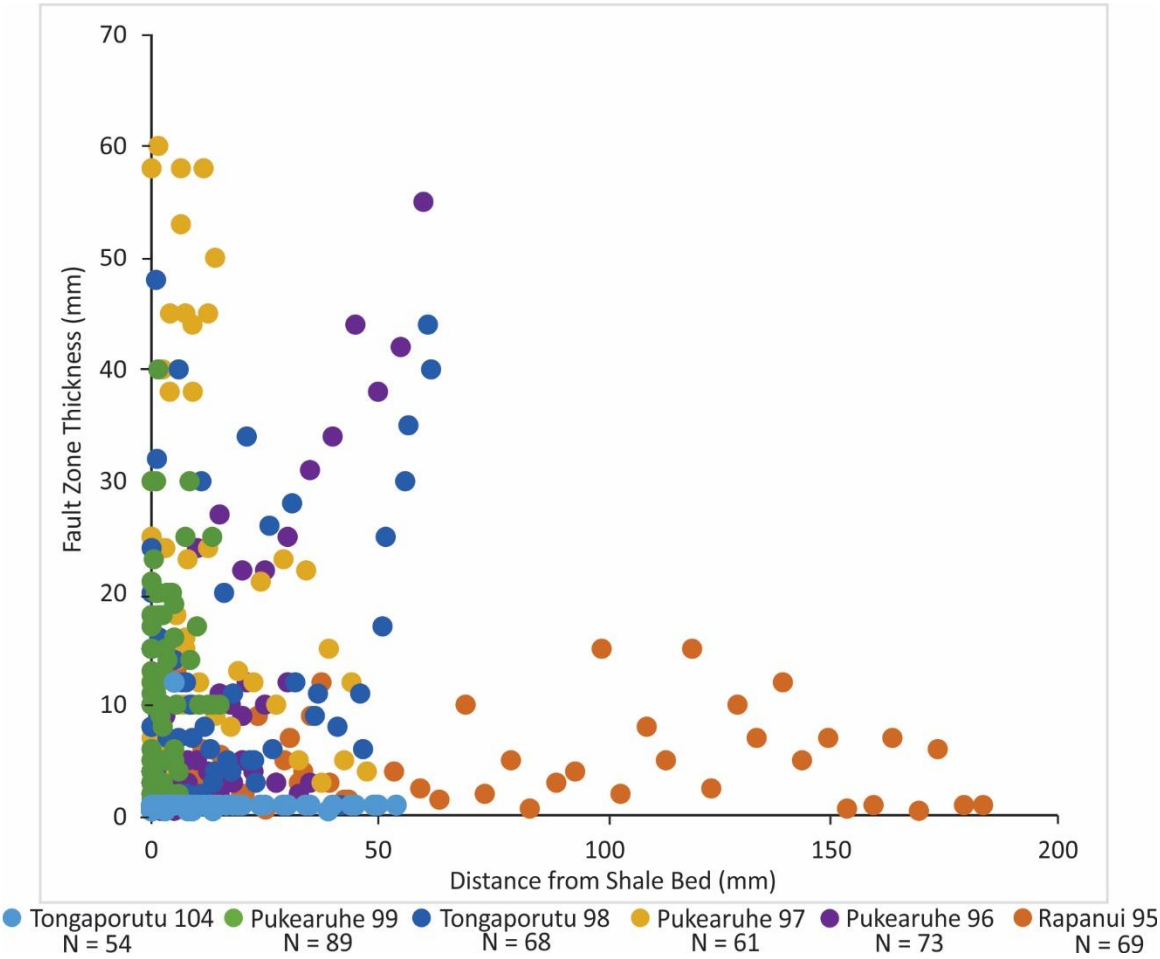

Figure 2.12 Fault-zone thickness plotted against the distance from siltstone beds for each profile. Data from Figure 1.4.3.

There is a positive correlation between fault displacement and both fault-rock and fault-zone thickness for all fault data (Figure 2.13), with thicknesses ranging by two to three orders of magnitude for a given displacement. These data are consistent with previous work conducted on the MMF and with research for other siliciclastic sequences (Blenkinsop 1989; Cartwright et al. 1995; Little 1995; Foxford et al. 1998; Bailey et al. 2005; Childs et al. 2007; Childs et al. 2009; Nicol

et al. 2013; Seebeck et al. 2014). Comparison of data for the fault population (N=184) and for the profiles provide a measure of the variability of thicknesses that can be expected for individual faults over dip distances of ~2-7 m. Inspection of Figure 2.13 suggests that the range of fault-rock and fault-zone thicknesses for individual faults are between 10 and 90% of the total spread for all fault data. The results here suggest that the smaller the fault displacement the greater the proportion of total spread in thickness (observed for all data) is captured by the profiles sampled. The portion of the fault dip-dimension represented by each dip profile has been estimated by using the equation $D = cL^n$ to estimate the total dip length, where D is maximum displacement, c is a constant related to rock properties, L is length and n is an exponent (e.g. Cowie and Scholz 1992). Parameters for this displacement-length scaling equation were adopted from FIFT (2005) where $D = 0.001L^{1.35}$ (i.e. $L= (D/0.001)^{1/1.35}$). Using these equations and assuming that the maximum displacements measured on each profile are the maximum for the fault, the profiles may constitute between 5 and 80% of the total dip dimension. The spread of the recorded data, as a proportion of the total spread for all data, is higher when the profile length is a greater proportion of the total fault length. Therefore, we propose that the total spread for all data may represent a proxy for the range of thicknesses present on individual faults when viewed over the entire fault surface (see Discussion section for further comments). If this were true then it may be possible to use thickness-displacement plots to stochastically estimate fault-zone thicknesses over the entire fault surface for the purposes of estimating fault-seal potential.

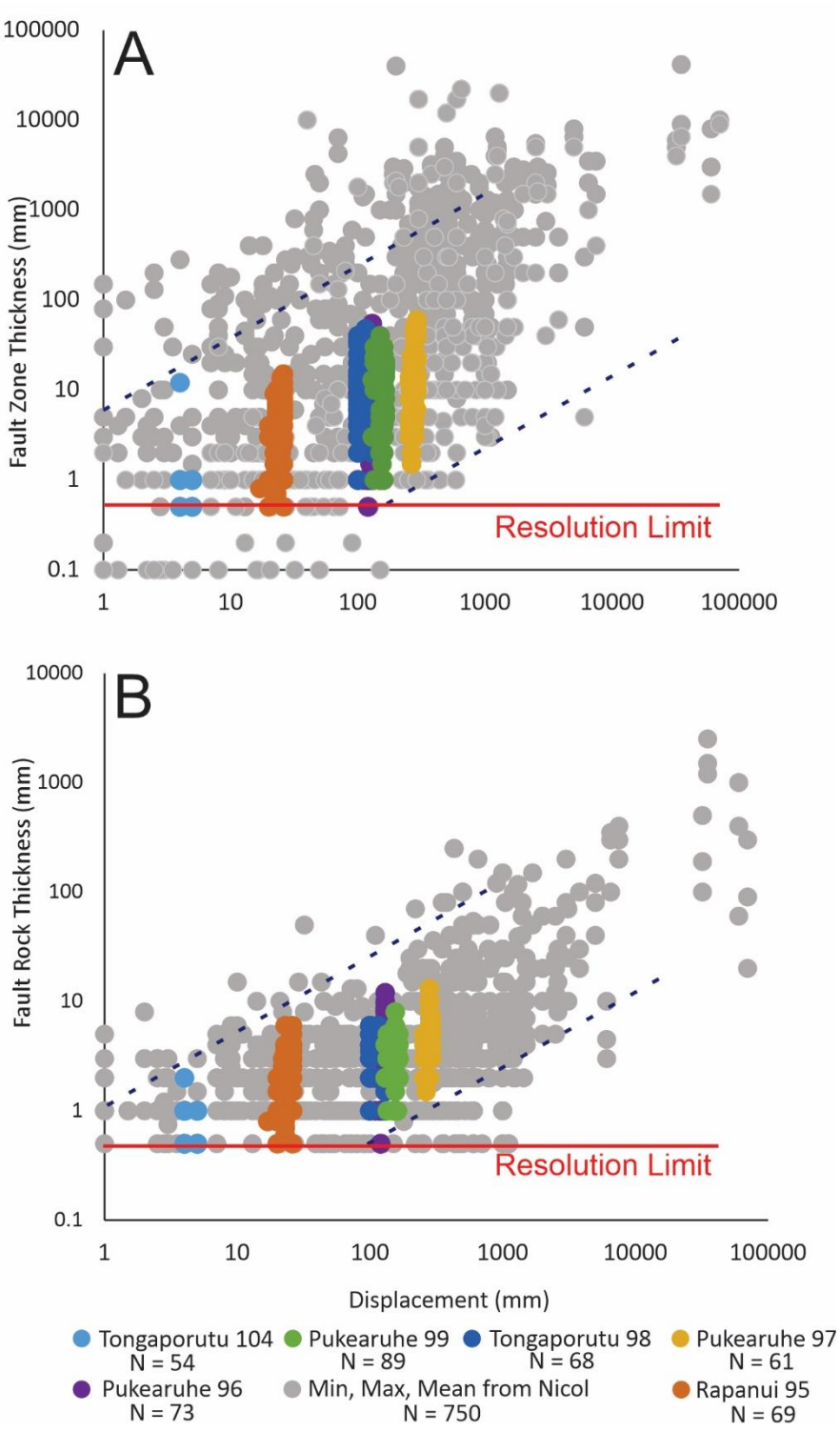

Figure 2.13 Graphs showing A) Fault-zone thickness and B) Fault-rock thickness variations with displacement. Measurements of fault-rock and zone vary over at least an order of magnitude for a given displacement. Below the lines of resolution limit sampling is incomplete.

2.5.4 Number of fault slip surfaces and deformation bands

Fault-rock for the studied faults is primarily a result of one or more deformation bands in sandstone beds. The number of these bands varied from 1 (single shear zone) to 20 (clusters of deformation bands). The minimum and maximum number of deformation bands along with the smallest and largest displacements were recorded for individual faults. These data are consistent with previous work and suggest a positive relationship between displacement and number of deformation bands (Nicol et al. 2013) (Figure 2.14).

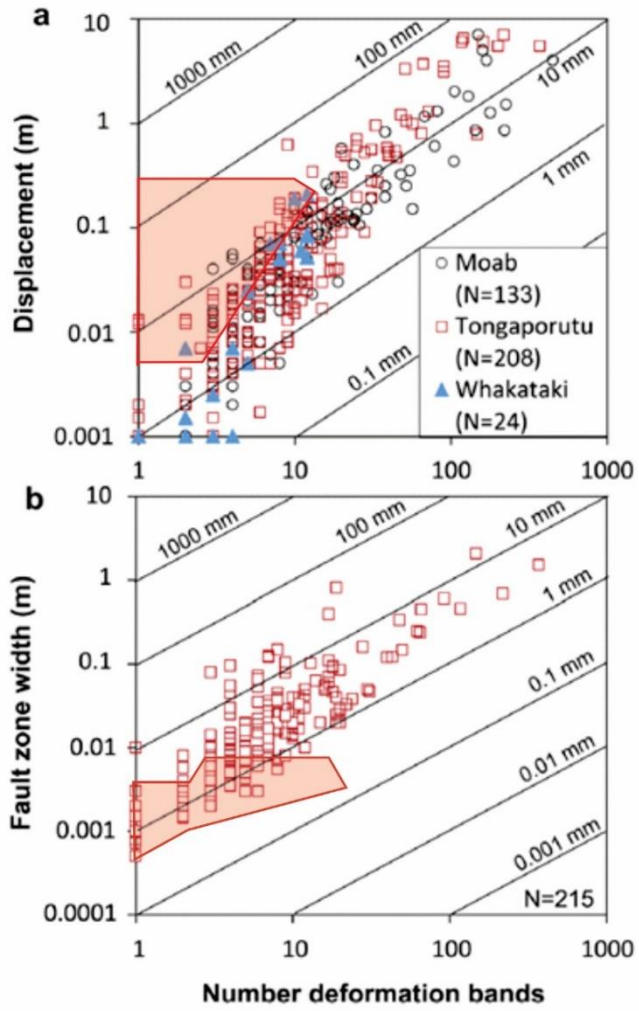

Figure 2.14 A) Displacement vs Number of Deformation bands from Moab (Utah, USA), Tongaporutu (Taranaki, New Zealand) and Whakataki (North Island, New Zealand). B) Fault zone width vs Number of deformation bands from Tongaporutu. Contours shows the average spacing between bands. Red polygons show where the 6 down fault profiles used in this study would plot. N.B. Number of Deformation Bands is the Maximum number observed for an outcropping section of fault. Both graphs modified from Nicol et al. (2013).

This positive relationship is interpreted to reflect a growth progression with additional bands added as fault displacement increases (Nicol et al. 2013). There is also a positive relationship between the number of bands and the fault-rock and fault-zone thicknesses (Figure 2.16B). The positive relationship between the number of deformation bands and fault-rock thickness is to be expected as deformation bands are the main source of fault-rock and areas of deformation band clusters correlate with areas of maximum fault-rock thickness. These clusters are generally <1 m wide and their dimension does not relate to displacement. Rather, it is inferred to reflect early segmentation which may be partly controlled by propagation of faults through heterogeneous host stratigraphy (Childs et al. 2009). The deformation band clusters only form within the sandstone beds and are therefore constrained to these horizons.

Increases in fault-zone thickness are often accompanied by an increase in the number of fault slip surfaces that displace siltstone beds. In Figure 2.15B, the number of slip surfaces was plotted against fault-zone thickness for 142 faults where, for each fault, the number of faults in the zone and the fault-zone thickness was averaged between the siltstone bed cut offs. For this sample, fault-zone thickness is highly variable and ranges from 1.5 mm to 320 mm where displaced by a single slip surface. The range of fault-zone thickness decreases with increasing number of faults which is in contrast to the observations of other fault studies in the MMF (e.g. Nicol et al. 2013). The decrease in the range of fault-zone thickness with increasing number of faults reflects the negative and positive slopes on the upper and lower bounds of the distribution, respectively. The relationships between fault-zone width and the number of faults displayed in Figure 2.15B is unexpected and is here interpreted to be due to sampling rather than representative of the relationship between fault-zone thickness and slip surfaces. As this study was focussed on relatively thin beds (generally <40cm) it may have treated slip surfaces as individual faults rather than strands in a larger fault-zone. This would also explain the lack of data towards the higher values of slip surface numbers. The base of the distribution in Figure 2.15B represents the lower limit at which features could be accurately measured at outcrop. While individual deformation bands were assigned a thickness of 0.7mm if less than a millimetre thick, it was generally considered that any feature thinner than a millimetre could not be accurately measured.

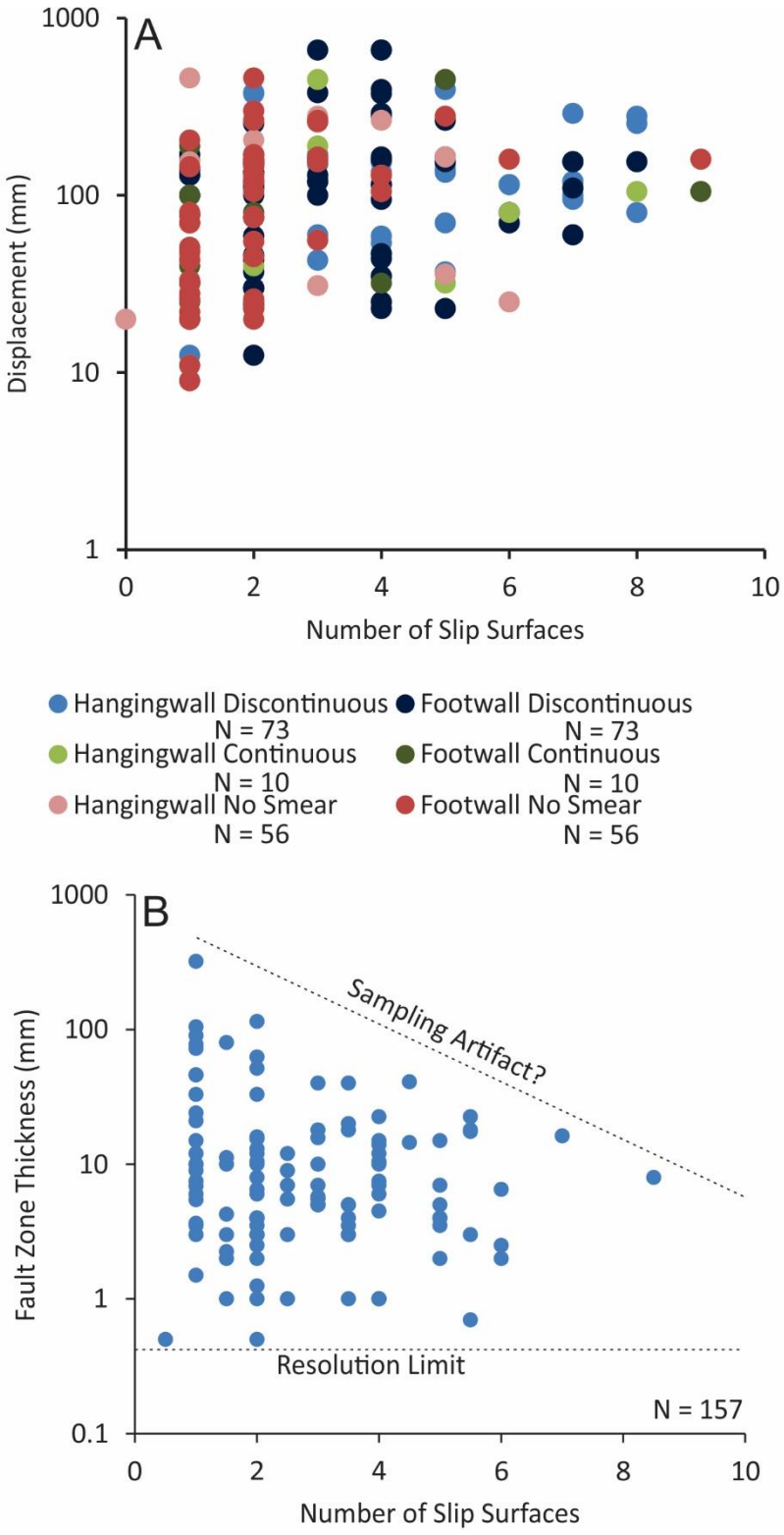

Figure 2.15. A) Displacement plotted against the number of slip surfaces at both hangingwall and footwall cut offs for no smear, discontinuous smear and continuous smear. B) Fault-zone thickness plotted against number of slip surfaces. The resolution limit of the data (assumed to be ~0.5 mm) and the upper limit of the data are shown. Analysis in A and B was conducted on the individual fault dataset and shows a decrease in variability with increasing displacement or fault-zone thickness which is likely to be a sampling artefact due to a decrease in the proportion of the fault population sampled that has large displacement/fault-zone thicknesses.

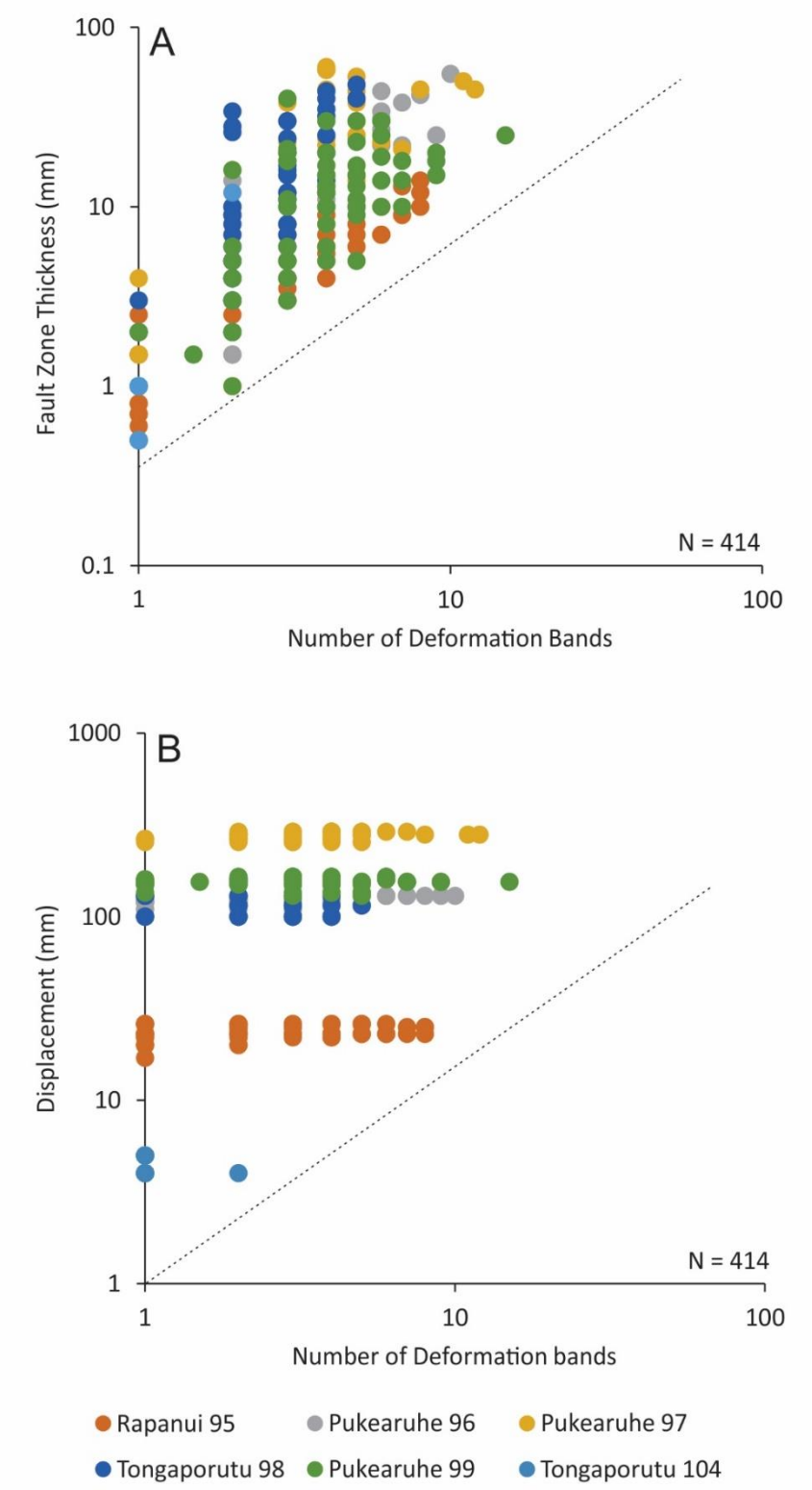

Figure 2.16 Plots of A) Fault-zone thickness and B) displacement against deformation band number for the six down fault profiles. There is a large range in number of deformation band that exceeds an order of magnitude. There is a positive relationship between the two variables.

In contrast to the fault slip surface data in Figure 2.15B, there is a positive relationship between fault-zone thickness and number of deformation bands (Figure 2.16A). There is a large degree of

variability in deformation band number for a given fault-zone thickness with band numbers ranging by more than an order of magnitude. This range suggests that the spacings between bands vary between faults with some clusters comprising closely spaced bands and others more widely spaced bands.

There is a difference in the trend and variability towards the higher end of displacement and fault-zone thickness for Figure 2.15 and Figure 2.16. Figure 2.15 displays a decrease in variability and maximum values for slip surfaces and deformation bands with increasing displacement and fault-zone thickness, which is likely a result of sampling trends from the Individual Fault Dataset. In our sample there was a higher proportion of faults with low displacements and a lack of data from larger faults (Figure 2.15). The data from Figure 2.16 was collected from the six down fault profiles which were more likely to capture the range in architectural values for a range of displacements and fault-zone thicknesses due to the repeated sampling of faults over short spacings (i.e. 5-10 cm) and longer sample lengths (i.e. 2-7 m). There is a negative relationship between the amount of fault displacement and the proportion of total range in fault-rock and fault-zone thickness captured by the profiles sampled, which is clearly demonstrated in Figure 2.15A and Figure 2.16B where up to 90% of the total spread (i.e. for all data) in thickness was sampled by a short 2D sample on an individual fault. To explore this negative relationship further and to examine what the spread data may indicate about fault-zone architecture, sample length and displacement these data are plotted on Figure 2.15 and Figure 2.16.

The number of faults observed within fault-zones is highly variable. These faults may comprise deformation bands within sandstone layers and slip surfaces within, or bounding, siltstone beds. They range in number from 1 to 9 and typically bound lenses of host rock. Where multiple faults are present within the fault-zone they can accommodate displacements of <10% to >90% of the total displacement accumulated across the zone. There is a positive correlation between the number of faults and the number of fault-bound lenses, as would be expected. In contrast to these relationships, the number of faults within the zone appears to be only weakly correlated with displacement. Given that there is a positive relationship between fault-zone thickness and displacement, and between number of deformation bands and displacement, the absence of a relationship between the number of faults and displacement is a surprise.

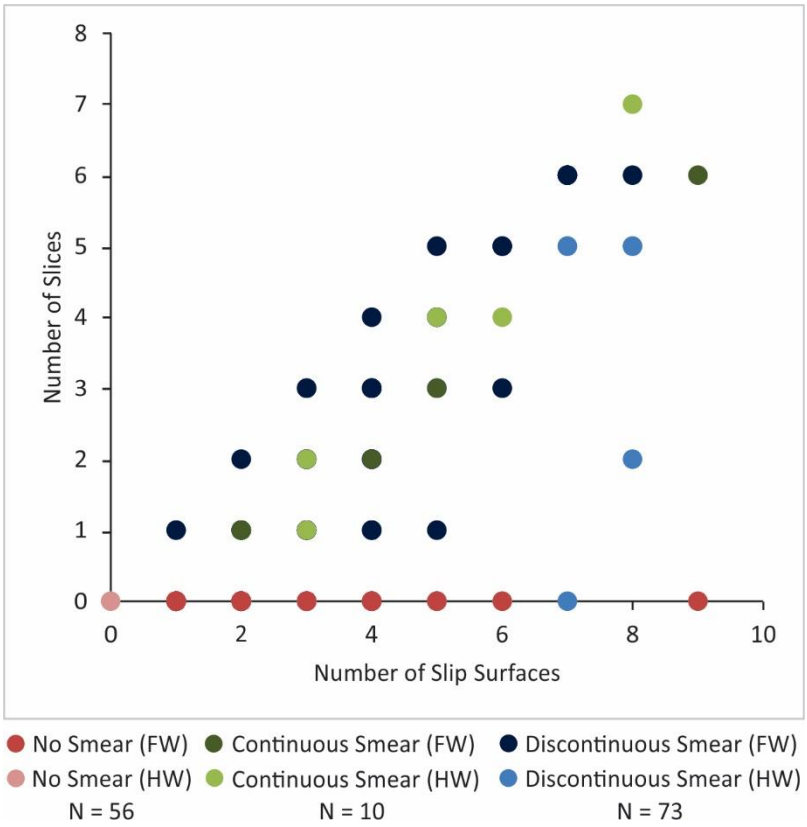

Figure 2.17 Number of slip surfaces vs the number of fault-bound slices for No Smear, Discontinuous Smear and Continuous Smear for both footwall and hangingwall cut offs.

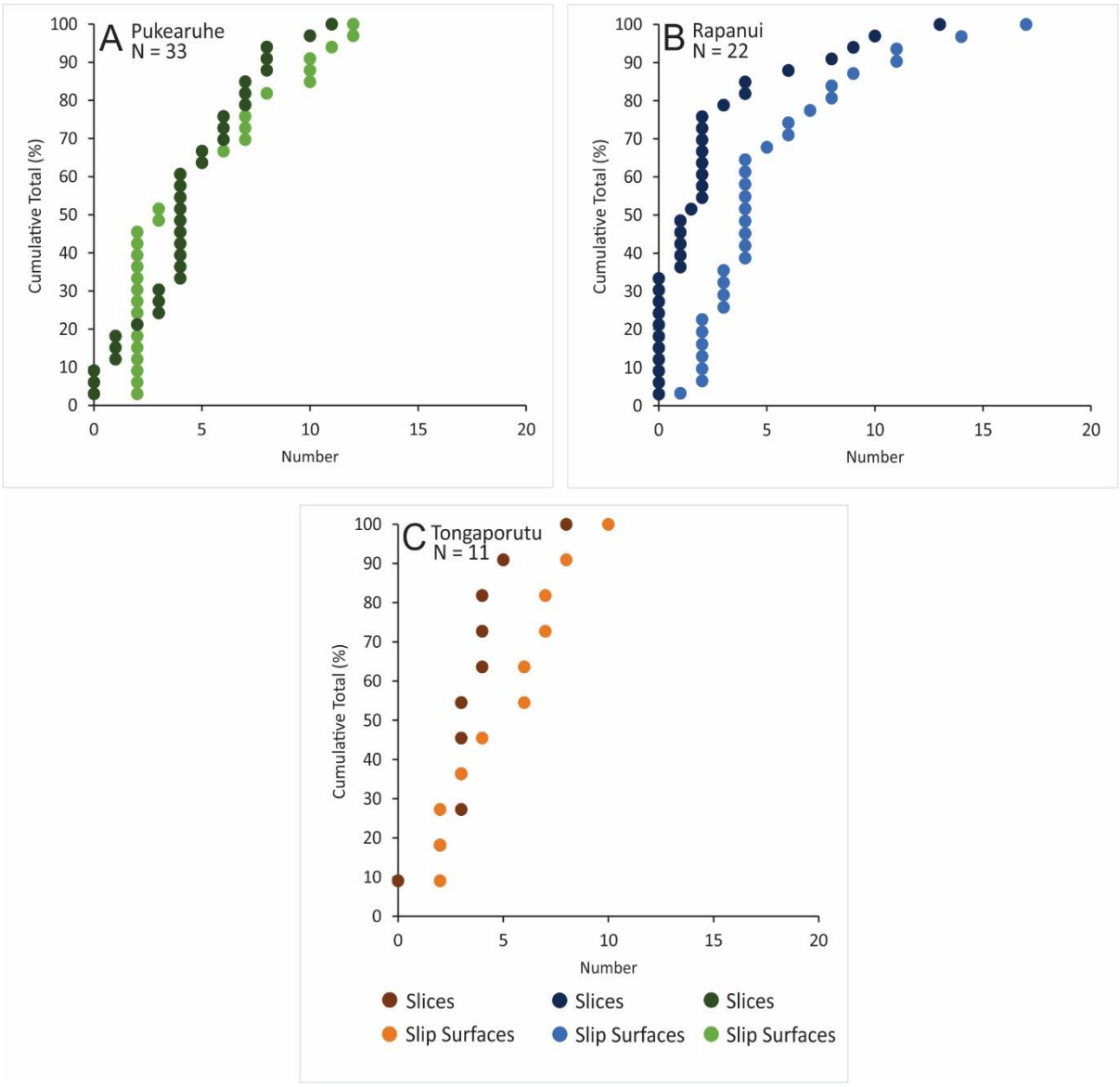

Figure 2.18 Cumulative frequency graphs for the number of faults (orange A, dark blue B, dark green C) and fault-bound lenses (brown A, light blue B and light green C) for the Pukearuhe (A), Rapanui (B) and Tongaporutu (C) locations. Each plot shows a positive correlation.

2.6 Discussion

Spatial variations of fault-zone and fault-rock over one to three orders of magnitude were recorded during this analysis. This study indicates that fault-zone architecture displays significant variation over short distances (cm to m) and that the controlling factors are likely to be numerous, a conclusion consistent with previous work (Caine et al. 1996; Evans et al. 1997; Foxford et al. 1998; Childs et al. 2007; Childs et al. 2009; Faulkner et al. 2010; Nicol et al. 2013; Seebeck et al. 2014). Structures that were visible at the outcrop scale, such as synthetic slip surfaces and host

rock slices, were also present in thin section studies suggesting that there is the potential for scaling up outcrop observations onto those observed on a seismic scale. Our data support the conclusions of Childs et al. (2009) that the widths of fault zones may be established early in the development of faulting with some degree of variability in fault dimensions and number of slip surfaces observed even for faults with small displacements (e.g. <10 mm). However, increases in the number of slip surfaces and deformation bands with increasing displacement appear to suggest that in many cases the densities of slip surfaces and deformation bands increase as displacement accrues within fault zones. We concur with Nicol et al. (2013) in suggesting that these increases in the densities of fault surfaces/deformation bands is most likely to occur at segment boundaries or irregularities on fault surfaces. It is possible that the addition of new slip-surfaces (or deformation bands) at complexities in fault surfaces reflects progressive strain localisation and associated asperity removal. However, it is worth noting that constraints on the absolute or relative ages of deformation bands at these irregularities is rare and it is possible that introduction of new slip surfaces produces new irregularities (i.e. fault zone delocalisation). Distal to these irregularities fault zones are generally less complicated with strains often localised into narrow zones, where shear strains localise from an early stage of faulting.

In Taranaki the generation of low permeability fault rock is a combination of both the cataclasis of host sandstone and smear of siltstone beds into the fault zone (Childs et al. 2007; Nicol and Childs 2018; this study). The along-fault profiles observed and it is worth noting that cataclastic deformation bands are often present alongside smear. There are significant variations in the amount, extent and type of fault-rock and these variations likely impact fault permeability. Of particular importance for across-fault permeability are the locations and frequency of patches of thin (e.g. <1 mm thickness on a 10 cm throw fault) fault rock. These patches are the sites within the fault zone is most likely to accommodate hydraulic break through. For the six faults studied in detail these patches occur at length scales of up to an order of magnitude larger than the displacement and typically have diameters comparable to, or smaller than the displacement. We believe that a large dataset of profiles of fault-rock thickness, similar to those presented in Figure 2.8, could provide a basis for quantifying the 2D spacing population and diameter of these low fault-rock thickness patches. Such data may be used in conjunction with juxtaposition analysis to predict the likelihood of ‘holes’ in the fault rock being located at sites of sand-on-sand juxtaposition. We concur with Yielding et al. (2016) in suggesting that improved understanding of fault-rock heterogeneity via outcrop studies could provide a means of improving fault seal prediction.

In addition to using the fault-profile data, fault-rock thickness measurements from many faults could provide a means of estimating the variability of fault –rock thicknesses over entire fault surfaces may provide a basis for estimating the range of thicknesses for a given displacement. Here we propose that the total spread for all data in Taranaki may represent a proxy for the range of fault-rock thicknesses present on individual faults when viewed over the entire fault surface. If this were true then it may be possible to use thickness-displacement plots to stochastically estimate fault-rock thicknesses over the entire fault surface for the purposes of estimating fault-seal potential.

2.7 Conclusions

This study measured and quantified the changes in fault-zone geometry both for individual faults and fault profiles at outcrop and sub-millimetre scale in the Mount Messenger Formation (MMF) in New Zealand. The collected data was used to constrain the variability in fault-zone architecture and the affect this may have on the distribution of low variability fault rock. Fault-zone geometries were found to vary by up to 3 orders of magnitude over sample lengths of several metres and displacements of <30 cm. Rapid changes in fault-zone architecture can often be attributed to the formation of deformation band clusters or the formation of lenses where host siltstone can become incorporated into the fault via multiple synthetic slip surfaces. The majority of fault profiles showed locations where fault rock was <1 mm, areas that are likely to act as conduits for fluid flow. No correlation was found between fault-rock minimums and architectural elements, making it hard to predict where and when holes may form along a fault length. To be able to more accurately predict fault permeability we suggest that a larger dataset of fault-zone and fault-rock thicknesses across a range of displacements should be compiled so that stochastic modelling can be used to identify likely locations for holes in fault seal.

2.8 References:

Annunziatellis A, Beaubien SE, Bigi S, Ciotoli G, Coltella M, Lombardi S. 2008. Gas migration along fault systems and through the vadose zone in the Latera caldera (central Italy): Implications for CO2 geological storage. Int J Greenh Gas Control. 2(3):353–372. doi:10.1016/j.ijggc.2008.02.003.

Aydin A. 2000. Fractures, faults, and hydrocarbon entrapment, migration and flow. Mar Pet Geol. 17(7):797–814. doi:10.1016/S0264-8172(00)00020-9.

Bailey WR, Walsh JJ, Manzocchi T. 2005. Fault populations, strain distribution and basement fault reactivation in the East Pennines Coalfield, UK. J Struct Geol. 27(5):913–928. doi:10.1016/j.jsg.2004.10.014.

Bense VF, Gleeson T, Loveless SE, Bour O, Scibek J. 2013. Fault zone hydrogeology. Earth-Science Rev. 127:171–192. doi:10.1016/j.earscirev.2013.09.008.

Blenkinsop TG. 1989. Thickness - displacement relationships for deformation zones: Discussion. J Struct Geol. 11(8):1051–1053. doi:10.1016/0191-8141(89)90056-4.

Browne GH, King PR, Higgs KE, Slatt RM, Browne GH, King PR, Higgs KE, Slatt RM, King PR, Higgs KE. 2005. Grain - size characteristics for distinguishing basin floor fan and slope fan depositional settings : Outcrop and subsurface examples from the late Miocene Mount Messenger Formation , New Zealand. New Zeal J Geol Geophys. 48:213–227. doi:10.1080/00288306.2005.9515111.

Caine JS, Evans JP, Forster CB. 1996. Fault zone architechture and permeability structure. Geology. 24(11):1025–1028. doi:10.1130/0091-7613(1996)024<1025.

Cartwright, JA, Trudgill, BD, Mansfield, Christopher S. 1995. Fault growth by segment linkage: an explanation for scatter in maximum displacement and trace length data from the Canyonlands grabens of SE Utah: Discussion. J Struct Geol. 22(1):135–140. doi:10.1016/S0191-8141(99)00136-4.

Cartwright J, Huuse M, Aplin A. 2007. Seal bypass systems. Am Assoc Pet Geol Bull. 91(8):1141–1166. doi:10.1306/04090705181.

Chester FM, Logan JM. 1986. Implications for mechanical properties of brittle faults from observations of the Punchbowl fault zone, California. Pure Appl Geophys. 124(1):79–106.

Childs C, Holdsworth RE, Jackson CAL, Manzocchi T, Walsh JJ, Yielding G. 2017. Introduction to the geometry and growth of normal faults. Geol Soc Spec Publ. 439(1):1–9. doi:10.1144/SP439.24.

Childs C, Manzocchi T, Walsh JJ, Bonson CG, Nicol A, Schöpfer MPJ. 2009. A geometric model of fault zone and fault rock thickness variations. J Struct Geol. 31(2):117–127. doi:10.1016/j.jsg.2008.08.009.

Childs C, Nicol A, Walsh JJ, Watterson J. 1996. Growth of vertically segmented normal faults. J Struct Geol. 18(12):1389–1397. doi:10.1016/S0191-8141(96)00060-0.

Childs C, Walsh JJ, Manzocchi T, Strand J, Nicol A, Tomasso M, Schopfer MPJ, Aplin AC. 2007. Definition of a fault permeability predictor from outcrop studies of a faulted turbidite sequence, Taranaki, New Zealand. Geol Soc London, Spec Publ. 292:235–258. doi:10.1144/SP292.14.

Childs C, Walsh JJ, Watterson J. 1997. Complexity in fault zone structure and implications for fault

seal prediction. Nor Pet Soc Spec Publ. 7:61–72. doi:10.1016/S0928-8937(97)80007-0.

Cowie PA, Scholz CH. 1992. Growth of faults by accumulation of seismic slip. J Geophys Res Solid Earth. 97(B7):11085–11095.

Dockrill B, Shipton ZK. 2010. Structural controls on leakage from a natural CO2 geologic storage site: Central Utah, U.S.A. J Struct Geol. 32(11):1768–1782. doi:10.1016/j.jsg.2010.01.007.

Evans JP, Forster CB, Goddard J V. 1997. Permeability of fault-related rocks, and implications for hydraulic structure of fault zones. 19(11).

Exner U, Tschegg C. 2012. Preferential cataclastic grain size reduction of feldspar in deformation bands in poorly consolidated arkosic sands. J Struct Geol. 43:63–72. doi:10.1016/j.jsg.2012.08.005.

Faulkner D. R., Jackson CAL, Lunn RJ, Schlische RW, Shipton ZK, Wibberley CAJ, Withjack MO. 2010. A review of recent developments concerning the structure, mechanics and fluid flow properties of fault zones. J Struct Geol. 32(11):1557–1575. doi:10.1016/j.jsg.2010.06.009.

Faulkner D.R., Jackson CAL, Lunn RJ, Schlische RW, Shipton ZK, Wibberley CAJ, Withjack MO. 2010. A review of recent developments concerning the structure, mechanics and fluid flow properties of fault zones. J Struct Geol. 32(11):1557–1575. doi:10.1016/j.jsg.2010.06.009.

Ferrill DA., Morris AP. 2002. Dilational normal faults. J Struct Geol. 25:183–196. doi:10.1016/S0191-8141(02)00029-9.

Fisher QJ, Knipe RJ. 1998. Fault Sealing processes in siliciclastic sediments. Geol Soc London, Spec Publ. 147:117–134.

Fisher QJ, Knipe RJ. 2001. The permeability of faults within siliciclastic petroleum reservoirs of the North Sea and Norwegian Continental Shelf. Mar Pet Geol. 18(10):1063–1081. doi:10.1016/S0264-8172(01)00042-3.

Fossen H, Schultz RA., Shipton ZK, Mair K. 2007. Deformation bands in sandstone: a review. J Geol Soc London. 164:755–769.

Fossen H, Schultz RA, Torabi A. 2011. Conditions and implications for compaction band formation in the Navajo Sandstone, Utah. J Struct Geol. 33(10):1477–1490. doi:10.1016/j.jsg.2011.08.001.

Foxford KA, Walsh JJ, Watterson J, Garden IR, Guscott SC, Burley SD. 1998. Structure and content of the Moab fault zone, Utah, USA, and its implications for fault seal prediction. Geol Soc London, Spec Publ.(147):87–103.

Fristad T, Groth A, Yielding G, Freeman B. 1997. Quantitative fault seal prediction: a case study from Oseberg Syd. Nor Pet Soc Spec Publ. 7(C):107–124. doi:10.1016/S0928-8937(97)80010-0.

Giba M, Nicol A, Walsh JJ. 2010. Evolution of faulting and volcanism in a back - arc basin and its implications for subduction processes. 29(November 2009):1–18. doi:10.1029/2009TC002634.

Giger SB, Clennell MB, Çiftçi NB, Harbers C, Clark P, Ricchetti M. 2013. Fault transmissibility in clastic-argillaceous sequences controlled by clay smear evolution. Am Assoc Pet Geol Bull. 97(5):705–731. doi:10.1306/10161211190.

Grant NT. 2016. A geometrical model for shale smear: implications for upscaling in faulted

geomodels. Pet Geosci. 23(1):39–55. doi:10.1144/petgeo2016-021.

Hermanrud C, Halkjelsvik ME, Kristiansen K, Bernal A, Strömbäck AC. 2014. Petroleum column-height controls in the western Hammerfest Basin, Barents Sea. Pet Geosci. 20(3):227–240. doi:10.1144/petgeo2013-041.

Hooper ECD. 1991. Fluid Migration Along Growth Faults in Compacting Sediments. J Pet Geol. 14(S1):161–180.

Van Hulten FFN. 2010. Geological factors effecting compartmentalization of Rotliegend gas fields in the Netherlands. Geol Soc London, Spec Publ. 347:301–315.

King P, Thrasher GP. 1996. Cretaceous-Cenozoic geology and petroleum systems of the Taranaki Basin, New Zealand. Institute of Geological & Nuclear Sciences.

Knott SD, Alastair BP, Brockbank J, Lawson BJ, McCallum JE, Welbon AI. 1996. Spatial and mechanical controls on fault populations. J Struct Geol. 18:359-372. doi: 10.1016/S0191-8141(96)80056-3.

Kristensen MB, Childs C, Olesen NØ, Korstgård JA. 2013. The microstructure and internal architecture of shear bands in sand–clay sequences. J Struct Geol. 46:129–141. doi:10.1016/j.jsg.2012.09.015.

Lindsay NG, Murphy FC, Walsh JJ, Watterson J. 1993. Outcrop Studies of Shale Smears on Fault Surface. Int Assoc Sedimentol Spec Publ.(15):113–123.

Little TA. 1995. Brittle deformation adjacent to the Awatere strike-slip fault in New Zealand : Faulting patterns , scaling relationships , and displacement partitioning. Geol Soc Am Bull. 107(11):1255–1271. doi:10.1130/0016-7606(1995)107<1255.

Mair K, Main I, Elphick S. 2000. Sequential growth of deformation bands in the laboratory. J Struct Geol. 22(1):25–42. doi:10.1016/S0191-8141(99)00124-8.

Manzocchi T, Childs C, Walsh JJ. 2010. Faults and Fault Properties in Hydrocarbon Flow Models. Geofluids:94–113. doi:10.1111/j.1468-8123.2010.00283.x.

Masalimova LU, Lowe DR, Sharman GR, King PR, Arnot MJ. 2016. Outcrop characterization of a submarine channel-lobe complex: The Lower Mount Messenger Formation, Taranaki Basin, New Zealand. Mar Pet Geol. 71:360–390. doi:10.1016/j.marpetgeo.2016.01.004.

Nicol A, Childs C, Walsh JJ, Schafer KW. 2013. A geometric model for the formation of deformation band clusters. J Struct Geol. 55:21–33. doi:10.1016/j.jsg.2013.07.004.

Nicol A, Childs C. 2018. Cataclasis and silt smear on normal faults in weakly lithified turbidites. J Struct Geol. 117(June):44–57. doi:10.1016/j.jsg.2018.06.017.

Peacock DCP, Knipe RJ, Sanderson DJ. 2000. Glossary of normal faults. J Struct Geol. 22(3):291–305. doi:10.1016/S0191-8141(00)80102-9.

Pei Y, Paton DA, Knipe RJ, Wu K. 2015. A review of fault sealing behaviour and its evaluation in siliciclastic rocks. Earth-Science Rev. 150(October):121–138. doi:10.1016/j.earscirev.2015.07.011.

Rotzien JR, Lowe DR, King PR, Browne GH. 2014. Stratigraphic architecture and evolution of a

deep-water slope channel-levee and overbank apron: The upper miocene upper mount messenger formation, Taranaki Basin. Mar Pet Geol. 52:22–41. doi:10.1016/j.marpetgeo.2014.01.006.

Scholz CH, Dawers NH, Yu JZ, Anders MH, Cowie PA. 1993. Fault growth and fault scaling laws: preliminary results. J Geophys Res. 98(B12):951–961. doi:10.1029/93jb01008.

Seebeck H, Nicol A, Walsh JJ, Childs C, Beetham RD, Pettinga J. 2014. Fluid flow in fault zones from an active rift. J Struct Geol. 62:52–64. doi:10.1016/j.jsg.2014.01.008.

Vrolijk PJ, Urai JL, Kettermann M. 2015. Clay Smear: Review of Mechanisms and Applications. J Struct Geol. doi:10.1016/j.jsg.2015.09.006.

Walsh JJ, Bailey WR, Childs C, Nicol A, Bonson CG. 2002. Formation of segmented normal faults: A 3-D perspective. J Struct Geol. 25(8):1251–1262. doi:10.1016/S0191-8141(02)00161-X.

Walsh JJ, Watterson J. 1988. Analysis of the relationship between displacements and dimensions of faults. J Struct Geol. 10(3):239–247. doi:10.1016/0191-8141(88)90057-0.

Wibberley CAJ, Shimamoto T. 2002. Internal structure and permeability of major strike-slip fault zones: The Median Tectonic Line in Mie Prefecture, Southwest Japan. J Struct Geol. 25(1):59–78. doi:10.1016/S0191-8141(02)00014-7.

Yielding G, Bretan P, Freeman B. 2016. Fault seal calibration : a brief review. Geol Soc London, Spec Publ. 347:243–255.

Yielding G, Freeman B, Needham DT. 1997. Quantitative fault seal prediction. Am Assoc Pet Geol Bull. 81(6):897–917. doi:10.1306/522B498D-1727-11D7-8645000102C1865D.

Van der Zee W, Urai JL. 2005. Processes of normal fault evolution in a siliciclastic sequence: a case study from Miri, Sarawak, Malaysia. J Struct Geol. 27(12):2281–2300. doi:10.1016/j.jsg.2005.07.006.

3 Shale smear geometries in a thinly bedded turbidite sequence

Abstract

The geometries of shale smears on small displacement normal faults in the MMF have been studied using a random sample of faults from coastal cliffs. Analysis was primarily conducted on outcrops of weakly lithified, thinly interbedded siltstones and sandstones with fault displacements of 2 cm to 1.1 m. Data were collected for over 180 individual faulted siltstone beds, with detailed measurements of shale smear geometries on 58 individual faulted beds. The data show that shale smear geometries are highly variable. At outcrop-scale shale smears are produced by a combination of ductile deformation and brittle faulting, with individual smears being produced by one or both processes. Individual beds can accommodate both brittle and ductile deformation, suggesting that apparent changes in the deformation style of beds is not entirely dependent on their mechanical properties. Thin sections of ductile smears indicate they are primarily deformed by micro-faulting and brittle deformation. Therefore, smearing in the MMF is primarily a brittle process, with the type of deformation observed sometimes being dependent on the scale of observation. Displaced siltstone beds in the MMF can produce no shale smear, discontinuous shale smear and continuous shale smear between the source beds. Analysis of the smear thicknesses suggests that on average the thickest smears are not located proximal to the source beds. Therefore, holes in shale smears do not appear to preferentially form at the midpoint between cut offs. The available smear data suggest that stochastic models may provide a means of populating shale smear thicknesses in fault zones.

3.1 Introduction

3.1.1 What are shale smears?

Lindsay et al. (1993) describe shale smear as a "shale or clay layer intervening between sandstone units juxtaposed across a fault". Shale smears are generally considered to be sourced from shale or clay beds in the host rock adjacent to the fault, with the smear thickness often observed (or inferred) to taper or thin with increasing distance from the source bed (Lindsay et al. 1993; Fulljames et al. 1997). The degree of smearing may be dependent on the proportion of clay or phyllosilicates present in the source bed. For this reason some prefer to use the term clay smear, where clay smear contains >40% clay/phyllosilicates and may comprise material entirely from clay-rich source beds or from mixing of a clay rich layer with other lithologies (Pei et al. 2015). However, many studies make no reference to the presence of clay in the smear or the source rock, which are often referred to as shales, a term poorly defined in the literature, while siltstone and sandstone beds have also been observed to smear (e.g. Kristensen et al. 2013; this study).

To describe and quantify the geometry of shale smears it is first necessary to clearly define what constitutes a shale smear and to understand how they form. Definitions of shale smear can include descriptions of their shape, bed composition and formation mechanisms. These definitions may be influenced by the data and techniques used in a given study or by the rock types associated with smearing and a range of parameters may be employed for defining shale smears. Shale smear studies are predominantly observed at outcrop-scale for normal faults within siliciclastic sequences (Lindsay et al. 1993; Lehner and Pilaar 1997; Van der Zee and Urai 2005; Childs et al. 2009; Kristensen et al. 2013; Vrolijk et al. 2016; Kettermann et al. 2016). Information gathered in these outcrop studies has been invaluable for our present understanding of shale smears, however, these data are predominantly two-dimensional (2D) and few examples provide a three-dimensional (3D) perspective of shale smear geometries and formation mechanisms (Kettermann et al. 2016). While many suggestions have been made as to the mechanism(s) of smear, no one clear controlling factor has been identified for the formation and, in some cases, destruction of shale smears (Kettermann et al. 2016).

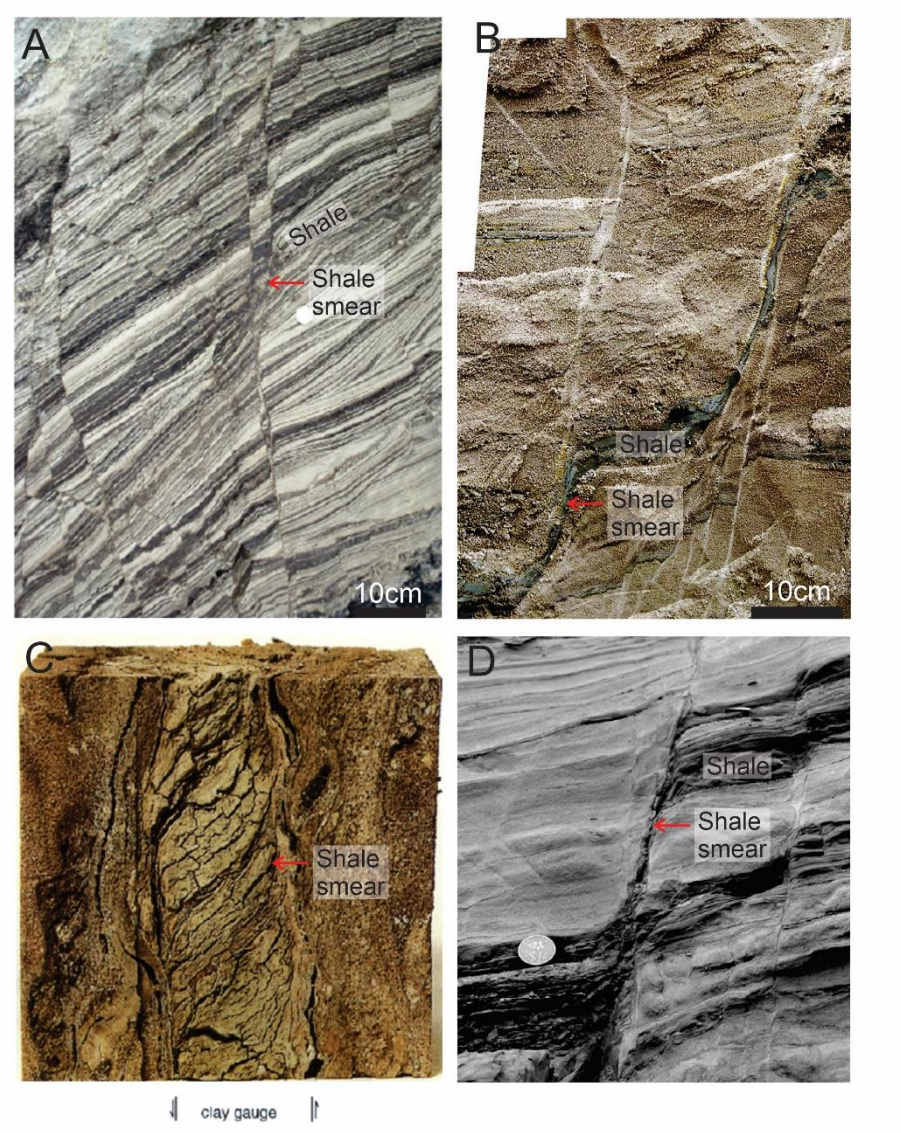

Figure 3.1 Photographs depicting the range of smears from previously published outcrop studies. A) Small scale shale smears from Jensgaard, Denmark from Kristensen et al. (2013) B) Continuous smears with lengths several times larger than the host bed thicknesses from Hambach Mine, Germany as published by Kettermann et al. (2016) C) Zoomed in section of internal structure of a shale smear that was traceable for~400m across the Frechen Lignite Mine, Germany as published by Lehner and Pilaar (1997)and D) A continuous smear from Miri, Malaysia published by Van der Zee and Urai (2005).

Shale smears are thought to be incorporated into fault-zones via four main mechanisms: abrasion, shear, injection and slicing (See Figure 3.2) (Lindsay et al. 1993; Giger et al. 2013; Pei et al. 2015; Vrolijk et al. 2016). The first and most common process associated with shale smear is abrasion, where the roughness of passing strata leads to the entrainment of clay from the host rock into the fault-rock creating a veneer of clay within the fault-zone. These abrasion smears can cover much of the fault surface, are usually very thin (<1mm) and may vary little in thickness (Lindsay et al. 1993; Giger et al. 2013). While sand beds can abrade clay into fault-zones they can also

erode the smear itself, which may occur where clay beds comprise a small proportion of the sequence thickness. By contrast, shear smears form where the fine-grained bed is sheared across the width of a fault zone (Lindsay et al. 1993; Giger et al. 2013; Vrolijk et al. 2016). In such cases, the source bed is part of a distributed shear zone and within this zone tapers with increasing distance from the source bed. In the ideal shear zone model, footwall and hangingwall shale beds thin towards the centre of the fault-zone, with the shale having the appearance of being dragged into the fault-zone. This type of smear is common in lithologies with a high shale to sand ratio where shale interbeds are common (Lindsay et al. 1993). Injection smears form by the injection of fluid-rich clays into the fault-zone creating characteristically thick clay smears that may exceed the thickness of the clay source bed (Lindsay et al. 1993). Injection occurs due to the sometimes-large difference in mechanical strength between clay and sand layers, with injection occurring as the clay deforms plastically under stresses induced by faulting. The thickest injection smears may occur at fault releasing bends where fault dilation provides space for the mobile clays (Van der Zee et al. 2003). Lastly, Giger et al. (2013) suggest that slicing is an important process by which shale smear forms. Slices are fragments of host rock that are bound by fault slip surfaces which displace shale or clay beds without significant interlayer mixing. Slicing has been widely reported in the literature (e.g. Van der Zee and Urai 2005; Giger et al. 2013; Kettermann et al. 2016), with Vrolijk et al. (2016) suggesting that brittle processes, such as the slicing of clay into the fault-zone, are more common than ductile processes, such as drag or plastic flow. Where numerous slices are closely spaced (e.g. <10 mm) and their displacements small, they can produce shale smear geometries that appear ductile. The absolute strength of the clay source bed, or its strength relative to surrounding sandstone beds, may control whether it smears or is faulted, with relatively incompetent clay beds most likely to deform in a ductile (Sperrevik et al. 2000). Conversely, post-lithification faulting may be more likely to produce brittle deformation and abrasion smears (Lindsay et al. 1993; Yielding et al. 2016). Other potential controls on shale smear formation include displacement, the rate of displacement, host rheology, depth of deformation, fault angle, net to gross of the sequence and shale bed distribution (Lindsay et al. 1993; Fulljames et al. 1997; Lehner and Pilaar 1997).

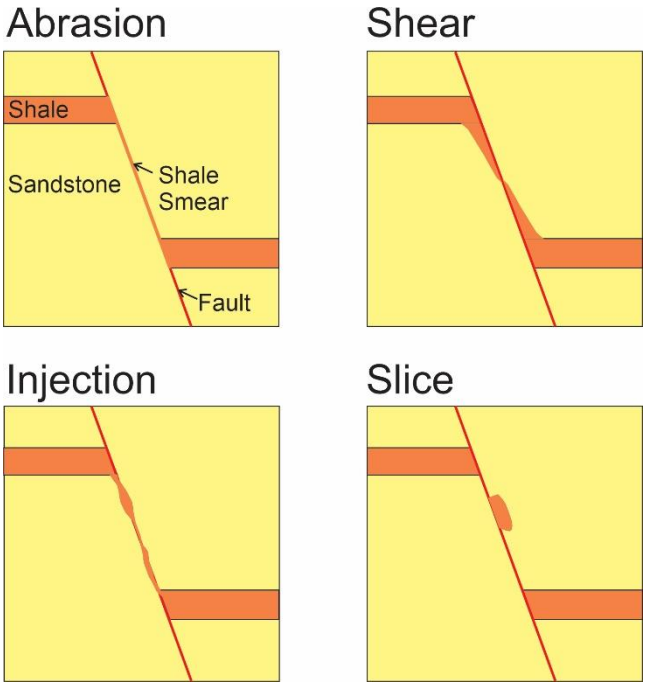

Figure 3.2 Schematic diagrams showing the variety of smearing processes described by previous studies.

The geometry of smears may be influenced by the stage they have reached in their evolution. Vrolijk et al. (2016) identified three distinct phases of clay smear formation. In the initial phase the incorporation of clay into the fault-zone first occurs. The clay then undergoes a second stage where it is smeared along the fault. Lastly, in the final stage the clay smear starts to develop holes and ceases to act as a coherent seal. As displacement progresses the relative importance of these holes increases. Childs et al. (2007) discovered that holes could form even when no significant thinning of the clay smear had occurred. Laboratory experiments using decimetre scale faults, suggest that from the outset of their formation smears can be smooth and evenly distributed ranging through to irregular and segmented (Ciftci et al. 2012). These laboratory studies suggest that the formation of holes in smears may not always be controlled by clay thickness and fault displacement. These experiments highlight the importance of secondary faults for smear geometry and continuity (Ciftci et al. 2012).

3.1.2 Why are shale smear important?

The ability of fluids to be transmitted across or along faults is predominantly dependent on the grain size of the host rock and fault-rock (Caine et al. 1996; Gartrell et al. 2004; Childs et al. 2007). In sequences where there is a high permeability contrast between the host lithologies, it is often the incorporation of the low permeability strata into fault-zones that leads to retarded lateral fluid flow. For example, Heynekamp et al. (1999) observed that the mixing of sand and clay within

the Sand Hill Fault-zone in New Mexico led to a reduction in permeability of up to six orders of magnitude. Such fault-rock has implications for sub-surface fluid flow as it controls migration pathways and the locations where fluids may accumulate or escape to the surface. Thus, faults can have serious ramifications for the carbon capture and storage, nuclear waste disposal, hydrocarbon and geothermal industries, as well as for water supplies globally (Gutierrez et al. 2000; Fisher and Knipe 2001; Caramanna et al. 2011; Cartwright 2011; Esposito and Benson 2011; Bense et al. 2013; Seebeck et al. 2014).

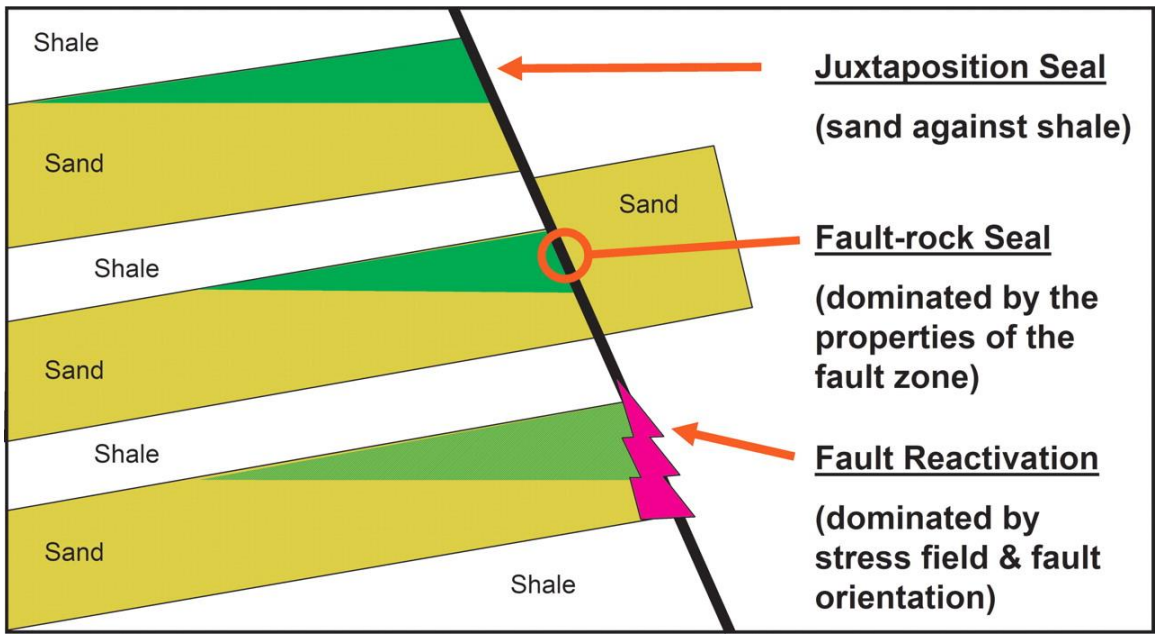

Figure 3.3 Schematic diagram from Yielding et al. (2010) showing the three controls on fault permeability.

Figure 3.3 highlights the three main controls on fault permeability. A juxtaposition seal occurs when a permeable horizon is displaced against an impermeable horizon, prevent across fault flow. Fault-rock seal occurs where impermeable fault-rock exists between two permeable horizons providing a baffle or barrier to flow. Fault reactivation is thought to allow the breaking of fault-rock seals and the dilation of the fault-zone, allowing fluids to travel vertically along a fault plane between two permeable horizons. As this thesis focuses on across fault fluid flow we will focus on the first two mechanisms.

There has been some debate as to whether juxtaposition seals or fault-rock seals are the dominant method of preventing across fault fluid flow. While some studies suggest that fault seal via fault-rock could be common (Bouvier et al. 1989, Lindsay et al. 1993, Gibson 1994, Fristad et al. 1997, Yielding et al. 1997), others indicate that fault-rock may be too thin and discontinuous to form a significant seal (James et al. 2004. Corona et al. 2010). Corona et al. (2010) suggest that

only when juxtaposition and stratigraphic sealing has been completely ruled out can a fault-rock seal be investigated. It is suggested that fault sealing not observed during structural modelling is most likely due to a lack of resolution, rather than low permeability fault-rock, with smaller beds and stratigraphic changes not resolvable on seismic or modelling software (James et al. 2004, Corona et al. 2010).

Shale smear is thought to be the main mechanism that leads to fault-rock seal and by better understanding the processes that produce smear and its distribution along fault-zones we can assess its impact on fault permeability and produce more robust prediction methods (Yielding et al. 1997; Ferrill and Morris 2002; Gartrell et al. 2004; Childs et al. 2007; M.B. Kristensen et al. 2013; Pei et al. 2015; Frischbutter et al. 2017). This could help identify faults that are sealing and those that act as conduits which has many implications for industries interested in the flow of fluids in the sub-surface, whether that be on production or geological timescales. Knowing where low permeability fault-rock may or may not be located within a fault zone helps map potential fluid pathways, as a fault is only as sealing as its most leaky part (Fulljames et al. 1997).

3.1.3 What is the scope of this chapter?

This chapter will examine the geometries and formation processes of shale smear geometries observed on small normal faults (<1m displacement) which displace turbidites exposed in cliffs along ~20 km of the Taranaki Coast, New Zealand (See Figure 2.3, Chapter 2). For the purposes of this study we use the term shale smear to describe both apparently ductile smear of fine-grained beds and the incorporation of siltstone beds into fault zones via a series of fault-bound slices (here referred to as slicing). We document the range of smear geometries and what effect these different geometries may have on lateral fault-zone permeability. We investigate whether smears generally taper with distance from their source bed or whether alternative geometries are more common. We also consider the role of secondary faults on the formation of shale smears and the importance of the slicing process. Differences in these geometries provides a basis for determining what factors control the geometry and formation of smears and whether it will be possible to predict their geometries on parts of faults where data are limited or absent. Our analysis suggests that smear geometries are highly variable. These variations reflect differences in the degree of smearing, and in the number and displacement of secondary faults within the fault zone. We contend that not all beds smear and that the results of previous studies may differ from those presented here because these earlier studies focused on strata and faults where

smears were well developed. Lastly, we argue that all smears in this study are brittle structures and that the distinction between ductile smears and smears formed by slicing is primarily the fault displacement and the scale of observation.

3.2 Data and methodology

Shale smears are examined for small normal faults that displace siltstone and sandstone beds in the Mount Messenger Formation (MMF). The MMF primarily comprises a Miocene age (~7-11 Ma) siliciclastic sequence of interbedded siltstone (1-45 cm) and sandstone (~1-150 cm) beds exposed in coastal cliffs up to ~200 m high and for ~25 km along the Taranaki Coast of New Zealand (Browne et al. 1996; King and Thrasher 1996; Masalimova et al. 2016). The sequence represents deepwater submarine fans, turbidite and mass transport deposits. The beds are displaced by normal faults ranging in displacement from a millimetre up to 70 m, which occurred at maximum burial depths of <1500m between 2 and 6 Ma (Nicol and Childs 2018). The resulting fault rock has permeabilities of six or more orders of magnitude less than the host sandstone (i.e. fault rock <0.0005mD and host sandstone >100 mD)(Childs et al. 2007).

The sandstone beds sampled contained an average of 69% fine to moderate sand sized grains, 25% silt size grains and 6% clay sized grains. The sandstones have a high percentage of lithic fragments (45%- 55%) and clays including kaolinite, smectite and illite (Higgs et al. 2015).The siltstone beds sampled were predominantly coarse silt with 20% sand sized grains, 69% silt sized grains and the remaining 16% being clay sized. XRD analysis of the host siltstones showed phyllosilicate contents between 36.5% and 53.8%.

One hundred and eighty-five shale smears were sampled along the Taranaki coastline from Pukearuhe in the South to Rapanui in the North (See Figure 1.3, Chapter 1). The number of samples on each beach was as follows: Pukearuhe (44), Waikiekie (2), Tongaporutu (43), Rapanui (57) and Mohakatino (25) with 14 Taranaki samples having no locality recorded. The samples from Pukearuhe were from the Upper MMF while the remaining sample sites were all within the Lower MMF. The majority of samples were from individual beds that were sampled once with only five samples from beds measured on multiple faults.

There is a possibility that by targeting beds that smear in an attempt to understand better the architecture and extent of smearing a bias has been introduced into the literature. As authors

have been conducting fieldwork with the primary aim of identifying smears, they may have sub-consciously overlooked beds that show no smear or even have consciously only chosen the best examples of smear to record. Therefore, this study takes a systematic approach to eliminate, or at least reduce, the perceived bias so that a representative sample of faulted beds (smeared and unsmeared) could be taken from the outcrop. However, not every bed could feasibly be used, and this study has its own limitations. These include a limited scale range of observations with no fault displacement measurements of dimensions <0.5 mm or >20 m observed and restricted in situ testing of fault-rock properties. Furthermore, larger faults were often unsuitable for sampling as beds were untraceable across the fault, their fault-rock was eroded and the area around the fault was unstable due to overhangs arising from erosion in the coastal cliffs.

In an attempt to remove bias from the sampling method, and to gain a representative overview of the faults within the MMF, a systematic approach was taken. Every fault that met the following criteria was cleaned down and measured:

1. Siltstone beds where the hangingwall and footwall could be unambiguously mapped across the fault.
2. Siltstone beds were displaced by more than their thickness so that fault-rock continuity between the two horizons could be assessed.
3. Each fault sampled displaced one siltstone bed between the horizon cut offs. This allowed the contribution of the siltstone bed to fault-rock to be determined with confidence.
4. For each fault the fault-zone/fault-rock were 100% exposed along the entire sample length of the displaced beds.

Measurements of fault-rock thickness, fault-zone thickness, number of slip surfaces and the thickness and geometries of shale smear were measured at both the hangingwall and footwall cut offs (See Figure 1.7, Chapter 1). These were taken from the middle of the beds and perpendicular to their long axis to give consistent readings. Fault-zone fine-grained material was summed across the fault-zone with both shale smear, shale slices and cataclastic deformation bands included. Where deformation bands were too fine to accurately measure, the number of bands was summed and multiplied by 0.7 mm to give the estimated width of cataclastic fault-rock in millimetres. The majority of measurements were taken in situ, although a small portion of measurements were from detailed photographs. Data from field and photograph measurements produced comparable results.

3.2.1 Thin section, photographs, down fault samples

Thin sections were used to examine sub-millimetre scale geometries of shale smears. Thin sections were sampled at locations of specific interest, such as across shale smears or

deformation bands. Once a sample site had been identified the area was cleaned down with scrapers and water. To keep thin section material in-tact, small (7 x 10 cm) plastic containers were carefully hammered into the outcrop. This greatly increased the chance of the sample coming off the outcrop whole and not splitting along the fault trace as the container helped provide a confining pressure. These samples were then impregnated with resin (while still in the container) and thin sectioned. Due to the weak nature of the rock, the samples could only undergo minimal abrasion to get a flat surface which meant samples were several grains thick in places.

A big question for outcrop studies is whether they can be up-scaled to the seismic scale structures. In the MMF, simply taking observations from larger (e.g. >10 m through) faults exposed in the coastal cliffs is unfeasible as it becomes difficult to trace individual beds across the fault making measurement of displacement and bed contribution to fault-rock difficult to estimate. Furthermore, the larger fault-zones in Taranaki are often areas of intense erosion, which removes important structure as well as leaving the overhanging cliff unstable and difficult to access safely. Therefore, this study focusses on whether there are similarities in structure between micrometre and metre-scale structures with the view that those that exist over several orders of magnitude are likely to be present on seismic-scale faults. If the geometries of fault-zones are independent of scale, then the results from outcrop studies can be upscaled for use in seismic-scale analysis. It has been suggested that the mechanisms for fault growth (i.e. initiation, propagation, interaction and linkage) are the same both for individual faults and larger fault systems (Childs et al. 2017). Therefore, the same features observed on small-scale faulting at outcrop are likely to be applicable to larger scale (decametre to kilometre displacement) fault systems. The shared mechanisms mean that while fault-zone properties show a high degree of variability, faults are fractal and show self-similar geometries at a range of scales. These shared features often mean that the distinction between individual faults and fault systems is dependent on the scale of observation (Childs et al. 2017). Therefore, we are of the opinion that characteristics observed at outcrop in Taranaki are potentially applicable to the larger fault systems in the offshore Taranaki Basin.

3.2.2 Investigation of slip surfaces

Shale smear algorithms and seismic interpretations often treat faults as 2D linear structures with a uniform geometry both along dip and strike. However, field observations show that faults are far more complex, sometimes with extensive antithetic and synthetic faults slip surfaces (Figure 3.4 and Figure 3.5). These over-simplifications are only of concern if smaller fault components influence fault permeability. Smaller synthetic and antithetic faults are often disregarded during

modelling as it is assumed that they have little effect on fluid flow at basin scales (Manzocchi et al. 2010). However, in a thinly bedded turbidite sequence, such as that seen in the MMF, small scale synthetic faulting may lead to the juxtaposition of permeable layers creating a stepped series of thin beds producing a conduit for fluid flow across a fault (See Figure 3.3). Therefore, an investigation on the effect of different fault architectures on shale smear was conducted. The down fault profiles also helped constrain the degree of variability that can be observed on faults and also helps ascertain the predictability of these variations along a fault's length.

The thicknesses, lengths and locations of shale smears relative to the source beds have been measured by detailed mapping of the smears. Mapping was primarily conducted in the field and was augmented by analysis of detailed photographs (e.g. Figure 3.4). These data were used to measure the thickness of shale smears at systematic distances (e.g. 1 cm) along the fault trace.

Figure 3.4 Small-scale faults observed in the footwall of a displaced siltstone bed that is highlighted by internal organic rich horizons which are preserved within the fault-bound (slices) lenses in the fault zone. Fault exposed at Rapanui Beach.

3.2.3 Measurement of smear dimensions

To quantify smear geometries the lengths and thicknesses of smears in fault footwalls and hangingwalls have been measured for 185 individual faults. The ratio of hangingwall and footwall smears lengths was determined to constrain the symmetry of smears and to assess whether host

beds in the footwall and hangingwall contribute equally to smear formation (Lindsay et al. 1993). In addition, the geometries of individual smears were examined using regular measurements of smear thickness between the hangingwall and footwall cut off for 58 faults displacing siltstone beds. For each fault, 20 smear thickness measurements were taken at even spacings between the top of the footwall cut off and top of the hangingwall. The data enabled us to test the tapering smear model often proposed in the literature (i.e. smears generally thin with increasing distance from the hangingwall or footwall source beds). Lastly, the relationship between shale smear length and fault-zone thickness was investigated to assess whether wider fault zones promoted the formation of shale smears.

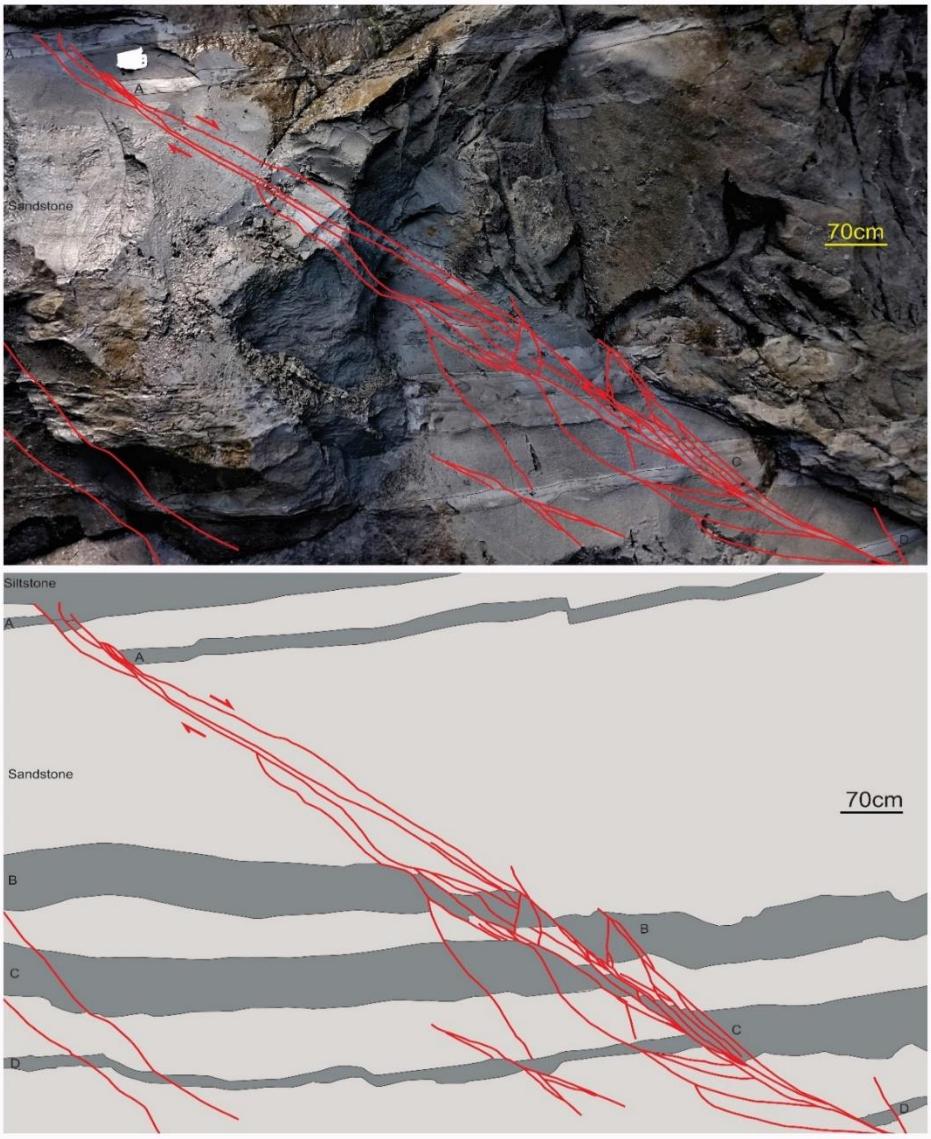

Figure 3.5 Fault from Rapanui Beach showing a complex fault-zone structure with both smearing and slicing. Slip surfaces regularly anastomose and bring host siltstone into the fault-zone. (A) Shows fault interpretation drawn over photograph. (B) Line drawing of fault in A.

3.3 Results

3.3.1 Shale smear geometries

A high degree of variation in smearing geometry, frequency and continuity is observed within the MMF. In this study 'siltstone' and 'shale' are used interchangeably to describe both host and fault rocks, a discussion of which is found in Chapter 1.3. A range of ductile shale smears (A-E) and no smear (F) geometries are as shown in Figure 3.7. By definition, what is typical of these ductile shale smears is the apparent absence of visible secondary faults which accommodate smear thickening or thinning. Photographs B-D show continuous smears with varying geometries, while A & E show discontinuous smears. In all of these cases the smears thin gradually away from the source bed, although detailed examination of the smear geometries suggests that this gradual thinning is not the norm (see section 3.3.2).

The production of shale smears by slip surfaces that bound lenses or slices are common in the MMF (Figure 3.7). As with the ductile shale smears, shale smears produced by slicing exhibit a range of geometries which reflect differences in the number of slices, the amount of overlap between slices and the location of the slice along a fault trace between the source beds. The examples of slices presented in Figure 3.7 show smearing that is being entirely accommodated by slicing (Figure 3.7A-C) and by a mix of slicing and ductile smearing (Figure 3.7D). At the scale of the individual faulted siltstone beds the individual slip surfaces may be approximately parallel to form rectangular bodies (B) but more often define lens-shaped bodies in the fault zone (Figure 3.7A, C & D).

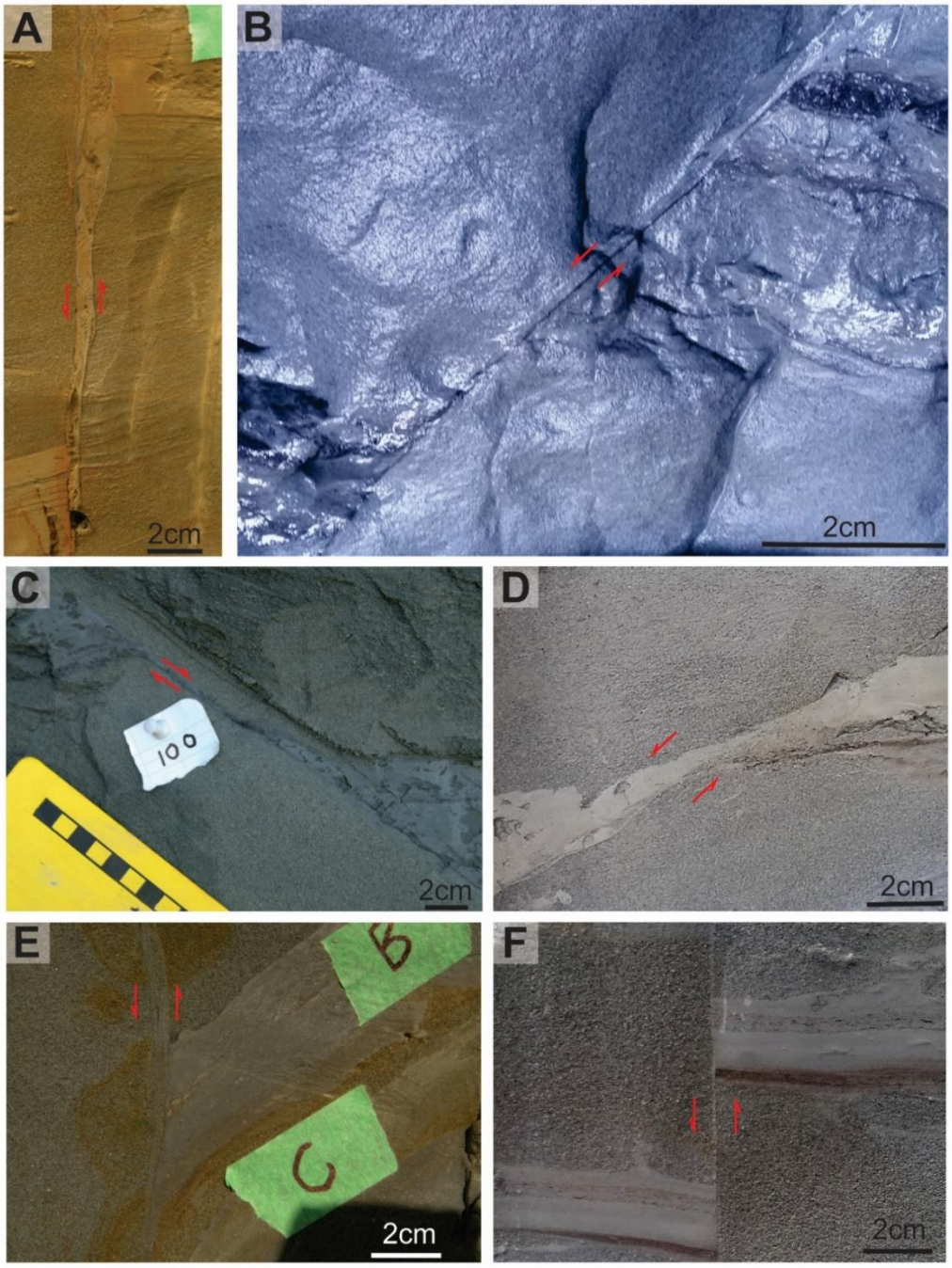

Figure 3.6 Photographs from the MMF, Taranaki, showing ductile smear and no-smear geometries. A) Discontinuous smear with a tapering geometry from Pukearuhe beach, B) thin continuous abrasion-type smear from Tongaporutu beach thought to comprise organic-rich material, C) continuous smear from Rapanui beach showing varying thickness along its length, D) continuous and relatively uniform thickness smear from Tongaporutu beach, E) bed B from Pukearuhe beach showing a short discontinuous smear and, F) example of beds showing no smear from Rapanaui beach (NB fine-grained light grey fault rock interpreted to be a cataclastic deformation band.

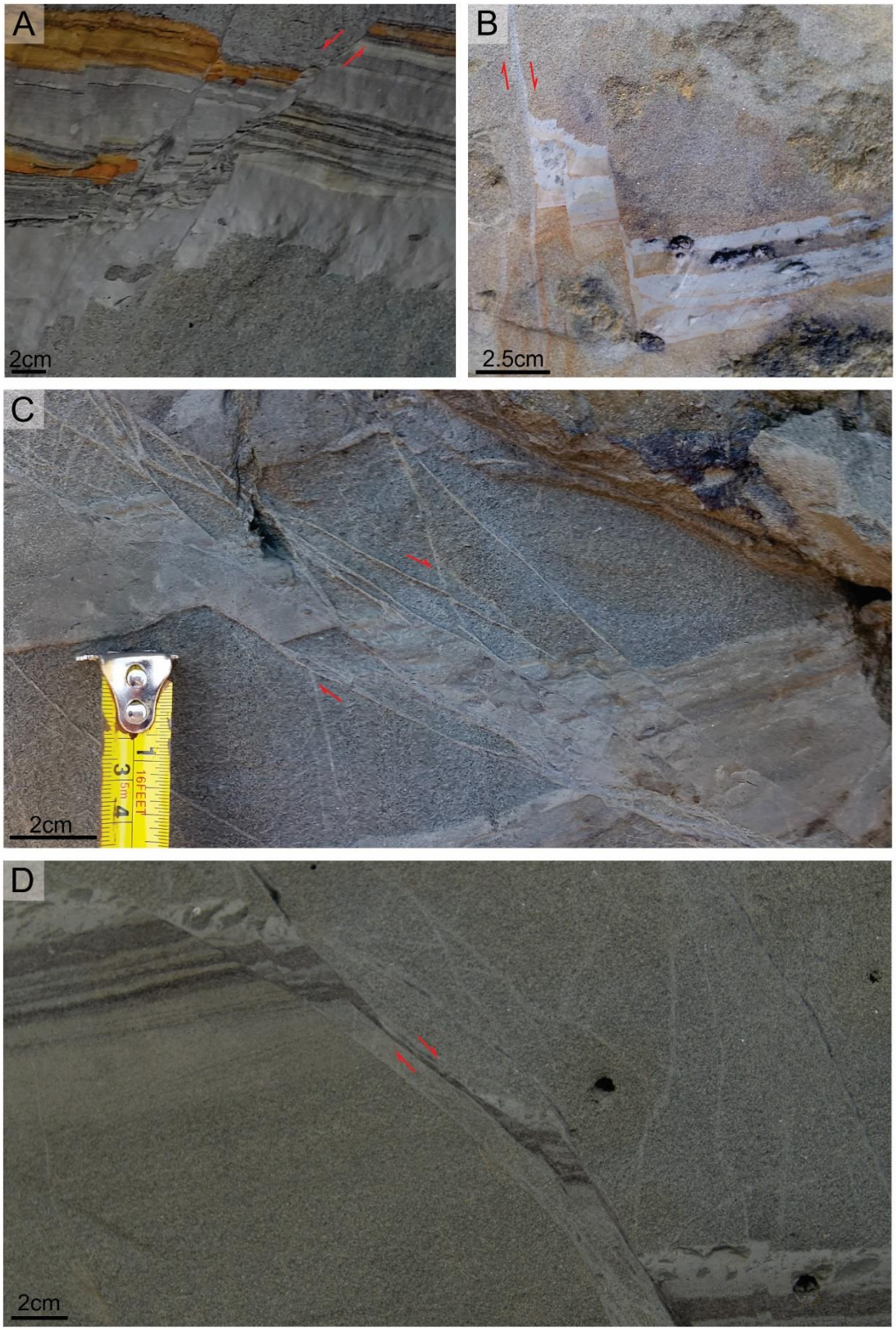

Figure 3.7 Compilation of faults showing slicing of siltstone beds in the MMF, Taranaki. A) Overlapping thin slices of bedded siltstone between the hangingwall and footwall source beds. B) Two slices that overlap and occur only a short distance from the hangingwall cut off, with no slicing along the rest of the fault. C) Large overlapping slices forming a continuous barrier of siltstone across the fault between source beds. D) Multiple slices that sit isolated between the two source beds. Dark brown source beds contain organic material.

In this study, shale smears formed by slicing of siltstone beds can be associated with up to nine slip surfaces (Figure 3.7 & Figure 3.8). In Figure 3.8 we have plotted the number of slip surfaces against the number of slices for footwall and hangingwall cut-offs from 139 fault zones in our shale smear dataset. As expected, the dataset shows a positive relationship between the number of siltstone bed slices and the number of slip surfaces. Siltstone beds with no smear (slicing) and multiple slip surfaces, plotted along the x axis of the graph, are formed in association with up to nine slip surfaces. In these cases, the slip surfaces are contained entirely within sandstone beds, forming deformation bands, and do not produce slices of siltstone beds.

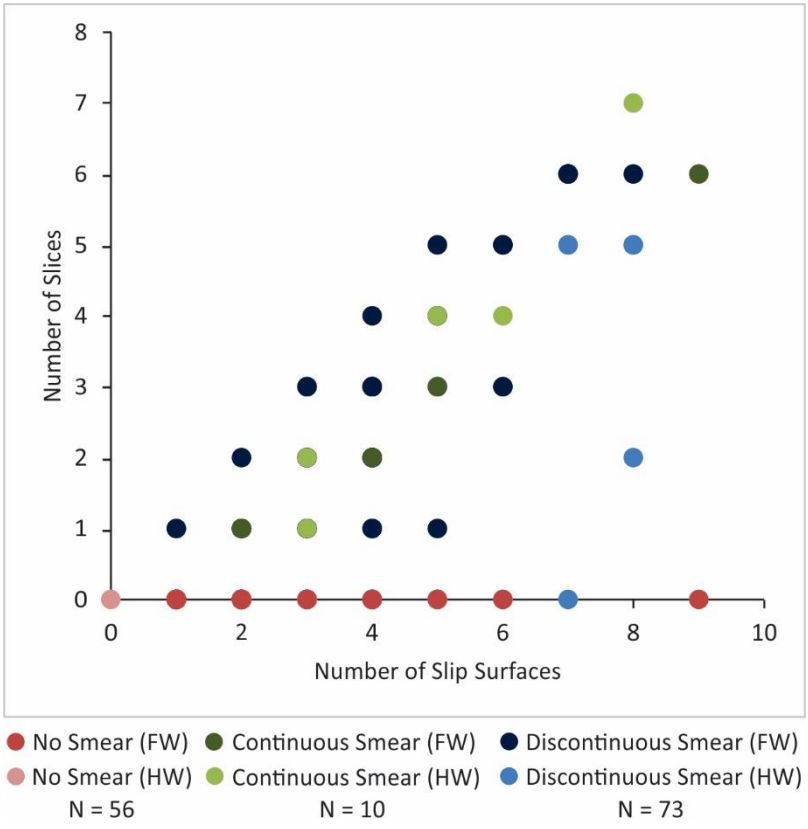

Figure 3.8 Graph showing the relationship between the number of slip surfaces and the number of slices for faults with no smear, discontinuous smear and continuous smear. There is a positive relationship between the two variables for discontinuous and continuous smears.

In summary, based on the observations from Taranaki, it is suggested that shale smear forms a spectrum of geometries with three end members. The ends of the spectrum includes beds that show no contribution to the fault-zone and instead are cleanly cut by slip surfaces with no evidence of shale becoming entrained into the fault. Shale smear of beds in a ductile fashion accounts for a second end member with the degree of smearing ranging from beds that show almost no smear to those that show a continuous smear veneer along the entirety of the fault

surface. The third end member are beds that have been sliced only. These slices are characterised by undeformed segments of host shale that still contain original structures within the fault-zone. They are bounded by slips surfaces and show little to no mixing with the surrounding host or fault-rock. There may be multiple overlapping slices providing a continuous barrier to flow between cut offs or a single isolated slice that exists anywhere between the host units. Finally, there are siltstone beds that show a mix of smear and slicing that range from minimal coverage of the displaced section to providing a clear continuum of low permeability fault-rock across the fault-zone. All three geometries have been encountered by other authors and therefore it is proposed that all previous results could be plotted on the below diagrams in a bid to describe and surmise their smearing styles.

3.3.2 Shale smear statistics

The results neither support the idea that all siltstone beds smear nor that the incorporation of fine-grained host rock into fault zones is always achieved by ductile shear processes. Of the 184 faulted siltstone beds sampled in the MMF, 71 beds showed no resolvable evidence of smear. In these cases the faults most often comprise a single slip surface (or deformation band) with sharp and often high-angle footwall and hangingwall horizon cut-offs (

Figure 3.6F). Of the remaining beds, 90 exhibited discontinuous smears between the siltstone bed cut-offs and 23 displayed continuous smear between the cut-offs. These general statistics were observed from the four different beaches, although the percentage of non-smeared beds decreased from Pukearuhe beach in the South to Mohakatino beach in the North (see Figure 3.9). Of the siltstone beds that show shale smear, ~50% (N=57) displayed a ductile smear geometry, ~30% (N=33) comprised entirely slices and ~20% (N=23) of beds displayed a combination of ductile smear and slicing (see Figure 3.7D). These statistics support the view that smear geometries can range from no smear, to ductile smear only, to slicing only and to a combination of both ductile and brittle smearing (see Figure 3.10). Our results are consistent with previous studies (e.g. Ciftci et al., 2012; Vrolijk et al,. 2016) in suggesting that secondary faulting within fault zones and associated slices produce an important form of shale smearing. In the MMF about half of all faults studied showed some siltstone bed slicing.

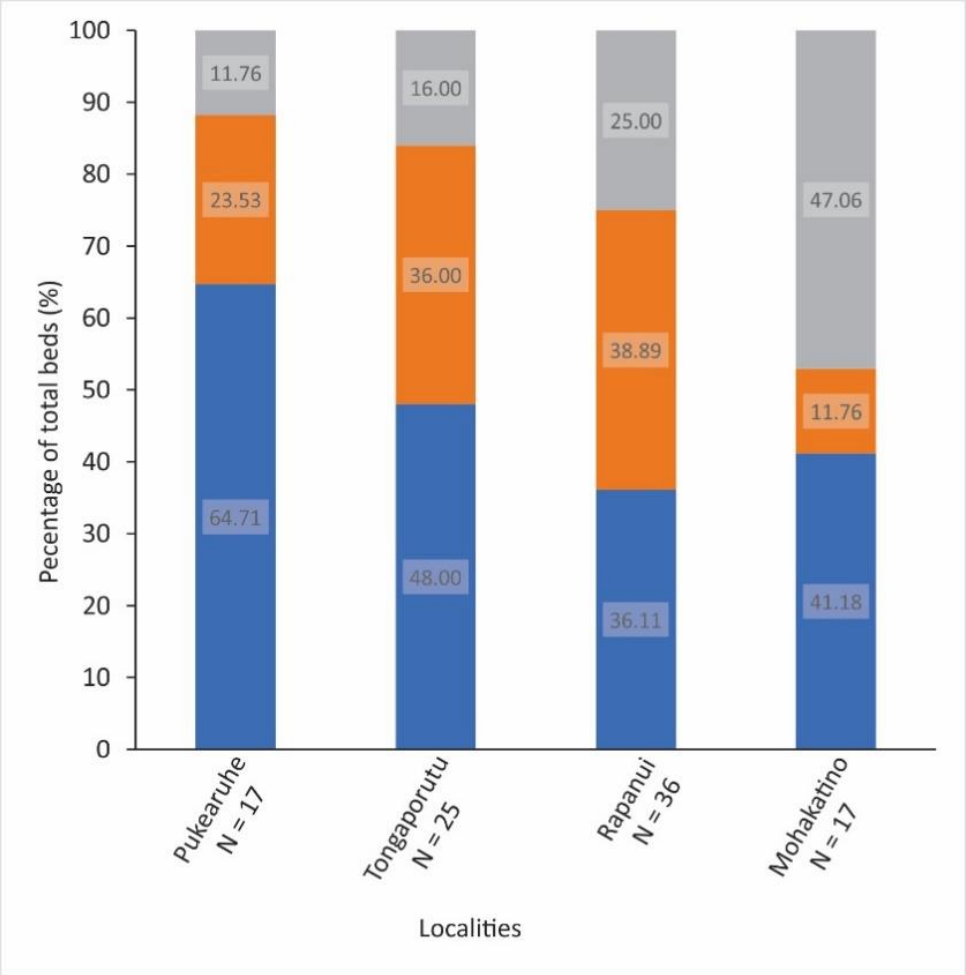

Figure 3.9. Graph showing shale smears from each beach in the MMF with the three types of smear (ductile smear, blue; slicing smear, orange; mixed ductile and slicing smear, grey). Percentages of each smear type are shown by numbers on the bars. Number of observations for each beach are given on the x-axis.

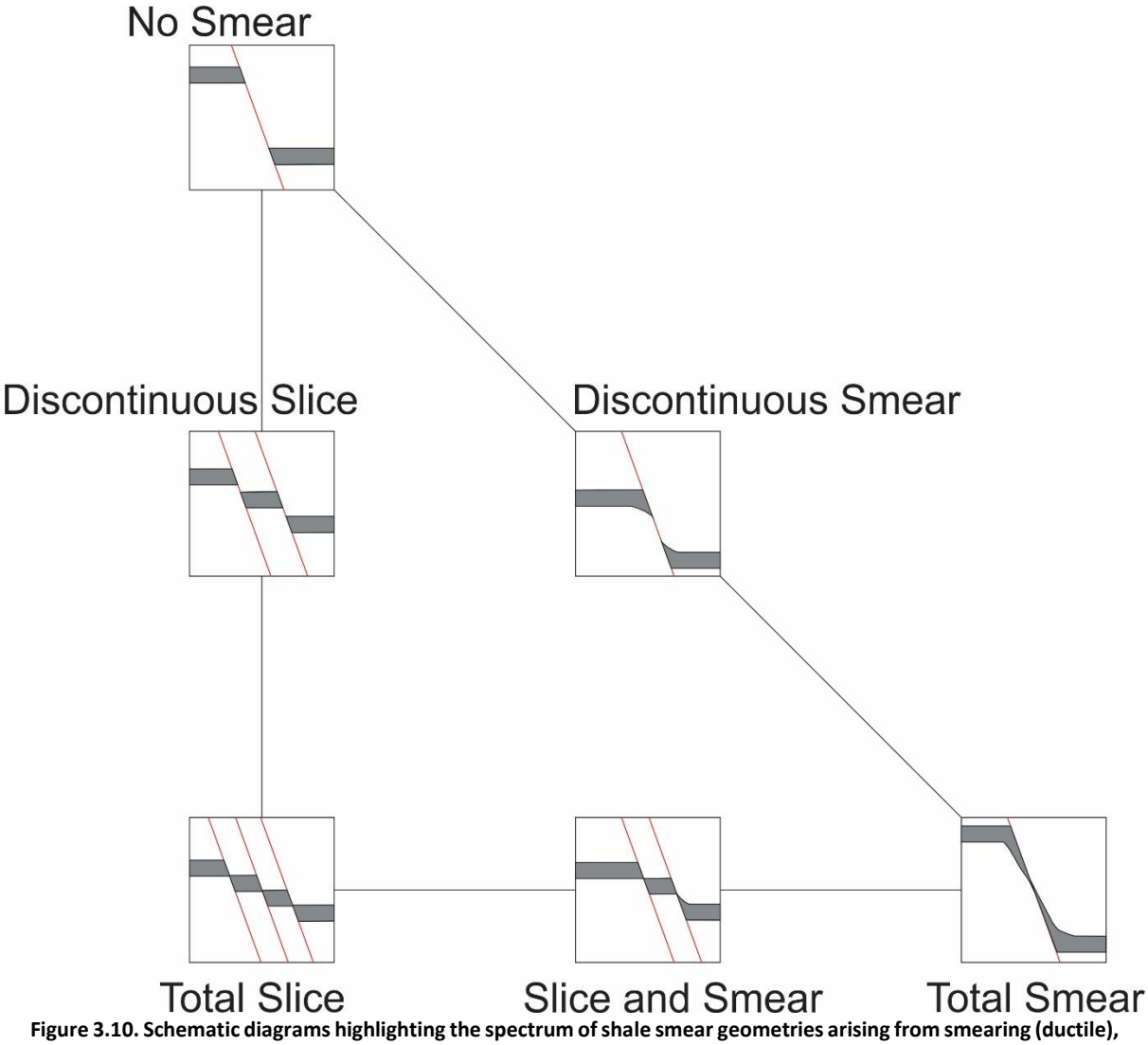

Figure 3.10. Schematic diagrams highlighting the spectrum of shale smear geometries arising from smearing (ductile), slicing and a combination of smearing and slicing.

The first-order numbers presented above provide little information about the detailed smear geometries and, for example, how many of the smears observed display tapering geometries consistent with a shear-zone model. To test for potential smear geometries that could have tapering forms we have measured the smear lengths for footwall and hangingwall beds on each fault and plotted these data in Figure 3.11. In this figure faults plotting close to the 1:1 line (i.e. smear lengths for footwall and hangingwall that differ by <20%) are characterised by smear that generally taper away from their respective sources towards the mid-point. The wide scatter in the graph about the red 1:1 line suggest that many of the observed smears do not display a tapering geometry (Figure 3.11). In fact, of the smears measured only 14% of the discontinuous smears sampled displayed a shear-zone tapering geometry. Approximately equal numbers of smears plot next to the x axis, y axis and the 1:1 line. These data suggest that many faults exhibited smear in only the footwall (i.e. plot on the x-axis) or hangingwall (i.e. plot on the y-axis). These results are

consistent with a previous study of shale smears in the MMF for which examples of tapering smears from both cut offs were found to be extremely rare (Childs et al. 2007).

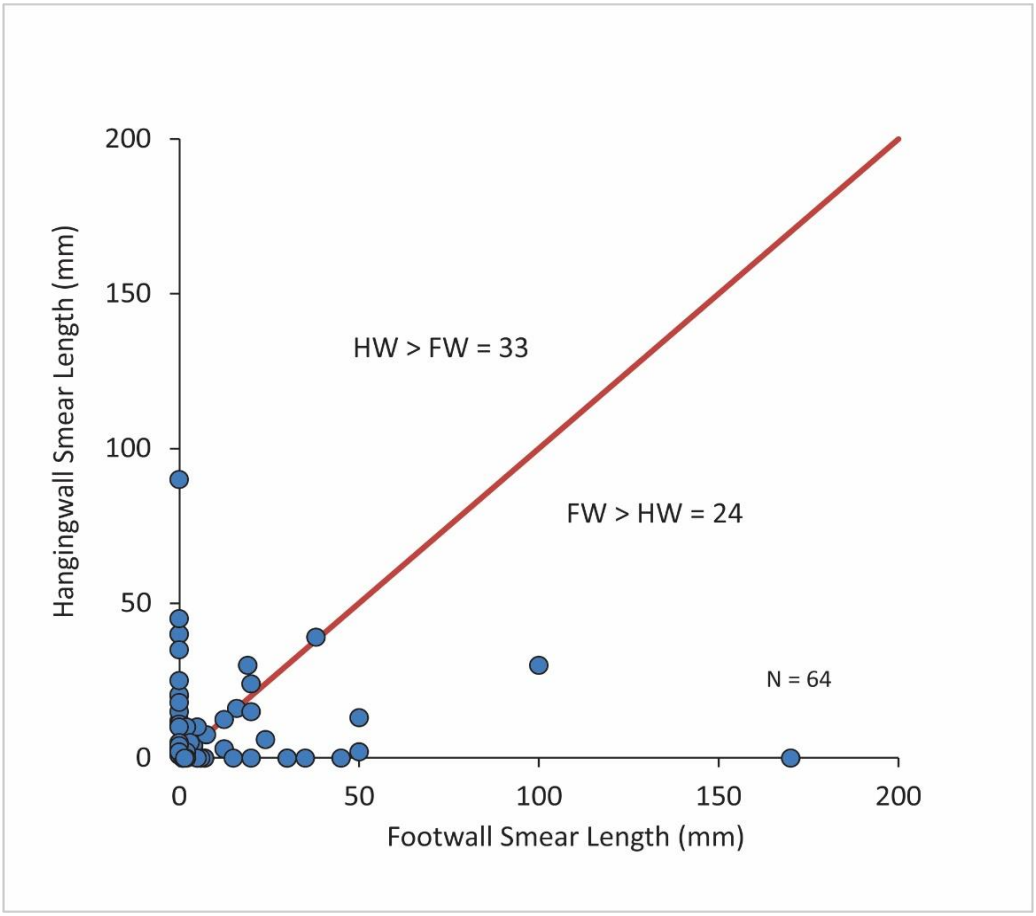

Figure 3.11. Measurements of smear lengths from hangingwall (y axis) and footwall (x axis) cut offs. Equal footwall and hangingwall smear lengths plot on the 1:1 line. For data above the 1:1 line hangingwall lengths exceed footwall and below the line footwall lengths are greatest.

In cases where smears are thickest at the host shale cut off and thin away from the bed until holes appear, it would be expected that the smear would most often break midway between the cut-offs leaving almost equal length sections of the smear in both the hangingwall and the footwall. Only about one third (~30%, N=19) of discontinuous smears were connected to both hangingwall and footwall cut offs, while only 13 % (N=8) had breaks in smears approximately midway between the cut-offs. In the majority of cases (~70%) smear was restricted to one side of the fault. These data indicate that breaks in smears are likely to occur anywhere between the cut-offs. Again, Childs et al. (2007) produced similar conclusions which led to their development of Probabilistic Shale Smear Factor (PSSF), where the locations of shale smears are equally as likely to occur at any location between the cut-offs (i.e. the locations of the smears are considered to be random). Lastly, shale smear length does not appear to increase with fault zone thickness (Figure 3.12). No

relationship was found between smear length and fault-zone thickness and data from both the hangingwall and footwall cut off plotted in the same area of the graph.

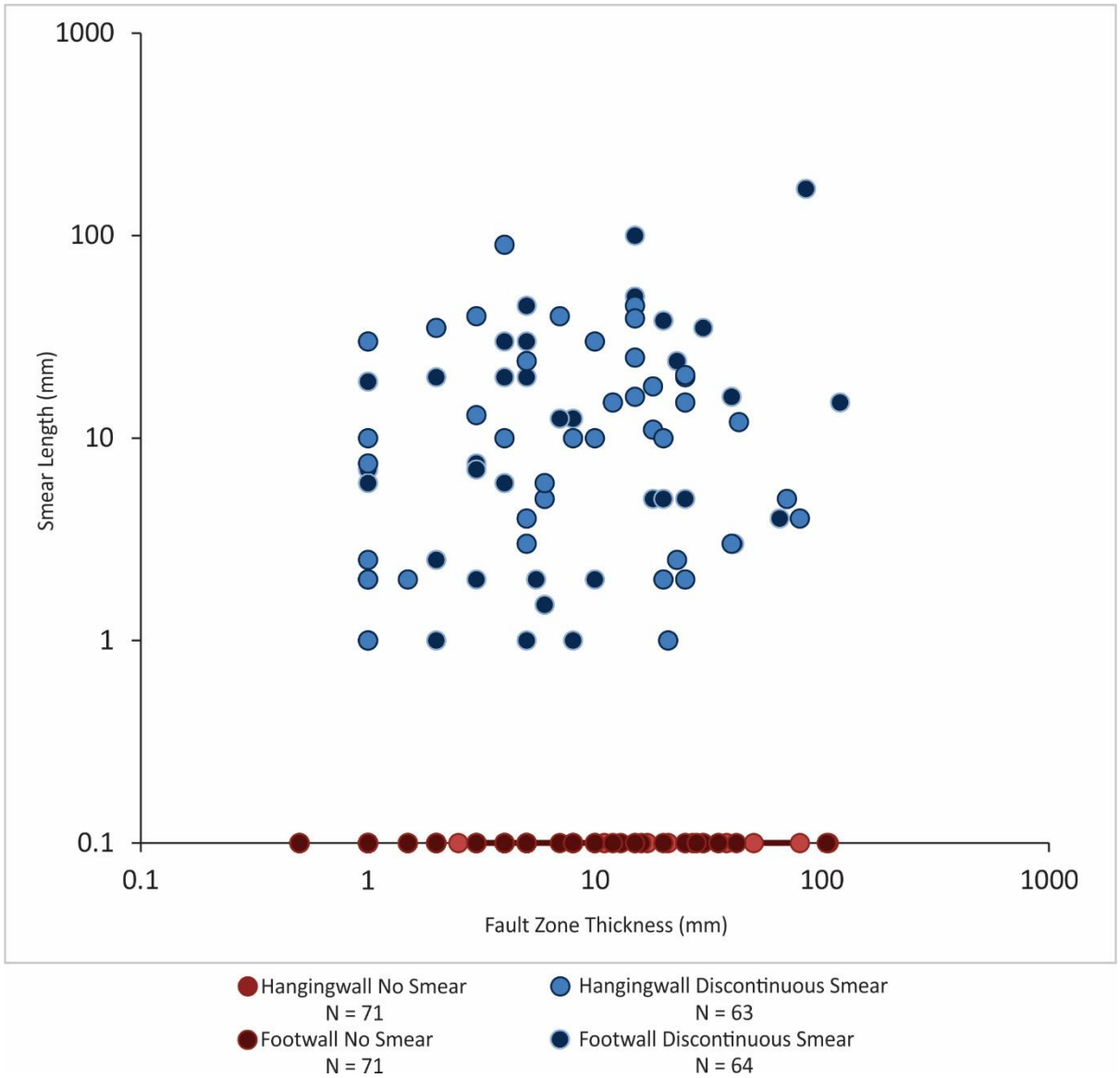

Figure 3.12. Fault-zone Thickness plotted against Smear Length. Both hangingwall and footwall cut offs show a similar spread of data with values for both smear length for a given fault-zone thickness and vice versa showing an nearly two orders of magnitude variation in places.

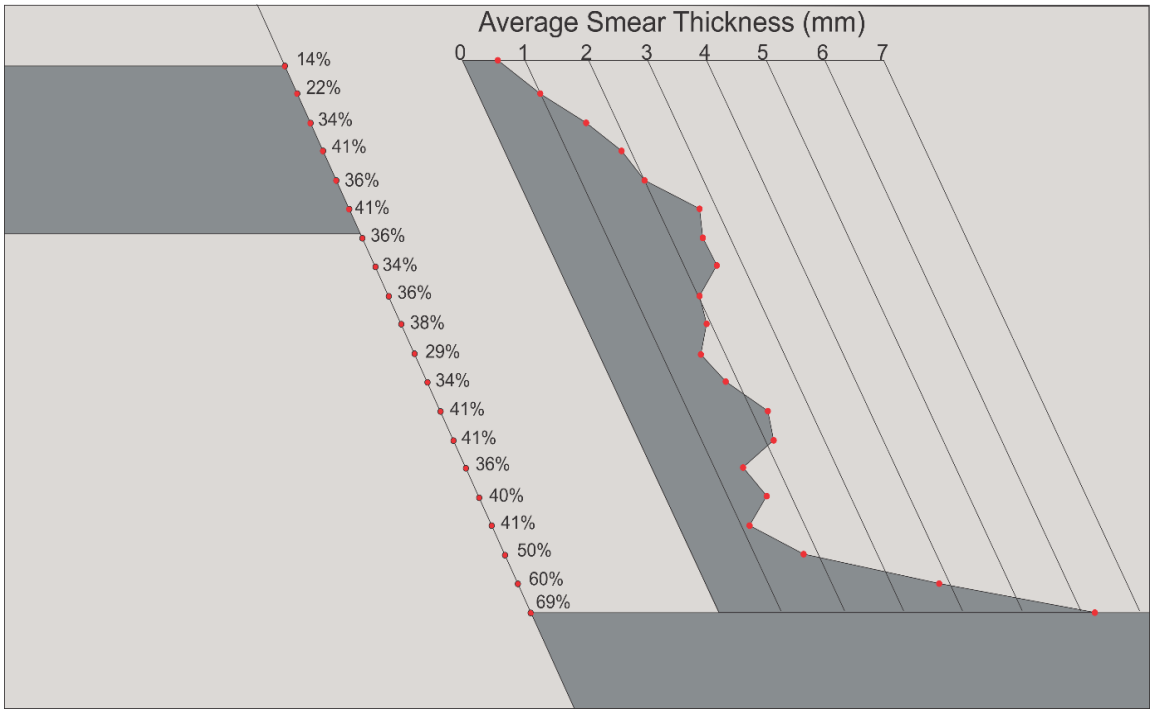

Figure 3.13 An infographic showing the average smear thicknesses for 58 individual displaced siltstone beds. The red dots represent the average thickness for each of 20 sample points (right graph) and the percentages (left numbers) are the chance of smear thickness. The grey horizontal polygons represent the host bed. Distance along the fault is normalised to the displacement.

In their study, Childs et al. (2007) measured smear thickness vs the distance from the host bed for 15 siltstone beds in the MMF, Taranaki. They found that shale smear was generally continuous when displacement was less than eight times the bed thickness. We expanded on the work of Childs et al. (2007) by conducting similar measurements for a larger number of beds (58) and calculating the likelihood of smear at numerous points between the two cut offs. Using a similar approach we measured the thickness of the clay smear at 20 evenly spaced intervals between the top of the footwall bed to the top of the hangingwall for 58 faulted siltstone beds (Figure 3.13). This was conducted to investigate the variation in shale smear thickness along fault-zones. While there is some smear thickening towards the hangingwall cut off, there is no systematic correlation between the location of the smears relative to the cut-offs and their thickness. Furthermore, there was no evidence for smears systematically thinning towards the mid-point between the host cut off as would be expected for a shear zone tapering geometry. Kettermann et al. (2016) also found that the tapering geometry was not always applicable and suggested that the geometry of the smears was controlled by locations and displacements of slip surfaces that intersect the smears. We believe that such slip surfaces may also be important for the MMF and discuss this further in section 3.4.1. Independent of the mechanisms that control smear thicknesses, the available data for smear thicknesses could be approximated by assuming that

there is no relationship between smear location relative to the source beds and smear thickness. If the distribution of low permeability fault-rock along a fault trace is random then it becomes difficult to predict the likelihood of smear continuity. Without knowing the controls on smear, a stochastic probabilistic approach could provide a useful means for approximating shale smear thicknesses in fault zones. The output of deterministic models is based entirely on the input parameters and initial conditions. Without knowing exactly what these inputs and conditions are there is uncertainty as to whether the results from such approaches are widely applicable representations of smears. Stochastic modelling includes inherent randomness, so that even with the same input parameters and initial starting conditions different results will be generated. Having a variety of results could help account for uncertainty and the high degree of variability associated with fault elements such as fault-rock thickness. It is hoped that by having a range of possibilities for the same data that the actual smear behaviour will fall between the end members of the range generated and different models can be constructed using the different results produced. The PSSF method developed by Childs et al. (2007) used stochastic modelling to produce a range of overlapping smears from multiple beds to assess the likelihood of smear continuity between host cut offs and the impact of smear holes on across fault flow.

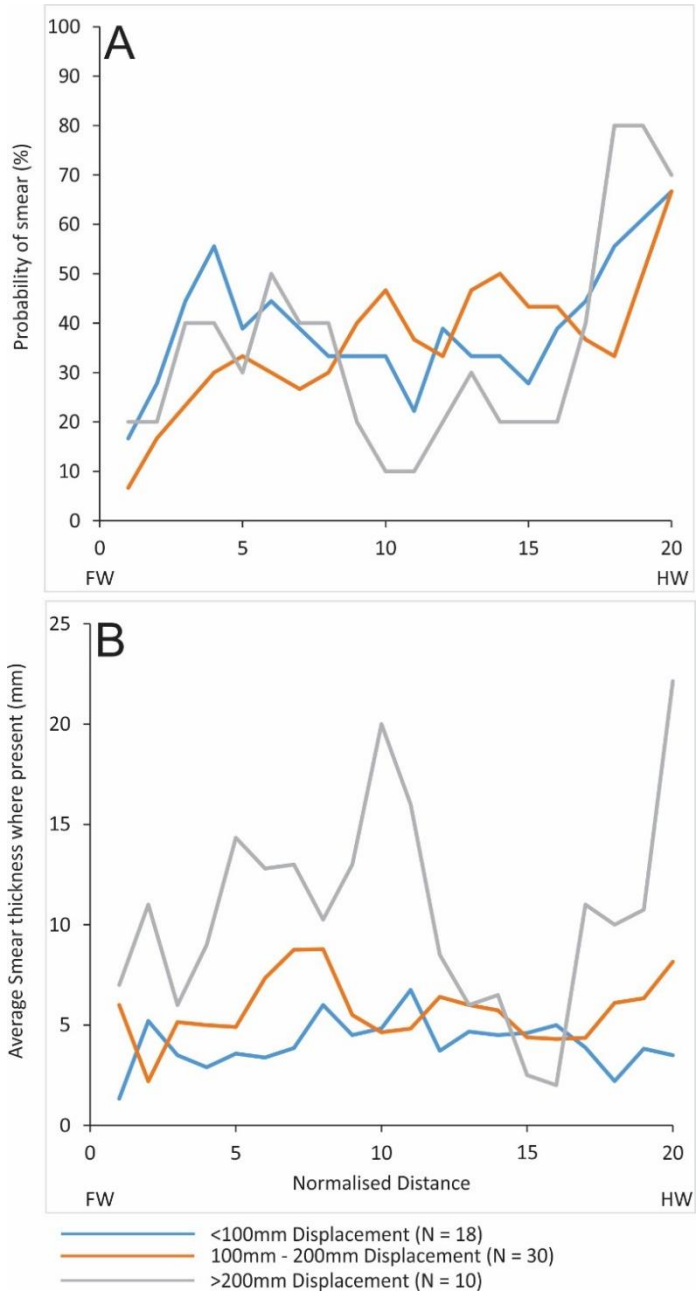

Figure 3.14 A) Graph depicting the probability of smear versus normalised distance between host cut offs for a range of displacements (see key below B). B) Graph showing the average smear thickness plotted against normalised distance along faults for three groups of fault displacements. Probability of smear was calculated by taking the number of faults that showed smear for a given point and dividing by the total number of beds to generate a percentage of beds that smeared at that point along the fault.

To assess what control the displacement had on smear thicknesses in the MMF the data was split into three categories according to the amount of displacement observed on the fault. These fault groups were: <100 mm (18 faults), 100-200 mm (30 faults), >200 mm displacement (10 faults).

In

Figure 3.14 the shapes of the curves are similar for faults with <100 mm and 100-200 mm displacements. The grouped displacement plots for displacements <200 mm are comparable to all 58 beds measured and suggest an elevated probability of smear adjacent to the hangingwall cut-off. The >200mm displacement group also displayed an increase in probability of smear adjacent to the hangingwall cut-off (i.e. three data points closest to the hangingwall cut-off)(

Figure 3.14). In the average thickness plot of

Figure 3.14B smear thicknesses for faults with <100 mm and 100-200 mm displacements are similar across the range of normalised distances, whereas smears for the >200 mm displacement faults are thickest midway between the cut-offs and immediately adjacent to the hangingwall cut-off. Interestingly, the smears appear to show no decrease in average thickness with increasing displacement, which is counter to a model in which smears progressively thin with accrual of displacement. If the observed thickening with increasing displacement is correct (and more data are required to test this observation), then the data suggest the addition of smear material with increasing displacement. The addition of new shale into the fault zone could reflect increased mixing of sandstone and siltstone, or possibly to the generation of 'smear' arising from cataclastic processes (see Nicol and Childs, 2018).

3.4 Discussion

3.4.1 Ductile vs brittle shale smear

Shale smears observed at outcrop scale have previously been described as ductile, with siltstone beds appearing to be dragged or abraded, and brittle with smears forming in association with slip surfaces (Vrolijk et al. 2016). Both brittle and ductile shale smears result in shale beds being incorporated into and along fault-zones (see Figure 3.15), however, they are often considered to be different processes. Differences in the deformation styles of shale beds is often attributed to changes in the mechanical properties of the deformed beds (Fulljames et al. 1997; Schmatz et al. 2010; Pei et al. 2015). However, in this study we have noticed that the same beds form both ductile and brittle shale smears. Because these beds do not vary in their mechanical properties, the question arises as to why they can display different types of deformation. Here we test the hypothesis that all shale smear structures form by brittle deformation processes and the difference between ductile and brittle deformation is due to the scale of faulting. In other words, ductile shale smears mainly form by brittle faulting that is too small to be observed at outcrop

scale, and the type of deformation is dependent on the scale of investigation. To test this idea we have thin sectioned a number of shale smears that primarily form by ductile smear.

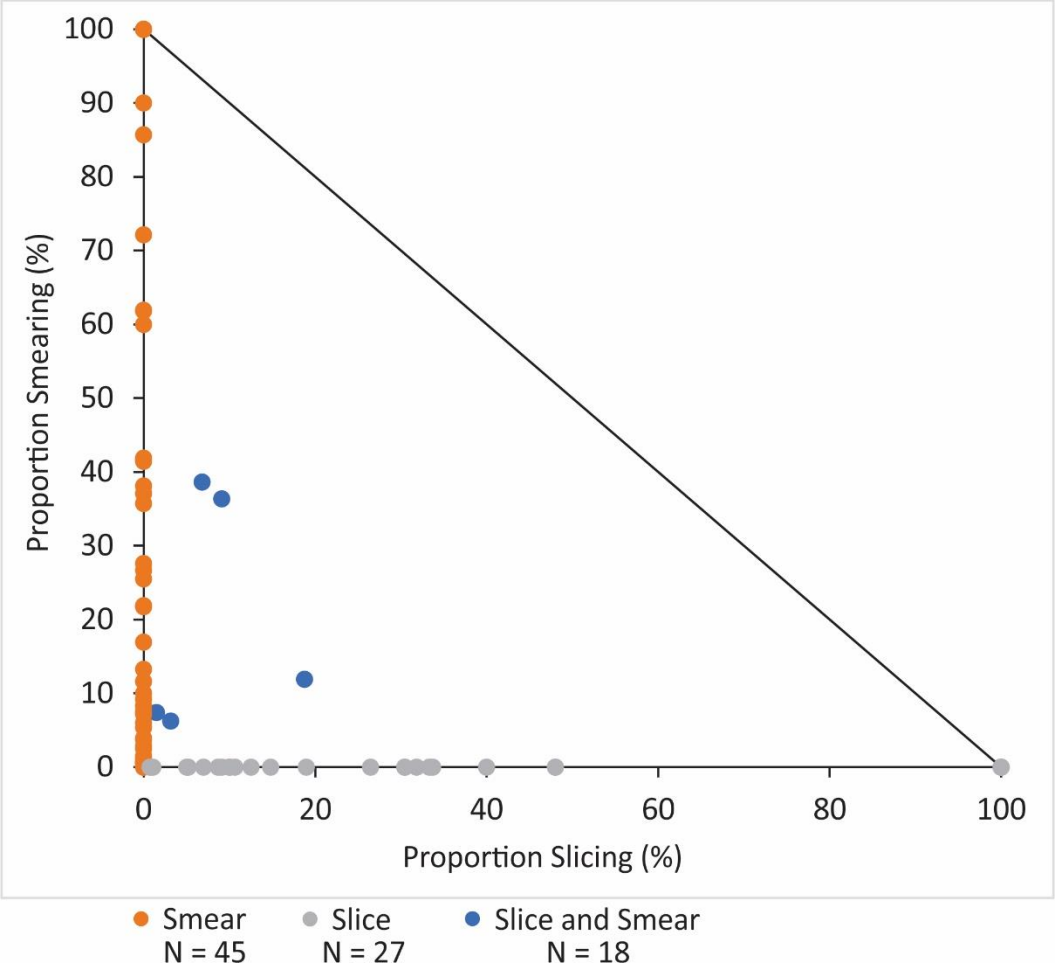

Figure 3.15 Graph depicting how siltstones beds from Taranaki would fall on the above spectrum. As can be seen beds are predominantly either sliced or smeared with very few exhibiting a combination of processes. The proportion of slicing and smearing was calculated by assessing what proportion of the fault trace between cut offs contained shale with this then being split according to the proportion of shale that showed internal deformation (smear) and shale that had sedimentary features intact (slice).

Thin sections of ductile shale smears from the MMF typically indicate that smearing is primarily accommodated by micro-scale faults. RAP 102 is a sample from a ductile shale smear that was taken at Rapanui Beach in the Lower MMF (Figure 3.16). The sample is 2.5 cm across and 7.5cm long and contains only smear from the footwall host units which comprise sand, shale and organic matter. The fault zone in the thin section is bounded by two slip surfaces which define a lens-shaped zone. Within the fault-zone lens there are many smaller synthetic and antithetic slip surfaces with displacements of mainly <500 µm that are present along the length of the sample. The micro-faults in the thin section define sharp boundaries between beds and there is little or no evidence of mixing or sand grains within the siltstone beds. The lack of mixing has been

previously studied by Giger et al. (2013) and supports the conclusion that the relative positions of individual layers within the slices are not changing significantly. Due to a lack of grain mixing or grain-size reduction, the original sedimentary fabric of host sandstone and siltstone in the fault zone can still be observed within micro-slices (Figure 3.16). In addition to the sandstone and siltstone beds a dark organic-rich unit appears to smear continuously along the slip surfaces. At thin section scale the organic smear thickness is ~200 µm and comprises a series of overlapping slices. It remains possible that the organic layer is also smearing by faults too small to be observed even in thin section or that the organic layer is weak and deforming plastically.

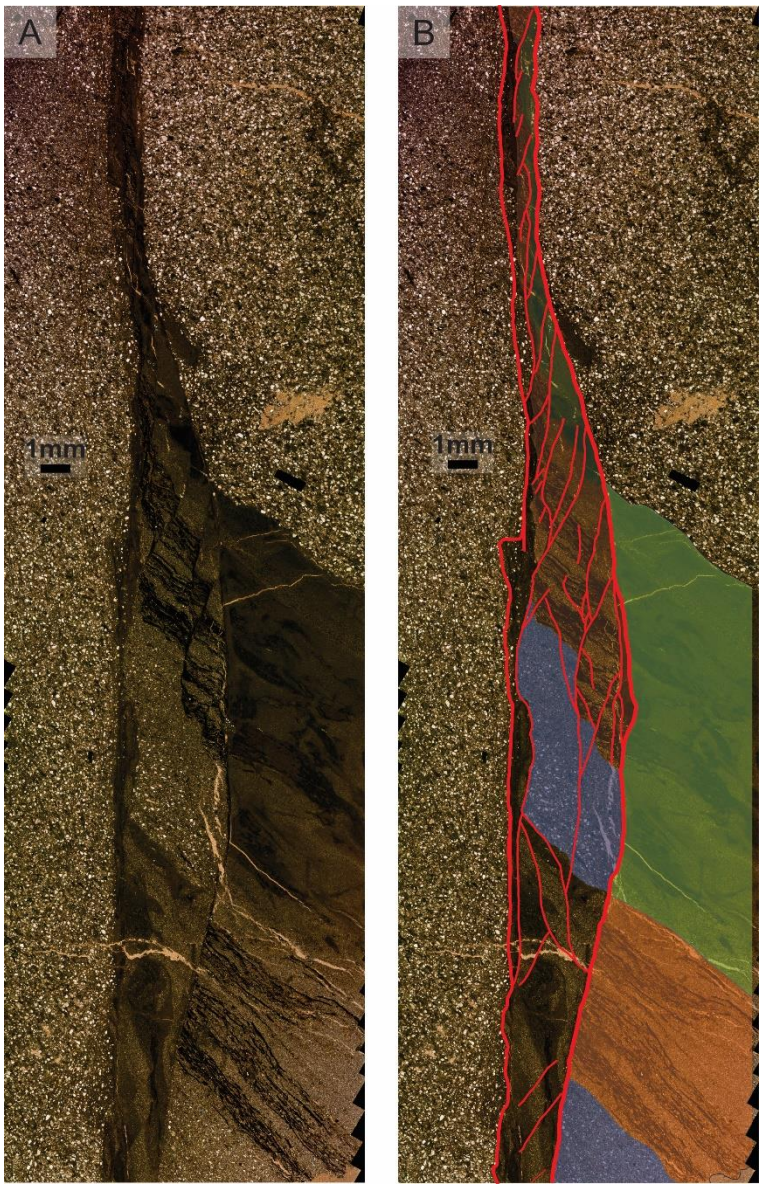

Figure 3.16. RAP 102 ductile shale smear thin section across the footwall of a smeared siltstone bed from Rapanui Beach showing micro scale slip surfaces and slices. A) Uninterpreted thin section. B) Interpreted thin section showing micro-faults and source beds. Blue granular unit is a fine sandstone, the orange unit is a siltstone with organic rich horizons (dark, long and thin layers), green is another siltstone.

3.4.2 Implications for fault permeability

The geometries of shale smears may have an impact on fault-rock permeability across some fault zones. In particular, the location, length and continuity of smears together with the number and spacing of small synthetic faults slicing up the shale beds in the fault zone could impact fault permeability.

Synthetic faults within fault zones are common in the MMF and may occur at any location relative to siltstone beds, making it difficult to predict where along the main fault slices are likely to be located. It is widely recognised that these secondary faults are often responsible for producing changes in the thickness of shale beds incorporated into fault zones. Kettermann et al. (2016) identified reidel shears locally displacing smear, leading to 'holes' and thinning of the smear within the fault-zone. We believe that slicing and ductile deformation are both part of a brittle process with both slices and apparently ductile shale smears being lensoid in shape. Thus, the incorporation of host siltstone into the fault zone typically produces a 'slice' geometry in 2D that is expressed as a lens in 3D; as illustrated in Figure 3.17. In addition, fault zones comprising smaller slip surfaces can lead to inaccuracies in juxtaposition predictions in cases where multiple slices of fault-rock in the fault-zone are not recognised and the fault is assumed to comprise a single slip surface (van der Zee and Urai 2005). This assumption is highly problematic, especially when considering large fault-zones with high displacements as these are more likely to be complex with multiple slip surfaces. Even on small-scale faults an increase in the number of slip surfaces can greatly impact the composition and juxtaposition of fault-rock against host rock.

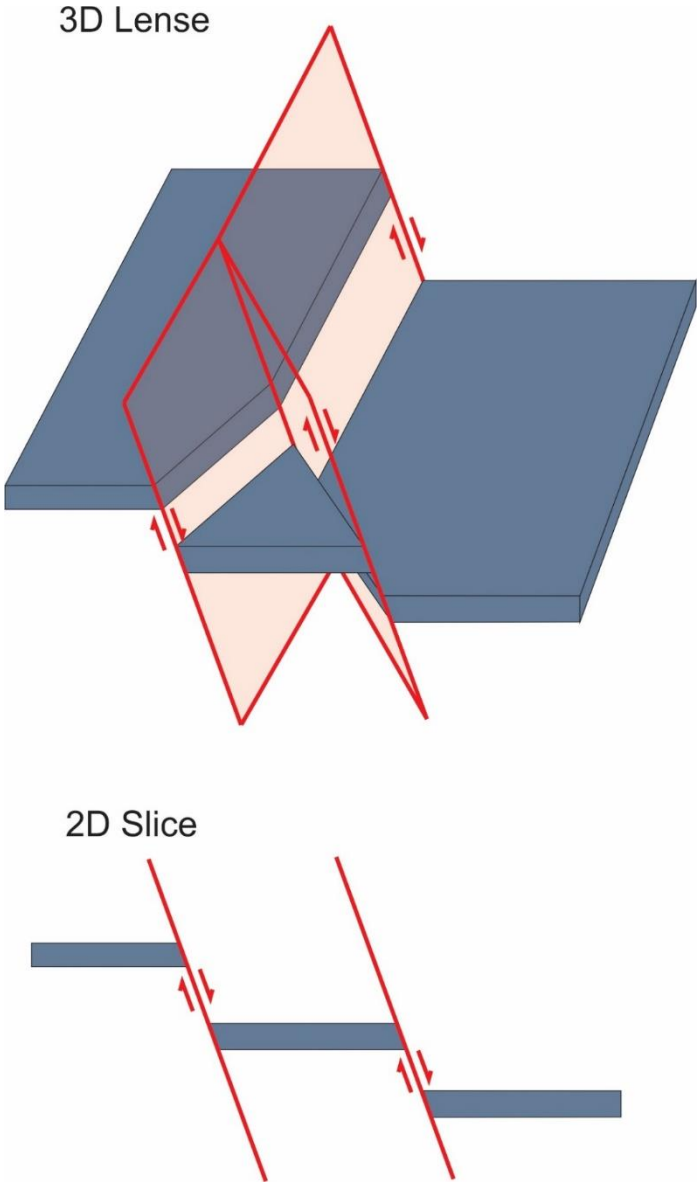

Figure 3.17 Schematic diagram showing how the siltstone slices observed at outcrop are likely to be a cross section of a fault lens when looked at in 3D.

The location of discontinuous smears could impact the accumulation of fluids adjacent to faults. Yielding (2012) raised the important issue of the location of holes or gaps in the smear. He showed that the amount of smear in the footwall controls the ability of a fault to pool fluids in a scenario where the smear is discontinuous. By contrast, the hangingwall smear length is less relevant (than footwall smear) as it will not prevent fluids flowing laterally out of the trap on the upthrown side of a fault. Figure 3.18 shows a schematic diagram which highlights the importance of footwall derived smear in trapping fluids. In the case of the MMF, where hangingwall smears appear to be slightly more common than footwall smears, reservoir rocks in the footwall may be less likely to host fluids than if most smears were located adjacent to the siltstone bed in fault footwalls (Figure 3.18). Individual shale smears may be less continuous on larger faults (compared to small) as fault-

zones will be more complex for larger displacements with more smaller synthetic faults. The focus therefore would be on the continuity of low permeability fault rock as a whole, either as overlapping smears sourced from multiple beds or the affect of cataclasites and phyllosilicate framework rocks bridging the gaps between smears. For both small and large faults the length of the seal from the footwall shale bed is the primary control on the volume of fluid trapped by the fault. Any hole or gap in the seal that exists would act as the spill point, meaning any low permeability seal located near or at the hangingwall would have a negligible affect on in place reserves.

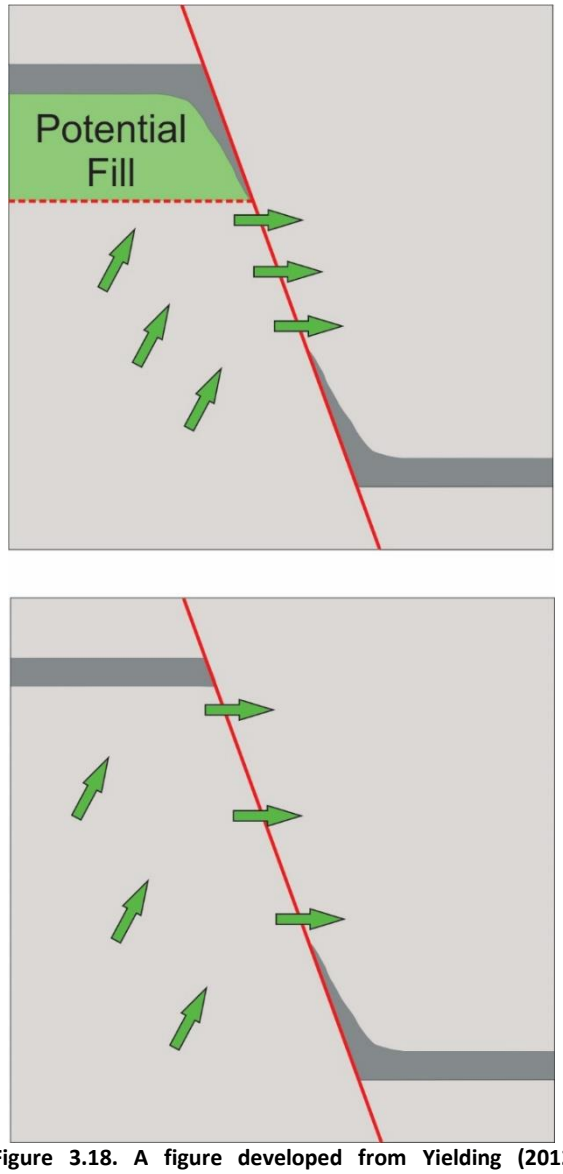

Figure 3.18. A figure developed from Yielding (2012) showing the impact of hangingwall and footwall smears on fluid accumulation. In this scenario it is only the length of the footwall smear that is important, with fluids able to migrate elsewhere even at almost continuous hangingwall smears.

3.5 Conclusions

The geometries of shale smears on small displacement (<1 m) normal faults in the MMF are highly variable. At outcrop-scale shale smears appear to be produced by a combination of ductile deformation and brittle faulting, with individual smears being produced by one or both of these processes. Individual beds can accommodate both brittle and ductile deformation, suggesting that apparent changes in the deformation style of beds is not entirely dependent on their mechanical properties. Thin sections of ductile smears indicate that they are primarily deformed by micro-faulting and brittle deformation. Therefore, smearing in the MMF is primarily a brittle process, with the type of deformation observed sometimes being dependent on the scale of observation. Displaced siltstone beds in the MMF can produce no shale smear, discontinuous shale smear and continuous shale smear between the source beds. Analysis of the smear thicknesses suggests that on average the thickest smears are not located proximal to the source beds. Therefore, holes in shale smears do not appear to preferentially form at the midpoint between cut offs. The available smear data suggest that stochastic models may provide a means of populating shale smear thicknesses in fault zones.

3.6 References

Bense VF, Gleeson T, Loveless SE, Bour O, Scibek J. 2013. Fault zone hydrogeology. Earth-Science Rev. 127:171–192. doi:10.1016/j.earscirev.2013.09.008.

Browne GH, McAlpine A, King PR. 1996. An outcrop study of bed thickness, continuity and permeability in reservoir facies of the Mt. Messenger Formation, North Taranaki. In: New Zealand Petroleum Conference Preceedings. p. 154–163.

Caine JS, Evans JP, Forster CB. 1996. Fault zone architechture and permeability structure. Geology. 24(11):1025–1028. doi:10.1130/0091-7613(1996)024<1025.

Caramanna G, Fietzek P, Maroto-Valer M. 2011. Monitoring techniques of a natural analogue for sub-seabed CO2 leakages. Energy Procedia. 4:3262–3268. doi:10.1016/j.egypro.2011.02.245.

Cartwright J. 2011. Diagenetically induced shear failure of fine-grained sediments and the development of polygonal fault systems. Mar Pet Geol. 28(9):1593–1610. doi:10.1016/j.marpetgeo.2011.06.004.

Childs C, Holdsworth RE, Jackson CAL, Manzocchi T, Walsh JJ, Yielding G. 2017. Introduction to the geometry and growth of normal faults. Geol Soc Spec Publ. 439(1):1–9. doi:10.1144/SP439.24.

Childs C, Manzocchi T, Walsh JJ, Bonson CG, Nicol A, Schöpfer MPJ. 2009. A geometric model of fault zone and fault rock thickness variations. J Struct Geol. 31(2):117–127. doi:10.1016/j.jsg.2008.08.009.

Childs C, Walsh JJ, Manzocchi T, Strand J, Nicol A, Tomasso M, Schopfer MPJ, Aplin AC. 2007. Definition of a fault permeability predictor from outcrop studies of a faulted turbidite sequence, Taranaki, New Zealand. Geol Soc London, Spec Publ. 292:235–258. doi:10.1144/SP292.14.

Ciftci BN, Giger SB, Clennell MB. 2012. Testing Fault Seal Prediction Algorithms Using Geomodels of Experimentally Produced Fault Zones. 3rd EAGE Int Conf Fault Top Seals.(October). doi:10.3997/2214-4609.20143014.

Corona FV, Davis JS, Hippler SJ, Vrolijk PJ. 2010. Multi-fault analysis scorecard: testing the stochastic approach in fault seal prediction. Geol Soc London, Spec Publ. 347:317-332. doi: 10.1144/SP347.18.

Esposito A, Benson SM. 2011. Remediation of possible leakage from geologic CO2 storage reservoirs into groundwater aquifers. Energy Procedia. 4:3216–3223. doi:10.1016/j.egypro.2011.02.238.

Ferrill D a., Morris AP. 2002. Dilational normal faults. J Struct Geol. 25:183–196. doi:10.1016/S0191-8141(02)00029-9.

Fisher QJ, Knipe RJ. 2001. The permeability of faults within siliciclastic petroleum reservoirs of the North Sea and Norwegian Continental Shelf. Mar Pet Geol. 18(10):1063–1081. doi:10.1016/S0264-8172(01)00042-3.

Frischbutter AA, Fisher QJ, Namazova G, Dufour S. 2017. The value of fault analysis for field development planning. Pet Geosci. 23(1):120–133.

Fulljames JR, Zijerveld LJJ, Franssen RCMW. 1997. Fault seal processes: systematic analysis of fault seals over geological and production time scales. Nor Pet Soc Spec Publ. 7(C):51–59.

doi:10.1016/S0928-8937(97)80006-9.

Gartrell A, Zhang Y, Lisk M, Dewhurst D. 2004. Fault intersections as critical hydrocarbon leakage zones: Integrated field study and numerical modelling of an example from the Timor Sea, Australia. Mar Pet Geol. 21(9):1165–1179. doi:10.1016/j.marpetgeo.2004.08.001.

Giger SB, Clennell MB, Çiftçi NB, Harbers C, Clark P, Ricchetti M. 2013. Fault transmissibility in clastic-argillaceous sequences controlled by clay smear evolution. Am Assoc Pet Geol Bull. 97(5):705–731. doi:10.1306/10161211190.

Gutierrez M, Øino LE, Nygård R. 2000. Stress-dependent permeability of a de-mineralised fracture in shale. Mar Pet Geol. 17(8):895–907. doi:10.1016/S0264-8172(00)00027-1.

Heynekamp MR, Goodwin LB, Mozley PS, Haneberg WC. 1999. Controls on Fault-Zone Architecture in Poorly Lithified Sediments, Rio Grande Rift, New Mexico: Implications for Fault-Zone Permeability and Fluid Flow. In Faults and Subsurface Fluid Flow in the Shallow Crust (eds W. Haneberg, P. Mozley, J. Moore and L. Goodwin). doi:10.1029/GM113p0027

Higgs KE, Arnot MJ, Brindle S. 2015. Advances in grain-size, mineral and pore-scale characterization of lithic and clay-rich reservoirs. Am Assoc Pet Geol Bull. 7(7):1315–1348. doi:10.1306/01271513101.

James WR, Fairchild LH, Nakayama GP, Hippler SJ, Vrolijk PJ 2004. Fault-seal analysis using a stochastic multifault approach. AAPG Bull. 88:885–904. doi:10.1306/02180403059.

Kettermann M, Thronberens S, Juarez O, Urai JL, Ziegler M, Asmus S, Krüger U. 2016. Mechanisms of clay smear formation in unconsolidated sediments-insights from 3-D observations of excavated normal faults. Solid Earth. 7(3):789–815. doi:10.5194/se-7-789-2016.

King P, Thrasher GP. 1996. Cretaceous-Cenozoic geology and petroleum systems of the Taranaki Basin, New Zealand. Institute of Geological & Nuclear Sciences.

Kristensen M.B., Childs C, Olesen NØ, Korstgård JA. 2013. The microstructure and internal architecture of shear bands in sand–clay sequences. J Struct Geol. 46:129–141. doi:10.1016/j.jsg.2012.09.015.

Lehner FK, Pilaar WF. 1997. The emplacement of clay smears in synsedimentary normal faults-inferences from field observations near Frechen , Germany. NPF Spec Publ. 7:39–50.

Lindsay NG, Murphy FC, Walsh JJ, Watterson J. 1993. Outcrop Studies of Shale Smears on Fault Surface. Int Assoc Sedimentol Spec Publ.(15):113–123.

Manzocchi T, Childs C, Walsh JJ. 2010. Faults and Fault Properties in Hydrocarbon Flow Models. Front Geofluids.:94–113. doi:10.1111/j.1468-8123.2010.00283.x.

Masalimova LU, Lowe DR, Sharman GR, King PR, Arnot MJ. 2016. Outcrop characterization of a submarine channel-lobe complex: The Lower Mount Messenger Formation, Taranaki Basin, New Zealand. Mar Pet Geol. 71:360–390. doi:10.1016/j.marpetgeo.2016.01.004.

Nicol A, Childs C. 2018. Cataclasis and silt smear on normal faults in weakly lithified turbidites. J Struct Geol. 117(June):44–57. doi:10.1016/j.jsg.2018.06.017.

Pei Y, Paton DA, Knipe RJ, Wu K. 2015. A review of fault sealing behaviour and its evaluation in siliciclastic rocks. Earth-Science Rev. 150(October):121–138. doi:10.1016/j.earscirev.2015.07.011.

Schmatz J, Vrolijk PJ, Urai JL. 2010. Clay smear in normal fault zones - The effect of multilayers and clay cementation in water-saturated model experiments. J Struct Geol. 32(11):1834–1849. doi:10.1016/j.jsg.2009.12.006.

Seebeck H, Nicol A, Walsh JJ, Childs C, Beetham RD, Pettinga J. 2014. Fluid flow in fault zones from an active rift. J Struct Geol. 62:52–64. doi:10.1016/j.jsg.2014.01.008.

Sperrevik S, Færseth RB, Gabrielsen RH. 2000. Experiments on clay smear formation along faults. Pet Geosci. 6(2):113–123. doi:10.1144/petgeo.6.2.113.

Vrolijk PJ, Urai JL, Kettermann M. 2016. Clay Smear: Review of Mechanisms and Applications. J Struct Geol. doi:10.1016/j.jsg.2015.09.006.

Yielding G. 2012. Using Probabilistic Shale Smear Factor to Relate SGR Predictions of Column Height to Fault-zone Heterogeneity. Pet Geosci. 18:33–42. doi:10.3997/2214-4609.20147179.

Yielding G, Bretan P, Freeman B. 2010. Fault seal calibration : a brief review. Geol Soc London, Spec Publ. 347:243–255.

Yielding G, Freeman B, Needham DT. 1997. Quantitative fault seal prediction. Am Assoc Pet Geol Bull. 81(6):897–917. doi:10.1306/522B498D-1727-11D7-8645000102C1865D.

Van der Zee W, Urai JL. 2005. Processes of normal fault evolution in a siliciclastic sequence: a case study from Miri, Sarawak, Malaysia. J Struct Geol. 27(12):2281–2300. doi:10.1016/j.jsg.2005.07.006.

Van der Zee W, Urai JL, Richard PD. 2003. Lateral clay injection into normal faults. GeoArabia. 8(3):501–522.

4 Frequency of shale smear and factors that influence their formation

4.1 Abstract

Fault-seal algorithms developed for the petroleum industry primarily use shale-bed thickness and displacement to estimate seal potential. Fault-seal equations were mainly developed from outcrop observations and assume that all shale beds smear and contribute to fault rock. Here we test the assumption that all shale beds smear by quantifying the proportion of faulted beds that smear for a turbidite sequence that comprises interbedded siltstone (beds ~1-45 cm thick) and sandstone (beds ~1-150 cm thick). Data are from coastal outcrops comprising small normal faults (displacements 2 cm to 1.1 m) which displace poorly lithified beds (burial depths ~1-1.5 km) of the Mount Messenger Formation in Taranaki, New Zealand. Over 180 faulted siltstone beds with 100% exposure were randomly sampled and show that 39% (N=71) of beds have no smear, 53% (N=97) discontinuous smear and 8% (N=15) continuous smear. The median smear continuity is ~3%, while half of the discontinuous smears have continuity of <23% and ~83% of all smears have continuity of <50% (Figure 4.1). The majority of smears have variable thicknesses which were often unrelated to source-bed thickness or distance from the source bed. These thickness variations can result from secondary faults within the fault zone which locally thicken or thin the smear depending on their geometries and displacements. Analysis of shale smears from different localities suggests that increasing phyllosilicate content may provide a first-order increase in the number and continuity of shale smears. However, individual shale beds displaced by adjacent normal faults, with comparable orientations, kinematics and timing of formation, can be smeared and not smeared, suggesting that in these cases variations in bed composition (e.g., phyllosilicate or organic material content), grain-size distribution, moisture content or lithification do not produce the observed variations in smear occurrence. Instead, shale smearing appears to be common where fault displacement is distributed across relatively wide fault zones. Independent of the factors contributing to shale smear, absence of shale smear on many beds has not previously been widely discussed in the literature and should be accounted for in shale-smear algorithms.

4.2 Introduction

Low permeability fault-zones can retard fluid flow in sub-surface reservoirs on geological and production timescales. Their ability to retard or restrict fluid flow is of importance to many industries that rely on the economic extraction or injection of fluids. Reduction of permeability in fault zones that displace reservoir units has been attributed to a number of processes including, cementation, cataclasis and smear or incorporation of low permeable units from the wallrock (Yielding et al. 1997; Foxford et al. 1998; Aydin 2000; Faulkner et al. 2010; Manzocchi et al. 2010; Pei et al. 2015). Of these mechanisms, shale smear is by far the most widely investigated in fault-seal studies.

Shale smears are broadly defined as clay or shale host rock that is entrained into a fault zone between the host shale-bed cut offs (Figure 4.1). Shale smears are most likely to be identified where they separate sandstone units juxtaposed across a fault and are primarily thought to form by drag and shear of mudstone layers between the displaced bed(s) (Lindsay et al. 1993; Ciftci et al. 2012; Vrolijk et al. 2016). The formation of shale smears can be influenced by a number of factors, including the lithification of the faulted strata (and associated maximum burial depth), stress regime and strain rate together with bed mineralogy, water content and thickness (Lindsay et al. 1993; Yielding et al. 1997; Fisher and Knipe 2001; Giger et al. 2013; Pei et al. 2015; Vrolijk et al. 2016). At shallow depths (e.g. < 3 km) it is often assumed that all shale beds will smear to some degree, however, non-smearing beds could be more common than first thought. The detailed geometries of smears may also be depend on the mechanism by which they become entrained in the fault zone, with abrasion style smears typically producing uniform, millimetre thick smear between bed cut offs. By contrast, injection smears can produce smears with fluctuating thickness and shear smears lead to a tapering smear that thins with increasing distance from the source bed (Figure 3.2) (Lindsay et al. 1993). Current algorithms use relationships between displacement and shale bed thickness to predict smear continuity and constrain fault seal, with lower displacement and higher bed thickness more likely to produce a continuous smear.

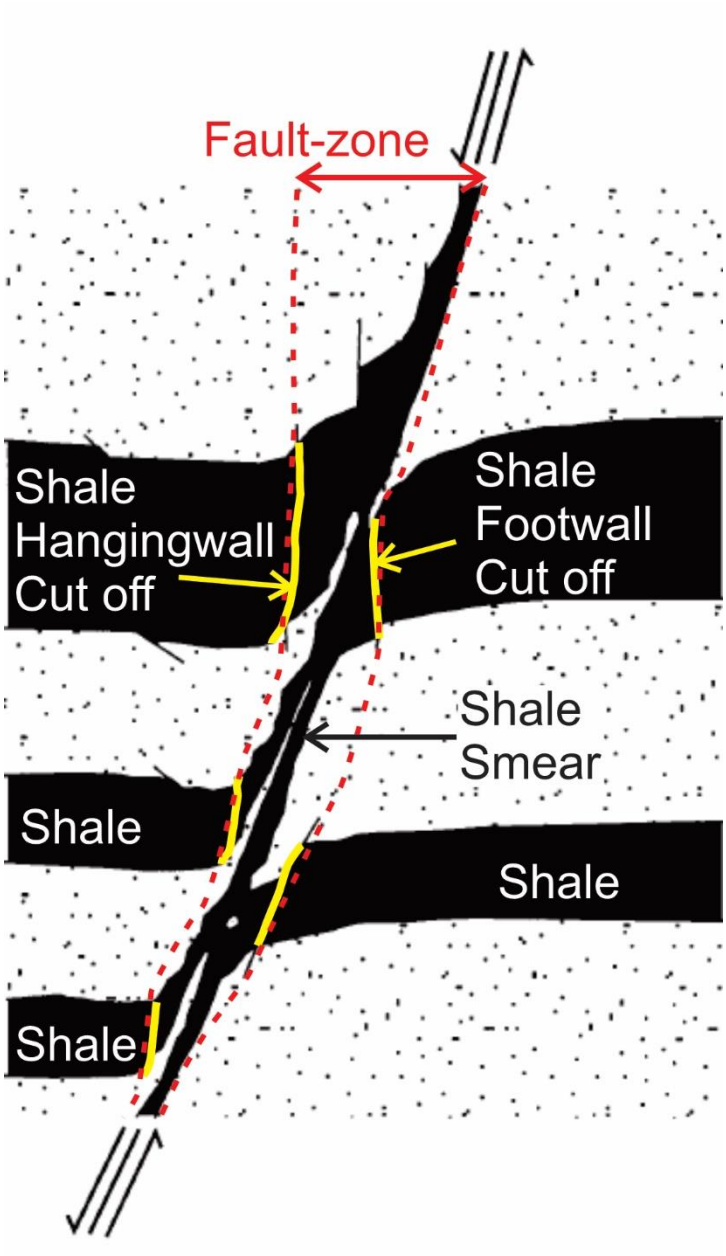

Figure 4.1 Line drawing of offset shale (black) and sandstone interbeds modified from Yielding et al. (1997). Note how the shale smear prevents juxtaposition of sandstone beds either side of the fault.

Research to date has focussed on the distribution of shale smear within fault zones in a bid to accurately predict where smear may create a seal between displaced reservoir units. Shale smears have been widely investigated using outcrops, laboratory models, seismic reflection lines and borehole cores (Lindsay et al. 1993; Fristad et al. 1997; Yielding et al. 1997; Sperrevik et al. 2000; Fisher and Knipe 2001; Schmatz et al. 2010). In order to generate sufficient data these studies typically focus on strata where shale smears are abundant, however, this focus may lead to a bias in the literature towards outcrops where they are more likely to be present. In this study we

systematically sample faulted siltstone beds from the Late Miocene (~11-7 Ma) Mount Messenger Formation in Taranaki, New Zealand. We sampled all faulted siltstone beds that were 100% exposed in coastal cliffs to generate a representative dataset of 186 faults that record a range of shale smear geometries. Results from the Mount Messenger Formation are compared to shale smears from The Late Cretaceous Conway Formation at Gore Bay and Early Miocene Waitemata Formation at White Bluff, both locations in New Zealand. These datasets are used to examine the frequency of shale smears and the variability in their geometries. The available data suggest that it is rarely the case that all shale beds smear and that the proportion of smearing beds varies between outcrops and formations. The phyllosilicate, organic matter, and fluid content together with the angle between the fault and host bed, and the fault zone width could all influence the frequency and continuity of smear.

4.3 Data and methods

This study exclusively uses 2D outcrop data of small displacement (<1.1 m) normal fault. Data are from six coastal localities in New Zealand. All outcrops are siliciclastic sequences comprising sandstone, siltstone and mudstone units exposed in coastal cliffs displaced by normal faults.

4.3.1 Study sites and lithologies

Fieldwork was conducted at six field sites across New Zealand from Gore Bay in the South Island to White Bluff in the North Island.

Table 4.1 Summary of the fault strata studied at field sites used for this study showing the similarities and difference between the sites

LOCALITY	LOCATION (LAT/LONG)		FORMATION	AGE	LITHOLOGY	DEPOSITIONAL ENVIRONMENT	FAULTING	NUMBER OF FAULTS	BURIAL DEPTH AND LITHIFICATION	SILTSTONE BED THICKNESS	FAULT THROW
WHITE BLUFF	1	36°56'12.4"S	Waitemata	Early Miocene	Interbedded sandstone and muddy siltstones. Lithic Subgreywackes	Turbidite	Normal	17	< 1 km Uncemented and poorly lithified	Range: 21.5-60mm	Range: 36-210mm
AUCKLAND	2	174°43'40.2"E		(23-16 Ma)	(Ballance 1964)				(Ballance 1964)	Average: 37.5mm	Average: 147mm
TARANAKI*	Pukearuhe:	38°53'31.1"S 174°31'03.0"E	Mount Messenger	Late Miocene (11-7 Ma)	Interbedded sandstone, siltstone and mudstone	Turbidite	Normal	184	1-1.5 km (Childs et al. 2007) Weakly Lithified	Range: 1.5-450mm Average: 44mm	Range: 9-5100mm Average: 192mm
	Tongaporutu:	38°49'14.9"S 174°34'51.3"E									
	Rapanui:	38°47'55.8"S 174°35'26.2"E									
	Mohakatino:	38°44'12.8"S 174°36'29.9"E									
GORE BAY, CANTERBURY	3	42°52'18.0"S	Conway	Late Cretaceous	Interbedded siltstone and very fine sandstone	Deep Marine	Normal	13		Range: 1-45mm	Range: 4.5-380mm
	4	173°18'38.5"E		(100-66 Ma)	(Rattenbury et al. 2006)					Average: 9.8mm	Average: 66mm

Four locations along the Taranaki Coast were studied. These are: Pukearuhe Beach for 1.5 km north of the Totahiapuru Stream mouth, Tongaporutu Beach for 2 km south of the Tongaporutu River mouth, Rapanui Beach for 0.5 km north of the Rapanui Stream mouth and Mohakatino Beach 1 km south of the Mokau river mouth (see Figure 4.2). In addition to the Taranaki outcrops data were collected from Gore Bay and White Bluff. Location, stratigraphic, lithification and burial depth information for all sites is summarised in Table 4.1.

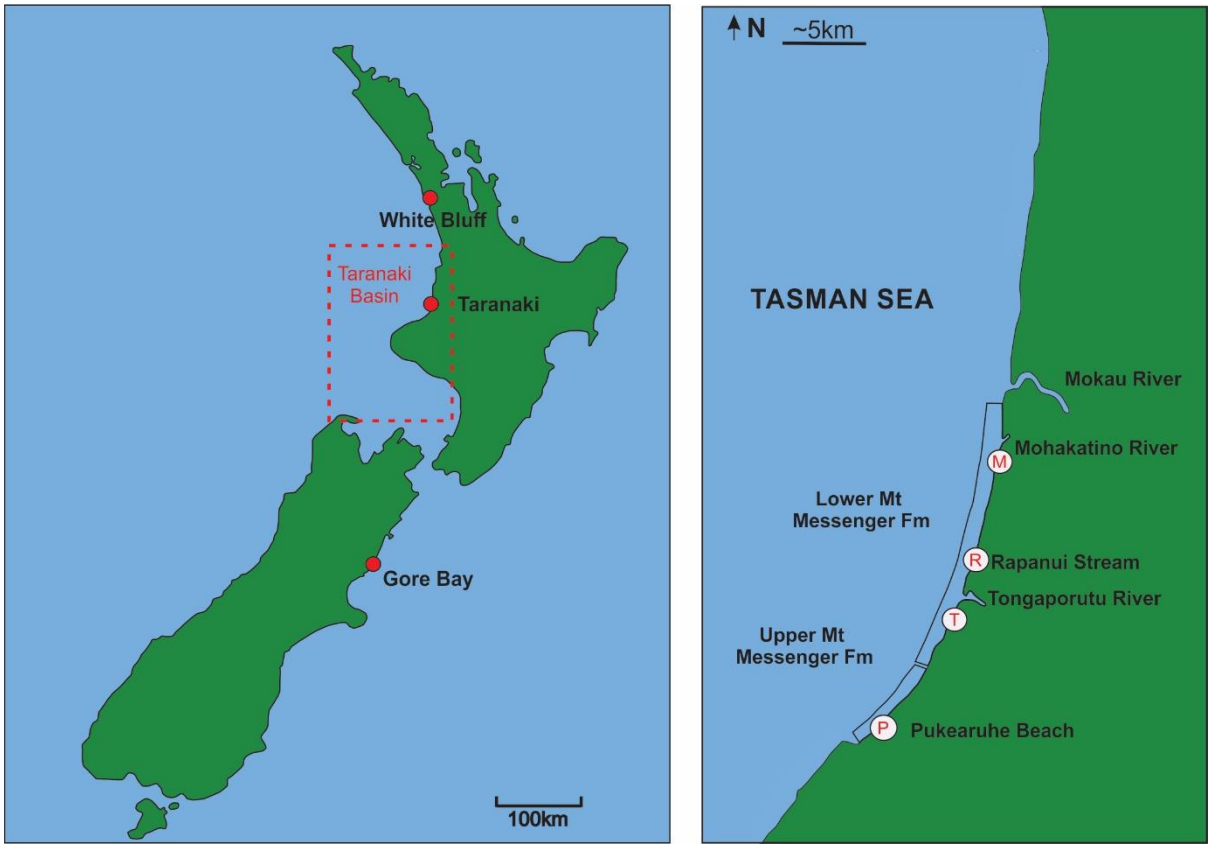

Figure 4.2 Map showing the locations of the sample sites at Gore Bay, Taranaki and White Bluff (left) and the Taranaki Coast (right). The localities used for this study are Mohakatino (M), Rapanui (R), Tongaporutu (T) and Pukearuhe (P).

The locations studied share a number of stratigraphic similarities and differences. All outcrops are poorly lithified and appear to have been buried to shallow depths. White Bluff and Taranaki strata are both examples of Miocene turbidites, although they typically display very different smear geometries and frequencies. Late Cretaceous deposits exposed at Gore Bay are more siltstone dominated than the other outcrops, while mudstones at Gore Bay and White Bluff anecdotally show a higher organic matter content than observed in Taranaki outcrops, with White Bluff comprising abundant 'carbonised plant matter' in mudstone beds (Ballance 1964).

The majority of faults examined in this study were from Taranaki (184 of 250 faults). All faults sampled in Taranaki were from the Mount Messenger Formation. The Mount Messenger Formation consists of strata with varying proportions of sandstone and siltstone and variable bed thicknesses. The net to

gross for the Mount Messenger Formation varies from 0.2-0.9, although in this study we have focused on sites with values of 0.4-0.6 and siltstone beds generally <20 cm thick. Sixty-two siltstone beds were sampled and run through the laser sizer and the average grain size was determined to be 16% clay, 64% silt and 20% sand sized particles. XRD data taken from 13 samples in the fault seals database by GNS show that siltstone beds within the Mount Messenger formation have phyllosilicate values ranging from 38.5% to 53.8% (GNS Science, 2018).

4.3.2 Sampling strategies and techniques

To prevent unconscious bias in this study (i.e., primarily studying outcrops where shale smear is ubiquitous or focusing on faults where smear geometries were well defined), we have sampled all faulted silt beds observed. That is, we have sampled 100% of fault-silt bed couples where the footwall and hangingwall sections of the bed and the intervening fault zone are 100% exposed (see Figure 4.3). This approach reduces the potential for sampling biases that may arise by focussing on the best examples of shale smear. We assume that our dataset is a random sample of the shale smear population which provides a representative range of shale-smear geometries in the outcrops studied.

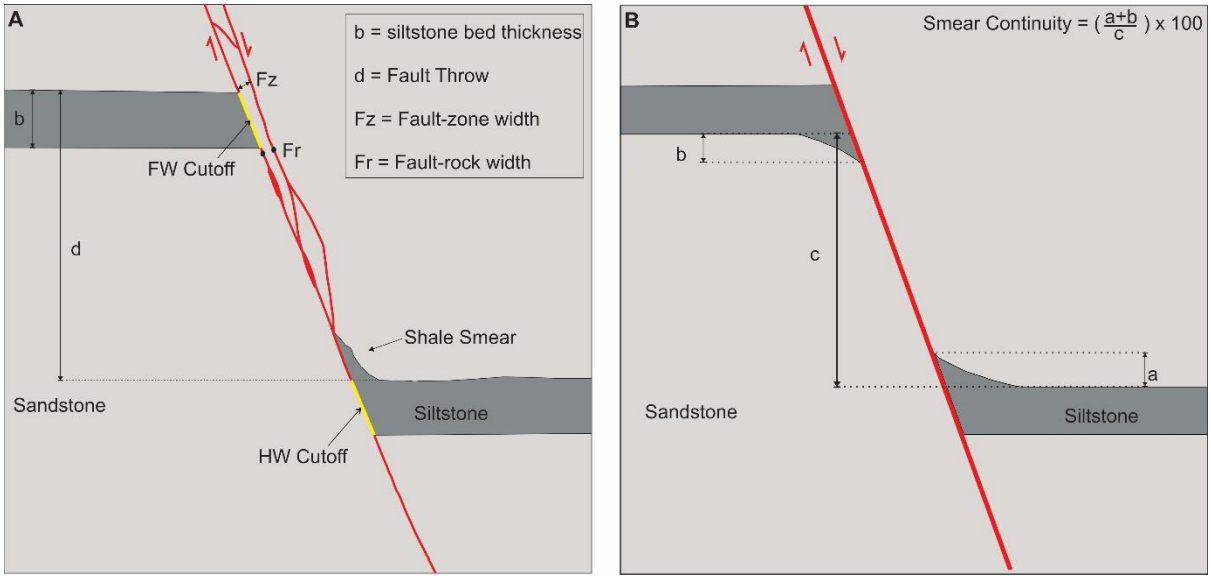

Figure 4.3 Schematics showing the measurements taken (left) and the calculation of shale smear continuity (right).

In addition to ensuring 100% exposure, the faults studied were required to meet the following conditions:

1. The footwall and hangingwall siltstone beds were displaced by more than the bed thickness. This permitted the fault rock between the footwall and

hangingwall cut offs to be analysed so that the geometry of shale smear could be recorded where it separates sandstone beds.

2. Displacement was sufficiently small that smear within the fault zone could be attributed to a single siltstone bed. In situations where multiple siltstone beds had moved past the sampled point on a fault it is often difficult to determine which beds had contributed which proportions of siltstone to the fault rock.

3. Hangingwall and footwall beds could be correlated across the fault and within the fault zone. This allowed the contributions of siltstone beds to the fault rock to be assessed and permitted accurate measurements of the smear geometries.

4. Beds are continuous and traceable within 1-2 m of the primary fault surface.

Faults and displaced beds were cleaned down using scrapers to remove weathered surface material and to provide a flat surface for measurements to be taken. Typically, several centimetres of the exposure was stripped to expose a fresh surface which ensured that samples were from fresh rock and not contaminated by surface deposits (e.g., salt infiltration and flora). The resulting observations and measurements were mainly 2D cross sections. Along-strike changes in shale smear geometries were observed over distances of no more than 2-3 cm, although no attempt was made to study the 3D geometries of shale smears systematically. Photos and measurements were taken of the cleaned surfaces and each faulted bed assigned a sample number. For each fault sampled measurements of smear length, smear thickness, silt bed thickness, fault displacement, fault rock thickness, fault zone thickness and the number slip surfaces were collected (see Figure 4.3). Fault zone thickness, fault rock thickness and the number of slip surfaces were measured at the mid-point of each cut off. For each fault-shale bed couplet the continuity and geometry of smears were recorded, along with any internal structure of the fault rock (e.g., internal layering and minor faults). Smear continuity is defined as the distance between host cut offs where smear is present. A complete range of scenarios from displaced beds producing no smear to those that produced continuous smear were recorded, with a maximum smear length of up to 1300mm. Smear continuity is here given as a percentage and provides an indication of how much of the fault surface may be sealed and allows faulted silt beds to be easily compared and displayed on graphs. Smear continuity is a first order number and provides no spatial context for where the smear may lie between the shale bed cut offs.

A total of displaced shale beds were measured and analysed of which 180 were individual shale beds. These faulted beds were sampled predominantly from Tongaporutu, Pukearuhe, Rapanui and

Mohakatino. Table 4.1 summarises the strata, estimated burial depth and number of fault/bed observations for each beach. For more information on the lithological variations within the MMF see 1.4.1.1 in Chapter 1.

4.4 Shale smear geometries and continuity

Shale smears and fault zones in general display a range of geometries both in individual outcrops, where the lithologies are approximately uniform, and between localities (See Figure 3.10 for smear spectrum). In Taranaki, faults zones show a variety of geometries, from a single slip surface (Figure 4.4A) to multiple small-scale synthetic slip surfaces that bound lenses that may contain slices of low permeability shale and stacked across the fault zone (Figure 4.4B & C)(Childs et al. 2007; Childs et al. 2009; Nicol and Childs 2018). These fault-zone geometries may be associated with a range of shale smear geometries and continuity. For example, in Figure 4.4A there is no smear, while Figure 4.4D shows continuous smear. There can also be a combination of synthetic faulting and shale smear dependent on the host rock properties and fault zone architecture (Figure 4.4C). Slices of shale tend to be thicker than shale smears while shale smears tend to be more continuous and cover more of the primary fault surface.

Shale smears and shale slices both have the potential to impact across fault permeability. We believe that shale smear and shale slicing are primarily scale-dependent manifestations of brittle deformation. Examination of thin sections supports the view that shale smear is predominately achieved by micro-scale faulting, which is typically sub-resolution at outcrop scale (see Chapter 3 Figure 3.16). Therefore, we have measured shale smears (N=43), shale slices (N=29) and mixed smears-slices (N=23) in our sample population. Because our sample was random the relative numbers of shale smears to shale slices may be representative of the entire population, however, we acknowledge that faults comprising multiple slip surfaces may be prone to coastal erosion and could be undersampled. Irrespective of whether shale slices have been undersampled, fewer shale slices were sampled than shale smear, and the exclusion of shale slices from the sample would only slightly reduce the number of shale beds incorporated into the fault zones.

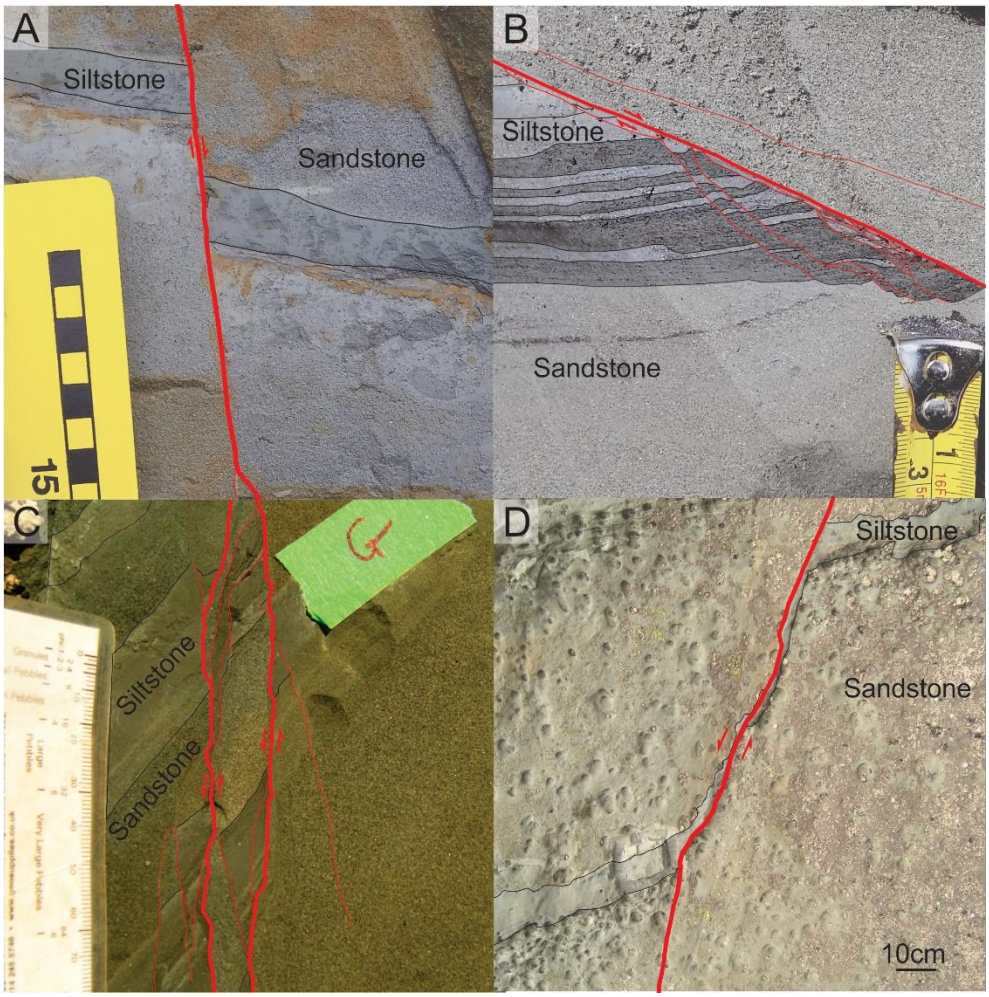

Figure 4.4 A series of images showing the range in smear geometries and continuity in Taranaki. A) No smear, B & C) slicing of silt beds, D) Continuous Smear.

The silt beds sampled were split into three groups according to the degree of smearing and slicing observed. These groups were discontinuous smear or slicing (N=90) (Figure 4.4B & C), no smear or slicing (N=71) (Figure 4.4A) and continuous smear or slicing (N=23) (Figure 4.4D). No smear refers to beds where both hangingwall and footwall cut offs terminate abruptly on the fault surface and the fault zones contain neither entrained (smeared) or sliced shale in the fault zone. Discontinuous beds are those that range from at least one millimetre of smear up to a millimetre less than continuous smear between the hangingwall and footwall cut offs (1 millimetre is considered to be the resolution limit of outcrop data in this study). Smears in the discontinuous category tend to vary greatly in appearance from beds with a small drag at the fault contact, to beds with a near continuous gradually thinning smear, to siltstone that exists in discontinuous isolated fragments along the fault trace. By

comparison, continuous smears or slices must cover the entire distance between the hangingwall and footwall cut offs.

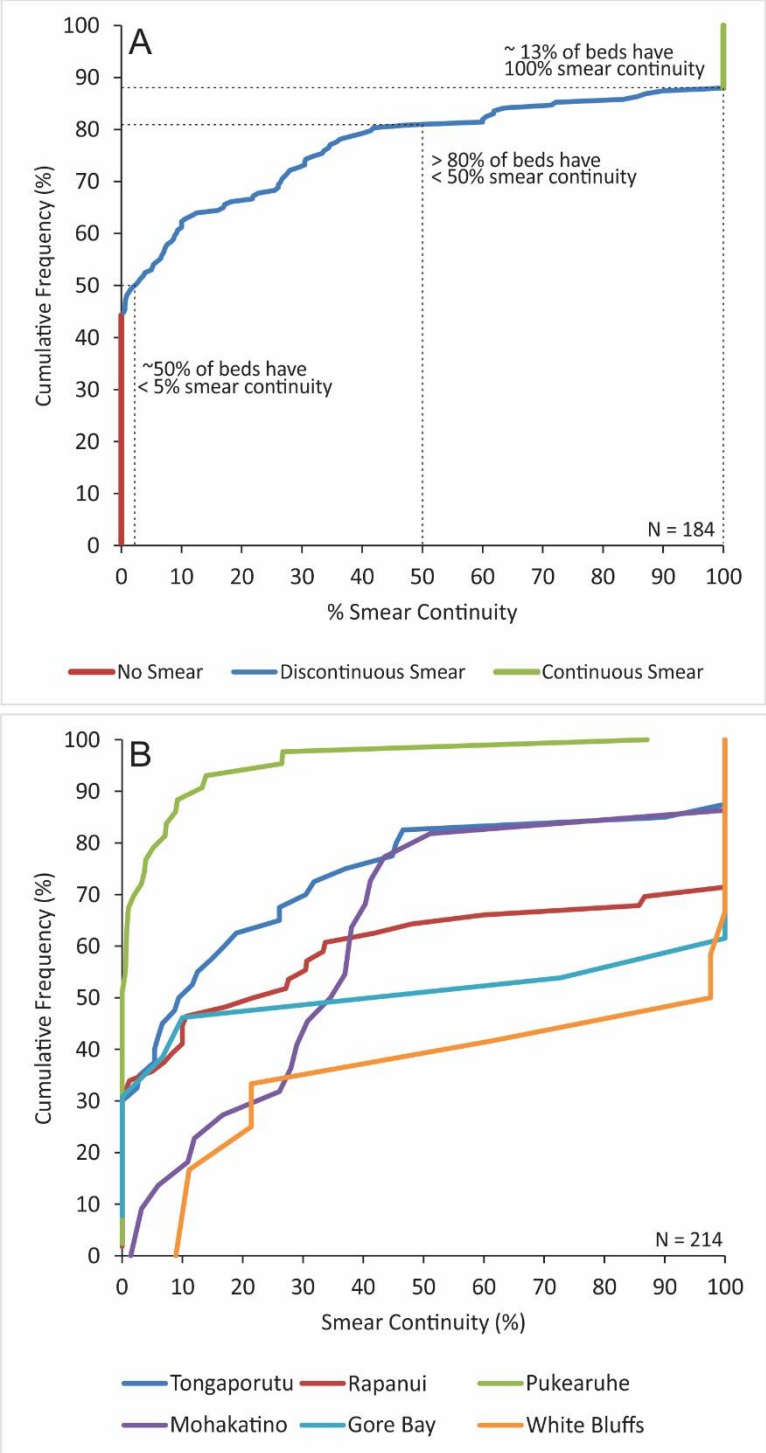

Figure 4.5 A) Cumulative frequency graph showing the range of smear/slice continuity for all faulted siltstone beds sampled from Taranaki, New Zealand. B) Cumulative frequency graphs showing fault-zone shale bed continuity for individual outcrops in Taranaki (Tongaporutu, Rapanui, Pukearuhe and Mohakatino), Gore Bay and White Bluff.

The cumulative frequency curve in Figure 4.5A shows the continuity of shale smears and shale slices for all Taranaki data. For the faults sampled ~50% show little to no evidence of incorporation of silt

beds into the fault zones (< 5 % continuity), while only a small percentage (~13 %) of faults displayed continuous smear/slicing. Between these two extremes (i.e. no smear and continuous smear) the cumulative frequency curve is convex upwards with ~80 % of faults having smear continuity <50 %, ~10 % of faults with continuity of ~50% to 99% and the remaining faults having continuous shale smear. These values indicate a predominance of faults with discontinuous smears that cover <50% of the fault surfaces and suggest that in Taranaki it is often not the case that shale beds are incorporated into fault zones either via smearing or slicing.

To further examine these data we have analysed faults from six localities (beaches) using separate cumulative frequency plots (Figure 4.5B). The plots show that the shapes of the cumulative frequency curves, and the relative proportions of non-smear, discontinuous smear and continuous smear, can vary significantly for outcrops within the same formation and in some cases for the same bed. For example, the Taranaki localities are all from within the Mount Messenger Formation and yet they appear to show a wide range of cumulative frequency distributions. The shapes of the cumulative frequency curves appear to change in a systematic way geographically with the proportion of 'non-smearing' faults decreasing northwards along the coast. The faults from Gore Bay and White Bluff contained a higher proportion of smeared beds than the Taranaki localities. At White Bluff, for example, none of the faulted beds displayed <~10% smear, while 40% of all beds showed continuous smear. The factors that may control the shape of the cumulative frequency curves and the proportions of shale beds that are incorporated into fault zones is discussed in the following section.

4.5 Factors controlling shale smear geometries

Lehner and Pilaar (1997) suggested that "the production of extensive smears requires a slow rate of displacement coupled with shale deforming in a ductile manner". They also indicated that bed thickness was a key control, observing that higher smear continuity was more likely for smears sourced from thicker beds. The influence of shale bed thickness is reflected in the shale smear algorithms, which use the relationship between bed thickness and displacement to predict smear continuity (i.e. the lower the displacement and the thicker the bed the more likely the chances of continuous smear). Many additional factors could also influence the continuity of shale smear including strata lithification, effective stress, confining pressure, strain rate, grain size, water content and mineralogy (Lindsay et al. 1993; Pei et al. 2015). For example, the brittleness of the host bed along with the amount and type of stress during deformation has been proposed to affect the resulting smear geometry (Vrolijk et al. 2016).

In Taranaki the importance of shale smear generally increases northwards along the coast and a number of factors can be discounted as primary controls for the abundance of shale smear. Initially this increase seems counterintuitive as smearing is more abundant deeper in the section. However, rock properties that are consistent or change gradually across the Mount Messenger Formation are unlikely to have been a primary control on shale smear given the spatial distribution of smear and no smear that were observed. Therefore, it is unlikely that any regional characteristic such as the burial depth, depth of faulting or lithification control the frequency of shale smear, at least within the Mount Messenger Formation. In contrast, the stratigraphy is not uniform along the coast, and it remains possible that these changes could influence the frequency of shale smears. In particular, the maximum siltstone content for all Taranaki localities is observed at Pukearuhe (where the fewest smears are observed), the maximum organic material in the siltstone beds at Rapanui and evidence of elevated fluid content at Mohakatino. Below we discuss how these lithological factors may influence the formation of shale smears.

4.5.1 Bed thickness and fault displacement

Bed thickness and its relationship to fault displacement are thought to be an important control on shale continuity. Shale Smear Factor (SSF) was developed from an outcrop study investigating displaced shale beds in a carboniferous fluvio-deltaic sequence (Lindsay et al. 1993). All shale beds studied by Lindsay et al. (1993) show smear to some degree, with the continuity of smear being dependent on the amount of displacement and the net:gross of the sequence. Shale smears were found to be most continuous when fault displacement was <50% of the bed thickness. Our analysis of the relationships between bed thickness, fault displacement and shale smear continuity supports the general conclusions of Lindsay et al. (1993), and indicates that continuous smears are most likely to occur when the bed thickness is more than 20% of displacement (Figure 4.6). While increasing displacement ultimately results in smear discontinuity arising from the rising shear strains, bed thickness relative to displacement does not appear to provide a primary control for which beds smear in the Mount Messenger Formation. This inferred lack of control is supported by Figure 4.6 on which continuous, discontinuous and no-smear faults occupy similar parts of the graph. These relationships suggest that the ratio of displacement to shale-bed thickness cannot be used to determine which beds are mostly likely to smear.

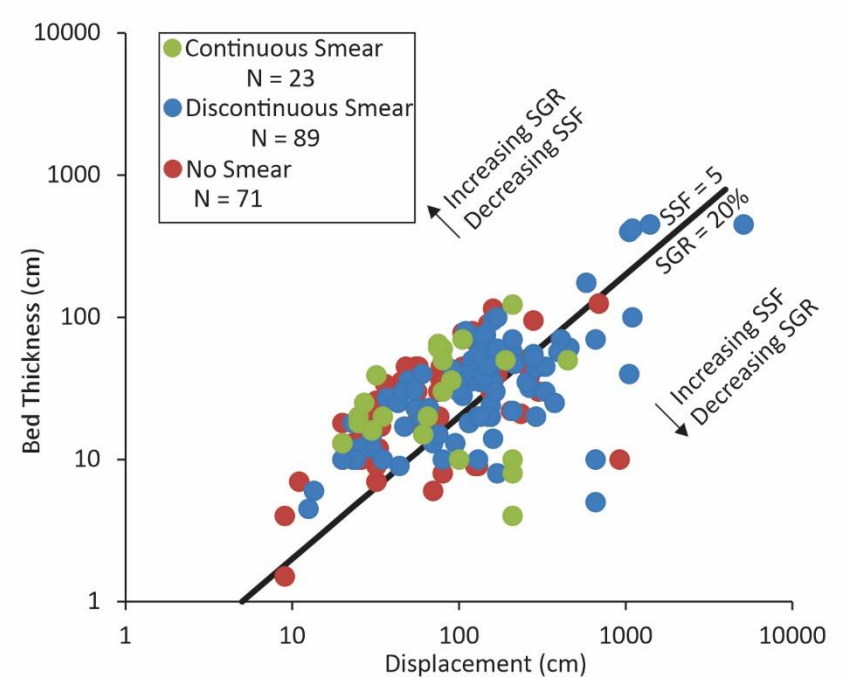

Figure 4.6 Bed Thickness vs Displacement graph for No, Discontinuous and Continuous Smear beds. No correlation between smearing and the ratio of bed thickness to displacement is found. Lines for SSF =5/SGR = 20% and SGR=30% show some typical cut offs used in previous studies with the intervening interval highlighted.

4.5.2 Silt bed phyllosilicate content and grain size

The grain size and composition of the host bed may control the frequency and continuity of shale smears. It has been proposed that the proportion and size of phyllosilicate grains could impact the continuity of shale smears. Fisher and Knipe (2001) suggest that in host rocks with a high clay content, burial and faulting leads to the production of a fault rock associated with the infilling of macroporosity by fine-grained clays and may lead to the formation of shale smears. The geometry and formation of the clay may be influenced by the effective stress, temperature history and amount of clay within the shale source rock. Fisher and Knipe (2001) also show that grain size of phyllosilicates might impact the geometries of smears, with phyllosilicate grains larger than 20µm observed within continuous smears and finer-grained material present in discontinuous smears. However, increase in smear continuity with increase of grain size also leads to a rise in the pore throat size of the fault rock and therefore to higher permeability than in finer grained fault rock (Fisher and Knipe 2001).

To assess whether the composition of the host shale impacts the likelihood of the shale bed smearing, XRD analysis was conducted on 17 faulted siltstone samples from five beaches with a range of smear geometries (i.e., continuous smear, discontinuous smear and no smear)(Table 4.2 and Figure 4.7). For each sample the percentage of Illite, Mica, Smectite, Chlorite and Kaolin were summed to estimate the total phyllosilicate content. The phyllosilicate content for each bed was used to calculate the

average for each beach (Table 4.2). These data support two important conclusions. First, for individual beds at a given beach there appears to be no substantial difference in the phyllosilicate content of siltstones that smear and do not smear. In some outcrops siltstone beds that showed no smear had higher phyllosilicate percentages than beds with substantial shale smear. Therefore, the phyllosilicate content cannot be called upon to explain the variability in smear geometry between individual beds. Second, while the phyllosilicate content of individual beds showed no correlation with the amount of smear, the average phyllosilicate content for each beach shows a positive correlation with the median smear continuity at each beach (Figure 4.7). Given that the bed thicknesses and fault displacements are comparable between beaches, these data support the notion that, on average, increasing the phyllosilicate content of silt beds in general increases both the likelihood and continuity of shale smear. The White Bluff locality provides the clearest example of this relationship with these strata having both the highest phyllosilicate content and the greatest proportion of beds with significant smear continuity (Table 4.2, Figure 4.7 and Figure 4.8). Despite the apparent correlation between smear continuity and phyllosilicate content at a regional scale, there is no clear relationship between phyllosilicate content and smearing for individual faulted beds with, in some cases, more smearing observed for beds with lower phyllosilicate (e.g., compare samples RAP 93 C and RAP 95 NO which smeared and did not smear, respectively; Figure 4.7). Our analysis suggests that while the phyllosilicate content can produce an overarching control on the frequency and continuity of shale smear, it is not the only factor influencing smearing. Secondary controls must impact the formation of smears on bed scale.

Table 4.2 Summary of XRD results from five locations across New Zealand. Samples were run by Equinor.

LOCALITY	NUMBER OF SAMPLES	PHYLLOSILICATE RANGE (%)	PHYLLOSILICATE AVERAGE (%)	MEDIAN SMEAR CONTINUITY (%)	COMMENTS
PUKEARUHE	2	19%-24%	21%	5%	
TONGAPORUTU	6	16%-25%	21%	28%	
RAPANUI	4	22%-27%	24%	42%	Organic rich layers No smear bed has 25% phyllosilicates
MOHAKATINO	2	23%-27%	25%	40%	Flame structures and organic rich layers
WHITE BLUFF	4	37% -46%	40%	68%	

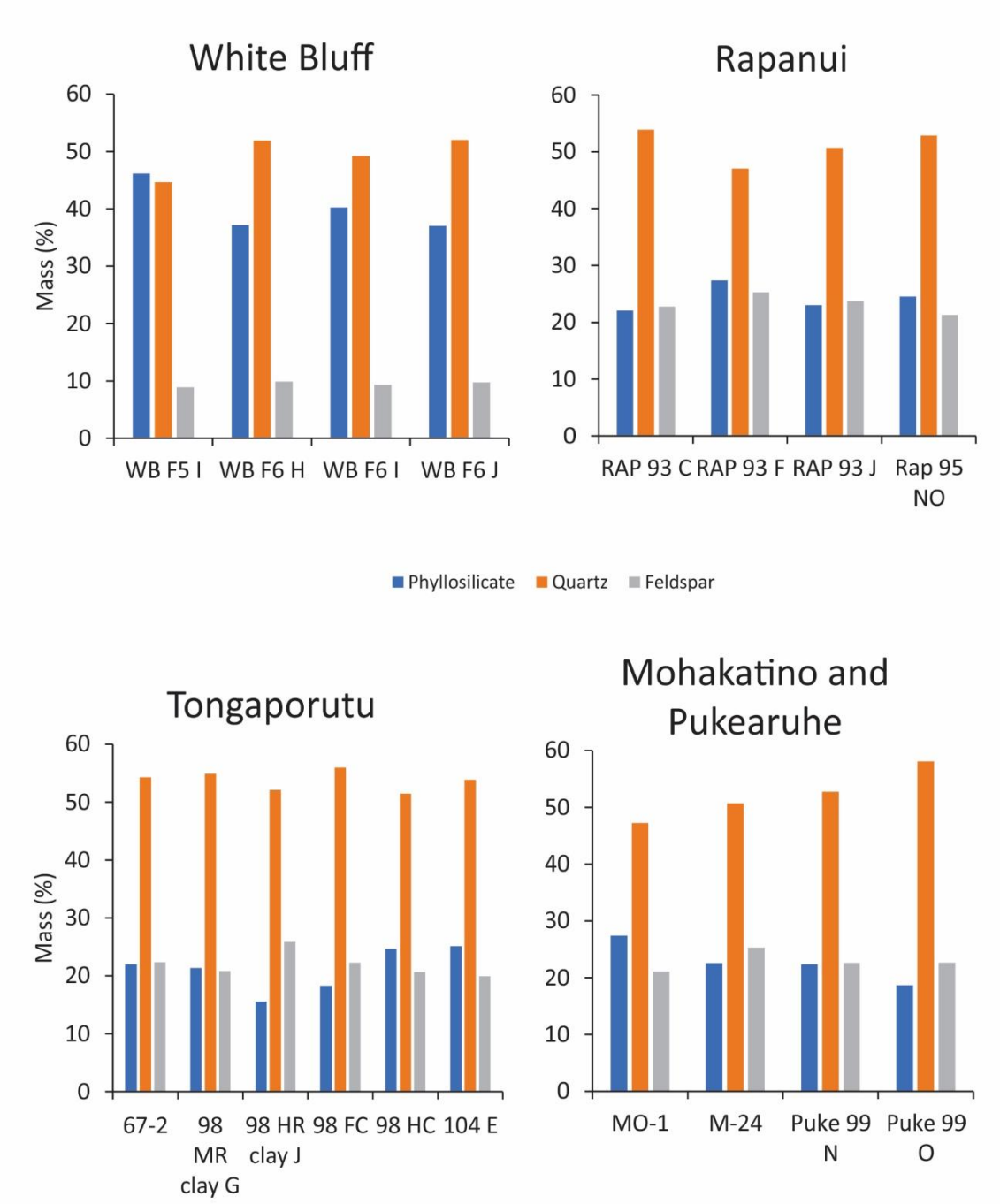

Figure 4.7 XRD results from Taranaki showing Phyllosilicate, Quartz and Feldspar percentages for several beds per locality. Samples collected in the field were sent to Equinor for XRD anlaysis.

In addition to the phyllosilicate content, there is some anecdotal evidence that elevated organic content of siltstone beds may promote shale smear. The contribution of organic matter (primarily fragments of plant material up to ~5 mm in maximum dimension) to the formation of shale smears is inferred from visual inspection of faulted beds at outcrop and thin section scales. From these data we noted that beds with higher organic material content appeared to be more likely to smear. In

particular, siltstone beds at Rapanui frequently contain black carbonaceous fragments that are easily smeared in hand specimen and may have locally promoted the formation of shale smears. To quantify this potential relationship 5 samples were submitted to Equinor to measure the Total Organic Carbon (TOC) of faulted siltstone beds from Taranaki. At the time of writing the TOC results were not available and will not be discussed further in this thesis.

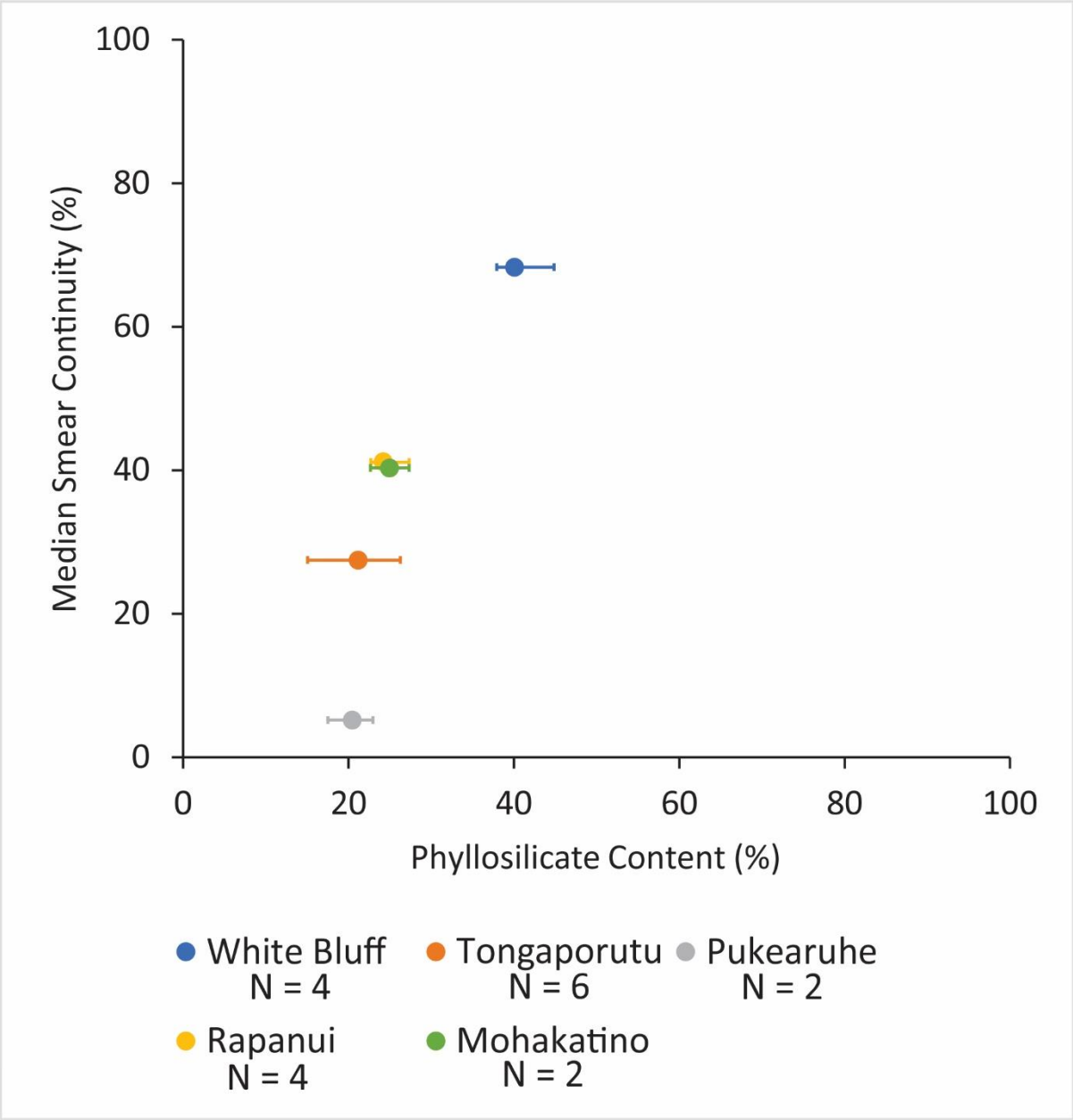

Figure 4.8 Graph showing the average phyllosilicate percentage for each locality plotted against the median smear continuity.

In Figure 4.10, for example, the general forms of the frequency histograms of faulted shale beds at Pukearuhe 99 (Figure 4.9), Pukearuhe 96, Pukearuhe 97, Tongaporutu 98, and Rapanui 95 are comparable, although the mode and median (45 and 32 µm, respectively) are higher for Pukearuhe

than the other two localities (compare Fig. 8A, B, C & D). The Pukearuhe locality displays the least shale smearing of the three locations studied and this may be partly due to the larger particle sizes of shales at this location (mode of 45 µm compared to 16-20 µm), which is consistent with the results of Fisher and Knipe (2001). The grain size distributions at Tongaporutu 98 and Rapanui 95 are comparable (i.e. modes 16-20 µm) and cannot account for the differences in smearing between these localities. In addition, there is no discernible difference in grain sizes between shale beds that smeared and did not smear at each locality. In these cases we infer that grain size did not control which beds smeared in this study and focus the following discussion on the phyllosilicate content of shale beds.

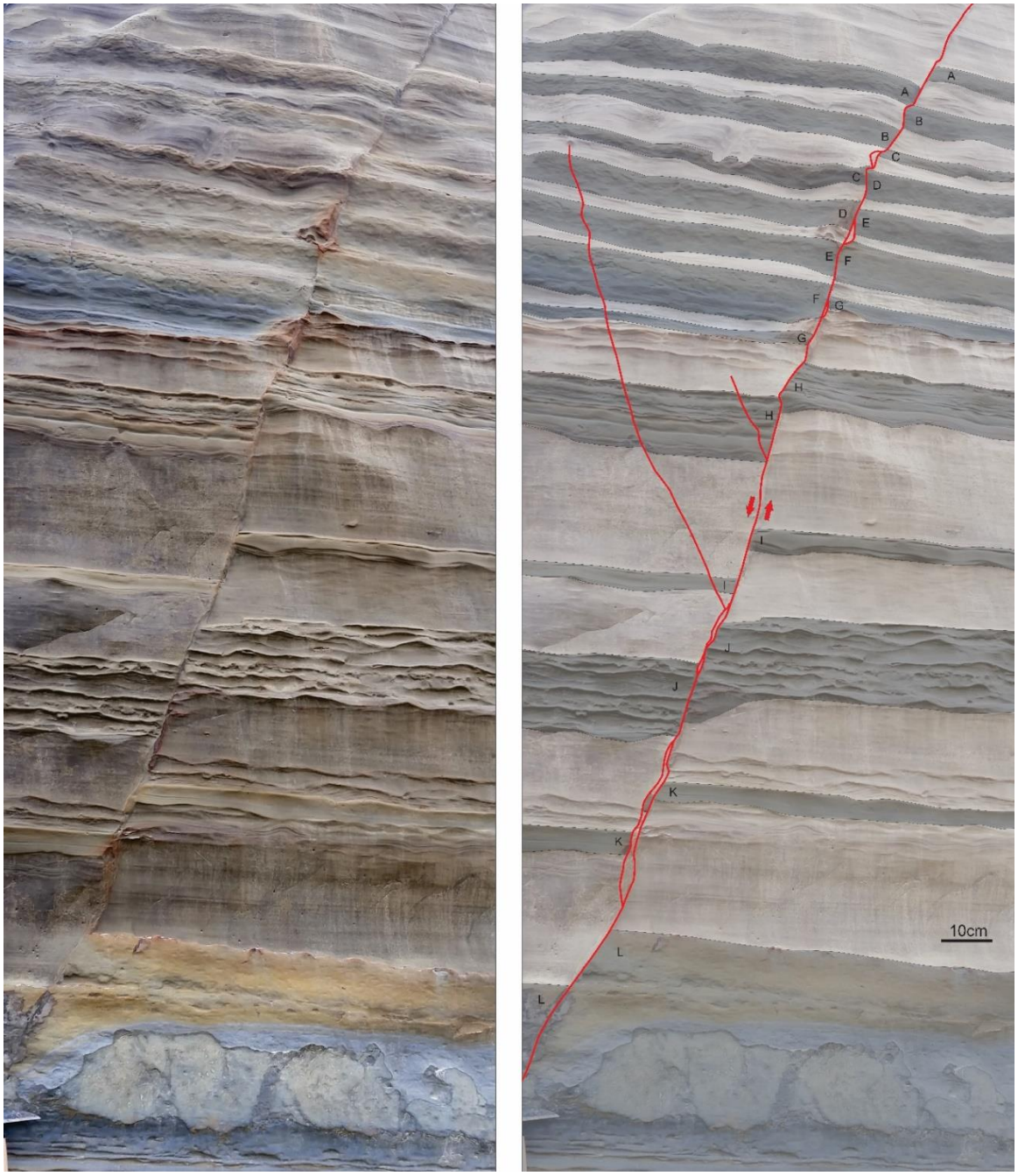

Figure 4.9 Uninterpreted (left) and interpreted (right) photograph of fault Pukearuhe 99 showing the displaced beds and major fault traces. See Figure 2.6 for photograph and fault location.

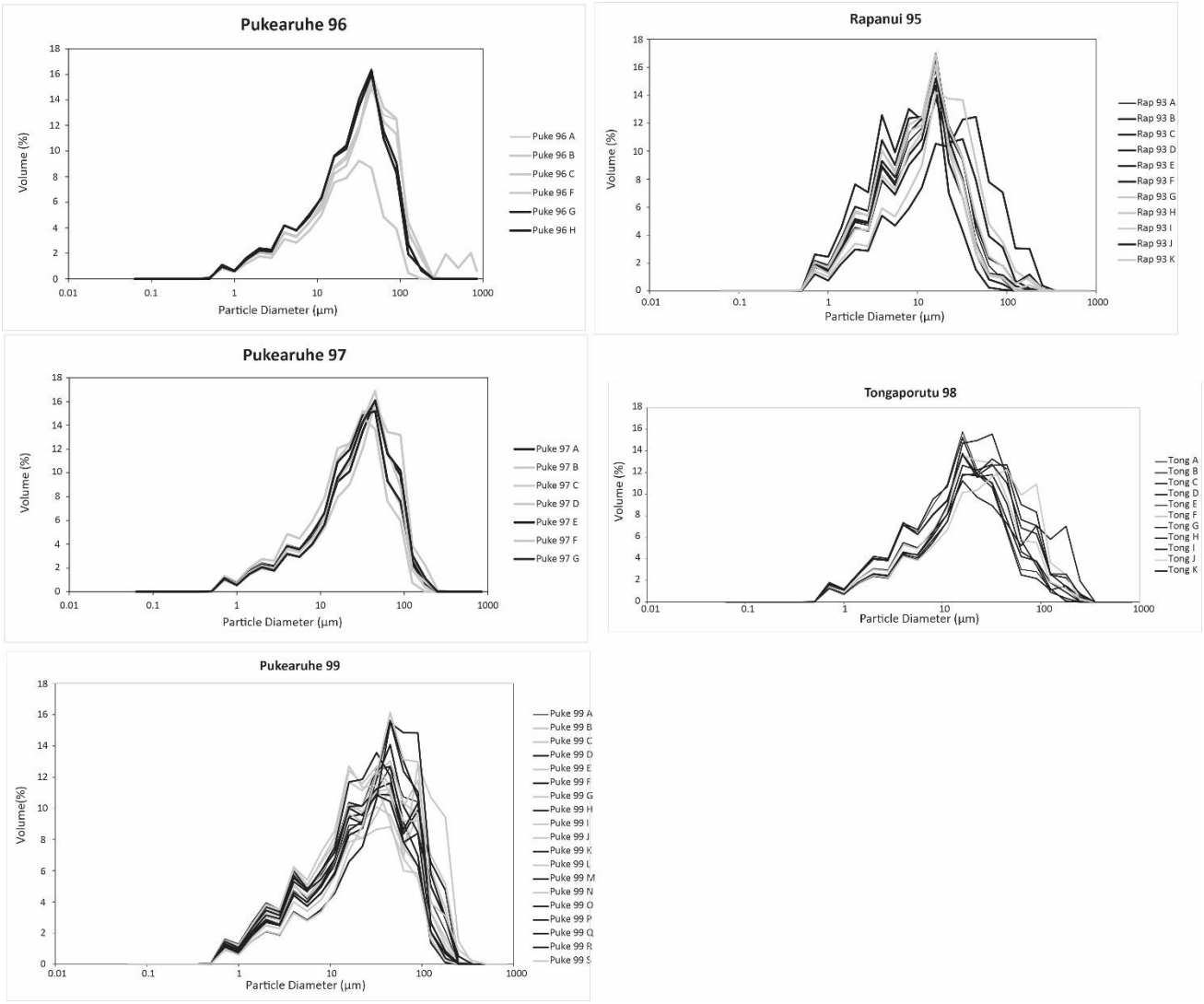

Figure 4.10. Graph of host siltstones from 5 faults in Taranaki coloured according to whether they smeared. Black = smeared, Grey = no smear. There appears to be no correlation between the host siltstone grain size distribution and likelihood of smear.

4.5.3 Shale bed water content

The water content of siltstone beds at the time of faulting could influence the formation of shale smears. Siltstone beds with high water content may, for example, promote injection of silt along faults during slip (Pei et al. 2015). Information on the fluid content of silt beds at the time of faulting are rare and the impact of fluid content on siltstone smear difficult to access. The Mohakatino locality is within a slumped interval where both the shale beds and the shale smears have ragged boundaries formed in part by flame structures. These flame structures suggest that the siltstone beds were deformed by faulting when the sequence contained interstitial water and burial depths were low (e.g., <200 m). These conditions would have favoured the mobilisation of the silts and may help account for the importance of continuous shale smears at this locality. In Figure 4.4D, for example, the shale smear is continuous despite the displacement being almost a factor of 10 larger than the bed thickness.

Displacement-bed thickness ratios of this order are rare along the Taranaki coast for continuous smears and could reflect high fluid content at the time of faulting.

4.5.4 Shale bed strength

Mechanical weakness of shale beds, both in absolute terms and relative to sandstone beds, is often quoted as being an important factor for the formation of shale smear (Giger et al. 2013). Schmidt (rebound) Hammer measurements from the Mount Messenger Formation suggest that siltstone beds may be stronger than sandstone beds in Taranaki. Relative Schmidt hammer tests conducted on each host bed for six down fault profiles showed that the siltstone beds were relatively harder than the sandstone interbeds (Table 4.3). These differences in hardness are supported by examination of eroding sandstone and siltstone beds in the coastal cliffs, where the siltstones often appear to be eroding more slowly (they slightly protrude from the outcrop) and may be more resistant to erosion (than the sandstone beds). Similarly, sandstone samples can be easily extracted from the outcrop, whereas siltstone beds can require a hammer and chisel to remove samples. Lastly, siltstone samples also stand up better to lab preparations and have a much higher survival rate when being analysed. Collectively these observations suggest that siltstone beds are marginally stronger than sandstone beds and that sandstone smear could be at least as common as shale smear. Our field observations confirm that sandstone smear occurs frequently in Taranaki, although we have not collected sufficient sandstone smear data to determine whether it occurs more frequently than siltstone smear.

We have also examined the Schmidt Hammer results to determine if they are negatively related to the occurrence of smear (i.e., stronger beds have less smear). The results show that at individual outcrops the rebound measurements do not vary significantly between beds, while the full range of continuous smear, discontinuous smear and no smear are typically observed. These data provide little support for the idea that siltstone bed strength is a controlling factor for the formation of smear.

We acknowledge that the mechanical strength of the beds at outcrop is not necessarily a reflection of the relative strengths at maximum burial and faulting. However, previous outcrop studies have noted that sandstone interbeds have been more consolidated than the shale where exposed and therefore the relative strength of beds at outcrop is commonly considered to be important when investigating controls on shale smear (Lindsay et al. 1993, Lehnar and Pillar 1997, Giger et al. 2013, Kristensen et al. 2013).

Table 4.3 A table showing average Schmidt hammer readings for siltstone and sandstone beds displaced by five faults. For descriptions of each fault see Chapter 2. A summary of the faults is shown in Table 2.1 in Chapter 2. Number of readings used to calculate average values are shown in brackets.

LITHOLOGY	RAPANUI 95	PUKEARUHE 96	PUKEARUHE 97	TONGAPORUTU 98	PUKEARUHE 99
AVERAGE SILTSTONE	10.2 (N=55)	22.7 (N=40)	23.7 (N=40)	28.6 (N=55)	20.4 (N=95)
AVERAGE SANDSTONE	8.7 (N=55)	20 (N=40)	22.3 (N=45)	28.3 (N=55)	19.9 (N=100)

4.5.5 Fault-zone architecture

Fault-zone architecture and the extent to which secondary faults within the zones accommodate displacement may play a role in the formation of shale smears and shale slices. Foxford et al. (1998) indicate that the number of slip surfaces within a fault zone could influence the formation of shale smears, with a higher number of slip surfaces producing more fault-bound slices of shale in the fault zone and a greater chance of shale smear. In addition, secondary faults within faults zones can locally impact the thickness of smears, in some cases removing the smear altogether. In Taranaki secondary faults with in fault zones may be the primary mechanism by which smear thicknesses change in dip sections (Childs et al. 2007; Nicol and Childs 2018). The impact of secondary faults in fault zones on the formation of shale smears and shale slices is dependent on several factors including, the number of secondary faults within the zone, how much of the total fault displacement is accommodated on these distributed faults, the spacing of the faults (and the width of the fault zone) and the resolution limit of the data. In cases where all displacement is accommodated on a single slip surface, by definition smearing and slicing of shale beds must be absent. Similarly, where there is no principal slip surface and displacement is distributed across the fault zone on multiple slip surfaces, then by definition shale slicing must occur.

Observations of faults in Taranaki support the view that shale slicing is common in cases where displacements are distributed across multiple slip surfaces (e.g., compare Figure 4.4, B and C). However, the role of fault-zone faulting in forming shale smears is much more difficult to observe at outcrop scale and to convincingly demonstrate without the aid of thin sections. In addition, due to the complex interplay of fault zone parameters and shale smear formation, the relationships between fault-zone architecture and shale smear formation is not always clear. For example, the plots of fault zone width or number of slip surfaces against smear continuity for faults in the Mount Messenger Formation show only weak correlations at best (Figure 4.7 and Figure 4.8). In cases where the locations

of shale smear or shale slicing are controlled by fault-zone architecture the occurrence of smears and slices are primarily influenced by the processes that produce segmentation, bending and stepping of the primary fault surface. In heterogeneous sedimentary sequences, where bedding exerts a control on fault propagation, the formation of fault-zone will be influenced by the physical properties of all beds and the mechanical discontinuities at their boundaries, rather than being entirely related to the properties of the shale beds (Childs et al. 2009).

4.5.6 Fault dip

In some cases decrease in fault dip can increase the amount of shale smear (Fulljames et al. 1997). For cross sections approximately parallel to fault dip the angle between the fault and shale bed could impact the amount of smearing observed (Fulljames et al. 1997). Here we have adopted the approach of Fulljames et al. (1997) and measured the bed-fault angle for both footwall and hangingwall cutoffs and the length of shale smear for 128 siltstone bed fault couples (see Chapter 2). Although this analysis is only in 2D, it provides a means of testing the potential role of fault dip on shale smear occurrence. Of the sampled faults 49% (63) were from beds that exhibited discontinuous smear, 40% (51) were from beds that showed no smear and 11% (14) were from beds that exhibited continuous smear. All three categories saw a similar range in angles recorded from ~ 30^{o} to 150^{o} (see Figure 2.7). There was a weak trend between the angle and the type of smear, with non-smeared beds more likely to have hangingwall and footwall cutoff angles and fault dips approaching ~90^{o} (median footwall angle 73^{o} and the median hangingwall ~108^{o} with an estimated median fault dip of ~75 ^{o}). By contrast, discontinuous smears showed greater variation with very few faults (< 10%) having cutoff angles of ~90^{o} with a median footwall and hangingwall cutoff angles of 60^{o} and 120^{o}, respectively. Similarly, continuous smears had no beds with angles of ~90^{o}, with footwall and hangingwall median values of ~63^{o} and ~122^{o}, respectively. While there is little difference between the cutoff angles for discontinuous and continuous smears, the available data from Taranaki may support the view non-smearing shale beds are more likely (than smeared beds) to have steep dips (e.g., >70°).

4.6 Discussion and conclusions

The study of larger scale faults is required to assess if the processes seen at the centimetre scale are also reflected in those resolvable on seismic sections (e.g. faults with displacements of decametres to kilometres). However, this can be difficult as finding a fault that has a large displacement, is accessible

and has beds that can easily be traced either side of the fault is uncommon and limits the amount we can investigate these processes at outcrop. While the analysis of the fault rock content can be conducted, both displaced beds need to be present for algorithms to be calculated so that their predictive abilities can be analysed.

Overall, the results from this study and from the literature indicate how much is unknown about the controls on shale smear formation and the process and evolution of low permeability fault entrained along a fault surface. Only by identifying the controlling factors on shale smear generation can accurate predictive models be produced and for this to be possible more work needs to be carried out to constrain the variability, as well as similarities, in fault zones globally.

While phyllosilicate content has been shown to control the degree of smear continuity within this study it only does so at the outcrop scale. At the smaller bed to bed scale it does not correlate well with the frequency or continuity of smear suggesting that secondary factors may play a role. This study suggests that the total organic carbon content, the fault architecture and the fluid content of the beds at the time of deformation could all influence the degree of smearing observed. Further work would be required to constrain the effect of each of these variables.

Fault seal may be influenced by both the continuity and frequency of shale smear. In cases where smear amalgamation is not common the continuity of smears will have a critical influence on fault seal. Shale smears may be common along faults, but if all smears are highly discontinuous and extend only a short distance from the source bed, then their effect on fluid flow will be minimal. At the other end of the spectrum there may be few shale smears but the smears may be continuous between cut offs and will impact fault seal. Therefore, the results of this chapter could have significant implications for fault seal. In particular, it is clear from faults in Taranaki that in some sequences many shale beds contribute little to the formation of low permeability fault rock and in these cases fault seal algorithms, such as Shale Smear Factor (SSF), Clay Smear Potential (CSP) and Shale Gouge Ratio (SGR), may over-estimate the amount of low permeability fault rock sourced directly from wallrock beds.

In Taranaki overestimates of the contribution of silt beds to the generation of fault rock may be partly, or entirely, countered by the production of fault rock by cataclasis of phyllosilicate-rich grains in faulted sandstone beds (Nicol and Childs 2018). The Mount Messenger Formation sandstones comprise about 50% lithic grains and are considered ‘dirty’ sands (Higgs et al. 2015). Therefore, for such ‘dirty’ sands it may be necessary to combine or sum the phyllosilicate content of both the shales and the sands to estimate the seal potential of the fault rock (see Chapter 5 for further discussion).

At present it seems unrealistic to assume that the controlling factors for the production of low permeability fault rock have been identified, especially since the process of smear formation and development over time is still relatively unknown. Bed thickness and displacement may play a role in this, and there are many compelling arguments that they do, however it is unlikely they are the only variables and therefore further work needs to be done to understand how we can further constrain these processes.

4.7 References

Aydin A. 2000. Fractures, faults, and hydrocarbon entrapment, migration and flow. Mar Pet Geol. 17(7):797–814. doi:10.1016/S0264-8172(00)00020-9.

Ballance PF. 1964. The Sedimentology Of The Waitemata Group In The Takapuna Section,Auckland. New Zeal J Geol Geophys. 7(3):466–499. doi:10.1080/00288306.1964.10422096.

Childs C, Manzocchi T, Walsh JJ, Bonson CG, Nicol A, Schöpfer MPJ. 2009. A geometric model of fault zone and fault rock thickness variations. J Struct Geol. 31(2):117–127. doi:10.1016/j.jsg.2008.08.009.

Childs C, Walsh JJ, Manzocchi T, Strand J, Nicol A, Tomasso M, Schopfer MPJ, Aplin AC. 2007. Definition of a fault permeability predictor from outcrop studies of a faulted turbidite sequence, Taranaki, New Zealand. Geol Soc London, Spec Publ. 292:235–258. doi:10.1144/SP292.14.

Ciftci BN, Giger SB, Clennell MB. 2012. Testing Fault Seal Prediction Algorithms Using Geomodels of Experimentally Produced Fault Zones. 3rd EAGE Int Conf Fault Top Seals.(October). doi:10.3997/2214-4609.20143014.

Faulkner DR, Jackson CAL, Lunn RJ, Schlische RW, Shipton ZK, Wibberley CAJ, Withjack MO. 2010. A review of recent developments concerning the structure, mechanics and fluid flow properties of fault zones. J Struct Geol. 32(11):1557–1575. doi:10.1016/j.jsg.2010.06.009.

Fisher QJ, Knipe RJ. 2001. The permeability of faults within siliciclastic petroleum reservoirs of the North Sea and Norwegian Continental Shelf. Mar Pet Geol. 18(10):1063–1081. doi:10.1016/S0264-8172(01)00042-3.

Foxford KA, Walsh JJ, Watterson J, Garden IR, Guscott SC, Burley SD. 1998. Structure and content of the Moab fault zone, Utah, USA, and its implications for fault seal prediction. Geol Soc London, Spec Publ.(147):87–103.

Fristad T, Groth A, Yielding G, Freeman B. 1997. Quantitative fault seal prediction: a case study from Oseberg Syd. Nor Pet Soc Spec Publ. 7(C):107–124. doi:10.1016/S0928-8937(97)80010-0.

Fulljames JR, Zijerveld LJJ, Franssen RCMW. 1997. Fault seal processes: systematic analysis of fault seals over geological and production time scales. Nor Pet Soc Spec Publ. 7(C):51–59. doi:10.1016/S0928-8937(97)80006-9.

Giger SB, Clennell MB, Çiftçi NB, Harbers C, Clark P, Ricchetti M. 2013. Fault transmissibility in clastic-argillaceous sequences controlled by clay smear evolution. Am Assoc Pet Geol Bull. 97(5):705–731. doi:10.1306/10161211190.

GNS Science 2018, Petroleum Basin Explorer, Fault Seals Database, viewed 20th February 2019.

Higgs KE, Arnot MJ, Brindle S. 2015. Advances in grain-size, mineral and pore-scale characterization of

lithic and clay-rich reservoirs. Am Assoc Pet Geol Bull. 7(7):1315–1348. doi:10.1306/01271513101.

Lehner FK, Pilaar WF. 1997. The emplacement of clay smears in synsedimentary normal faults-inferences from field observations near Frechen , Germany. NPF Spec Publ. 7:39–50.

Lindsay NG, Murphy FC, Walsh JJ, Watterson J. 1993. Outcrop Studies of Shale Smears on Fault Surface. Int Assoc Sedimentol Spec Publ.(15):113–123.

Manzocchi T, Childs C, Walsh JJ. 2010. Faults and Fault Properties in Hydrocarbon Flow Models. Geofluids:94–113. doi:10.1111/j.1468-8123.2010.00283.x.

Nicol A, Childs C. 2018. Cataclasis and silt smear on normal faults in weakly lithified turbidites. J Struct Geol. 117(June):44–57. doi:10.1016/j.jsg.2018.06.017.

Pei Y, Paton DA, Knipe RJ, Wu K. 2015. A review of fault sealing behaviour and its evaluation in siliciclastic rocks. Earth-Science Rev. 150(October):121–138. doi:10.1016/j.earscirev.2015.07.011.

Rattenbury M., & Townsend D., Johnston M. (2000). Geology of the Kaikoura Area. Tech. rep.. 13.

Schmatz J, Vrolijk PJ, Urai JL. 2010. Clay smear in normal fault zones - The effect of multilayers and clay cementation in water-saturated model experiments. J Struct Geol. 32(11):1834–1849. doi:10.1016/j.jsg.2009.12.006.

Sperrevik S, Færseth RB, Gabrielsen RH. 2000. Experiments on clay smear formation along faults. Pet Geosci. 6(2):113–123. doi:10.1144/petgeo.6.2.113.

Vrolijk PJ, Urai JL, Kettermann M. 2016. Clay Smear: Review of Mechanisms and Applications. J Struct Geol. doi:10.1016/j.jsg.2015.09.006.

Yielding G, Freeman B, Needham DT. 1997. Quantitative fault seal prediction. Am Assoc Pet Geol Bull. 81(6):897–917. doi:10.1306/522B498D-1727-11D7-8645000102C1865D.

5 Implications of outcrop observations of small faults for the utility of fault-seal algorithms

5.1 Abstract

Using the available data and published shale-smear algorithms we calculate Shale Smear Factor (SSF), Clay Smear Potential (CSP) and Shale Gouge Ratio (SGR) for over 180 siltstone beds displaced on small normal faults in thinly bedded sandstones and shales. The algorithms were applied both to a series of detailed down fault profiles from Taranaki and also a larger dataset on individual faulted beds from Gore Bay, Taranaki and White Bluff. Outcrop data for small faults have been studied to determine if the output from three fault-seal algorithms (CSP, SSF and SGR) are compatible with the observed shale smear continuity and fault-rock thicknesses. Our data show both shale smear continuity and fault-rock thickness are highly variable at length scales of <1 m. Shale smears have been divided into three groups of continuous smear, discontinuous smear and no smear. These groups have been compared to bed thickness, displacement and outputs from the three fault-seal algorithms. The data show little correlation between bed thickness, displacement and the continuity of shale smears. Fault seal CSP and SSF algorithms use bed thickness and fault displacement as input parameters and these algorithms also show no correlation with the occurrence of discontinuous and non-smears. Consistent with previous studies, continuous smears are found to be most common when they are derived from thick beds with low displacements. Comparison of fault-rock thickness measurements and fault-seal estimates from the three algorithms indicate that the algorithms do not reproduce the short wavelength (<0.5 m) up to order of magnitude variations in fault-rock thickness. The algorithms are unlikely to identify locations of minimum fault-rock thickness on the fault surfaces which are the most likely sites of across-fault flow. The poor correlations between outputs from the algorithms and outcrop observations may arise because the algorithms over simplify fault-zone structure and shale smear geometries, and do not explicitly account for processes other than shale smear that produce fault rock (e.g. cataclasis).

5.2 Introduction

Faults can affect reservoir compartmentalisation, the integrity of seals and the migration of fluids between traps in interbedded sequences (Figure 5.1) (Fisher and Knipe 2001; Cartwright et al. 2007). Fault rocks generated during displacement have the potential to impede or retard across-fault flow of fluids (Lindsay et al. 1993; Caine et al. 1996; Lehner and Pilaar 1997; Yielding et al. 1997; Foxford et al. 1998; Aydin 2000; Childs et al. 2007; Manzocchi et al. 2010). Fault sealing is of significant interest to many industries including, but not limited to, those involved in groundwater and hydrocarbon extraction, and CO_2 sequestration (Gutierrez et al. 2000; Bense et al. 2013). These industries are concerned with fluid movement on production (e.g., <100 years) and geological timescales of millions of years (Childs et al. 1997). To assess if a fault is sealing for fluid flow it is important to understand what controls a fault's ability to transmit fluids. There are four main ways in which fault seal can be produced: (i) juxtaposition of impermeable and permeable beds across a fault-zone, (ii) the formation of impermeable shale smear, (iii) the production of cataclastic fault-rock within the fault-zone and/or, (iv) the cementation of the fault-zone by diagenetic or mineralisation processes. These processes may not necessarily act independently and could change over geological time. Processes (i) and (ii) are most often assessed using Allan Diagrams of fault surfaces (Allan 1986) and fault-seal algorithms (Lindsay et al. 1993; Lehner and Pilaar 1997; Yielding et al. 1997; Childs et al. 2007; Giger et al. 2013; Pei et al. 2015; Vrolijk et al. 2016), respectively, while cataclasis and cementation are rarely explicitly accounted for in fault-seal analysis. Shale-smear algorithms are often combined with Allan diagrams to highlight areas of reservoir to reservoir juxtaposition where across-fault fluid flow is most likely. Combining these data with well pressures and/or flow rates increases the chance of an accurate prediction of fault seal (Fristad et al. 1997; Fulljames et al. 1997; Yielding et al. 1997; Yielding 2002; Yielding et al. 2010; Vrolijk et al. 2016).

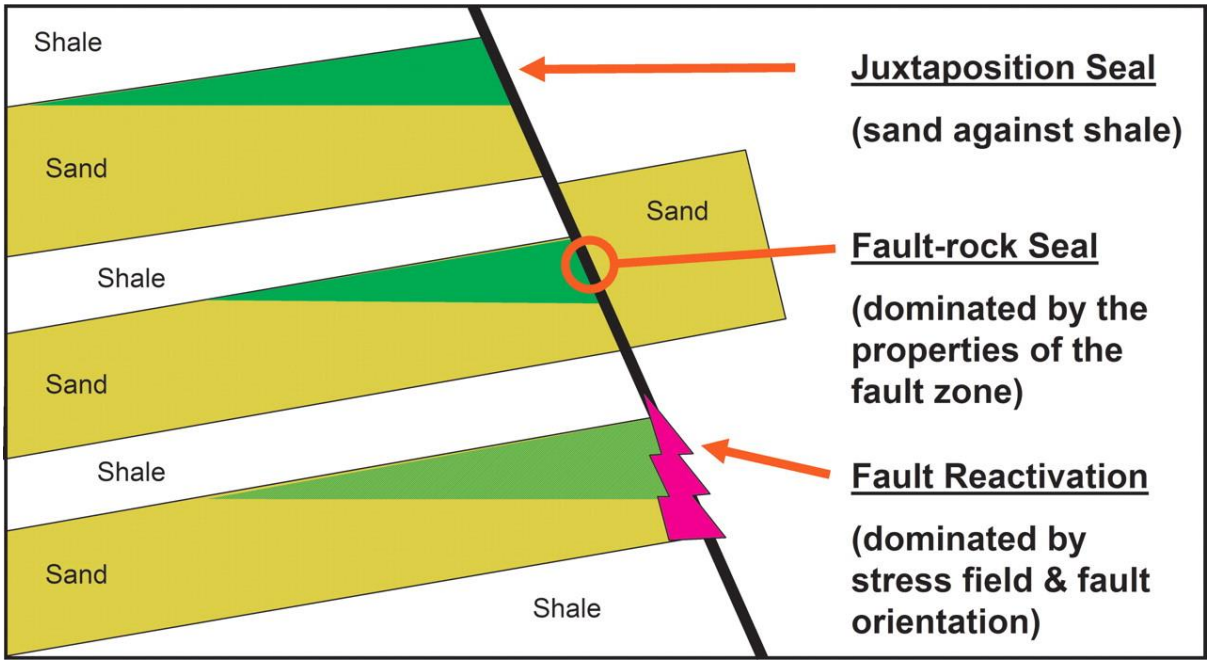

Figure 5.1 Schematic from Yielding et al. (2010) showing the three main influences on fault permeability.

Three main shale-smear algorithms have been developed to estimate fault-seal potential of normal faults in siliciclastic sequences (Bouvier et al. 1989; Lindsay et al. 1993; Fristad et al. 1997; Fulljames et al. 1997; Lehner and Pilaar 1997; Childs et al. 2007). These algorithms are referred to as Clay Smear Potential (CSP), Shale Smear Factor (SSF) and Shale Gouge Ratio (SGR). A summary of these main algorithms, their variants and the publications on which they are based is provided in Figure 5.2 and Table 5.1. Although subtly different, the algorithms primarily utilise estimates of shale thickness in the faulted wall rock and fault displacement. Implicit in these equations is the assumption that fine-grained fault rock is mainly sourced from mudstone beds in the wall rock adjacent to the fault. For fault seal analysis in petroleum reservoirs it is typically measured from seismic reflection lines, while VShale well logs are used to estimate the amount of shale in the faulted sequence. Using VShale data the algorithms focus on the amount of clay within the sedimentary host units rather than the processes that lead to smear and fault-rock formation (Vrolijk et al. 2016). The algorithms assume that the fault-rock at a given point will be a deformed representation of the host rock composition that has been displaced past that point (Noorsalehi-Garakani et al. 2013), with little consideration given to the complexity of fault-zone structure (Childs et al. 2009). The existence of multiple fault slip surfaces or throw partitioning across relay zones can create across fault juxtapositions not predicted by algorithms meaning reservoir-reservoir contacts may be overlooked and a fault may be predicted to be sealing when in reality it is not (Childs et al. 2009; Kettermann et al. 2016).

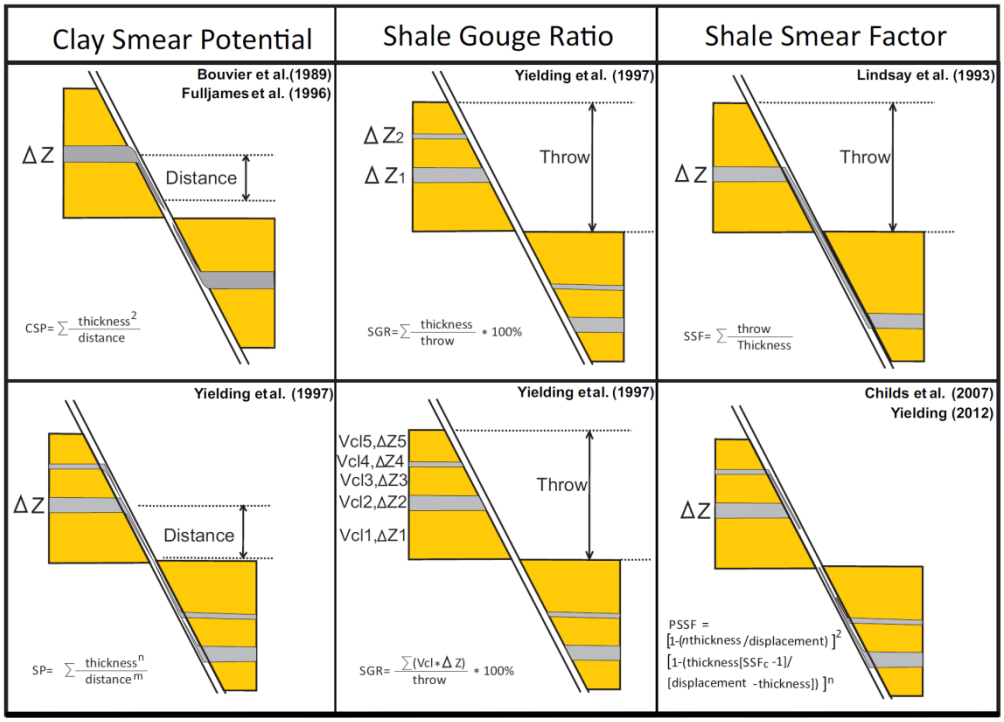

Figure 5.2 Infographic showing the different shale-smear algorithms and how they are calculated. All three algorithms use the relationship between the host shale-bed thickness and the vertical distance the beds have been displaced along the fault. In all diagrams yellow beds are sandstone and grey beds shale. All models use planar faults, common fault dips and uniform fault-zone widths (modified from Childs et al. 2007; Vrolijk et al. 2016).

Table 5.1 A summary table of the three main shale smear algorithms used to predict the presence and distribution of low permeability fault-rock (Giger et al. 2013).

Algorithm	Formula*	Predictive Application	Mechanisms	References
Clay smear potential (CSP)	$CSP = c \times \sum t_{sh}^{n}/d^{m}$ $c = 1, m = 1, n = 2$	Thickness of clay smear	Injection, flow	Bouvier et al., 1989; Lehner and Pilaar, 1997
Variations: Calibration factor $c \neq 1$ to account for rheology and stress dependency				Fulljames et al., 1997
Smear factor (SF = CSP, but where $c = 1$, $m \neq 1$, $n \neq 2$)[1],				[1]Yielding et al., 1997
also referred to as generalized smear potential (GSP) by[2]				[2]Doughty, 2003
Shale smear factor (SSF)	$SSF_{[c]} = S_{t[c]}/t_{sh}$**	Continuity of clay smear, seal breakdown for SSF = SSF_c	Abrasion, shear/drag, injection/flow	Lindsay et al., 1993
Variation: Probabilistic shale smear factor (PSSF)				Childs et al., 2007
Shale gouge ratio (SGR)	$SGR = \sum[V_{sh(i)} \times t_{sh(i)}]/S_t$	Distribution of phyllosilicates along fault zone, seal strength when calibrated	Abrasion, wear, grain-scale mixing	Fristad et al., 1997; Yielding et al., 1997
Variation: Effective shale gouge ratio (ESGR) with weighting factor, essentially a hybrid of CSP and SGR				Knipe et al., 2004; Freeman et al., 2010

*c = constant to calibrate for rheology and stress; d = distance between the shale/clay source layer and a point in the fault zone; m and n = scaling exponents; S_t = cumulative or total slip; t_{sh} = thickness of phyllosilicate-rich (clay/shale) layer; V_{sh} = volumetric fraction of phyllosilicates.
**The subscript $_{[c]}$ denotes the critical S_t at which clay smears become discontinuous (seal breakdown).

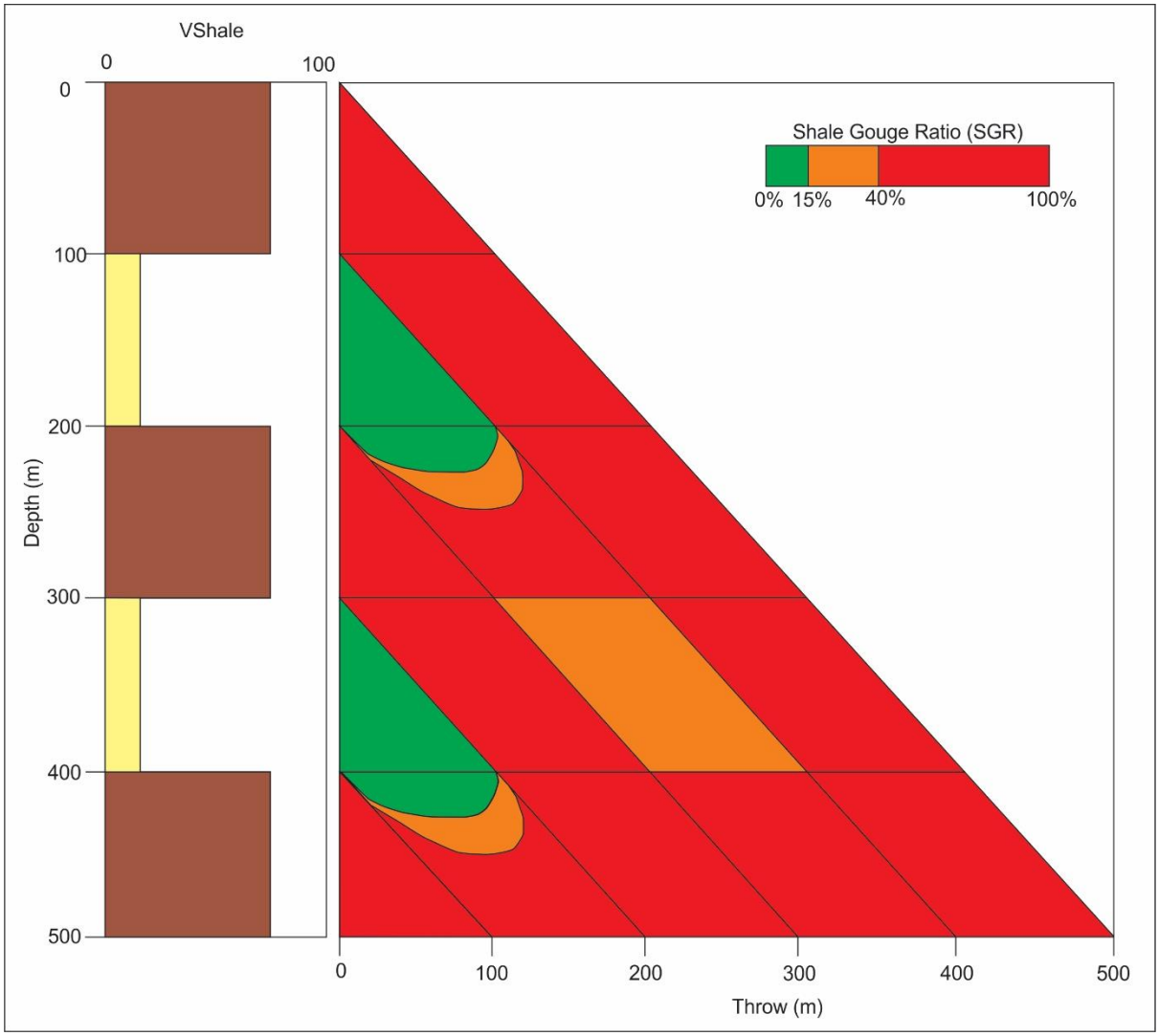

Figure 5.3 An example of how the Shale Gouge Ratio (SGR) can be combined with a traditional Allan diagram to create a predictive tool for fault-rock seal. The Vshale log is used to inform the phyllosilicate content for stratigraphic units, with the throw taken from seismic. The combination of SGR and Allan Diagram allows for both fault juxtaposition seal and fault-rock seal to be assessed and the likelihood for fault-rock seal at reservoir/reservoir juxtapositions.

Although the fault seal predictions using SGR have been tested using oil column heights and reservoir pressures (Yielding et al. 1997; Foxford et al. 1998), many fault-seal predictions are either not validated or calibrated using independent datasets. Calculations typically use data from well logs, seismic imaging or well pressures, which are not direct measurements of fault attributes; this means that the input data contains a degree of uncertainty. In the absence of column height, pressure data or fluid flow information across faults, we test the assumption that fault-seal predictions are positively related to fault-rock thickness, where fault-rock thickness is a key parameter for calculating fault permeability (Manzocchi et al. 2010). In particular, we focus on shale-smear algorithms and how well they predict the distribution of fault-rock across a fault surface. In this chapter, we review the literature for the formation of low permeability fault-rock and the current predictive algorithms to highlight how and why each algorithm was designed, as well as the shortcomings of each. We use

detailed measurements of fault-rock thickness and calculated CSP, SSF and SGR for six dip-profiles from small normal faults in the Mount Messenger Formation of northern Taranaki. The algorithms produced fault-seal predictions that appear to be unrelated with the measured thicknesses of fault rock. In addition, none of the algorithms could be used to differentiate between continuous, discontinuous or non-smearing beds. It is proposed that SGR may be the best algorithm to use as it considers the clay fraction in the host sandstone as well as the host siltstone and allows cataclasis and phyllosilicate framework rocks to be included in fault-seal predictions. To improve SGR predictions further it is suggested that they should be combined with frequency distributions of smear continuity so that it can be calibrated for a given location.

5.3 Fault Seal

Faults exhibit a range of fluid-flow behaviours in the subsurface. Fault-zones can act as conduits, barriers and dual conduit/barrier systems for fluid flow (Caine et al. 1996; Cartwright et al. 2007; Bense et al. 2013), with variations possible along both strike and dip directions, and over production or geological timescales. For example, fault ruptures may be associated with transient dilation of a fault surface (and/or fractures within fault zones) and increase the ability of fluids to use the fault as a conduit. There can also be variations in across- and along-fault flow depending on the juxtaposition of beds across the fault and the permeability and distribution of low permeability fault-rock within the fault-zone.

Fault rock in siliciclastic sequences can be divided into four categories based on the host lithology (Fisher and Knipe 2001). These are: i) disaggregation zones which occur in clean sandstones (<14% clay) with no grain damage and deformation is taken up in grain rearrangement, ii) cataclastic faults in clean sandstones that show decreases in permeability and porosity due to a decrease in grain size as a result grain fracturing, iii) faulting of phyllosilicate framework rocks in dirty sandstones (14%-40% clay) that show a decrease in porosity and permeability due to the replacement of macroporosity with microporosity as clays are mixed in with framework grains, iv) clay smears in sediments with over 40% clay (Fisher and Knipe 1998; Fisher and Knipe 2001). Within a siliciclastic sequence of interbedded sandstone and siltstone the permeability difference between fault-rock and the associated siltstone host rock is far less than the permeability difference between the two lithologies, and the biggest control of fault rock on fluid flow is the incorporation of low permeability host rock in parts of fault-zones that separate sandstone beds (Childs et al. 2007). Fisher et al. (2018) suggest that fault-rock permeability is not strongly linked to the clay content of the host rock or to the type of fault-rock as clay content is not the sole control on permeability. Corroborating this idea is work conducted by

Frischbutter et al. (2017) who looked at syn-depositional normal faults in Upper Jurassic reservoirs in the North Sea. They suggest that while a relationship between fault-rock type and permeability reduction exists it is not as strong as previously thought. However, the controls on how often and how much low permeability host material is incorporated within a fault zone still remains unknown and therefore further work is required if fault permeability in such sequences is to be fully understood.

5.3.1 Low Permeability Fault-rock Generation

Low permeability fault-rock is a term typically applied to material in fault zones that can retard or prevent fluid flow. Research into low-permeability fault rock has been focussed on the production of shale smears, which form by the inclusion of low permeability mudstone (i.e. siltstone, shale and clay) from the wall rock into the fault-zone. The entrainment and distribution of low permeability host units into the fault-zone via abrasion, shearing, injection and slicing has been documented by many authors (e.g. Lindsay et al. 1993; Lehner and Pilaar 1997; Yielding et al. 1997; Giger et al. 2013). Efforts to predict the location, extent and geometries of shale smears have been limited in number and success due to the number of parameters that are needed to accounted for their formation (Welbon et al. 1997).

To quantify the distribution of shale smears it is important to first have an unambiguous definition of smear. While there is agreement that shale smear is formed by fine-grained host rock becoming entrained within the fault-zone, there are a number of ways in which this can occur and consequently a diversity of views on what the resulting fault-rock may look like. For example, there is no description on what degree of deformation or mixing a host bed needs to have undergone to be defined as a smear rather than a lens of host rock within the fault-zone. The resulting discrepancies between authors for the definition of shale smears are indicated by the following quotes. Shale smears are described by Vrolijk et al. (2016) as “a type of clay gouge that develops by mechanical processes alone” and by Lindsay et al. (1993) as a “shale or clay layer intervening between sandstone units juxtaposed across a fault”. Shale smear is similarly summarised as “clay smear loosely incorporates all processes that transfer clay from the host rock into the fault-zone” (van der Zee and Urai 2005). Fisher et al. (2018) used fault-rock microstructure to define clay smear, suggesting that it incorporates all clay supported fault-rocks. A more detailed description is given by Ciftci et al. (2012) who describe shale smear as “a laminar volume of phyllosilicate-rich material that is entrained in a fault-zone between offset mudstone layers of the hangingwall and footwall blocks”.

To be able to predict the distribution of smear, there needs to be a basic understanding of what controls shale smear formation in the first place. Current studies suggest that there are a broad range of controls, conditions and influences on the generation of fault-rock. These are summarised very briefly below to display the range of proposed conditions that may influence the composition and geometry of fault-rock on a given fault surface.

The type of sediments within a sequence has a significant role in determining the type of fault-rock deformation, the petrophysical properties and the structures of fault-rock (Pei et al. 2015). Estimating the phyllosilicate content of the host rock is often used as an approximate indictor of fault permeability. These variables have an inverse relationship with lower phyllosilicate content of the host rock generally associated with higher fault permeability. The phyllosilicate percentage is sometimes used to differentiate which fault-rocks can be deemed clay smear, with Pei et al. (2015) suggesting that fault-rocks with >40% clay/phyllosilicates are called shale smears. XRD analysis conducted by GNS of siltstones sampled from the Mount Messenger Formation (MMF) indicate an average phyllosilicate content of ~46%, with values ranging from 36.5% to 53.8% and only two of 14 samples having a phyllosilicate percentage below 40%. Therefore, shale smears in the MMF satisfy the definition of Pei et al. (2015).

The mechanisms of shale smear generally require that there is a considerable difference between the mechanical strength of shale and sandstone beds being displaced, with the shale considered to be the weaker of the two. This strength contrast results in either the shale being abraded into the fault by the mechanically stronger sandstone as the units are displaced past each other or as the shale migrating into the fault-zone via ductile flow. Such ductile flow may reflect injection or shearing processes, with shearing most often considered to produce the classical tapering smear geometry. At the point where the shale begins to deform in a brittle manner it will no longer form one smooth or continuous smear, but will be faulted into the zone by one or more small-scale synthetic slip surfaces. As discussed in Chapter 2, the perceived transition from ductile to brittle deformation of shale beds is dependent on the scale of observation.

5.4 Fault-Seal Algorithms

Three predictive algorithms have been developed to provide an indication of the likelihood of fault seal. These are: clay smear potential (CSP), shale smear factor (SSF), and shale gouge ratio (SGR) (see Figure 5.2). While these algorithms all work in slightly different ways and produce different indicators for fault seal, they are all based upon the notion that bed thickness and displacement are primary

controls on the incorporation of low permeability material into a fault-zone. The algorithms are not predictions of fault sealing but more the likelihood of clay smear developing along a fault surface (Yielding et al. 1997). This chapter tests the accuracy of the three most common shale smear algorithms by applying them to faulted siltstone and sandstone interbeds of the MMF, Taranaki. CSP models ductile smears that typically develop in non-lithified clays (Lehner and Pilaar 1997). CSP values rise with increasing bed thickness and the number of beds displaced past a point on the fault trace and can decrease with increasing throw. The constants M and N were added to the CSP equation by Yielding et al. (1997) in an attempt to make the algorithm more flexible allowing it to be applied across a range of interbedded sequences. SSF is designed to model the behaviour of abrasion type smears and is constant between host cut offs as it contains no measure of the distance from the source bed (Lindsay et al. 1993). SGR records the proportion of shale source beds in a sequence that has moved past a point on a fault and, like the other two algorithms assumes that fine-grained fault rock is primarily derived from shale beds next to the fault in the host rock. SGR was primarily developed for situations where multiple shale beds contribute to the fault rock. It is less of a measure of smear continuity than SSF and CSP and is more focussed on predicting the percentage of shale/clay within the fault-rock. Below we summarise the CSP, SSF and SGR fault-seal algorithms and their application.

5.4.1 Clay Smear Potential (CSP)

Clay Smear Potential (CSP) is calculated by measuring the distance between the host bed and the midpoint between the hangingwall and footwall cut offs and dividing this value by the clay bed thickness squared (Figure 5.4). In general, the higher the CSP the greater likelihood of producing continuous smear. The CSP algorithm is based upon the observed characteristics of deformed non-lithified clays that produce ductile smears (Dockrill and Shipton 2010). Several fault sealing cut-off values have been proposed for CSP which, as with the other algorithms, vary from area to area. Jev et al. (1993) used faults from the Akaso Field in the Niger Delta to determine the CSP cut off for sealing and non-sealing faults. The faults studied gave a CSP cut off of 15 and below for non-sealing faults and 30 and above for faults that bounded prospects. Bentley and Barry (1991) conducted a similar investigation on Comorant Block IV in the Brent Province and found that a CSP value of 5 provided a cut off between sealing and non-sealing faults. A key difference between CSP and the other algorithms is that CSP takes into account the viscosity of clay and therefore incorporates fluid dynamics based on research by Lehner and Pilaar (1997). This is represented by the bed thickness being raised to the power of two. CSP can also be adjusted to account for differences in host clay composition and therefore accounting for different clay flow viscosities.

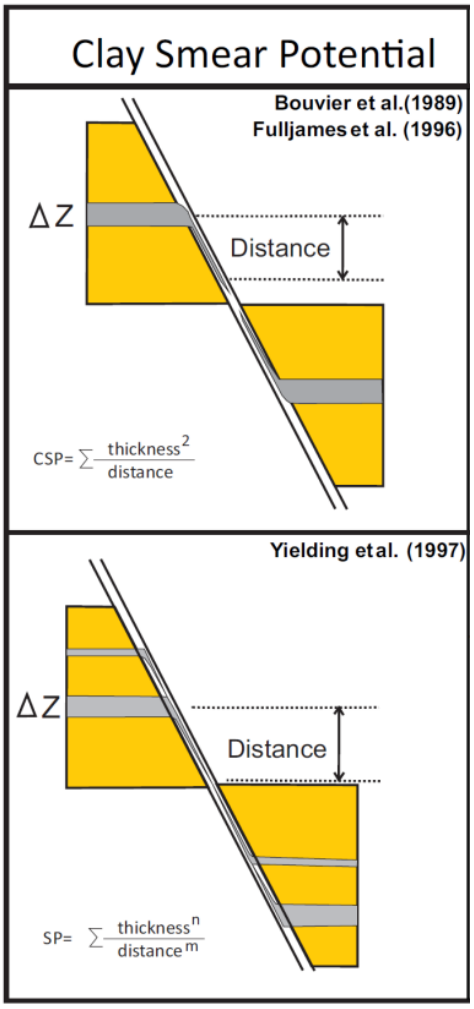

Figure 5.4 Schematic diagram showing the CSP algorithms calculated for individual beds (above) and multiple beds (below). Sandstone units are in yellow and shale units in grey (modified from Childs et al. 2007; Vrolijk et al. 2016).

5.4.2 Shale Smear Factor (SSF)

Shale smear factor (SSF) divides the distance that the bed is displaced vertically along a fault by the thickness of the shale bed (Figure 5.5) (Lindsay et al. 1993; Yielding et al. 1997; Childs et al. 2007). SSF is constant along the fault plane between the displaced cut-offs of a bed and increases with displacement accumulation for a bed of thickness that may occur along a strike. In general, the lower the SSF value the higher the chance of having produced continuous smear between beds (Lindsay et al. 1993). Key for estimating fault seal is establishing the SSF value below which continuous shale smears (i.e. no break in the smear between the source beds) are likely to occur. Previous field studies

suggest that a critical ratio of fault displacement (throw) to bed thickness can be identified at which smears become discontinuous (Childs et al. 2007). Lindsay et al. (1993) proposed a cut off at a SSF Factor of 7 between continuous smearing and non-continuous smearing beds, but this has been disputed as continuous smears have been observed up to SSF of 50 (Gibson 1994). Dockrill and Shipton (2010) on the other hand suggested that smears can start to become discontinuous and seals can be breached at SSF values as low as 5-10. Furthermore, Fisher and Knipe (2001) suggest that discontinuous smears have been observed on faults with an SSF of <2, while faults with an SSF of greater than 15 have displayed continuous smears. The SSF values below which the smears are continuous for individual fields and faults can vary depending on a range of factors.

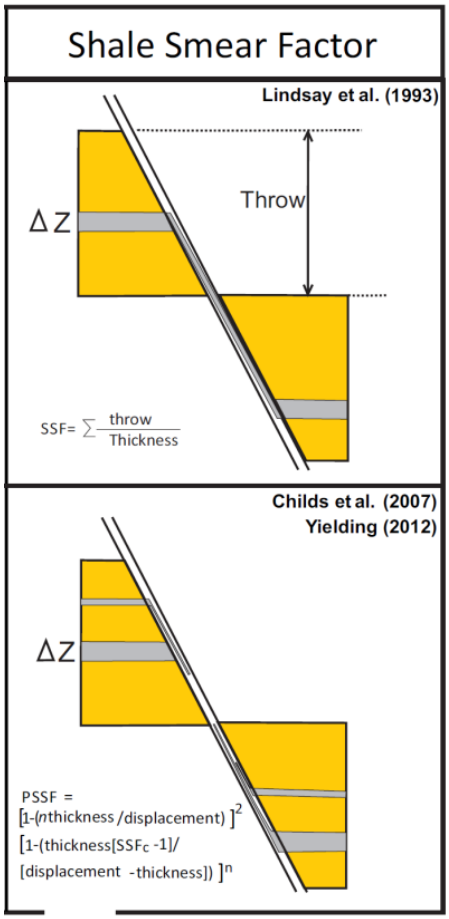

Figure 5.5 Schematic diagram showing the SSF algorithm calculated for individual beds (above) and the PSSF calculated for multiple beds (below). Sandstone units are in yellow and shale units in grey (modified from Childs et al. 2007; Vrolijk et al. 2016).

The Probabilistic Shale Smear Factor (PSSF), a modified SSF, was proposed by Childs et al. (2007) based on an outcrop study of normal faults from the Mount Messenger Formation in New Zealand. The

equation was developed in an effort to predict when and where holes within clay smear may form. For this approach the SSF below which all smears are continuous is defined and used to calculate the smear length for a shale bed of known thickness. Shale smears for one or more beds are randomly placed between bed cut-offs. PSSF uses the formula 1 – (Tx(SSFc -1)/(D-T))(where T= bed thickness, D=displacement and SSFc is the SSF value below which the smears are likely to be continuous), incorporating the shale smear factor to produce a probability that holes in the shale smear will occur. The holes represent areas of weakness within a seal through which fluids may be transmitted. Being able to predict if and where these holes exist has significant implications for fault seal integrity.

5.4.3 Shale Gouge Ratio (SGR)

Shale gouge ratio (SGR) is applied by calculating the average shale fraction of the units that have been displaced past a point on the fault, multiplying each fraction by the thickness of the shale bed, summing the fraction-thickness product for each bed, dividing the sum for all beds by the fault throw and multiplying by 100 to produce a prediction of the percentage of the fault-rock that is composed of shale (Figure 5.6) (Faulkner et al. 2010). SGR = (sum[(zone thickness)x(zone clay faction)]/fault throw)x100% (Yielding et al. 1997). SGR attempts to predict the composition of the fault-rock at a specific point along a fault using the sand and shale percentages of the host units that have moved past that section of the fault. It achieves this by assuming that the composition of fault-rock anywhere along a fault will be relative to the proportions of different lithologies that have moved past that point and that different host lithologies contribute equally to the resultant fault-rock (Faulkner et al. 2010). Whether this takes the form of unmixed sections representing the different lithologies than have been displaced or a more homogenous mixing of all beds to form a single low permeability fault-rock is not defined. The higher (>40-50%) the SGR the higher the shale volume percentage and the more likely the fault-rock is dominated by shale smears. Conversely, the lower the SGR (<15-20%) the lower the shale content in the fault-rock and the more cataclasites are inferred to dominate (Yielding et al. 2010). An SGR of 20% was suggested by Yielding et al. (1997) to separate sealing (>20%) and non-sealing (<20%) faults, however variation is expected from fault to fault and field to field (Childs et al. 1997) so a range of between 15% to 25% SGR is generally considered as the threshold between sealing and leaking fault behaviours (Dockrill and Shipton 2010).

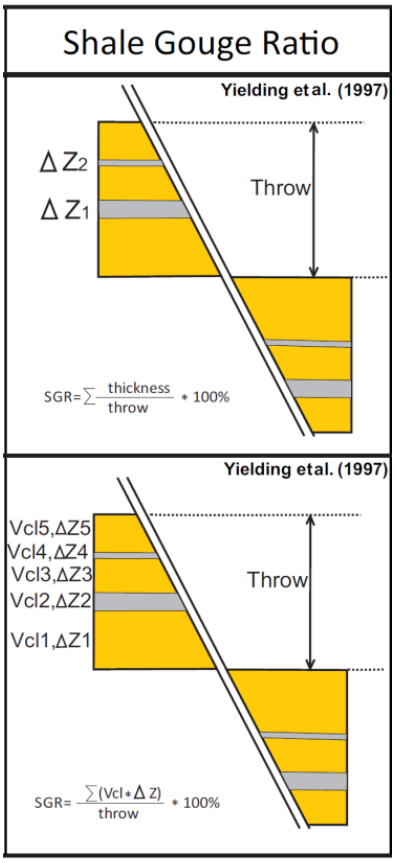

Figure 5.6 Schematic diagram showing the SGR algorithm calculated for shale beds (above) and calculated using the shale fraction of all units displaced (below). Sandstone units are in yellow and shale units in grey (modified from Childs et al. 2007; Vrolijk et al. 2016).

5.4.4 Comparison and Assumptions of Algorithms

To understand the limitations and applicability of different algorithms it is important to examine the scenarios (i.e. processes) that they were developed for and the assumptions that underpin them. CSP and SSF were originally developed from observations of fluvio-deltaic units raising the question of whether they are accurate when applied to units comprising different lithologies and depositional environments (Vrolijk et al. 2016). CSP and SSF differ from SGR in that they are intended to describe shale smear processes, while SGR describes the incorporation of phyllosilicates from the wallrock without identifying a specific process (N.B. SGR is often described as a mixing algorithm, but this is not

necessarily the case as it specifies the proportion of sand and shale present rather than their geometry in the fault). CSP and SSF aim to predict the continuity of a smearing clay bed, with greater continuity more likely to generate sealing fault-rock and impede across-fault flow. SGR produces a ratio of clay to sand for a specific point on a fault with the assumption that the higher the clay content the more likely the fault will seal. In this sense SGR could be applied to other fault-rock generating processes, such as cataclasis and the production of phyllosilicate framework rocks, whereas SSF and CSP are used solely to predict the presence of shale smear (Faulkner et al. 2010; Giger et al. 2013). SSF and CSP could potentially underestimate the amount of shale within fault-zones derived from the wall rock, especially for sequences containing dirty sands (e.g. sands comprising clay-rich grains).

The formation of holes within shale smears is a crucial element of fault seal, however, it remains unclear how or why these holes occur. Probablistic Shale Smear Factor (PSSF) is the only algorithm that takes account of these holes when predicting clay smear seals. Childs et al. (2007) suggest that shale smears can have irregular geometries and holes could form due to rapid thinning of the clay smear. In many cases rapid changes in shale smear thickness may be induced by secondary faults within the fault zone (Childs et al. 2007; Ciftci et al. 2012; this study Chapter 2).

Algorithms are designed to predict the likelihood of continuous shale smear and are based on the assumption that once a bed has reached a certain displacement the smear will thin to a point where it becomes discontinuous. Predictions are based on the relationship between bed thickness and displacement; the greater the bed thickness and the lower the displacement the more likely a smear is to be continuous and act as an effective seal (Lindsay et al. 1993; Lehner and Pilaar 1997; Yielding et al. 1997). There are many limitations associated with these algorithms. Of primary concern is the fact that the algorithms are a simplified description of the fault rock and neither take account of the detailed geometries of the fault nor the variety of processes that result in its formation. Three main limitations of the algorithms have been identified. Firstly, they don't take into account the numerous factors that are thought to influence the likelihood of smear such as stress regime, shale composition and bed lithification, which may be impacted by a number of factors including the depth of burial (Childs et al. 2007, Pei et al. 2015, Ketterman et al. 2016, Vrolijk et al. 2016). Secondly, fault-zones are often represented as a single plane whereas this is rarely the case in nature (Foxford et al. 1998, Childs et al. 2007, Dockrill and Shipton 2010, Pei et al. 2015, Ketterman et al. 2016, Vrolijk et al. 2016). Fault zones are typically heterogeneous over small distances (i.e. less than the fault displacement) which may make it difficult to accurately predict fault sealing behaviour. Due to the high degree of variation in sealing lithologies and fault-rock composition often recorded along faults, the effectiveness of shale smear algorithms has been questioned (Childs et al. 1997). However, Yielding et al. (1997) described the algorithms by stating that "Although this is undoubtedly an oversimplification of the detailed

processes occurring in the fault-zone, it represents a traceable upscaling of the lithological diversity at the fault surface." Thirdly, most algorithms treat shale beds individually rather than considering the contribution not only from other shale intervals but also intervals that have a high clay percentage (e.g. lithic sands) (Vrolijk et al. 2016). For example, within the Mount Messenger Formation the sandstone units contain a high percentage of lithics and clays which have the potential to form a significant percentage of the low permeability fault-rock.

The algorithms are based on several assumptions, some of which are not globally applicable. For example, currently the effects of cataclasis or phyllosilicate framework rocks are not accommodated by SSF or CSP despite their ability to act as barriers or baffles to flow. The focus on solely the shale horizons may lead to an underestimating of the shale percentage of the resulting fault-rock and a misinterpretation of the type of sealing that is occurring. In addition, it is assumed that host rock properties control shale smear and that all beds are incorporated to the same extent in the fault-zone. Data presented in Chapter 3 of this thesis clearly demonstrate that the smearing of beds is highly variable and independent of key parameters. SSF and SGR use only the displacement and bed thickness as the basis for their calculations meaning an array of variables are unaccounted for. These variables include the number of synthetic slip surfaces within a fault-zone, which increase with increasing fault-zone thickness (Seebeck et al. 2014). The present algorithms infer a single slip surface which in many cases is likely to be an over simplification (Vrolijk et al. 2016). Furthermore, assumptions that shale smear thickness will decrease with increased distance from the source bed, that thicker and more numerous shale beds will form thicker smears and that thicker smears will be more continuous have been topics of debate (Lindsay et al. 1993; Fulljames et al. 1997; Lehner and Pilaar 1997; Yielding et al. 1997; Pei et al. 2015; Vrolijk et al. 2016).

Finally, being able to upscale fault attributes is important when applying observations from core, outcrop or well logs to faults in seismic reflection lines. Outcrop studies are limited in their applicability, as the scale of observation as well as the degree of variability is often difficult to relate to seismic scale features. More often than not fault-rock is observed in two dimensions and while this provides an indication of the structures that are likely to be present in the subsurface it is a sub-sample of a 3D structure. While upscaling of core data is routinely performed for reservoir models (Manzocchi et al. 2010), the change from 2D to 3D is rarely considered.

5.4.5 Application and Calibration of Algorithms

Despite the limitations discussed in the previous section, predictive fault-seal algorithms remain important tools, particularly for the oil and gas industry (Manzocchi et al. 2010). The utility of these tools for discriminating between sealing and non-sealing faults has been tested using downhole wireline logs for capillary pressure, gas saturations and oil/gas column heights (Vrolijk et al. 2016). A number of studies have utilised the algorithms to identify capillary pressure cut offs for petroleum fields below and above which faults are sealing and non-sealing, respectively (Bouvier et al. 1989; Jev et al. 1993; Fristad et al. 1997; Yielding et al. 1997). These calibrations typically assume that the relationships observed on one fault can be extrapolated to other faults within a field or region. Calibration of datasets using SGR can be undertaken using deterministic or empirical approaches. A deterministic approach involves using samples from nearby outcrops or wells to assess the amount of shale fault-rock present and to calculate the resulting capillary threshold pressures. By using SGR, these values can then be assigned to known faults and the capillary threshold values calculated. By contrast, an empirical approach, known capillary threshold pressures for defined hydrocarbon column heights are assigned to the respective SGR values and these are then plotted to show where the cut off in SGR values for a sealing fault may be (Yielding et al. 2016).

Despite the success of these calibration exercises, the relationships between fault seal, capillary pressure and column height are variable (Vrolijk et al. 2016). Local differences in fault-zone properties and the lithologies of faulted strata are likely to mean that universal calibration of fault-sealing behaviour and reservoir pressures is not possible. It may be, for example, that fault sealing properties may vary for different faults in the same petroleum field or for the same fault. These differences in fault seal are expected to be at least partly due to fault-zone heterogeneity over short distances, with Foxford et al. (1998) unable to predict the structure of the fault-zone at a point only 10 m from the original sample point. A 10 m length-scale is below seismic resolution and typically much smaller than the spacing of wells. Thus, fault data collected from wells may not be representative of other parts of faults in the same area. However, with ongoing research into the controls and processes of fault-rock production fault-seal algorithms can continue to be refined and improved. For example, it is important to consider other processes that may be contributing to the fault seal, one of which could be cataclasis, with a view to explicitly incorporating these processes into the algorithms. In the interim, being aware of the limitations of algorithms allows users to get the most out of the predictions.

5.5 Data and Methods

5.5.1 Fault Data

The aim of this chapter is to use the available data to determine if there is a positive relationship between fault-rock thickness and the outputs of CSP, SSF and SGR fault seal algorithms. Using outcrop measurements we test the assumption that fault rock is predominantly derived from host-rock siltstone beds and controlled by the thickness of the host bed and the displacement along the fault. Fault-rock thickness and fault-seal algorithm analysis in this chapter were conducted for ~180 normal faults that displace individual siltstones in Taranaki, Gore Bay or White Bluff and displaced multiple beds for six along-fault profiles from the Mount Messenger Formation (MMF) in Coastal Taranaki. Data for these detailed profiles were collected to aid interpretation of the larger dataset of individual displaced beds and to assess the heterogeneity of fault-rock thickness (see Chapter 4 for more detailed discussion of the fault-profile data). Displacements for the entire dataset (individual beds and fault profiles) ranged from millimetre to 15 m and bed thickness from ~1 – 150 cm. The stratigraphic sequence comprises thinly interbedded sandstone and siltstone that are exposed in coastal cliffs. The majority of the shale beds analysed were several centimetres thick. Of the faults recorded, any siltstone beds that had a displacement greater than the bed thicknesses were used for the fault-seal calculations.

The faults sampled were 100% exposed and included measurements of fault-rock thicknesses, fault displacements and bed thicknesses. In most cases outcrop cleaning was required to maximise the resolution of the available data. Fault cleaning was undertaken by scraping the outcrop flat and removing the weathered surface. After cleaning the lower resolution limit of the data was about 1 mm and smaller features (e.g. displacements, deformation bands, grains and layers) could only be reliably measured from thin sections. A more detailed description of the cleaning process can be found in Chapter 1 and Chapter 2.

5.5.2 Fault-seal calculations

The algorithm formulas used in this study for CSP, SSF and SGR are presented in Table 5.1 and Figure 5.2. These algorithms are summarised in Giger et al. (2013) and from a number of sources (see Table 5.1 right column). The algorithms (CSP, SSF and SGR) for individual and multiple beds are comparable and differ in that for multiple beds we use the sum of the thickness of siltstone beds past a point on

the fault and for individual beds the thickness of the bed. For individual beds and the CSP calculation, the midway point between siltstone bed cut offs was used to calculate the distance. SGR equations for individual and multiple beds also vary because clay content for sandstones and shales are only available for the Taranaki profile data. Therefore, SGR calculations for multiple silt beds use average clay content values for siltstone and sandstone beds derived from unpublished XRD data (N= 16, this study) and from the published results of QEMSCAN analysis (Higgs et al. 2015). No XRD or QEMSCAN data are presently available for siltstone or sandstone beds from Gore Bay or White Bluff so we have elected to use binary estimates of phyllosilicate content (sandstone = 0% and siltstone = 100%). In detail we know from Taranaki QEMSCAN data (Higgs et al. 2015) that this binary system can be approximate only and infer that it provides a first-order estimate of SGR for individual beds.

We have not been able to calibrate the algorithm results to fault seal as part of this study. Therefore, in this study we have adopted limiting values for continuous smear and fault seal from the literature. For the purposes of this study we use limiting values of SSF <5 and CSP >30 for continuous smear and SGR >20% for sealing faults (Jev et al. 1993; Lindsay et al. 1993; Fristad et al. 1997; Yielding et al. 1997; Childs et al. 2007; Vrolijk et al. 2016). These values are used for the purposes of discussion only and it is recognised that continuous smear and fault seal may occur for SSF <7, SGR >15% and CSP >15.

Several relationships were tested to determine if some of the underlying assumptions made by shale smear algorithms are applicable to the Mount Messenger Formation or whether these assumptions are more restricted in application and less representative of global processes than first thought.

5.6 Results

5.6.1 Shale Smear and Algorithm Outputs

Shale smears are thought to make a significant contribution to fault rock and to the permeability structures of fault zones (Lindsay et al. 1993; Fristad et al. 1997; Childs et al. 2007; Faulkner et al. 2010; Giger et al. 2013; Pei et al. 2015; Vrolijk et al. 2016; Fisher et al. 2018). Underpinning the CSP and SSF algorithms is the belief that for a given bed thickness, rising displacement reduces the likelihood of continuous smear and fault seal. To test these relationships we have compared smear continuity, displacement and siltstone bed thickness with CSP, SSF and SGR values using the dataset for individual beds (Figure 5.7-Figure 5.9). In addition we compare smear continuity and algorithm outputs for the five fault profiles.

For the individual beds dataset all three algorithms use a combination of bed thickness and displacement to discern the likelihood of shale smear and fault seal. The relationships are examined in Figure 5.3. These were the first relationships to be tested. The above attributes were plotted against smear continuity to test the relationship between the two variables and the presence of smear (Figure 5.7). For these figures, faults with continuous smear, no smear and discontinuous smear have been differentiated, with an expectation that decreasing displacement and increasing bed thickness will produce increasing smear continuity. However, no such relationships were found between bed thickness and the continuity of shale smears or between displacement and smear continuity (Figure 5.7). Although data from different strata have not been discriminated in Figure 5.7, inspection of the datasets suggests that the absence of relationships between smear continuity and displacement occurs at each of the three sites studied (i.e. Gore Bay, Taranaki and White Bluff).

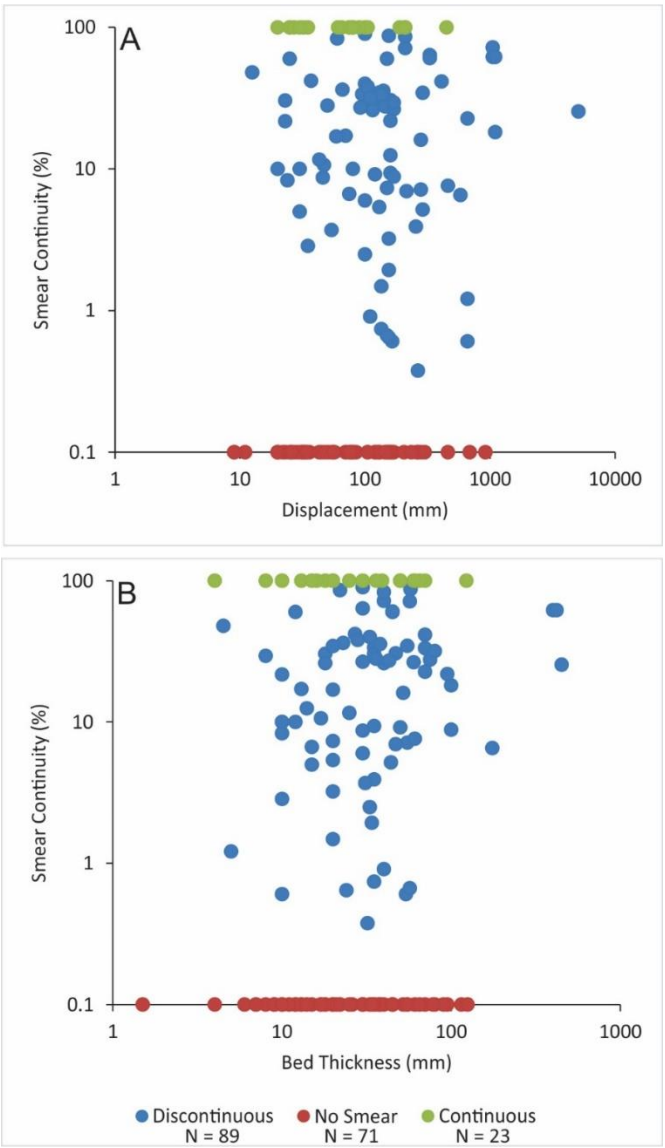

Figure 5.7 Graphs of A) Displacement vs Shale smear continuity and, B) Bed Thickness vs Shale smear continuity for fault with no smear, discontinuous smear and continuous smear for individual beds (total N=184).

To further test relationships between displacement, bed thickness and smear continuity we have plotted these variables on Figure 5.8. Displacement and bed thickness show a weak positive relationship on Figure 5.8 for continuous, discontinuous and no smears, however, this relationship is predominantly due to the near-linear upper bound of the data along the 1:1 line. The upper bound of the data is defined by our sampling strategy, as smear was only measured for faults where each siltstone bed had been entirely displaced and faults with displacements of less than the bed thickness were not sampled. The distribution of data points for continuous, discontinuous and no smear faults is similar, consistent with the non-relationship in Figure 5.7. The data broadly straddle lines with a slope of 1 representing SSF=5 and SGR=20%, with continuous smears mostly to the left of these lines (i.e. SSF values of <5 and SGR > 20%). The predominance of continuous smears left of the SSF=5 and

SGR=20% lines is consistent with previous studies in suggesting that lower (than 5) SSF and higher (than 20%) SGR are more likely to result in continuous smear and fault seal (Lindsay et al. 1993; Yielding et al. 1997; Childs et al. 2007; Dockrill and Shipton 2010; Pei et al. 2015; Vrolijk et al. 2016). While the predominance of continuous smears at SSF<5 was expected, there are also many faults with discontinuous and no smear for SSFs of <5 and SGR >20%.

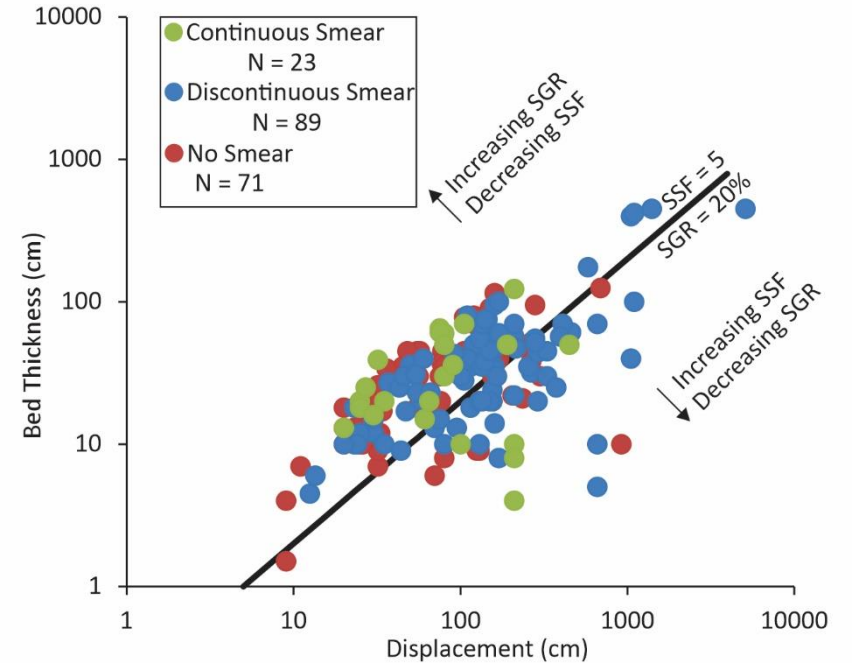

Figure 5.8 Bed thickness plotted against displacement for siltstone beds displaying no smear, discontinuous smear and continuous smear. All three groupings plot within the same range suggesting that the ratio of bed thickness to displacement does not control smear formation. Lines of equal bed thickness and displacement, SGR=20% and SSF=5 are shown. See Table 5.1 for equations used to calculate SGR and SSF.

These relationships between CSP, SSF and SGR and smear continuity are further explored in Figure 5.9 and Figure 5.10. Figure 5.9 shows the continuous smear, discontinuous smear and no smear in cumulative frequency space and clearly shows that continuous smears are distinct from no smears and discontinuous smears. These graphs show that when the entire population of data are considered CSP and SGR are generally larger for continuous smears (than for discontinuous and no smears), while SSF is smaller than the other two groups. The distinction between discontinuous smear and no smear is not as clear in Figure 5.9, with no smear typically plotting between or, coincident with, discontinuous smear. These relationships do not suggest a progressive increase in smear continuity with, for example, decreasing SSF. Figure 5.10 shows the range in values that continuous, discontinuous and no smear beds have for the three algorithms. At first glance, continuous smears appear to conform well to the algorithms with the majority of beds having high SGR and CSP values and low SSF, which is

to be expected for sealing beds. However, it is also worth noting that ~20% of continuous smears have SGR values of <20% which would indicate that the bed would be non-sealing. Furthermore, the apparent correlation between the majority of continuous smears and algorithms is not found in the values for discontinuous or no smear beds, which show a similar distribution in SGR, SSF and CSP as their sealing counterparts. Therefore, it is more likely coincidence than correlation that the continuously smeared beds conform so well with the algorithm cut offs. The conclusion that we draw from Figure 5.8 and Figure 5.9 is that, perhaps with the exception of continuous smears, smear continuity cannot be predicted using bed thickness and displacement alone.

The relatively poor correlations between smear continuity and the fault-seal algorithms partly arises because many of the siltstone beds studied do not smear or smear very little. Recognition that shale smearing is not ubiquitous departs from the findings of previous studies which suggest that the majority of shale beds smear. For smear to affect fault permeability it should be continuous between cut offs and prevent communication between juxtaposed reservoir units. Therefore, the continuity of smears within the Individual Fault Dataset was calculated. Around 50% of beds have less than 3% smear continuity and only 12% of beds were continuous (Figure 5.10). When separated by locality, only White Bluff and Mohakatino contained displaced siltstone beds that all smeared to some degree. Therefore, smearing may be less common than first thought and the algorithms may, in some sequences, be overestimating the degree of smear.

These available data from New Zealand call into question the predictive utility of fault-seal algorithms which rely largely on the shale smear process. As can be observed from the plots in Figure 5.7-Figure 5.10 the correlations of SSF, SGR or CSP with smear continuity are weak. Therefore, the algorithms that primarily use bed thickness and displacement parameters cannot be used to predict the presence or absence of shale smear or low permeability fault rock, at least on faults with displacements less than a metre in the MMF. This suggests that factors other than bed thickness and displacement may control whether a bed smears or not, and different process for generating low permeability fault rock should be considered.

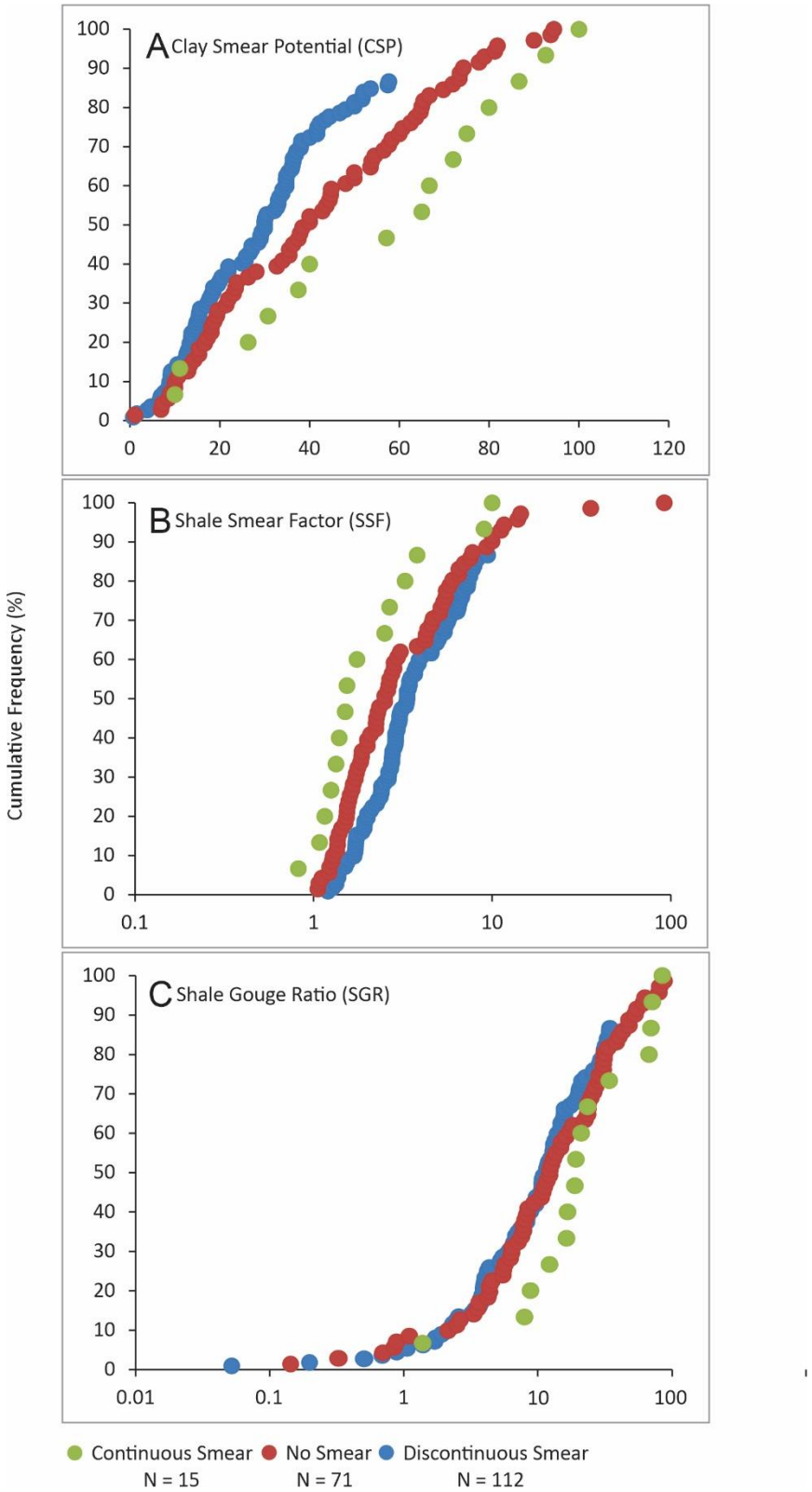

Figure 5.9 Cumulative frequency curves showing the relationships between faults with continuous smear, discontinuous smear and no smear for values of CSP, SSF and SGR. In all graphs continuous smear are green symbols, discontinuous smear blue and no smear red. See Table 5.1 for algorithms used to calculate CSP, SSF and SGR. Refer to key at base of figure for number of data on each graph.

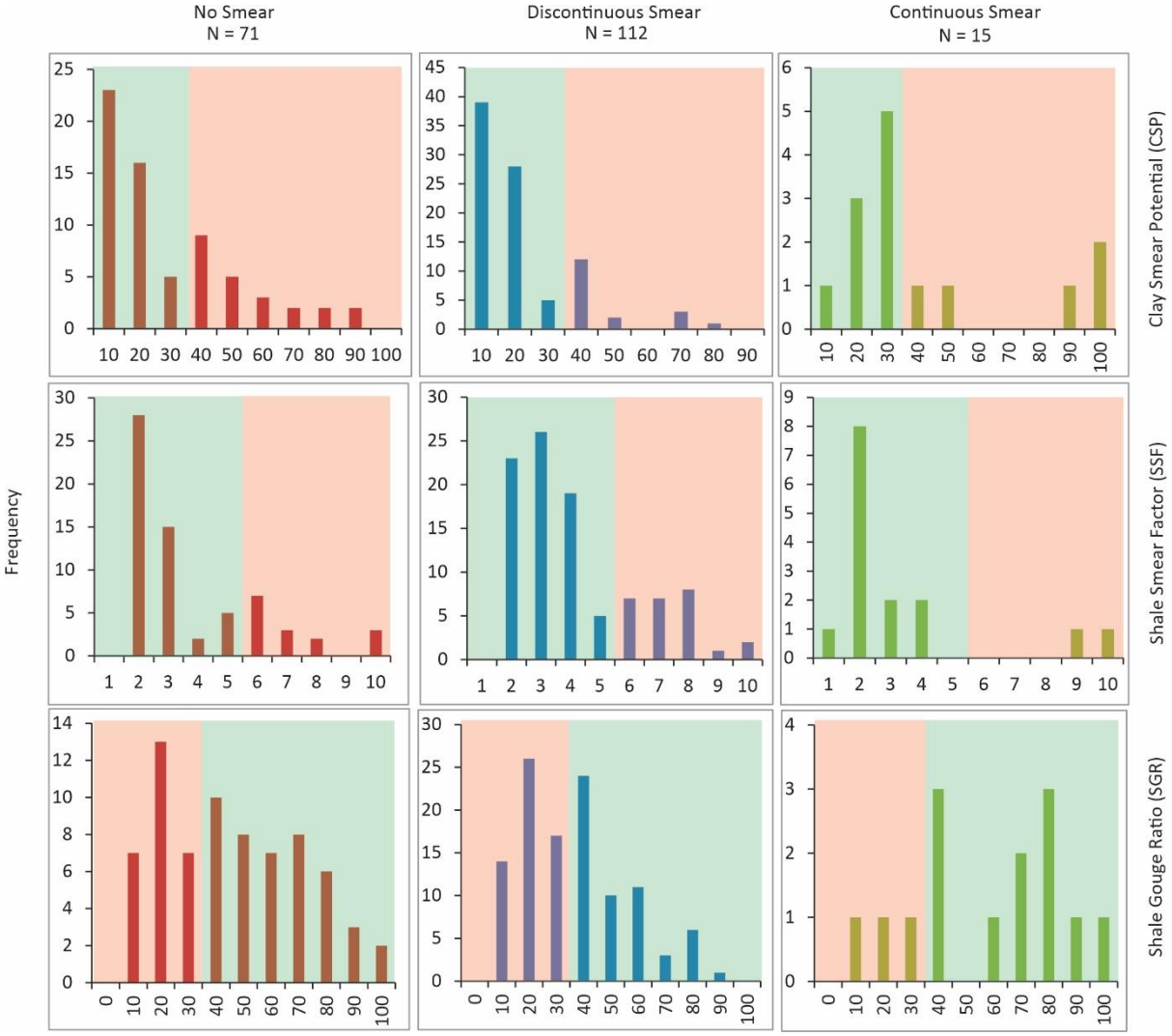

Figure 5.10 Frequency histograms showing the range of CSP (top graphs), SSF (middle graphs) and SGR (bottom graphs) values for no smear (red, left), discontinuous smear (blue, middle) and continuous smear (green, right). Beds predicted to produce continuous smear plot in the green area and those that don't are in red polygons. Number of data for each graph are shown at the top of each column of graphs.

5.6.2 Fault-Rock Thickness and Algorithm Outputs

The previous section focuses on the relationships between shale smear and the outputs of fault-seal algorithms, however, it is clear from previous studies of the MMF that multiple processes may contribute to fault-rock generation (Childs et al. 2007; Nicol and Childs 2018). In particular, Nicol and Childs (2018) indicate that about half of the fault rock observed within fault zones of the MMF may be produced by cataclasis of sandstones that comprise weak lithic and feldspar grains that were partly or entirely altered to clays. In cases where non-smear processes contribute to fault-rock production the CSP and SSF algorithms could have limited value for predicting fault-seal. To test the utility of all three algorithms here we compare fault-rock thicknesses to algorithm outputs for the six down-fault profiles collected from the MMF in Taranaki. For these profiles, fault-rock thicknesses were measured at 5-10

cm sample intervals and fault seal calculated along the length of each fault trace. These resulting data are plotted for three faults in Figure 5.11.

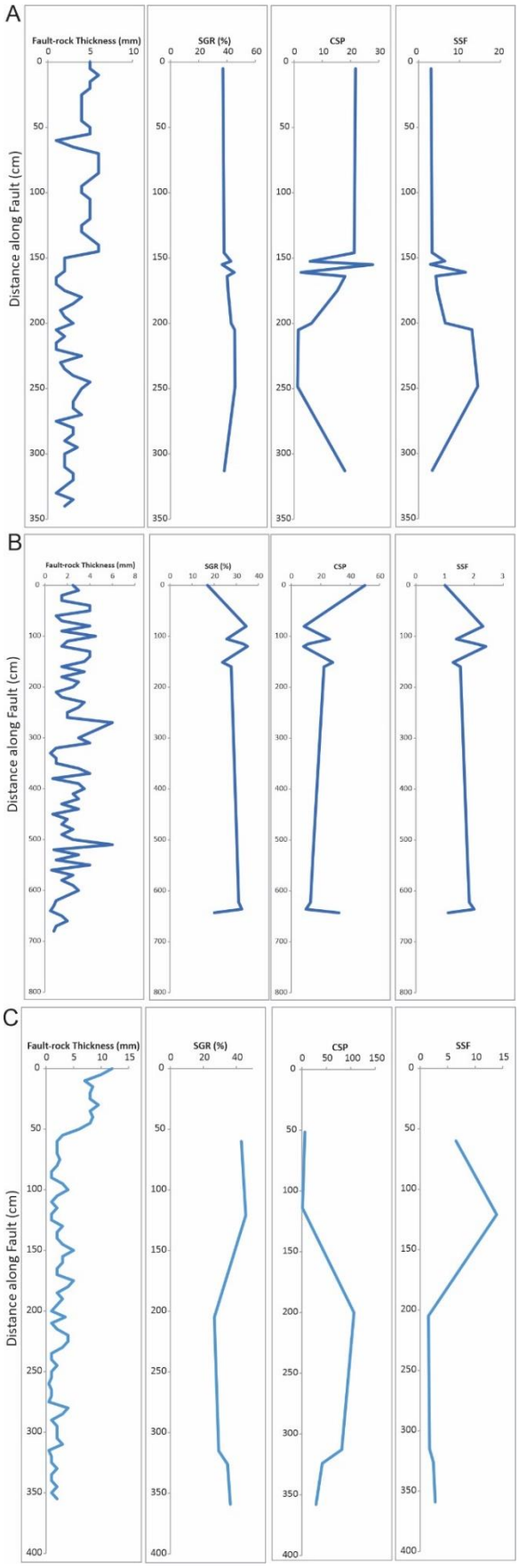

Figure 5.11 Fault-rock thickness (mm), SGR, CSP, SSF vs distance along each fault (in cm). A) Fault Tongaporutu 98 displacement 13 cm, B) fault Rapanui 95 displacement 2.3 cm and, C) Pukearuhe 96 displacement 12 cm. For details of each profile see Table 4.1 in Chapter 4.

Fault-rock thicknesses on the faults examined are highly variable (Figure 5.11). The graphs in Figure 5.7 show up to an order of magnitude variation in thickness (e.g. 0.5 to 6 mm, Figure 5.11B distance 280-320 cm) over distances of as little as 20 cm. The wavelengths of fault-rock thickness variations of at least a factor of two are typically 30-100 cm and are greater than the thicknesses of siltstone beds. These variations partly arise due to changes in the number and thickness of cataclastic deformation bands and also to local shale smear. CSP, SSF and SGR curves on Figure 5.11 also display order of magnitude changes in values, however, these changes generally occur on metre length scales. The long wavelength of CSP, SSF and SGR is partly a combination of the bed thickness, bed spacing and displacement. CSP and SSF values are broadly consistent (i.e. highs in SSF coincide with lows in CSP), which is to be expected given that they use the same input parameters. Given the different wavelength of changes in fault-rock thickness and in fault-seal values (i.e. CSP, SSF and SGR) it is not possible to infer the detailed values of fault-rock thickness from the algorithms being used. In addition, it does not appear to be possible to predict the broad-scale variations in fault-rock thickness from the algorithms. For example, in Figure 5.11A fault rock thickness shows a broad high between ~70 and 150 cm, yet SGR, CSP and SSF are not appreciably higher or lower in this interval than elsewhere along the fault. The available data suggests that, at least for these small normal faults in the MMF of Taranaki, that the current algorithms do not provide sufficient resolution to determine if fault seal is possible. For example, in Figure 5.11B SGR values typically exceed 20% (and might be predicted to seal) along much of the fault dip length and yet fault-rock thickness of ~0.5 mm was observed at no fewer than six locations along the fault trace; such thin fault rock could locally promote across-fault leakage. While the algorithms are not designed to predict fault-rock thickness, it is an important measurement for fault seal and prediction accuracy could be increased if small-scale fluctuations in fault-rock thickness were taken into account when constructing fault-seal models.

5.7 Discussion

5.7.1 Limitation of Shale Smear Algorithms

Although output from fault-seal algorithms have been calibrated using data from oil and gas fields, our analysis suggests that in some cases they may not provide robust estimates of the distribution of shale smear or fault-rock thickness. In this study, where we have randomly sampled almost 200 faults, the correlations between shale bed-thickness, displacement and smear continuity are weak, suggesting that the fundamental relationship the algorithms are built upon may not be applicable to some faults. CSP and SSF algorithms require that all siltstone beds smear, but this is not the case and in Taranaki about 40% of beds displayed no smear at all. If it is assumed that all shale beds produce shale smear and that shale smear is the primary source of low permeability fault rock in fault zones,

then CSP and SSF algorithms will produce over-estimates of the volume of low permeability fault rock. In addition to over-estimating the volume of fault rock, fault-seal calculations may require over-simplified fault-zone structure. The algorithms assume only a single slip surface despite faults regularly displaying more slip surfaces at outcrop (Foxford et al. 1998; Childs et al. 2009). This over-simplification of fault-zone structure may also result in algorithms leading to over-prediction of sealing faults, as fault-surface heterogeneities may lead to gaps or breaks in shale smears (Dockrill and Shipton 2010). At the present time fault-zone complexities are not considered in the basic CSP, SSF and SGR calculations, although multiple slip surfaces and smear amalgamation have been included in the PSSF algorithm (Childs et al. 2007).

As SGR is not process specific and instead describes (and predicts) fault rock sourced from both sandstone and siltstone lithologies, it could be used to assess the fault-rock derived from multiple mechanisms. Rather than assuming that smear and fine grained impermeable fault-rock can only be formed from smeared shale rich beds, SGR allows the incorporation of lithic and clay material within sandstones to also contribute to the overall makeup of the fault-rock (Dockrill and Shipton 2010). The SGR method could be improved further by taking account of additional factors that may contribute to the generation of fault rock. These factors may include the mechanical strength of the host shale, the mechanical strength contrast between host units, and the architecture of the fault-zone. These factors will require information about the geological history, including the maximum burial depth, the burial depth at the time of faulting, and host-rock lithologies. Including more information in the algorithms may or may not improve their predictive value, but it remains unclear whether the additional predictive power of the algorithms will warrant the additional work required.

Scale is also an important factor to consider when assessing and testing algorithms. A problem that currently affects the petroleum industry is that it is only possible to observe faults on two scales: the seismic scale and the well scale (Gillespie et al. 1993). However, it may be the structures between these two scales, too large to be fully constrained from a well but too small to be observed on seismic, that affect the sealing potential of a fault (e.g. Figure 5.12). Even studies at outcrop scale struggle to incorporate more than one or two orders of magnitude due to beds being difficult to trace in complex fault-zones and that displacement exceeding the portion of fault exposed, leaving only the hanging wall or footwall present (Gillespie et al. 1993). While outcrop observations were used to create and refine the algorithms the ultimate goal is to be able to accurately predict the sealing of faults on the seismic scale. A difficulty of this is that a pair of faults closely spaced at outcrop may appear as only one fault plane at seismic scale (van der Zee and Urai 2005). If small scale fault structures play a role in shale smear then applying algorithms to structures mapped through seismic may lead to predictions either overestimating or downplaying the degree of fault sealing present. Small-scale faulting,

something that is often overlooked during modelling, can have a large impact on the flow potential of faults that disrupt thinly interbedded sequences such as turbidite deposits (Manzocchi et al. 2010). In this scenario even small-scale faults may be able to connect reservoir units. This would suggest that even a sub-seismic scale fault could influence the fault system's ability to act as a conduit or a seal and will have a big impact on fluid migration regardless of whether it can be accurately mapped on seismic.

Oil column heights and capillary pressure data have been interpreted to support fault seal in some cases (Fristad et al. 1997; Yielding et al. 1997; Yielding 2002; Yielding et al. 2010; Pei et al. 2015; Vrolijk et al. 2016). However, uncertainties remain about whether the algorithms work because they accurately predict the behaviour of shale smear or whether they accurately predict the behaviour of low permeability fault-rock, of which shale smear is only a part of the control. Fault seal may be produced by a multitude of processes many of which are not explicitly incorporated into the existing algorithms. While attempts to combine multiple processes into a single algorithm have been conducted (Welbon et al. 1997), isolating the controlling factors is often difficult (Vrolijk et al. 2016). For example, the effects of cataclasis and phyllosilicate rich frame-work rocks are not incorporated into algorithms, although it is clear that both are important for the MMF in New Zealand (Childs et al. 2007; Nicol and Childs 2018). Similarly, it is uncertain what contribution sands make to clay rich fault-rock. Yielding et al. (2016) described the correlation between well data and predictive algorithms as potentially "largely coincidental and likely to be a response to the heterogeneity of fault-zone structure". They also state that the results from flow tests are a product of fluid flow measured between two wells and do not actually measure the fault-zone permeability itself (Yielding et al. 2016). Other studies have suggested that the amount of fault sealing due to low permeability fault-rock has been greatly over estimated (James et al. 2004; Corona et al. 2010). These authors indicate that fault-rock is rarely continuous or thick enough to provide a reliable seal and that fault seal is often achieved by unresolved stratigraphic variation or structural juxtaposition (Corona et al. 2010). Based on previous publications and our analysis of data from New Zealand, it seems likely that the algorithms will always be inaccurate to some degree, as we don't currently have the knowledge to make more informed predictions.

5.7.2 Implications for shale smear algorithms?

Fault-seal information are converted to fault transmissibility multipliers for use in fluid-flow models of reservoirs. Fisher and Jolley (2007) suggested that the most important factors when predicting fault

fluid flow and transmissibility multipliers are accurate juxtaposition, permeabilities and thicknesses. In addition, two phase fault-rock properties should be considered in simulations where capillary effects are likely to influence flow (Manzocchi et al. 2010). Fault transmissibility multipliers define the extent to which fluids can move through faults and can be determined in two ways (Manzocchi et al. 2010). Firstly, they can be estimated by modifying the fault transmissibility multipliers until the reservoir model history matches the pressure and production data from a field. However, this approach can be problematic as a single multiplier is used for the entire fault surface and any potential heterogeneity of fault permeability observed along strike and dip is unlikely to be captured. The history matching approach provides little information on the underlying controls on fault permeability, making it difficult to convincingly draw conclusions on the likely transmissibility of faults beyond the region for which history matching was performed.

A second method of calculating fault transmissibility is to use fault-seal algorithms to determine the faults and locations on faults that may act as conduits, baffles or barriers to flow. Fault permeability is usually calculated using SGR and a predetermined relationship either from previous studies (see Table 5.2) (Manzocchi et al. 2010) or from analogue fields. The relationship between SGR and fault permeability can be estimated from laboratory studies where fault-rock permeabilities are measured from core and from measurements of fault-rock thickness. Fault-rock thickness is often determined based on a pre-set positive relationship with displacement that is determined from outcrop studies (Childs et al. 1997; Manzocchi et al. 2010). Where input parameters are calibrated using existing relationships, the better the analogue used and the greater the proximity to the field in question the data has been sourced, then the more likely the prediction is to be accurate (Manzocchi et al. 2010).

Table 5.2 Summary of published studies that have used SGR based method of fault fluid flow predictions from Manzocchi et al. 2010

STUDY	AREA	PREDICTION ACCURACY	IMPROVEMENT MADE/NEEDED
KNAI AND KNIPE (1998)	Heidrun Field, North Sea	Success	
YIELDING (2002)	Scott Field	Success	
RIVENÆS AND DART (2002)	Brage and Oseberg Fields, North Sea	Overestimated	Values reduced by 2 – 3 orders of magnitude
SVERDRUP ET AL. (2003)	Snorre Field, North Sea	Success for oil Unsuccessful for gas	Two phase needed to include gas
AL-BUSAFI ET AL. (2005)	Pierce Field, North Sea	Improved history match	Improved further with two phase capillary entry height method (see below)
JOLLEY ET AL. (2007)	North Cormorant, Brent and Pelican Fields	Success	
MYERS ET AL. (2007)	Ringhorne Field	Success	
ZIJLSTRA ET AL. (2007)	Rotliegend reservoirs	Unsuccessful using single-phase multipliers	Developed a method called capillary entry height method for better results

Transmissibility multipliers derived from SGR and outcrop-derived fault thickness information must be upscaled to produce reservoir models of fluid flow. In many cases this upscaling is likely to result in an averaging of fault properties. The present study (and many previous investigations) have highlighted the heterogeneity of fault seal and fault-rock thickness at outcrop scale (e.g. Figure 5.11), which will

not be captured in reservoir fluid flow models (see Figure 5.12). The successful prediction of hydrocarbon flow associated with faults in some reservoir studies provides some support for the fault-seal algorithms and for their application to reservoir models. However, doubts remain about whether the current strategies for predicting fault seal can be used to identify the locations and numbers of 'holes' (i.e. zones of thin fault rock) in the fault seal that will promote across-fault flow at reservoir pressures and temperatures. Therefore, further work is required to determine if inclusion of the heterogeneities of fault rock at outcrop scale in reservoir models will improve their predictive power.

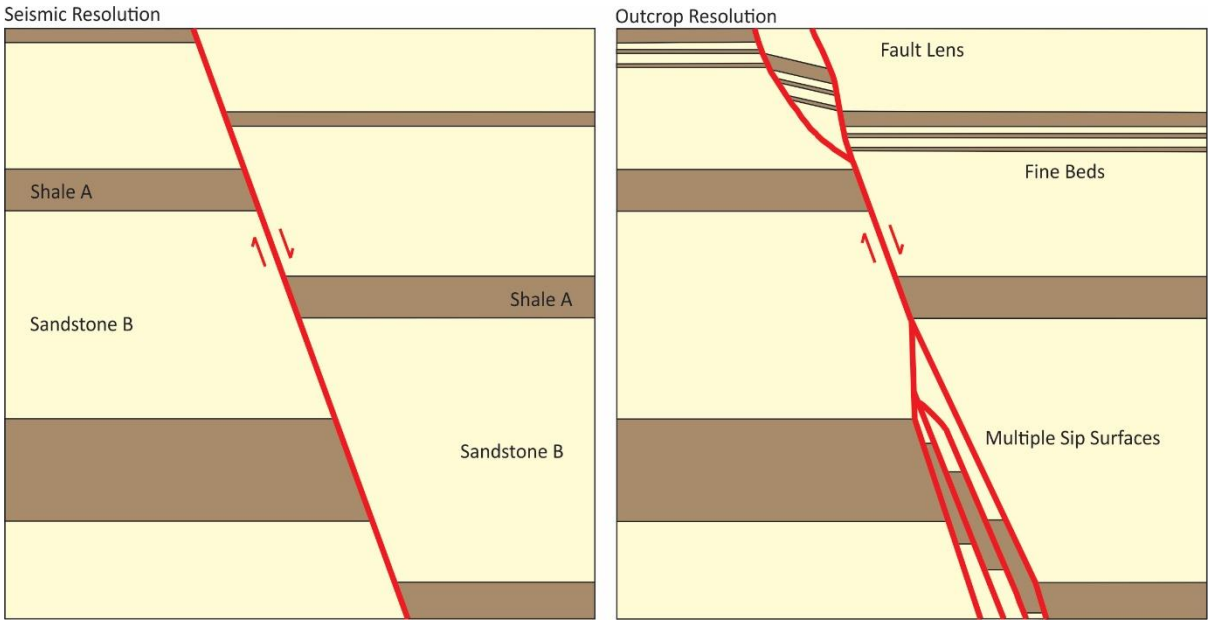

Figure 5.12 Schematic diagrams developed from Xie et al. (2018) showing faults at seismic (left) and outcrop (right) scales. The outcrop scale diagram shows small scale structures within the fault zone that change the geometry and juxtaposition of shale beds across the fault. These small-scale faults within the zone may change the seal properties of the fault.

5.8 Conclusion

Outcrop data for nearly 200 small faults was studied to determine if the output from three fault-seal algorithms (CSP, SSF and SGR) were compatible with the observed shale smear continuity and fault-rock thicknesses. Our data show both shale smear continuity and fault-rock thickness are highly variable at length scales of <1 m. Shale smears were divided into three groups of continuous smear, discontinuous smear and no smear and these groups compared to bed thickness, displacement and outputs from the three fault-seal algorithms. The data show little correlation between bed thickness, displacement and the continuity of shale smears. Given that fault seal CSP and SSF algorithms use bed thickness and fault displacement as the sole input parameters it is not surprising these algorithms

show no correlation with the occurrence of discontinuous and non-smears. Comparison of fault-rock thickness measurements and fault-seal estimates from the three algorithms indicate that the algorithms do not reproduce the short wavelength (<0.5 m) up to order of magnitude variations in fault-rock thickness, most likely due to the calculations being based off only two variables. The algorithms are not designed to identify locations of minimum fault-rock thickness on the fault surface despite these being the most likely sites of across-fault flow. The poor correlations between outputs from the algorithms and outcrop observations may arise because the algorithms oversimplify fault-zone structure and shale smear geometries, and do not fully represent all mechanisms of low permeability fault-rock generation.

5.9 References

Al-Busafi. B, Fisher. Q, Harris. S, Kendall. M. (2005). The Impact of Faults Representation on History Match and Future Generated Seismic Impedance Response in Reservoir Models - Case Study for Pierce Field North Sea. 10.2118/93429-MS.

Aydin A. 2000. Fractures, faults, and hydrocarbon entrapment, migration and flow. Mar Pet Geol. 17(7):797–814. doi:10.1016/S0264-8172(00)00020-9.

Bense VF, Gleeson T, Loveless SE, Bour O, Scibek J. 2013. Fault zone hydrogeology. Earth-Science Rev. 127:171–192. doi:10.1016/j.earscirev.2013.09.008.

Bentley MR, Barry JJ. 1991. Representation of fault sealing in a reservoir simulation: Cormorant block IV UK North Sea. 66th Annu Tech Conf Exhib Soc Pet Eng Dallas, Texas.:119–126.

Bouvier JD, Sijpesteijn K, Kleusner DF, Onyejekwe CC, Van Der Pal RC. 1989. Three-dimensional seismic interpretation and fault sealing investigations, Nun River field, Nigeria. Am Assoc Pet Geol Bull. 73:1397–1414.

Caine JS, Evans JP, Forster CB. 1996. Fault zone architechture and permeability structure. Geology. 24(11):1025–1028. doi:10.1130/0091-7613(1996)024<1025.

Cartwright J, Huuse M, Aplin A. 2007. Seal bypass systems. Am Assoc Pet Geol Bull. 91(8):1141–1166. doi:10.1306/04090705181.

Childs C, Manzocchi T, Walsh JJ, Bonson CG, Nicol A, Schöpfer MPJ. 2009. A geometric model of fault zone and fault rock thickness variations. J Struct Geol. 31(2):117–127. doi:10.1016/j.jsg.2008.08.009.

Childs C, Walsh JJ, Manzocchi T, Strand J, Nicol A, Tomasso M, Schopfer MPJ, Aplin AC. 2007. Definition of a fault permeability predictor from outcrop studies of a faulted turbidite sequence, Taranaki, New Zealand. Geol Soc London, Spec Publ. 292:235–258. doi:10.1144/SP292.14.

Childs C, Walsh JJ, Watterson J. 1997. Complexity in fault zone structure and implications for fault seal prediction. Nor Pet Soc Spec Publ. 7:61–72. doi:10.1016/S0928-8937(97)80007-0.

Ciftci BN, Giger SB, Clennell MB. 2012. Testing Fault Seal Prediction Algorithms Using Geomodels of Experimentally Produced Fault Zones. 3rd EAGE Int Conf Fault Top Seals.(October). doi:10.3997/2214-4609.20143014.

Corona FV, Davis JS, Hippler SJ, Vrolijk PJ. 2010. Multi-fault analysis scorecard: testing the stochastic approach in fault seal prediction. Geol Soc London, Spec Publ. 347:317-332. doi: 10.1144/SP347.18.

Dockrill B, Shipton ZK. 2010. Structural controls on leakage from a natural CO2 geologic storage site: Central Utah, U.S.A. J Struct Geol. 32(11):1768–1782. doi:10.1016/j.jsg.2010.01.007.

Faulkner DR, Jackson CAL, Lunn RJ, Schlische RW, Shipton ZK, Wibberley CAJ, Withjack MO. 2010. A review of recent developments concerning the structure, mechanics and fluid flow properties of fault zones. J Struct Geol. 32(11):1557–1575. doi:10.1016/j.jsg.2010.06.009.

Fisher Q, Jolley S. 2007. Treatment of faults in production simulation models. Geol Soc London, Spec Publ. 292:219–233.

Fisher QJ, Haneef J, Grattoni CA, Allshorn S, Lorinczi P. 2018. Permeability of fault rocks in siliciclastic reservoirs: Recent advances. Mar Pet Geol. 91(July 2017):29–42. doi:10.1016/j.marpetgeo.2017.12.019.

Fisher QJ, Knipe RJ. 1998. Fault Sealing processes in siliciclastic sediments. Geol Soc London, Spec Publ. 147:117–134.

Fisher QJ, Knipe RJ. 2001. The permeability of faults within siliciclastic petroleum reservoirs of the North Sea and Norwegian Continental Shelf. Mar Pet Geol. 18(10):1063–1081. doi:10.1016/S0264-8172(01)00042-3.

Foxford KA, Walsh JJ, Watterson J, Garden IR, Guscott SC, Burley SD. 1998. Structure and content of the Moab fault zone, Utah, USA, and its implications for fault seal prediction. Geol Soc London, Spec Publ.(147):87–103.

Frischbutter AA, Fisher QJ, Namazova G, Dufour S. 2017. The value of fault analysis for field development planning. Pet Geosci. 23(1):120–133.

Fristad T, Groth A, Yielding G, Freeman B. 1997. Quantitative fault seal prediction: a case study from Oseberg Syd. Nor Pet Soc Spec Publ. 7(C):107–124. doi:10.1016/S0928-8937(97)80010-0.

Fulljames JR, Zijerveld LJJ, Franssen RCMW. 1997. Fault seal processes: systematic analysis of fault seals over geological and production time scales. Nor Pet Soc Spec Publ. 7(C):51–59. doi:10.1016/S0928-8937(97)80006-9.

Gibson RG. 1994. Fault zones seals in siliciclastic strata of the Columbus Basin, offshore Trinidad. Am Assoc Pet Geol Bull. 78:1372–1385.

Giger SB, Clennell MB, Çiftçi NB, Harbers C, Clark P, Ricchetti M. 2013. Fault transmissibility in clastic-

argillaceous sequences controlled by clay smear evolution. Am Assoc Pet Geol Bull. 97(5):705–731. doi:10.1306/10161211190.

Gillespie PA, Howard CB, Walsh JJ, Watterson J. 1993. Measurement and characterisation of spatial distributions of fractures. Tectonophysics. 226(1–4):113–141. doi:10.1016/0040-1951(93)90114-Y.

Gutierrez M, Øino LE, Nygård R. 2000. Stress-dependent permeability of a de-mineralised fracture in shale. Mar Pet Geol. 17(8):895–907. doi:10.1016/S0264-8172(00)00027-1.

Higgs KE, Arnot MJ, Brindle S. 2015. Advances in grain-size, mineral and pore-scale characterization of lithic and clay-rich reservoirs. Am Assoc Pet Geol Bull. 7(7):1315–1348. doi:10.1306/01271513101.

James WR, Fairchild LH, Nakayama GP, Hippler SJ, Vrolijk PJ 2004. Fault-seal analysis using a stochastic multifault approach. AAPG Bull. 88:885–904. doi:10.1306/02180403059.

Jev BI, Kaars-Sijpesteijn CH, Peters MPAM, Watts NL, Wilkie JT. 1993. Akaso field, Nigeria: Use of integrated 3-D seismic, fault-slicing, clay smearing and RFT pressure data on fault trapping and dynamic leakage. Am Assoc Pet Geol Bull. 77:1389–1404.

Jolley S, Dijk H, Lamens J, Fisher QJ, Manzocchi T, Eikmans H, Huang Y. 2007. Faulting and fault sealing in production simulation models: Brent Province, northern North Sea. Pet Geosci. 13:321–340.

Kettermann M, Thronberens S, Juarez O, Urai JL, Ziegler M, Asmus S, Krüger U. 2016. Mechanisms of clay smear formation in unconsolidated sediments-insights from 3-D observations of excavated normal faults. Solid Earth. 7(3):789–815. doi:10.5194/se-7-789-2016.

Knai TA, Knipe RJ. 1998. The impact of faults on fluid flow in the Heidrun field. Geol Soc London, Spec Publ. 147:269–282.

Lehner FK, Pilaar WF. 1997. The emplacement of clay smears in synsedimentary normal faults-inferences from field observations near Frechen , Germany. NPF Spec Publ. 7:39–50.

Lindsay NG, Murphy FC, Walsh JJ, Watterson J. 1993. Outcrop Studies of Shale Smears on Fault Surface. Int Assoc Sedimentol Spec Publ.(15):113–123.

Manzocchi T, Childs C, Walsh JJ. 2010. Faults and Fault Properties in Hydrocarbon Flow Models. Front Geofluids.:94–113. doi:10.1111/j.1468-8123.2010.00283.x.

Myers RD, Allgood A, Hjellbakk A, Vrolijk P, Briedis N. 2007. Testing fault transmissibility prediction in a structurally dominated reservoir: Ringhorne Field, Norway. Geol Soc London, Spec Publ. 292:271–294.

Nicol A, Childs C. 2018. Cataclasis and silt smear on normal faults in weakly lithified turbidites. J Struct Geol. 117(June):44–57. doi:10.1016/j.jsg.2018.06.017.

Noorsalehi-Garakani S, Kleine Vennekate GJ, Vrolijk P, Urai JL. 2013. Clay-smear continuity and normal fault zone geometry - First results from excavated sandbox models. J Struct Geol. 57:58–80. doi:10.1016/j.jsg.2013.09.008.

Pei Y, Paton DA, Knipe RJ, Wu K. 2015. A review of fault sealing behaviour and its evaluation in siliciclastic rocks. Earth-Science Rev. 150(October):121–138. doi:10.1016/j.earscirev.2015.07.011.

Rivenæs JC, Dart C. 2002. Reservoir compartmentalisation by water saturated faults: is evaluation possible with today's tools? Nor Pet Soc Spec Publ. 11:173–186.

Seebeck H, Nicol A, Walsh JJ, Childs C, Beetham RD, Pettinga J. 2014. Fluid flow in fault zones from an active rift. J Struct Geol. 62:52–64. doi:10.1016/j.jsg.2014.01.008.

Sverdrup E, Helgesen J, Vold J. 2003. Sealing properties of faults and their influence on water alternating-gas injection effeciency in the Snorre field, northern North Sea. Am Assoc Pet Geol Bull. 87:1437–1458.

Urban S. Allan. 1986. Model for Hydrocarbon Migration and Entrapment Within Faulted Structures. Am Assoc Pet Geol Bull. 70. doi:10.1306/94885962-1704-11D7-8645000102C1865D.

Vrolijk PJ, Urai JL, Kettermann M. 2016. Clay Smear: Review of Mechanisms and Applications. J Struct Geol. doi:10.1016/j.jsg.2015.09.006.

Welbon AI, Beach A, Brochbank PJ, Fjeld O, Knott SD, Pedersen T, Thomas S. 1997. Fault seal analysis in hydrocarbon exploration and appraisal, examples from offshore mid-Norway. Nor Pet Soc Spec Publ. 7:125–138.

Yielding G. 2002. Shale Gouge Ratio - calibration by geohistory. Nor Pet Soc Spec Publ. 11:1–15.

Yielding G, Bretan P, Freeman B. 2010. Fault seal calibration: a brief review. In: Reservoir Compartmentalization. Geological Society Special Publicaiton. p. 243–255.

Yielding G, Michie E, Bretan P, Fisher Q. 2016. Workflows for Fault Seal Prediction in Siliciclastics and Carbonates. *AAPG/EAGE Hydrocarbon Seals of the Middle East*, Muscat, Oman, January 18-20. AAPG Datapages.

Yielding G, Freeman B, Needham DT. 1997. Quantitative fault seal prediction. Am Assoc Pet Geol Bull. 81(6):897–917. doi:10.1306/522B498D-1727-11D7-8645000102C1865D.

van der Zee W, Urai JL. 2005. Processes of normal fault evolution in a siliciclastic sequence: a case study from Miri, Sarawak, Malaysia. J Struct Geol. 27(12):2281–2300. doi:10.1016/j.jsg.2005.07.006.

Zijlstra E, Reemst R, Fisher Q. 2007. Incorporation of fault properties into production simulation models of Permian reservoirs from the southern North Sea. Geol Soc London, Spec Publ. 292:295–308.

6 Conclusions and Future Work

6.1 Conclusions

This thesis aimed to address the questions set out in Chapter 1 by exploring different aspects of shale smear and fault architecture through Chapter 2 to Chapter 5. Below we present the titles (in bold text), key questions (in bold text) and conclusions for chapters 2-5 (Chapter 1 being the introduction and Chapter 6, this chapter).

Chapter 2: **Fault zone architecture and the production of low-permeability fault rock.**

Most faults comprise high strain, and low permeability, fault rock and lower shear strain fault zone. Questions remain about how these high and lower shear strain fault-zone components relate to each other. How is low permeability fault rock distributed within fault-zones, both in 2D and 3D? What relationships exist between displacement and fault architecture and what are the implications for predicting the impact of faulting on fluid flow?

This study measured and quantified the changes in fault-zone geometry both for individual faults and fault profiles at outcrop and sub-millimetre scale in the Mount Messenger Formation (MMF) in New Zealand. The collected data was used to constrain the variability in fault-zone architecture and the affect this may have on the distribution of low variability fault rock. Fault-zone geometries were found to vary by up to 3 orders of magnitude over sample lengths of several metres and displacements of <30 cm. Rapid changes in fault-zone architecture can often be attributed to the formation of deformation band clusters or the formation of lenses where host siltstone can become incorporated into the fault via multiple synthetic slip surfaces. The majority of fault profiles showed locations where fault rock was <1 mm, areas that are likely to act as conduits for fluid flow. No correlation was found between fault-rock minimums and architectural elements, making it hard to predict where and when holes may form along a fault length. To be able to more accurately predict fault permeability we suggest that a larger dataset of fault-zone and fault-rock thicknesses across a range of displacements should be compiled so that stochastic modelling can be used to identify likely locations for holes in fault seal.

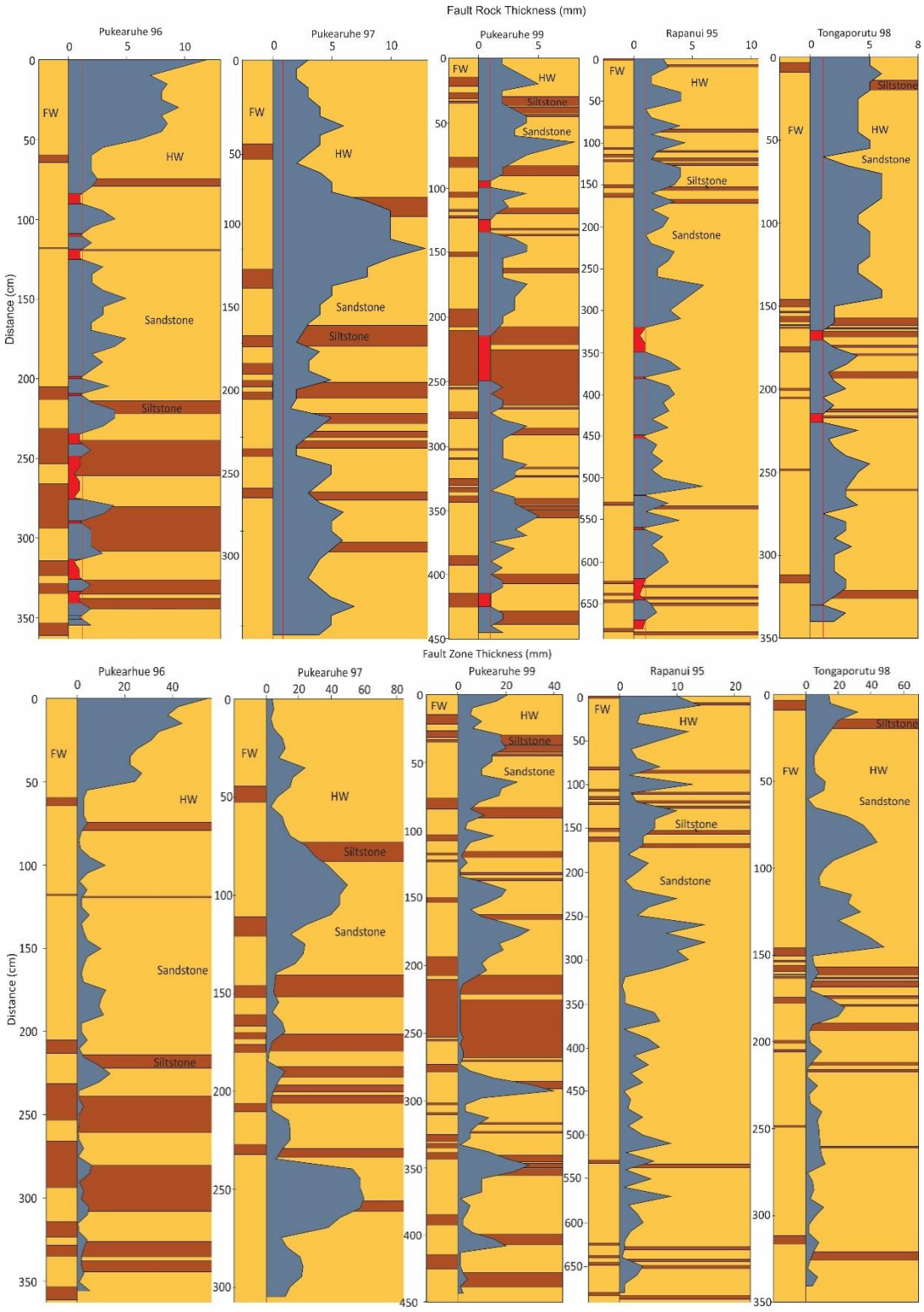

Figure 6.1 Five down fault profiles showing the variability of fault-rock (top graphs) and fault-zone (bottom graphs) thickness along dip traces of small faults. Sections of fault-rock with thicknesses of <1 mm are highlighted in red to show the distribution of holes along the fault trace. Hangingwall and footwall cut offs of siltstone (brown) and sandstone (yellow) beds are shown with no apparent correlation between fault-rock thicknesses and proximity to certain lithologies (i.e. siltstone or sandstone beds).

Chapter 3: **Shale smear geometries in a thinly turbidite sequence.**

Shale smears have a range of geometries and here we examine what are the range of geometries? Are different geometries representative of different processes (brittle or ductile), different shale-bed properties or a product of the scale of observation? How do the geometries of shale smears vary between sequences? What is the impact of shale smear and their varying geometries on fluid flow?

The geometries of shale smears on small displacement (<1 m) normal faults in the Mount Messenger Formation (MMF) are highly variable (see Figure 6.2). At outcrop-scale shale smears are produced by

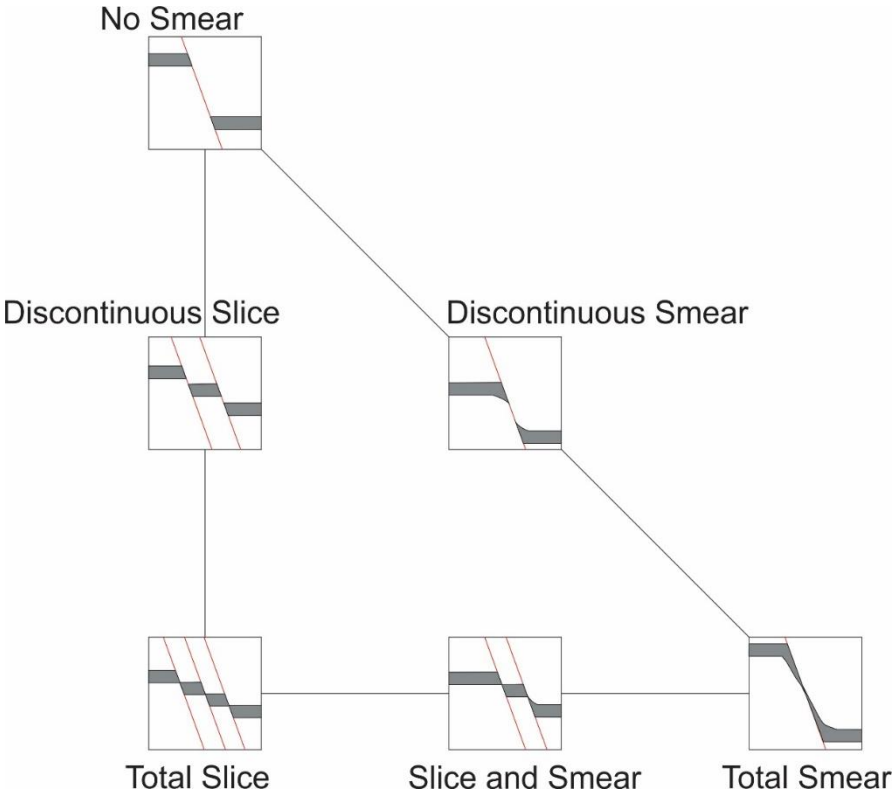

Figure 6.2 Schematic diagram depicting the variation on smear type and geometry observed for this study and previous papers on the MMF (Childs et al. 2007; Nicol and Childs 2018). Grey polygons are shale beds or shale smears and white polygons sandstone. Total smear and total slice indicates that there in each case there is no sand-on-sand juxtaposition across the fault.

a combination of ductile deformation and brittle faulting, with individual smears being produced by one or both of these processes. Individual beds can accommodate both brittle and ductile deformation, suggesting that apparent changes in the deformation style of beds is not entirely dependent on their mechanical properties. Thin sections of ductile smears show that they are primarily deformed by micro-faulting and brittle deformation. Therefore, smearing in the MMF is primarily a brittle process, with the type of deformation observed sometimes being dependent on the scale of observation. Displaced siltstone beds in the MMF can produce no shale smear, discontinuous shale smear and continuous shale smear between the source beds. Analysis of the smear thicknesses

suggests that on average the thickest smears are not located proximal to the source beds. Therefore, holes in shale smears do not appear to preferentially form at the midpoint between cut offs. The available smear data suggest that stochastic models may provide a means of populating shale smear thicknesses in fault zones.

Chapter 4: **Frequency of shale smear and factors that influence their formation.**

The implicit assumption in many shale smear analyses is that all shale or siltstone beds smear, however, questions remain about the frequency of shale smears. For example, how common are shale smears and what percentage of smears are continuous between the host shale-bed cut offs? What are the potential controls on the formation of smears on individual beds, for individual stratigraphic sequences and between different stratigraphic sequences? How do statistics on shale smear occurrence in this study relate to previous work?

Coastal outcrops comprising small normal faults (displacements 2 cm to 1.1 m) that displaced poorly lithified beds (burial depths ~1-1.5 km) of the Conway Formation (Gore Bay, New Zealand), Mount Messenger Formation (Taranaki, New Zealand) and Waitemata Group (White Bluff, New Zealand) were used to quantify the proportion of beds that smeared into fault-zones. In all cases the faulted beds were randomly sampled and characterised by 100% exposure with a lower resolution limit of about 1 mm. The majority of the data were from the Mount Messenger Formation, where from a sample of over 180 faulted siltstone beds 39% (N=71) displayed no smear, 53% (N=97) discontinuous smear and 8% (N=15) continuous smear (Figure 6.3A). The median smear continuity is ~3%, while half of the discontinuous smears have continuity of <23% and ~83% of all smears have continuity of <50%. The frequency of continuous smear varies between different sequences with almost 50% continuous smear observed at White Bluff and Gore Bay (Figure 6.3B). These differences are primarily thought to reflect changes in the composition of the shale beds with Gore Bay and White Bluff having a higher proportion of carbonaceous material and clay than the Taranaki outcrops, respectively. However, both no smear and continuous smear are also observed on the same beds and these differences do not appear to reflect within bed changes in composition or grain size. In such cases fault zone architecture may be an important factor for the formation of shale smear, with more distributed deformation likely to promote shale smear and slicing. Further work is required to constrain the effect of fault zone geometry on smearing.

Fault seal may be influenced by both the continuity and frequency of shale smear. In cases where smear amalgamation is not common the continuity of smears will have a critical influence on fault seal. Shale smears may be common along faults, but if all smears are highly discontinuous and extend only a short distance from the source bed, then their effect on fluid flow will be minimal. At the other

end of the spectrum, there may be few shale smears but the smears may be continuous between shale-bed cut offs and will impact fault seal. Therefore, the results of this chapter could have significant implications for fault seal. In particular, it is clear from faults in Taranaki that in some

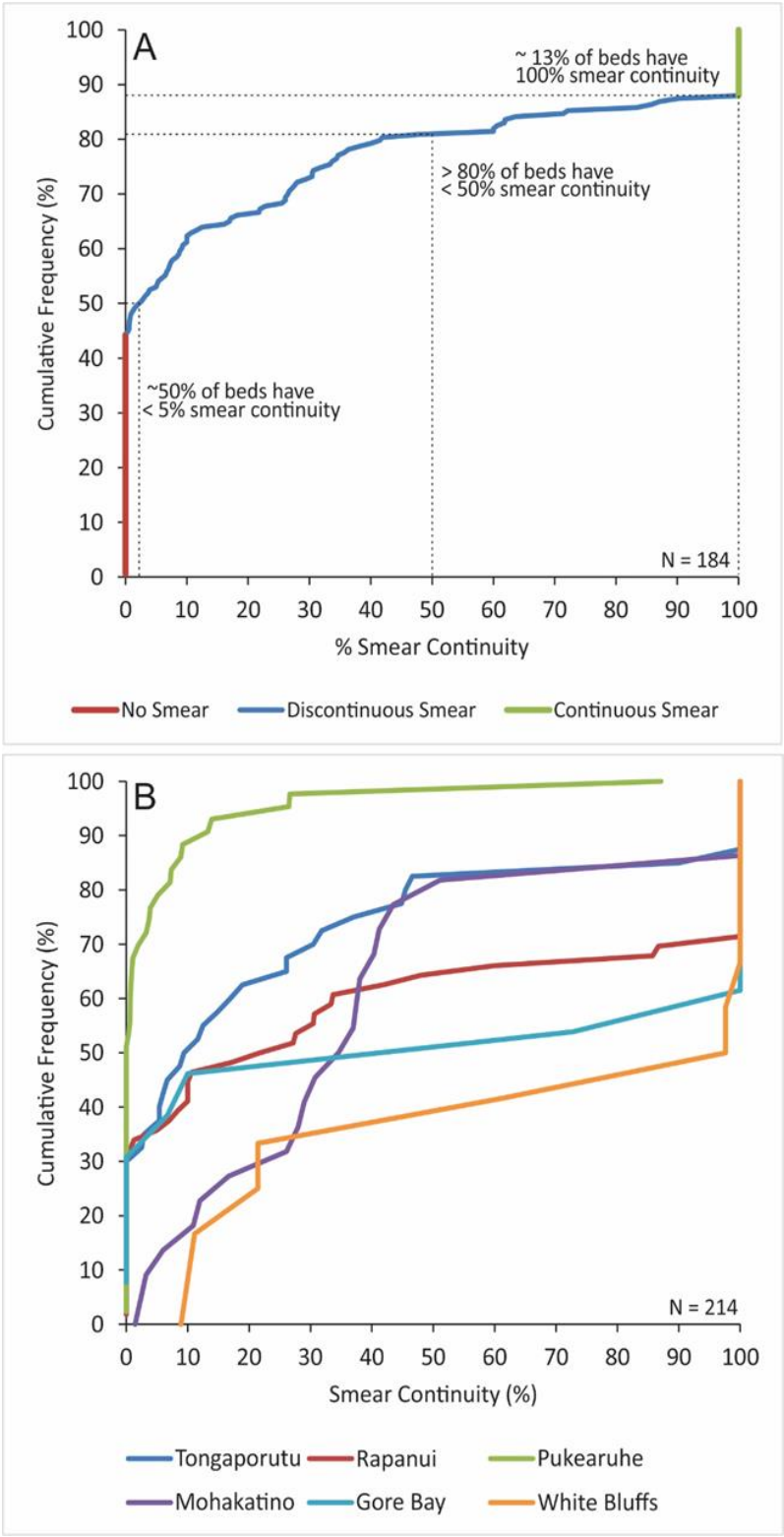

Figure 6.3 Frequency graphs showing the range in smear continuity for; A) all the sampled faulted siltstone beds in Taranaki and; B) individual localities throughout New Zealand. Shale smear continuity is the proportion of the distance along the fault between shale-bed cut-offs and with sand-on-sand juxtaposition that is covered by shale smear.

sequences many shale beds contribute little to the formation of low permeability fault rock and in these cases fault-seal algorithms, such as Shale Smear Factor (SSF), Clay Smear Potential (CSP) and Shale Gouge Ratio (SGR) may over-estimate the amount of low permeability fault rock sourced directly from wallrock beds.

In Taranaki, overestimates of the contribution of siltstone beds to the generation of fault rock may be partly, or entirely, countered by the production of fault rock by cataclasis of phyllosilicate-rich grains in faulted sandstone beds (Nicol and Childs 2018). Therefore, for such 'dirty' sands it may be necessary to combine or sum the phyllosilicates.

Chapter 5: **Implications of outcrop observations of small faults for the utility of fault-seal algorithms.**

H**ow accurate are the current shale-smear algorithms? Can they be used to predict the thickness of low permeability fault rock? What are the limitations of the current algorithms? What is the best way to use the algorithms going forward?**

Outcrop data for nearly 200 small faults have been studied to determine if the output from three fault-seal algorithms (CSP, SSF and SGR) are compatible with the observed shale smear continuity and fault-rock thicknesses. Our data show both shale smear continuity and fault-rock are highly variable at length scales of <1 m. Shale smears have been divided into three groups of continuous smear, discontinuous smear and no smear and these groups compared to bed thickness, displacement and outputs from the three fault-seal algorithms. The data show little correlation between bed thickness, displacement and the continuity of shale smears. Given that fault seal CSP and SSF algorithms use bed thickness and fault displacement as input parameters it is not surprising these algorithms also show no correlation with the occurrence of discontinuous and non-smears. Consistent with previous studies, continuous smears are found to be most common when they are derived from thick beds with low displacements. Comparison of fault-rock thickness measurements and fault-seal estimates from the three algorithms indicate that the algorithms do not reproduce the short wavelength (<0.5 m) up to order of magnitude variations in fault-rock thickness. The algorithms are unlikely to identify locations of minimum fault-rock thickness on the fault surface which are the most likely sites of across-fault flow. The poor correlations between outputs from the algorithms and outcrop observations may arise because the algorithms over simplify fault-zone structure and shale smear geometries, and do not explicitly account for processes other than shale smear that produce fault rock (e.g. cataclasis).

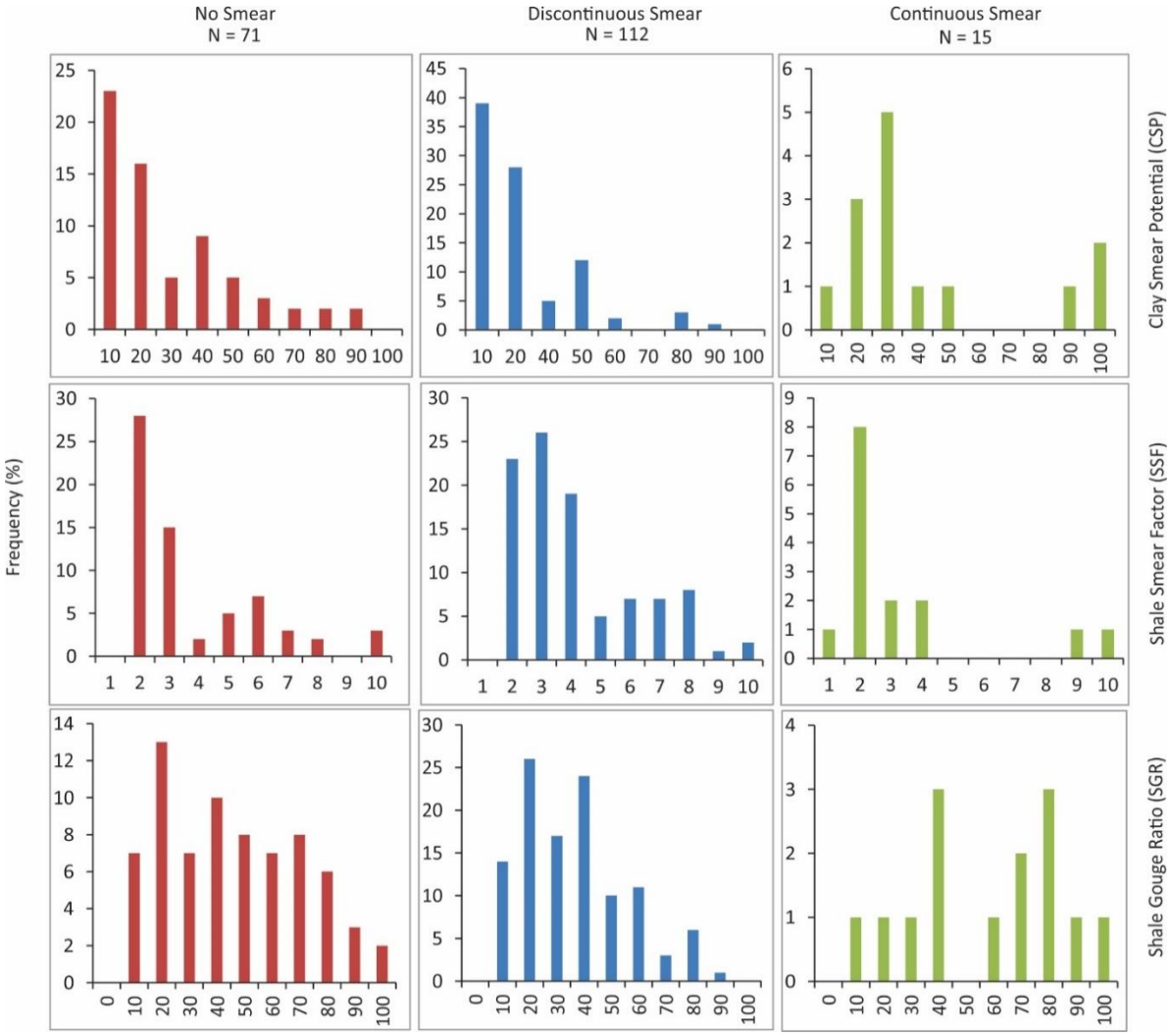

Figure 6.4 Graphs showing the range in algorithm values for no smear (red), discontinuous smear (blue) and continuous smear (green) beds. A similar range in values can be seen for all three smear types indicating that the algorithms struggle to differentiate between beds that do and don't smear for this dataset.

6.2 Further Work

Due to the time constraints of a PhD, several avenues of research were not undertaken during this project but are areas of potential interest for future work. The future work identified here can be broken down into seven main topics which are listed below and briefly discussed in the following sections.

1. Shale smears on Reverse and Strike Slip Faults,
2. Shale smear Evolution,
3. 3D geometries of smears,
4. Upscaling observations from outcrop,
5. Fault-rock and fault-zone variability,
6. Cataclasis and fault-rock generation,
7. Shale smears amalgamation.

6.2.1 Shale smears on Reverse and Strike Slip Faults

Shale smears on reverse and strike slip faults are rarely studied. This study (as with previous studies) focusses on normal faults to limit the number of variables that could be controlling smear. Nonetheless, work on reverse faults is sorely needed to assess the sealing properties of reverse faults in compressional regimes. During the early stages of this project several reverse faults were analysed with numerous measurements and pictures taken. However, in order to limit the scope of the present thesis these reverse faults were not studied in detail. From the preliminary data gathered it appears that different smear geometries can be generated in compressional and extensional regimes (e.g., reverse faulting may be associated with folding that extends beyond the fault zone, although significantly more data are required to test this possibility.

6.2.2 Shale smear Evolution

How fault zones in general and shale smears specifically evolve through time has been widely discussed in the literature (e.g. Childs et al. 2009; Faulkner et al. 2010; Nicol et al. 2013; Vrolijk et al. 2016) and yet consensus has not been reached as to how and why fault zones evolve. For example, while it is sometimes assumed that once a smear becomes discontinuous it ceases to lengthen, Childs et al. (2007) suggest that it is “far more likely that smears will continue to lengthen by shearing with increased fault displacement”.

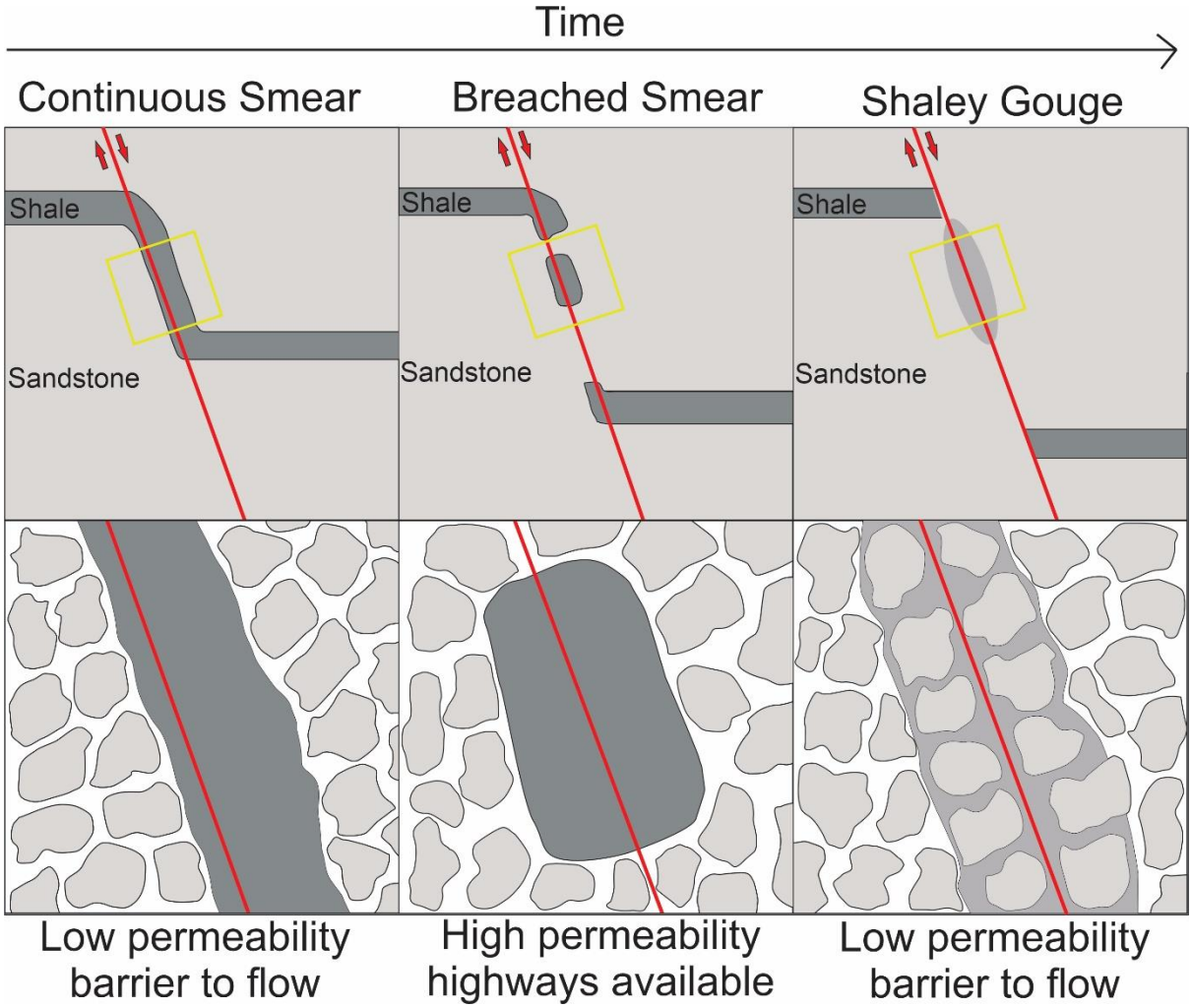

Figure 6.5. Schematic diagram depicting a simplified version of the three stages (1. continuous smear, 2. breached smear and 3. shaley gouge) that shale smears are thought to evolve through over time. The potential impact of each stage on fluid flow is indicated along the base of the figure.

In some cases, an improved understanding of fault permeability may require more information about how shale smears evolve. In particular, understanding how and when a low permeability shale smear changes from being continuous to completely abraded and infilling macroporosity is important when trying to predict fault sealing.

Three stages have been inferred for the life cycle of a shale smear: 1) The smear is continuous and acts as a barrier to across fault fluid flow, 2) the smear starts to become segmented potentially allowing permeability pathways between the segments and 3) the segments become abraded over time formed a clay gouge that infills macroporosity between grains and become a barrier or baffle to fluid flow (Vrolijk et al. 2016). Currently it is difficult to know if all smears go through these stages, how long each stage may last and if there are conditions that promote preservation of one stage over another. These questions could be addressed in future work.

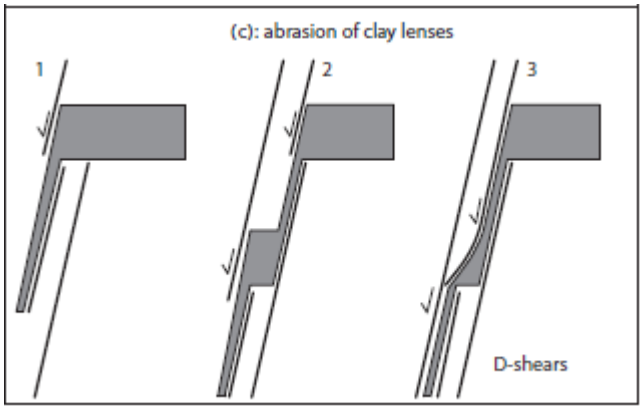

Figure 6.6. Diagram illustrating another potential style of evolution of shale smear within a fault-zone starting with a simple smear, followed by a fault bound lens forming and then the lens geometry becoming lengthened and thinned with increasing numbers of synthetic slip surfaces (Kettermann et al. 2016).

6.2.3 3D geometries of shale smears

This study, in common with the vast majority of field-based studies, is a 2D analysis of fault zones mainly observed in cross sections. The data used is a sub-sample of a 4D system in which little information is available on how smears change geometry in and out of the plane of observation and through time. During the course of this study we considered systematically 'mining' along faults to determine the 3D geometries of shale smears, however, due to limited time and resources such an approach was not taken. Limited ad hoc excavations (<20 cm into the outcrop) into several faults did confirm that for the MMF such excavation would be possible (assuming that permission to undertake these studies was granted by local authorities and Māori iwi). These excavations also demonstrated that in some cases shale smears changed dramatically in thickness over short distances in a horizontal direction (as has also been observed in vertical direction on some faults). These observations suggest that 3D studies of shale smear may be achievable and valuable and should be considered for future studies.

6.2.4 Upscaling observations from outcrop

The majority of studies of shale smear are conducted at outcrop scale or using 'table top' laboratory experiments. By and large we assume that fault zones are fractal (e.g. Childs et al. 2017) and that observations at outcrop and model scales apply at seismic or reservoir scale. Without the ability to accurately image smaller-scale features, seismic relies on the ability to upscale our observations when modelling the complexity and heterogeneity inherent to faults with large displacements. If the

upscaling is valid, then the use of outcrop (and model) data to constrain the form of fault-seal algorithms is also valid. The addition, if up scaling is valid, then small-scale slip surfaces observed in fault zones at outcrop scale should also be present at seismic scale. These intra fault-zone structures could significantly alter bed juxtapositions producing different fluid pathways and reservoir to reservoir connections than predicted with a single slip surface alone (van der Zee and Urai 2005). More research is required to test the upscaling assumption and identify what parts of faults are most likely to host sub-seismic structures that could locally modify the formation of shale smears and the across-fault juxtaposition of reservoir rocks.

6.2.5 Fault-rock and fault-zone variability

The variability of fault-zone architecture over a fault surface should be further investigated. Given the formation, migration and pooling of hydrocarbons and other fluids occurs on geological timescales it is important to be able to constrain better how fault architecture and permeability may fluctuate in space and time. To better constrain the influence and impact of small-scale faults more outcrop work could be undertaken to map the variation in fault-rock and fault-zone thickness. By creating a detailed and extensive database of fault profiles, stochastic methods could be used to predict the distribution of low permeability fault rock and areas of increased complexity along a fault trace. Research outlined in this thesis suggests that all outcrops can be plotted somewhere on the diagram shown in Figure 6.2 and that all shale smears exist between the no smear, continuous smear and total slicing end members. Populating this framework with data from a range of outcrops may assist us to better understand the processes that generate shale smears. A better understanding of these processes could lead to improvements in the shale smear algorithms.

6.2.6 Cataclasis and fault-rock generation

As highlighted by Figure 6.3 a large proportion of the siltstone beds sampled in New Zealand either did not smear or had smears that only covered a small proportion of the fault trace. The lack of shale smear in some cases suggests that incorporation of siltstone wallrock into fault zones may, in some cases, not be the primary process by which low-permeability fault rock is generated. We agree with Nicol and Childs (2018) that for the MMF cataclasis of ‘dirty’ sandstones is an important mechanism by which fault rock forms. Cataclastic processes can lead to permeability reductions of several orders of magnitude (Yielding et al. 1997; Fisher and Knipe 2001; Bense et al. 2013) and can create baffles and/or barriers to flow (Bense et al. 2013). In sandstones with a high proportion of clay (15 - 40%) or lithic grains, cataclasis can lead to the formation of phyllosilicate framework rocks (Fisher and Knipe 2001; Torabi 2014). SEM samples and thin sections from the MMF show the preferential breakdown of lithics and clays within deformation bands, leaving isolated quartz crystals floating in a fine grained

matrix (see Figure 6.7 and Figure 6.8). We believe that such cataclastic processes could significantly impact the permeability of some reservoirs. The available data suggest that further investigation into the impact of cataclasis on fault-rock properties (e.g. thickness and permeability) in lithic and clay rich sandstones and how best to ensure that cataclastic processes are incorporated within predictive algorithms and fault permeability calculations could be valuable.

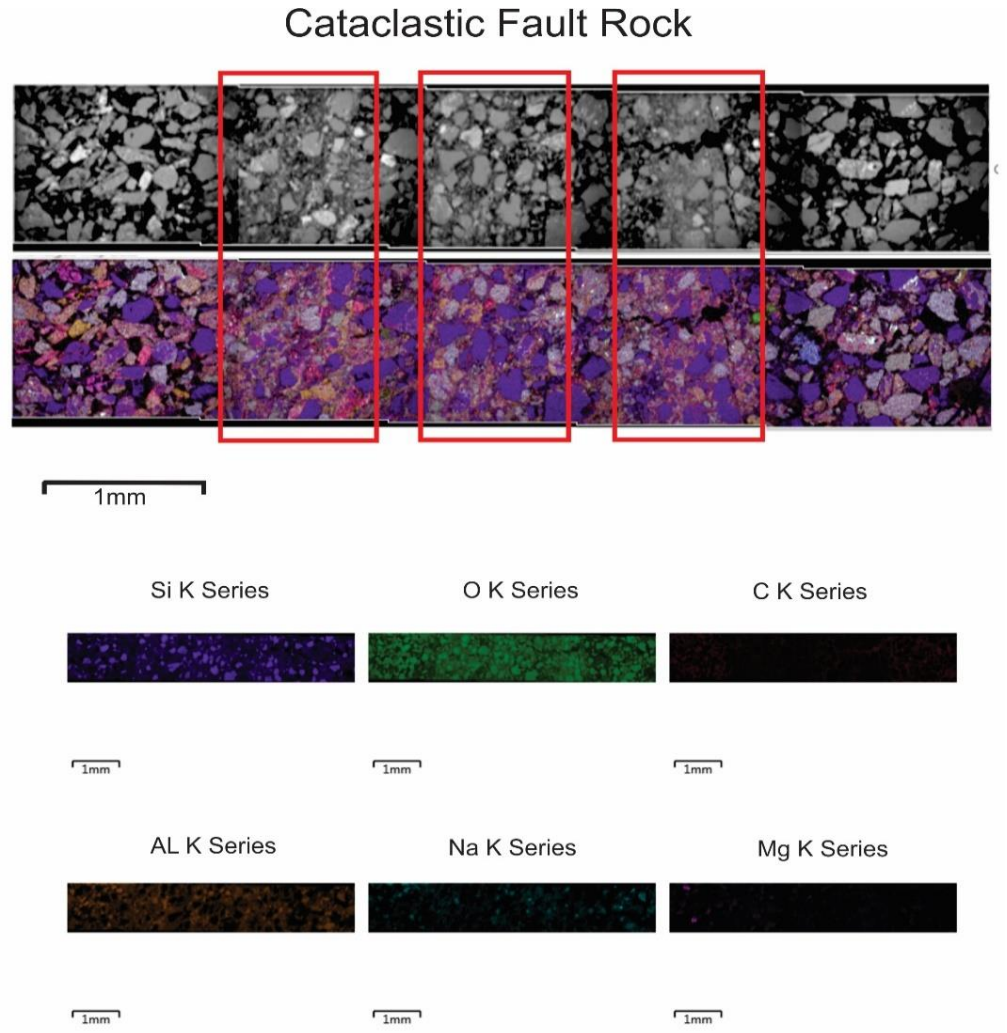

Figure 6.7 SEM image montage showing mutliple deformation bands within a sandstone from the MMF. The red boxes highlight the deformation bands - areas of grain breakdown can be seen as a cloudy background on the top BSE image and purple quartz crystals floating in a fine grained aluminium rich matrix on the chemscan image below.

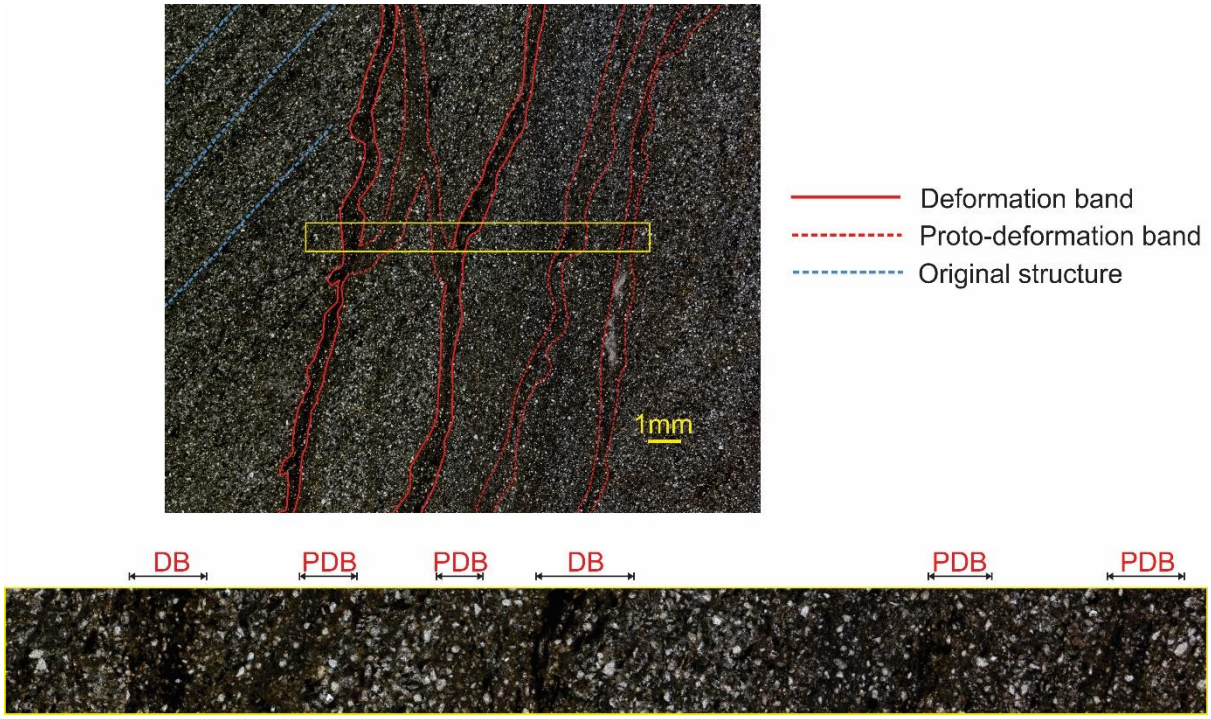

Figure 6.8 Thin section showing host sandstone with several deformation bands running from top to bottom bounded by the red lines (blue dashed lines are bedding). The magnified yellow section shows the grain size reduction inside the bands with isolated quartz crystals left floating in a fine grained matrix. DB = Deformation Band and PDB = Proto-Deformation Band.

6.2.7 Shale smears amalgamation

A brief analysis of multi-bed shale smears (i.e. sections of the fault surface that have been passed by multiple siltstone beds) was conducted in the MMF towards the end of this thesis. While it was expected that smears derived from multiple beds would amalgamate to form longer and/or thicker smears than those from individual beds, often this was not found to be the case. Multiple bed smears showed a similar continuity and degree of amalgamation to individual smears, suggesting that sand smears must also be prevalent. While a decrease in the sequence net:gross was found to increase smear continuity it was not found to increase amalgamation. A better understanding of multi-bed smears and how they behave within a fault-zone is needed as there are often thin interbeds of shale and sand that are not resolved on Gamma Ray or VShale curves, but still contribute to fault rock. Further investigation of shale smear amalgamation is required to test our tentative observations that such amalgamation may not be as common as previously thought. Such studies might also consider what factors influence the formation of amalgamated smears.

6.3 References

Bense VF, Gleeson T, Loveless SE, Bour O, Scibek J. 2013. Fault zone hydrogeology. Earth-Science Rev. 127:171–192. doi:10.1016/j.earscirev.2013.09.008.

Childs C, Walsh JJ, Manzocchi T, Strand J, Nicol A, Tomasso M, Schopfer MPJ, Aplin AC. 2007. Definition of a fault permeability predictor from outcrop studies of a faulted turbidite sequence, Taranaki, New Zealand. Geol Soc London, Spec Publ. 292:235–258. doi:10.1144/SP292.14.

Fisher QJ, Knipe RJ. 2001. The permeability of faults within siliciclastic petroleum reservoirs of the North Sea and Norwegian Continental Shelf. Mar Pet Geol. 18(10):1063–1081. doi:10.1016/S0264-8172(01)00042-3.

Kettermann M, Thronberens S, Juarez O, Urai JL, Ziegler M, Asmus S, Krüger U. 2016. Mechanisms of clay smear formation in unconsolidated sediments-insights from 3-D observations of excavated normal faults. Solid Earth. 7(3):789–815. doi:10.5194/se-7-789-2016.

Nicol A, Childs C. 2018. Cataclasis and silt smear on normal faults in weakly lithified turbidites. J Struct Geol. 117(June):44–57. doi:10.1016/j.jsg.2018.06.017.

Torabi A. 2014. Tectonophysics Cataclastic bands in immature and poorly lithified sandstone, examples from Corsica , France. 630:91–102.

Vrolijk PJ, Urai JL, Kettermann M. 2016. Clay Smear: Review of Mechanisms and Applications. J Struct Geol. doi:10.1016/j.jsg.2015.09.006.

Yielding G, Freeman B, Needham DT. 1997. Quantitative fault seal prediction. Am Assoc Pet Geol Bull. 81(6):897–917. doi:10.1306/522B498D-1727-11D7-8645000102C1865D.

van der Zee W, Urai JL. 2005. Processes of normal fault evolution in a siliciclastic sequence: a case study from Miri, Sarawak, Malaysia. J Struct Geol. 27(12):2281–2300. doi:10.1016/j.jsg.2005.07.006.